

**Environmental and Climatological Evolution  
of the early Paleogene Southern Ocean**

Peter Kristian Bijl

LPP Foundation 2011



Peter Kristian Bijl  
Biomarine Sciences  
Institute of Environmental Biology  
Department of Biology  
Faculty of Science  
Utrecht University

Laboratory of Palaeobotany and Palynology  
Budapestlaan 4  
3584 CD Utrecht  
the Netherlands

p.k.bijl@uu.nl

ISBN No. 978-90-39356548  
NSG Publication No. 20111130  
LPP Contributions Series No. 34

Printed by Wöhrmann Print Service, Zutphen

Cover: photos modified from originals made by Henk Brinkhuis and the Shipboard Scientific Party of IODP Leg 318. Dinocyst drawings obtained from Williams et al. (2004) and Lentin and Vozzhennikova (1989), with permission.

**Environmental and Climatological Evolution  
of the early Paleogene Southern Ocean**

**Milieu- en Klimaatsevolutie van de  
Zuidelijke Oceaan tijdens het vroeg Paleogeen**

(met een samenvatting in het Nederlands)

Proefschrift

ter verkrijging van de graad van doctor aan de Universiteit Utrecht op gezag van de rector magnificus, prof. dr. G.J. van der Zwaan, ingevolge het besluit van het college voor promoties in het openbaar te verdedigen op woensdag 30 november 2011 des middags te 12.45 uur

door

Peter Kristian Bijl

geboren op 21 oktober 1983 te Hoogeveen

**Promotoren:** Prof. dr. H. Brinkhuis  
Prof. dr. S. Schouten

**Co-promotor:** Dr. A. Sluijs

This research was funded by the LPP Foundation.

## **Members of the dissertation committee**

Prof. dr. Lucas Lourens – Universiteit Utrecht, the Netherlands

Prof. dr. Richard D. Pancost – Bristol University, United Kingdom

Prof. dr. Paul Pearson – Cardiff University, United Kingdom

Prof. dr. Jörg Pross – Frankfurt Universität, Deutschland

Prof. dr. ir. Jaap S. Sinninghe Damsté – Koninklijke NIOZ, Texel, and

Universiteit Utrecht, the Netherlands



*'It is only by combining the information furnished by all the Earth Sciences that we can hope to determine "truth" here'*

- **Alfred Wegener (1880-1930)**

# Contents



<b>General Introduction and Synopsis</b>	<b>11</b>
--	-----------



<b>Chapter 1</b> A magnetostratigraphically calibrated dinocyst zonation for the early Paleogene South Pacific Ocean <i>with Appy Sluijs and Henk Brinkhuis</i>	<b>23</b>
--	-----------



<b>Chapter 2</b> Early Paleogene temperature evolution of the southwest Pacific Ocean <i>with Stefan Schouten, Appy Sluijs, James C. Zachos, Gert-Jan Reichart and Henk Brinkhuis</i> <i>Published in Nature 461: pp. 776-779, 2009</i>	<b>71</b>
---	-----------



<b>Chapter 3</b> Environmental forcings of Paleogene Southern Ocean dinoflagellate biogeography <i>with Jörg Pross, Jeroen Warnaar, Catherine E. Stickley, Matthew Huber, Raquel Guerstein, Alexander J. P. Houben, Appy Sluijs, Henk Visscher and Henk Brinkhuis</i> <i>Published in Paleogeography 26: PA1202, 2011</i>	<b>87</b>
---	-----------



<b>Chapter 4</b> Southern Ocean warming, sea level and hydrological change during the Paleocene-Eocene Thermal Maximum <i>with Appy Sluijs, Stefan Schouten, Ursula Röhl, Gert-Jan Reichart and Henk Brinkhuis</i> <i>Published in Climate of the Past 7: pp. 47-61, 2011</i>	<b>113</b>
---	------------



<b>Chapter 5</b> Linkage between early opening of the Tasmanian Gateway and Antarctic cooling <i>with Appy Sluijs, Stefan Schouten and Henk Brinkhuis</i>	<b>131</b>
--	------------



## **Chapter 6**

**151**

Transient middle Eocene atmospheric CO<sub>2</sub> and temperature variations

*with Alexander J.P. Houben, Stefan Schouten, Steven M. Bohaty, Appy Sluijs, Gert-Jan Reichart, Jaap S. Sinninghe Damsté and Henk Brinkhuis  
Published in Science 330: pp. 819-821, 2010*



## **References**

**173**



## **Nederlandse Samenvatting**

**193**

## **Acknowledgements**

**205**

## **Curriculum Vitae**

**211**





# GENERAL INTRODUCTION AND SYNOPSIS



*Dinopterygium cladoides* Deflandre, 1935

Cyst is characterized by the possession of a narrow equatorial cingulum, with two very large membranes, and by the development of a system of fine wing-like, crested membranes, which delineate the tabulation. It has a goniodomecean tabulation and a disintegration archeopyle.



Since the beginning of the industrial revolution about 150 years ago, the burning of fossil hydrocarbons is increasing the partial pressure of atmospheric carbon dioxide ( $p\text{CO}_2$ ) at an unprecedented rate. If  $\text{CO}_2$  emissions continue unabated,  $p\text{CO}_2$  levels will approach 1,000 parts per million by volume (ppmv) at the end of the 21<sup>st</sup> century, much higher compared to  $\sim 390$  ppmv at present and  $\sim 280$  ppmv prior to massive industrialization (IPCC 2007).  $\text{CO}_2$ , as a greenhouse gas, absorbs outgoing long-wave radiation (heat) and emits it to all directions, also to the Earth's surface. Higher  $\text{CO}_2$  levels are therefore expected to result in a warming of the lower atmosphere. Moreover, the residence time of  $\text{CO}_2$  is long enough for the Earth to experience the effects: the emitted  $\text{CO}_2$  will reside in the atmosphere-ocean system for 100,000 years (Walker and Kasting 1992; Dickens 2003; Archer 2005). The climatic response to  $p\text{CO}_2$  increase is already detectable in field observations (IPCC 2007). Computer model experiments are conducted to predict the climatic and environmental effects of the predicted greenhouse gas increase. A fundamental assumption in these computer models is the principle of actualism: the forces and feedbacks at hand in present-day climates also apply in the future. The question is whether these feedbacks are similar in different climatic conditions. One way to test the validity of computer model output is to look in the Earth's geologic past: investigating what the Earth looked like in the past with conditions analogous to our future, but also how sensitive it responded to perturbations of the climate system, may provide insights in future climate change.

To study a world with  $p\text{CO}_2$  approaching that predicted for the future, paleoclimatologists are inspired to go far back in time. The available evidence suggests that  $p\text{CO}_2$  did not exceed 1,000 ppmv during the last 35 million years of Earth history. Most of that time,  $p\text{CO}_2$  was below 500 ppmv (Beerling and Royer 2011). The time period from beyond 35 million years ago (Ma) is characterized by  $p\text{CO}_2$  values that may have been well above 1,000 ppmv (Pearson and Palmer 2000; Pagani et al., 2005; Zachos et al., 2008). Evidence for much warmer climates in that time period is particularly convincing in polar regions. Vegetation reconstructions from northern high latitudes indicate that during the Eocene Epoch, 56 to 34 Ma, the continents fringing the Arctic Ocean were forested with (amongst others) *Metasequoia*, now flourishing in temperate rainforests (Francis 1988). Crocodile skulls were found in Alaska (Markwick 1998), and footprints reveal that ancestors of modern-day hippos roamed marshes on what now is Svalbard. In fact, some mammals were year-round residents of the high Canadian Arctic (e.g., Eberle et al., 2009). During the zenith of Eocene warmth, at  $\sim 54$  Ma, palms flourished on the landmasses fringing the Arctic Ocean (Sluijs et al., 2009a), and at  $\sim 50$  Ma, the Arctic Ocean itself was blanketed by thick mats of the free-floating fresh water fern *Azolla* (Brinkhuis et al., 2006; Collinson et al., 2010). The latter phenomenon and the reconstructed vegetation on land evidences that, at least seasonally, profound wet precipitation regimes existed in the northern high latitudes (Pagani et al., 2006; Speelman et al., 2010; Barke et al., 2011).

At southern high latitudes, Paleogene macrofossil remains have been found on outcrops on the Antarctic continent, evidencing angiosperm forests (Francis and Poole 2002). New Zealand ( $50^\circ$  South paleolatitude, Slat. (Crouch 2001)) biomes contained a diversity of palms in the late Eocene (Hartwich et al., 2010). Clay



mineralogical studies from Eocene Antarctic coastal sediments suggest wet weathering regimes in the Antarctic hinterland (Ehrmann 1998). The discovery of warm and wet conditions is enigmatic because polar environments in the Paleogene must still have been limited in daylight for half of the year. In order to explain the warmth on Eocene Antarctica, a hypothesis was proposed involving the effect of Southern Hemisphere continental configuration changes. Because Australia was still more or less attached to Antarctica during most of the Eocene (Lawver and Gahagan 2003) and also the conduit between South America and Antarctica was only shallowly open (Lagabrielle et al., 2009), the modern-day isolating Antarctic Circumpolar Current (ACC) could not circulate the Antarctic continent. Instead, low latitude, warm surface currents were thought to have reached and warmed Antarctica (Kennett 1977; Fig. 1). However, this hypothesis was later disputed by the results of general circulation model experiments (Sloan and Rea 1995). Applying these models to the Paleogene revealed that even in absence of an ACC, low latitude, warm currents could not reach the Antarctic coastline. Instead, large clockwise gyres existed in the Southern Ocean, which effectively prevented low latitude currents to reach Antarctica (Sloan and Rea 1995; Huber et al., 2004; Fig. 1). The currently leading hypothesis explaining the warmth of the early Paleogene now is related to the high concentrations of greenhouse gases, and associated feedbacks (Zachos et al., 2008), although sufficient direct evidence to support this statement is lacking.

In stark contrast to the overwhelming evidence for general warmth are the enigmatic findings of ice rafted debris, sea-ice diatoms and evidence for frost in the Arctic Ocean from 46 million years onwards (Eldrett et al., 2007; St. John 2008; Stickley et al., 2009). Although Paleogene climates seemed to have passed their warmest by then (Zachos et al., 2008), still both temperatures and  $p\text{CO}_2$  concentrations are considered too high to allow for the presence of large ice caps on the poles (DeConto et al., 2008). On the Southern Hemisphere, remains of surface-dwelling dinoflagellates show a dramatic shift towards dominance of forms that are endemic to the Southern Ocean (e.g., Wrenn and Beckman, 1982; Wrenn and Hart, 1988; Brinkhuis et al., 2003a; Warnaar 2006). Intuitively, such an endemic dinocyst community suggests cooling of Southern Ocean surface waters. This is in contradiction with the reduced meridional temperature gradients as inferred from fossil leaf analyses (Greenwood and Wing 1995), which would promote poleward migration of biota rather than polar endemism. Moreover, the absence of geographic barriers separating the Southern Ocean from adjacent, warmer basins would further promote proliferation of low-latitude dinoflagellates into the Southern Ocean.

In general, while a wealth of evidence suggests that the early Eocene was warm, and the remainder of the Eocene had experienced cooling towards the icehouse world of the Oligocene and Neogene, still many questions remain on timing, nature and causes of the greenhouse-icehouse transition. Improved understanding of high-latitude climate evolution of the Southern Ocean starts with continuous, chronostratigraphically well-constrained time series of early Paleogene high-latitude temperature, climatic and biotic changes. The record from the Arctic Coring Expedition (Moran et al., 2006) provides a unique first insight in Northern high-latitude paleo-environments in the Paleogene greenhouse, but the record is patchy, of



low resolution and with large hiatuses (Sluijs et al., 2008a). The Southern Ocean, however, has much better coverage of sedimentary archives provided by the Deep Sea Drilling Project (DSDP), and subsequently the Ocean Drilling Program (ODP) and the on going Integrated Ocean Drilling Program (IODP). One issue that hampers investigations of these cores has been the lack of biostratigraphic tools to date these sediments: conventional calcite-based microfossils are usually absent in high-latitude sediments. In part because of this, still relatively little is known about Southern high-latitude climate evolution in the early Paleogene.

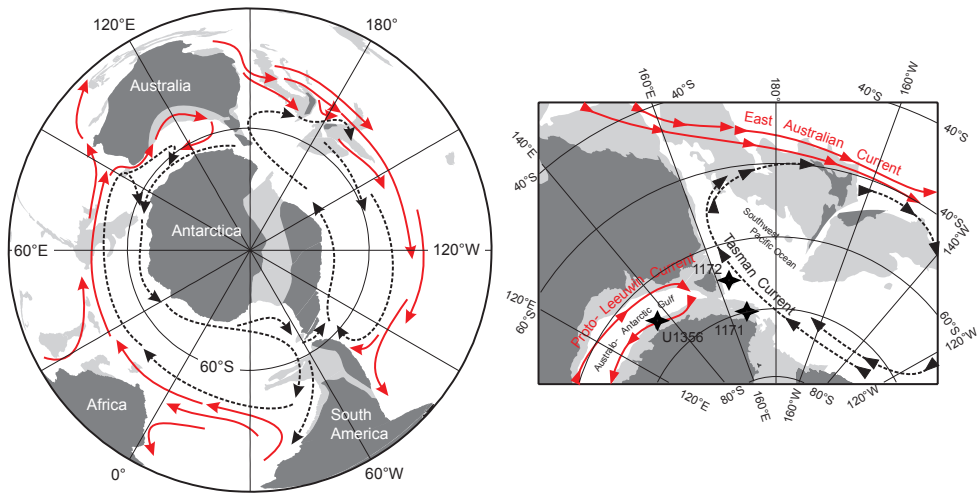


Figure 1. Left: Paleogeographic reconstruction of the Southern Ocean. Tectonic configurations were obtained from de odsn website: [www.odsn.de](http://www.odsn.de). Note that Australia was much closer to Antarctica than it is today. The light grey areas indicate continental blocks that were submerged in the Eocene. Also plotted is the generalized Eocene surface current configuration as interpreted from computer model studies applying the Eocene continental configuration (Huber et al., 2004). Right: detailed paleogeographic reconstruction of the southwest Pacific Ocean. Black asterisks indicates the main drill sites from which sediments were used in this thesis: Ocean Drilling Program (ODP) Site 1172 on the East Tasman Plateau (ETP); ODP Site 1171 on the South Tasman Rise (STR) and Integrated Ocean Drilling Program (IODP) Site U1356 on the Wilkes Land Margin.

An indirect approach to evaluate Paleogene Southern Ocean climate evolution may be captured in the compilation of benthic foraminiferal oxygen isotopes ( $\delta^{18}\text{O}$ ; Zachos et al., 2008). The  $\delta^{18}\text{O}$  value of benthic foraminifera is mainly influenced by water temperature and changes in  $\delta^{18}\text{O}$  of the seawater. The latter is, in turn, influenced by ice volume and salinity. In the absence of major continental ice, salinity changes mainly influence the seawater  $\delta^{18}\text{O}$  in these times. The salinity and temperature of intermediate and deep water depend on the source and mechanisms of deep and intermediate water formation. The Southern Ocean is thought to have been the main source for deep-water formation in the Eocene (Thomas et al., 2003). Hence, the signal obtained from benthic foraminiferal calcite produced within deep and intermediate waters may in fact bear the signatures of climatic evolution of Southern Ocean surface waters.



The benthic  $\delta^{18}\text{O}$  stack (Zachos et al., 2008) shows a general cooling from the Cretaceous-Paleogene boundary, towards a minimum in the mid-Paleocene (~58 Ma; Zachos et al., 2008; Fig. 2). Subsequently, temperatures rise gradually until ~52 Ma, where long-term Cenozoic peak temperatures are reached until ~50 Ma: the Early Eocene Climatic Optimum (EECO). Here, intermediate waters reached temperatures 13°C warmer than today, assuming ice-free conditions and normal salinity. The subsequent 15 million years, from 49 to 34 Ma, are characterized by gradual cooling of intermediate waters (Zachos et al., 2008; Fig. 2), eventually culminating in the onset of major glaciation of Antarctica (Zachos et al., 1992), at around 34 million years ago (Zachos et al., 2008). Because the presence of ice prior to the early Oligocene isotope step is still under debate (Eldrett et al., 2007; St. John 2008), it is as yet unknown how much of the middle and late Eocene  $\delta^{18}\text{O}$  increase is related to cooling, how much to ice volume and how much to a change in sources of deep water formation.

Superimposed on these trends, several intervals of more rapid climate change in a transient fashion have been recognized. The Paleocene-Eocene Thermal Maximum (PETM) is a brief (~150 kyrs) interval of 5-8°C warming documented in the tropics and in mid- and high-latitude sites on both hemispheres (Kennett and Stott 1991; Sluijs 2006; see Sluijs et al., 2007a for a review). Transient warming at this event is accompanied by a prominent negative excursion in the stable carbon isotopic composition of sedimentary components (Kennett and Stott 1991; Sluijs et al., 2007a). This evidences an input of  $^{13}\text{C}$ -depleted carbon into the global exogenic carbon pool. Because ample evidence shows that the amount of carbon being added to the exogenic carbon pool at the PETM is in the same order as is expected for the future after all fossil fuels have been burned, this climate event is seen as best analogue to future climate change. Younger, less extreme events with many similarities to the PETM are recognized in the interval from the PETM (~56 Ma) up to 51 Ma (e.g., Cramer et al., 2003; Nicolo et al., 2007; Stap et al., 2010; Zachos et al., 2010). These so-called 'hyperthermals' come with various acronyms, and are, like the PETM, characterized by a shift towards lower  $\delta^{13}\text{C}$  values of the exogenic carbon pool.

A younger prominent feature of relatively short-term climate warming is the 'Middle Eocene Climate Optimum' (MECO; Bohaty and Zachos 2003), occurring at ~39 Ma (Bohaty et al., 2009). Similar to the PETM and other hyperthermal phases, the MECO stands out in deep-sea records as a phase of carbonate dissolution (Bohaty et al., 2009), suggestive of involvement of changes in the carbon cycle. In contrast to the early Eocene hyperthermal phases, the MECO is not accompanied by a shift towards lighter carbon isotopes (Bohaty et al., 2009). This suggests that, if  $\text{CO}_2$  was involved in climate change, the source of carbon injected into the atmosphere is different compared to the early Eocene hyperthermal phases.

In this thesis, some of the outstanding questions will be addressed in order to better understand the climatic evolution of the Southern Ocean, such as: how did southern high-latitude surface waters evolve in the early Paleogene, particularly in comparison to that reconstructed for deeper waters? How sensitive were Southern Ocean surface waters to long- and short-term climatic oscillations in the early



Paleogene? What was the biotic response to the temperature and circulation changes? What was the role of atmospheric CO<sub>2</sub>, and what of the opening and subsequent deepening of the Tasmanian Gateway? What was the climate sensitivity of the Southern Ocean in the Paleogene greenhouse?

To answer these questions, a combination of techniques is applied that have proven particularly useful to reconstruct high-latitude climate change. In contrast to calcite-based microfossil groups, the fossil remains of surface-dwelling dinoflagellates, i.e., their organic-walled cysts (dinocysts) have been found abundantly in high-latitude settings. In most high-latitude settings, particularly further back in the geologic record, dinocysts are the only biostratigraphic tool to tie high-latitude sections to international time scales (Brinkhuis et al., 2003a; Eldrett et al., 2004; Williams et al., 2004). On top of this, dinocyst assemblages provide valuable qualitative information on a suite of physical properties of the surface waters, such as nutrients, temperature, salinity and coastal proximity (Dale 1996; Pross and Brinkhuis 2005). Specifically for southern high latitudes, dinocyst assemblages consist of species that are endemic to the Southern Ocean (Wrenn and Beckman 1982; Wrenn and Hart 1988). These species were referred to as transantarctic flora, because it was suggested that they evidence the existence of a transantarctic seaway (Wrenn and Beckman 1982), and because at that time, dinoflagellates were apparently considered flora. Although dinoflagellates constitute of both heterotrophic and autotrophic forms, and it can be debated whether the data from Wrenn and Beckman (1982) truly supports the presence of a transantarctic seaway, the name of this dinocyst community is maintained in this thesis. It was shown that transantarctic floral species dominate in regions that are under influence of Antarctic-derived surface currents (Huber et al., 2004). This observation intuitively argues for temperature as the controlling environmental factor on the biogeographic distribution of endemic dinocysts, although this has not yet been tested adequately.

In addition to the dinocyst assemblages, organic geochemical paleo-environmental tools can often be applied on dinocyst-bearing sediments, owing to the similarity in preservation requirements for both the organic compounds and dinocysts. The organic geochemical toolbox to reconstruct climate change has been widened in the recent years, with the invention of new tools, such as the TEX<sub>86</sub> proxy for sea surface temperature (SST; Schouten et al., 2002; Kim et al., 2010) and *p*CO<sub>2</sub> based on <sup>13</sup>C of long chain alkenones (Pagani 2002). Combining organic geochemical and palynological tools on the wealth of sedimentary records from the Southern Ocean may help to reconstruct the dynamics and high-resolution climatic evolution of the early Paleogene high southern latitudes.

This thesis provides new insights into the paleoenvironmental and paleoclimatological evolution of the early Paleogene Southern Ocean. In **Chapters 1, 2, and 3**, a framework for portraying the early Paleogene paleoclimatological and paleoenvironmental evolution in the Southern Ocean is provided, in terms of dinocyst bio-magnetostratigraphy, organic biomarker paleothermometry and dinocyst biogeographic evolution of the Southern Ocean. **Chapters 4, 5, and 6** zoom in on critical intervals of more rapid climate change, in chronological order (Fig. 2).





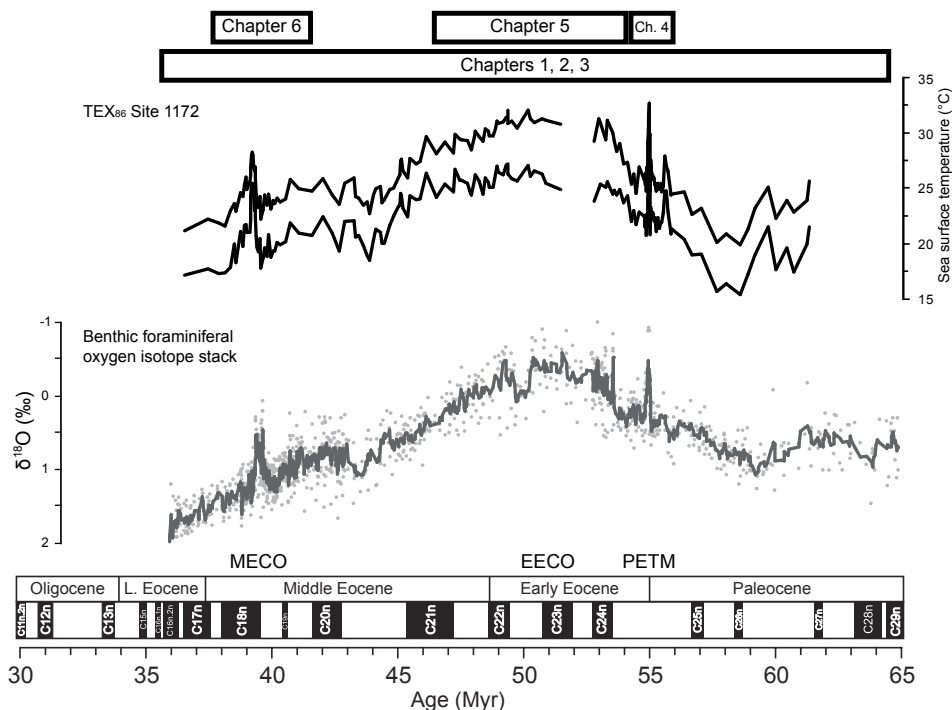


Figure 2. Early Paleogene Southwest Pacific Ocean TEX<sub>86</sub> sea surface temperature reconstructions, and the stack of benthic foraminiferal oxygen isotopes ( $\delta^{18}\text{O}$ ; as modified from Zachos et al. (2008); see Chapter 2). Two calibrations for TEX<sub>86</sub> are used (Kim et al., 2010). Also indicated is the structure of the thesis per chapter. Chapter 1, 2 and 3 cover the long-term Paleocene and Eocene climate development, Chapter 4 focuses on the Paleocene-Eocene Thermal Maximum, Chapter 5 focuses on the early-middle Eocene boundary and Chapter 6 concerns the Middle Eocene Climatic Optimum.

In **Chapter 1** a calibrated organic-walled dinoflagellate cyst biostratigraphic zonation scheme is proposed for upper Paleocene - upper Eocene sediments from the South Pacific Ocean. We compare chronologies from Ocean Drilling Program (ODP) Holes 1171D and 1172A/D to that of Integrated Ocean Drilling Program (IODP) Hole U1356A, and subsequently to dinocyst zonations from New Zealand. Based on these correlations, we present a revised magnetostratigraphic age model for ODP Holes 1171D and 1172A/D and propose a South Pacific dinocyst zonation scheme consisting of thirteen dinocyst zones. The South Pacific Dinocyst Zonation is calibrated to the International Time Scale of Gradstein et al. (2004) with additional independent age control from stable carbon isotope profiles, i.e., those correlated to the Paleocene-Eocene Thermal Maximum and the Middle Eocene Climatic Optimum, and magnetostratigraphy.

In **Chapter 2** a uniquely continuous and chronostratigraphically well-calibrated TEX<sub>86</sub> record of SST is provided from Ocean Drilling Program Leg 189 Site 1172 at the East Tasman Plateau (~65° Slat.; Fig. 1). We show that southwest Pacific



SSTs rose above present-day tropical values (to 34°C) during the early Eocene (53 Ma) and had gradually decreased to about 21°C by the early late Eocene (36 Ma). Our results suggest that there was almost no latitudinal SST gradient between sub-equatorial and sub-polar regions during the early Eocene (~55–50 Ma). The latitudinal gradient markedly increased in the middle Eocene. In theory, if Eocene cooling was largely driven by a decrease in atmospheric greenhouse gas concentration (Zachos et al., 2008, and references cited therein), additional processes are required to explain the relative stability of tropical SSTs (Pearson et al., 2007) given that there was significant cooling at higher latitudes.

Despite warm polar climates and low meridional temperature gradients, a number of different high-latitude plankton assemblages were, to varying extents, dominated by endemic species during most of the Paleogene. To document the evolution of Paleogene plankton endemism in the high southern latitudes, in **Chapter 3** the spatio-temporal distribution of dinocysts is investigated. Moreover, we assess their response to changes in regional SST. Paleocene and early Eocene (65–50 Ma) Southern Ocean dinocyst assemblages were largely cosmopolitan in nature, but a distinct switch from cosmopolitan-dominated to endemic-dominated assemblages (the so-called “transantarctic flora”) occurred around the early-middle Eocene boundary (50 Ma). The spatial distribution and relative abundance patterns of this transantarctic flora correspond well with surface water circulation patterns, as reconstructed through general circulation model experiments, throughout the Eocene. Dinocyst assemblages are quantitatively compared with the TEX<sub>86</sub>- based SST reconstructions of Chapter 2 through the lower and middle Eocene from ODP Site 1172. One conclusion is that the middle Eocene onset of the proliferation of the transantarctic flora is not linearly correlated with regional SST records. Only after the transantarctic flora became fully established later in the middle Eocene, possibly triggered by large-scale changes in surface-ocean nutrient availability, abundances of endemic dinocysts show a high degree of correlation with regional SST variations.

In **Chapter 4** a record of the PETM is presented from ODP Site 1172. The organic paleothermometer TEX<sub>86</sub> suggests that southwest Pacific sea surface temperatures increased from ~26°C to ~33°C during the PETM. Such temperatures before, during and after the PETM are >10°C warmer than predicted by paleoclimate model simulations for this latitude. Hence, not only Arctic, but also Antarctic temperatures may be underestimated in simulations of ancient greenhouse climates by the current generation of fully coupled climate models. An early influx of abundant *Apectodinium* is recognized at Site 1172, in accord with that in expanded PETM sections, such as those from New Jersey. This suggests once more that anomalous environmental change preceded the CIE on a global scale. Organic dinoflagellate cyst assemblages suggest a local decrease in the amount of river run-off reaching the core site during the PETM, possibly in concert with eustatic rise. Moreover, the assemblages suggest changes in seasonality of the regional hydrological system and perhaps storm activity. Finally, significant variation in dinoflagellate cyst assemblages during the PETM indicates that southwest Pacific climates varied significantly over time scales of 10<sup>3</sup> – 10<sup>4</sup> years during this event, a finding comparable to similar studies of PETM successions from the New Jersey Shelf.



In **Chapter 5** the role of the opening of a critical Southern Ocean gateway, the Tasmanian Gateway in Antarctic climate change is investigated. Proxy-records are presented from recently recovered sediments from the Wilkes Land Margin, Antarctica (Escutia et al., 2011), deposited west of the Tasmanian Gateway in the Australo-Antarctic Gulf. Integrated marine and terrestrial microfossil and organic geochemical analyses show a strong cooling of east Antarctic surface waters (3-4°C) and adjacent landmasses (~6°C), at ~50 Ma. Critically, this cooling coincides with the first incursion of typical southwest Pacific phytoplankton that migrated across an apparently shallow southern opening of the Tasmanian Gateway at that time. Collectively, this implies that the onset of the relatively cool westward Antarctic Counter Current through the Tasmanian Gateway diminished the influence the warmer Australo-Antarctic waters. This suggests a significant role of the shallow opening of the Tasmanian Gateway in East Antarctic cooling, pre-setting this region for massive cryosphere development at the Eocene-Oligocene boundary at ~34 Ma.

The long-term warmth of the Eocene (~56-34 Ma) is commonly associated with elevated partial pressure of atmospheric carbon dioxide ( $p\text{CO}_2$ ). However, a relationship between the two has not been established for short-term climate perturbations. In **Chapter 6** both  $p\text{CO}_2$  and SST are presented over an episode of transient global warming called the Middle Eocene Climatic Optimum (MECO; ~39 Ma). Organic molecular paleothermometry indicates a 3-6°C warming of southwest Pacific SSTs whilst reconstructions of  $p\text{CO}_2$  indicate a concomitant two- to three-fold increase. The marked consistency between SST and  $p\text{CO}_2$  trends during the MECO suggests that elevated  $p\text{CO}_2$  played a major role in global warming during the MECO.

In summary, this thesis provides a detailed image of the early Paleogene greenhouse-icehouse transition of the Southern Ocean. The dinocyst zonation for a large part of the early Paleogene may serve as guide for future biostratigraphy and age-assessment, which is crucial because few biostratigraphic tools are available in Eocene Southern high-latitude sediments. The SST evolution of the South Pacific Ocean mimics that of benthic foraminiferal oxygen isotopes, suggesting that the South Pacific Ocean was a region of deep-water formation. However, absolute temperatures seem much higher than those inferred from the benthic foraminifera. Part of this may be due to the effect of seasonal biases, i.e., that the deep water was formed mainly in winter and that the reconstructed Southern Ocean surface temperatures were skewed towards summer. The biotic response to the SST evolution in the Southern Ocean is controversial: dominance of endemic dinocyst assemblages seems unrelated to SST. The working hypothesis intuitively was that the proliferation of an endemic phytoplankton community at high latitudes was the result of outcompeting warm-water taxa when temperatures cooled. Because SST seems unrelated to the onset of proliferation of endemic dinocysts, an alternative suggestion is proposed relating the shift to an increase of surface-water nutrient levels in the middle Eocene. Indeed, several independent other proxies conspire to suggest a switch in nutrient input from the late early Eocene (~50 Ma) onwards, from basin-scale Pacific Ocean export productivity to inter-basin increase in benthic foraminiferal carbon isotopic gradients suggesting more effective aging of intermediate waters. The PETM interval in the South Pacific Ocean also stands out with a rapid sea surface temperature increase: 5-



8°C. Also an acme of the tropical dinocyst genus *Apectodinium* is observed. As for some other PETM sections, the PETM record from the South Pacific Ocean reveals major environmental change preceding the negative carbon isotope excursion (CIE). This is in concert with suggestions that initial climate changes preceded the release of carbon in the exogenic carbon pool that resulted in the CIE. In turn, this suggests that the carbon input in the exogenic carbon pool is a response rather than a forcing factor. Another ongoing debate that was touched upon in this thesis is the role of oceanic gateway openings and its role in climate change. Newly drilled (2010) sediment archives from the Wilkes Land Margin, Antarctica, showed that through flow of the Antarctic Counter Current was initiated around the early-middle Eocene boundary (~52-50 Ma), concomitant to amplified cooling of Antarctic continental and coastal temperatures. The opening of the Tasmanian Gateway occurred at the time when the Earth started cooling gradually towards the icehouse state of the past 35 million years. Hence, Tasmanian Gateway opening may have set the stage for climate deterioration, although atmospheric CO<sub>2</sub> was likely still the major forcing factor of early Paleogene climate evolution. Indeed, we still see that transient climate warming at the MECO coincides with increased concentrations of atmospheric CO<sub>2</sub>, suggesting an important role for atmospheric CO<sub>2</sub> as driver of climate.









**We propose an organic-walled dinoflagellate cyst (dinocyst) zonation for the late Paleocene to late Eocene (58 - 36 Million years ago; Ma) of the South Pacific Ocean, calibrated using magnetostratigraphy and stable isotope stratigraphy. Dinocyst chronologies were generated from Ocean Drilling Program (ODP) Holes 1171D on the South Tasman Rise, 1172A/D on the East Tasman Plateau and Integrated Ocean Drilling Program (IODP) Hole U1356A on the Wilkes Land margin. Correlation to dinocyst zonations from New Zealand lead to revisions of the magnetostratigraphic age model at Holes 1171D and 1172A/D. Stable carbon isotope profiles provide correlations to the Paleocene-Eocene Thermal Maximum (~56 Ma) and the Middle Eocene Climatic Optimum (~40 Ma). The resulting zonation consists of thirteen dinocyst zones and is calibrated to the International Time Scale of Gradstein et al. (2004).**





## 1. Introduction

Throughout the past decades, interest has risen for southern high-latitude sediments from the early Paleogene Greenhouse period (~65 to 35 Ma), particularly for paleoclimate reconstructions (Wrenn and Beckman 1982; Wrenn and Hart 1988; Hannah 1997; O'Brien et al., 1998, 2004). Precise dating of the sediments has proven to comprise the major obstacle, because the well-calibrated calcite fossil groups, such as foraminifera and calcareous nannoplankton, are typically poorly or not preserved in high-latitude settings (Wilson et al., 1998; Florindo et al., 2003; Barker et al., 2007). In addition, siliceous microfossils such as diatoms and radiolaria dissolve and are typically not preserved in lower Paleogene sediments in the southern ocean. Organic-walled dinoflagellate cysts (dinocysts) are, however, often abundant and well-preserved in southern high-latitude marginal marine sediments (Wrenn and Hart 1988; Brinkhuis et al., 2003a, b), but this group still lacks a well-calibrated biostratigraphic framework in the Southern Ocean.

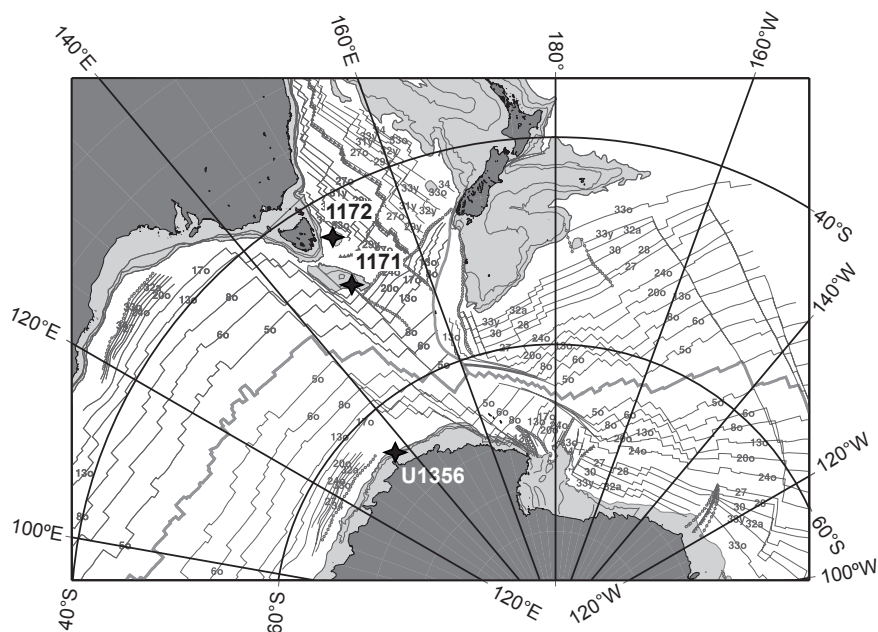


Figure 1. Present-day site locations of Ocean Drilling Program Sites 1172 and 1171 on the East Tasman Plateau (ETP) and South Tasman Rise (STR) in the Southwest Pacific, and Integrated Ocean Drilling Program Site U1356 on the Wilkes Land Margin, Antarctica (map modified from Cande and Stock (2004)). Dark grey areas indicate present-day shorelines, light-grey areas are submerged continental blocks above 3000 meters. White areas are below 3000 meters.

The Ocean Drilling Program (ODP) recovered early Paleogene sedimentary successions around Tasmania (Leg 189; at Sites 1171 and 1172; Fig. 1). An initial bio-magnetostratigraphic age model (including dinocysts) was published in the Scientific Results Volume (Stickley et al., 2004a). Extensive research at Site 1172 over the past



years has positively identified the Paleocene-Eocene Thermal Maximum (Chapter 4) and the Middle Eocene Climatic Optimum (Chapter 6), which represent chronostratigraphic tie points, and allows for a significant improvement of the age model. In addition, the recently recovered sedimentary succession at Site U1356 offshore the Wilkes Land Margin, Antarctica (Fig. 1) provides additional age constraints for early-middle Eocene dinocyst stratigraphy. We here evaluate the existing dinocyst chronology at Holes 1171D and 1172A/D and review the magnetostratigraphic calibrations made previously. Furthermore, we compare dinocyst chronologies at Holes 1171D and 1172A/D to that of Hole U1356A, and subsequently to dinocyst zonations from New Zealand. Based on these correlations, we present a revised bio-magnetostratigraphic age model for Holes 1171D and 1172A/D that allows for a South Pacific dinocyst zonation scheme.

## 2. Geological background and material

### *2.1 Tectonic evolution of the south Pacific and south Indian Ocean*

The breakup of supercontinent Gondwana around Jurassic-Cretaceous boundary times (~145 Ma; Willcox and Stagg 1990) resulted in rifting between Australia and Antarctica. Continental crustal stretching and thinning occurred pulsewise, and formed the Australo-Antarctic Gulf. Continued rifting eventually resulted in the formation of oceanic crust in the Australo-Antarctic Gulf by the late Cretaceous (~83 Ma; Close et al., 2009). Sea floor spreading rates were slow initially (1.5-7.5 mm/yr; Close et al., 2009), and Antarctica and Australia remained attached at the Tasmanian side at least until the early Paleocene (~64 Ma; Woodburne and Case 1996). Before 64 Ma, Australian and South American terrestrial mammal assemblages exchanged, via a land connection over the Tasmanian land bridge (Woodburne and Case 1996). Diversifying mammal assemblages on Australia from 64 Ma onwards thus signifies the formation of a marine barrier, the Tasmanian Gateway. This Gateway must initially have been shallow, because, e.g., dinoflagellate cyst assemblages from either side of the Gateway are distinctly different until 50 Ma (Fig. 2a; Chapter 6). Crustal anomaly studies have shown a distinct increase in sea floor spreading rates in the Australo-Antarctic Gulf from 50 Ma onwards (Fig. 2b, c; Close et al., 2009). Continental blocks surrounding the Tasmanian Gateway slowly deepened, such as the East Tasman Plateau (Röhl et al., 2004a) and the South Tasman Rise (Cande and Stock 2004). Gradual drowning ultimately evolved in rapid deepening of continental blocks surrounding Tasmania starting at ~35.5 Ma (Stickley et al., 2004b), when the northward drift of the Australian continent commenced (Fig. 2d). This tectonic evolution dictated the surface oceanic circulation and thereby the distribution of dinocysts around the Tasmanian sector, with differentiation of dinocyst assemblages on either side of the gateway until 50 Ma (Chapter 3, 6), and major reorganizations of the dinocyst assemblages occurred when the Tasmanian Gateway deepened (Sluijs et al., 2003; Stickley et al., 2004b; Warnaar 2006). These dinocyst distributions are closely consistent with the output of ocean current configurations from computer model experiments (Sloan and Rea 1995; Huber et al., 2004).



## 2.2 Site 1172

### 2.2.1 Site and lithology description Holes 1172A/D

Site 1172 is located on the submerged flat western side of the East Tasman Plateau (ETP), at 45° Southern latitude (Slat.), at a water depth of 2620 meters (Fig. 1; Exon et al., 2004). Four holes were drilled in total, of which Hole 1172A extends to the mid-Lutetian (bottom of the hole at ~504 meters below sea floor (mbsf)). Hole 1172D contains sediments from mid-Lutetian to upper Maastrichtian, with good overlap between the two holes. Sediments used in this study are from ~358-630 mbsf. Paleocene - lower Eocene sediments are olive grey, with some variations to greyish brown and to greenish grey, with abundant bioturbation (Exon et al., 2001).

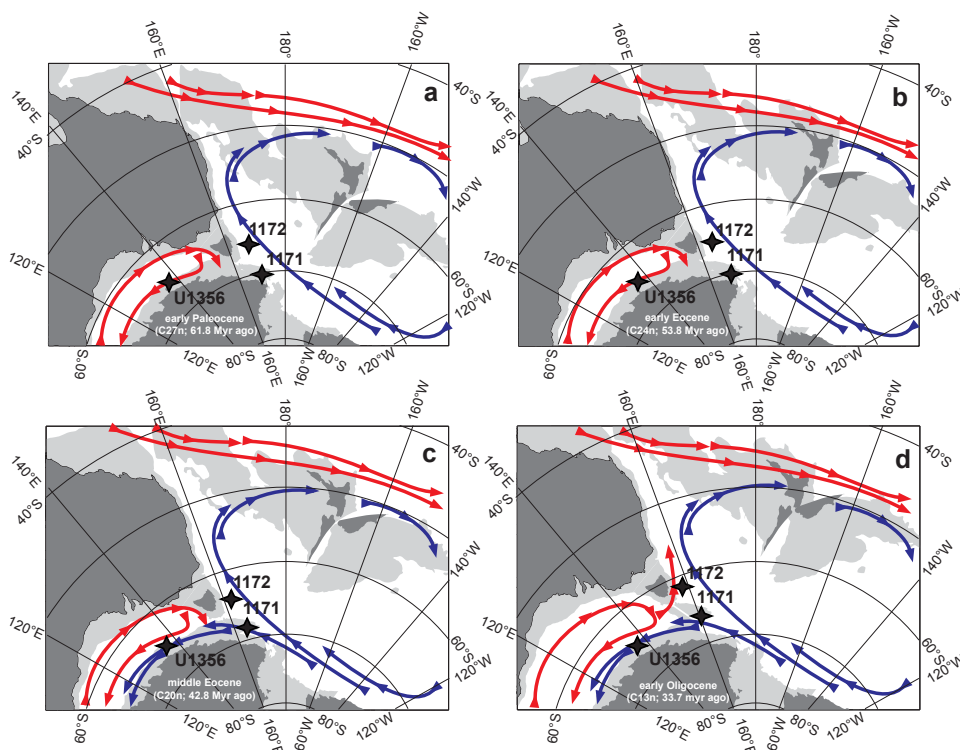


Figure 2. Paleogeographic reconstructions of the Australian Sector of the Southern Ocean, for (a) 61.1 Ma, (b) 53.3 Ma, (c) 43.8 Ma and (d) 33.5 Ma (maps modified from Cande and Stock (2004)). Also plotted are the reconstructed locations of the sites mentioned in this study, and the reconstructed surface current configurations. Shadings as in Fig. 1.

Sediments are virtually barren of any calcareous and siliceous microfossil groups, hampering conventional biostratigraphic dating (Stickley et al., 2004a). Middle - upper Eocene sediments contain increasing abundances of other microfossil groups, upsection, such as calcareous nannofossils, radiolarians and diatoms and eventually planktonic foraminifera (Stickley et al., 2004a). Prior to 35.5 Ma, lateral tectonic motion of the ETP was limited to slight eastward rift, away from Australia



(Fig. 2). Gradual subsidence of the East Tasman Plateau provided accommodation space for continuous shallow marine deposition. Middle Eocene strata are characterized by slightly deeper facies, increased carbonate content of the sediments and rapid shifts in dinocyst assemblages and elemental counts, all of which reflect third-order sea level cycles (Röhl et al., 2004a).

### 2.2.2 Age model Hole 1172A/D

Age control in the pre-Oligocene part of the succession relies on dinocysts, and occasionally on diatom and calcareous nannofossil stratigraphy, combined with magnetostratigraphy (Stickley et al., 2004a). Inclination data for Holes 1172A/D were published in the initial reports volume (Exon et al., 2001) and available on the ODP website ([www-odp.tamu.edu](http://www-odp.tamu.edu)), and magnetic reversals were identified from the inclination data as published by Fuller and Touchard (2004). Interpretation of the inclination data was complicated due to the strong normal overprint (Fuller and Touchard 2004). A first inventory of dinocyst species found during Leg 189 is published in the Scientific Results section of the Ocean Drilling Program (Brinkhuis et al., 2003a). The upper Paleocene and Eocene successions can be correlated to those in New Zealand, because many key dinocyst events were recognized at both locations (Brinkhuis et al., 2003a, b; Crouch and Brinkhuis 2005). Furthermore, high-resolution studies have added stratigraphic tie points and/or provided independent age constraints for Holes 1172A and D. For example, the identification of a ~3‰ negative excursion in the stable carbon isotopic composition ( $\delta^{13}\text{C}$ ) of total organic carbon in Section 1172D-15R-4 reveals the position of the Paleocene-Eocene Thermal Maximum (PETM), along with dominance of dinocyst *Apectodinium* spp. and a transient 5-8°C sea surface temperature rise (Chapter 4). Also, bulk carbonate carbon isotope analyses revealed a profile within Core 1172A-46X to -42X, which allowed correlation to the Middle Eocene Climatic Optimum (MECO; Chapter 6). We incorporated these new insights into a revised magnetostratigraphic interpretation of ODP Site 1172 in the range chart of selected dinocyst species (Fig. 3). The magnetostratigraphic interpretation follows that in Chapter 6.

## 2.3 Site 1171

### 2.3.1 Site and lithology description Hole 1171D

Site 1171 is located in lower bathyal water depths of about 2150 meters on a gently south-westerly slope on the southern part of the South Tasman Rise (STR), at 48° Slat. (Fig. 1; Stickley et al., 2004a). The age model for this site indicates the presence of strata from early Eocene (mid-Subchron C24n; Röhl et al., 2004b) to early Oligocene times. The middle Eocene section does contain occasional calcareous nannofossils, but the lithology is predominantly carbonate-low, dark greenish grey to olive grey claystone, with increasing abundance of calcareous nannofossils going upsection, rich in dinocysts throughout the section. High sedimentation rates of >12 cm/kyr evidence steady subsidence of the sub-basins that were formed during faulting of the STR.



# EARLY PALEOGENE DINOCYST ZONATION

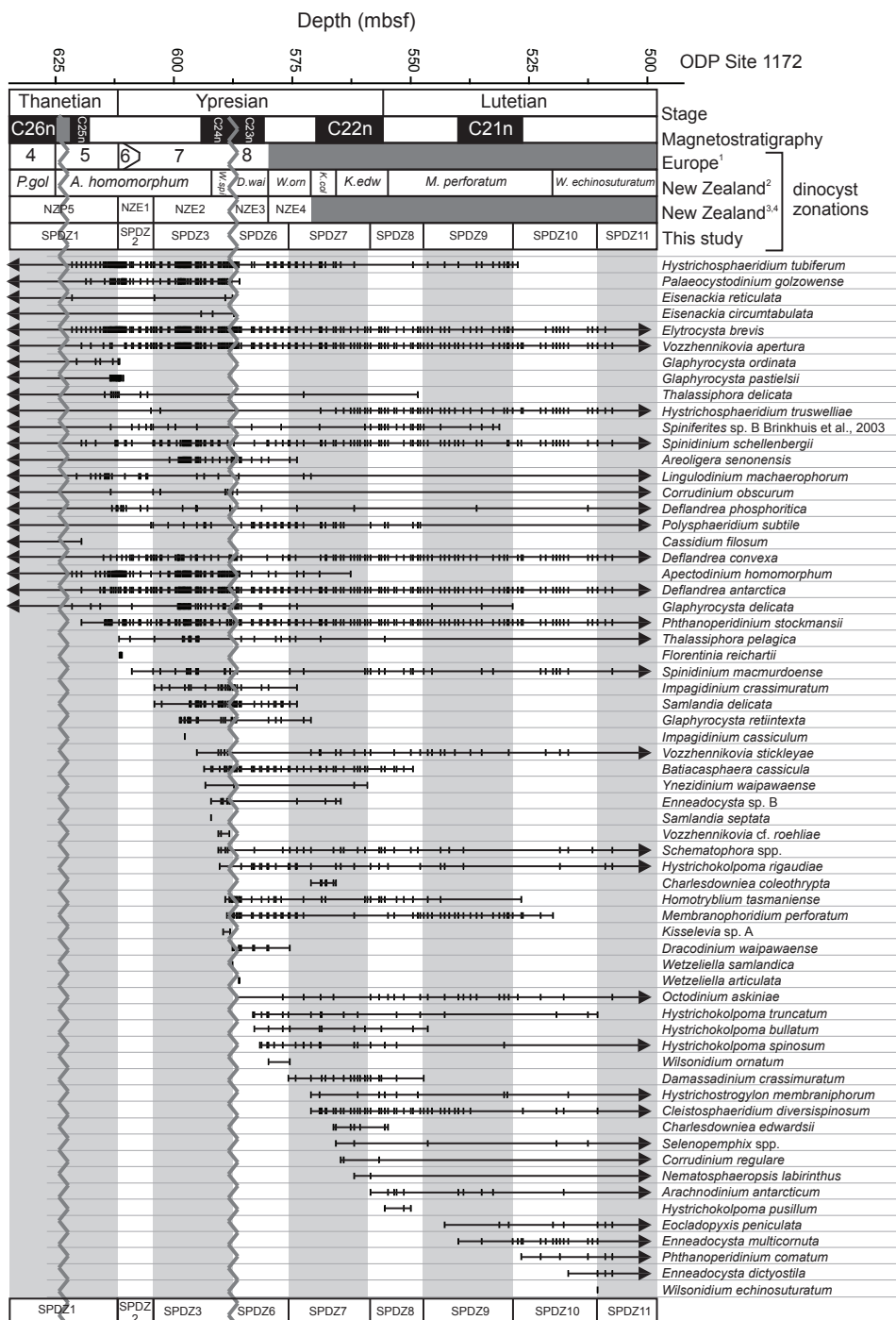


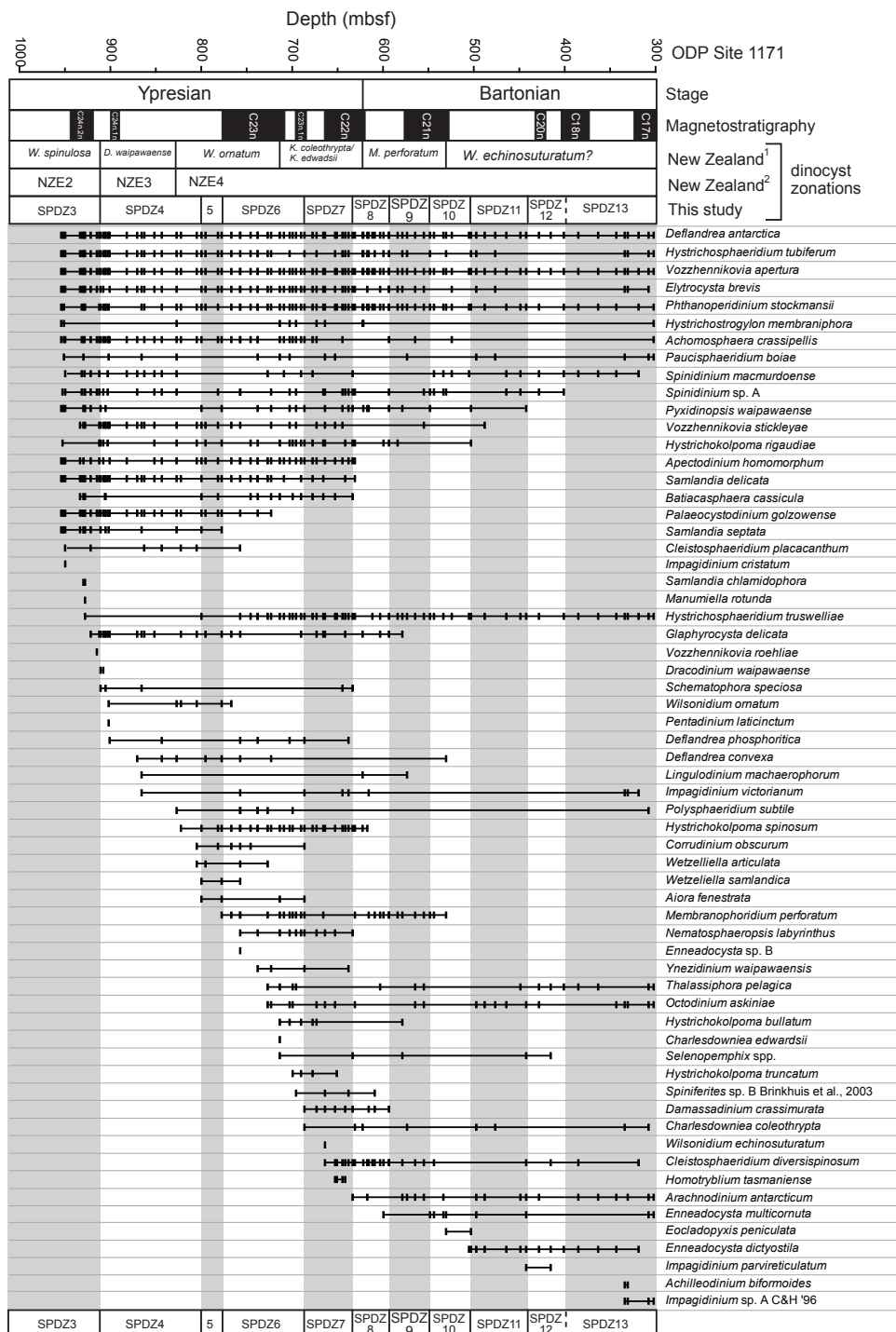


Figure 3 (this page and previous page). Ranges of dinocyst taxa for ODP Site 1172. a (previous page): Thanetian-Lutetian strata. b (this page): Lutetian – Priabonian strata. Also plotted are the magnetostratigraphic interpretation, and other dinocyst zonation schemes such as those from Heilmann-Clausen (1985)(1), Wilson (1988)(2), Crouch and Brinkhuis (2005)(3) and Crouch (2010)(4).

Figure 4 (next page). Ranges of dinocyst taxa for ODP Site 1171, with magnetostratigraphic interpretation and other dinocyst zonation schemes such as those from Wilson (1988)(1) and Crouch and Brinkhuis (2005)(2).



# EARLY PALEOGENE DINOCYST ZONATION





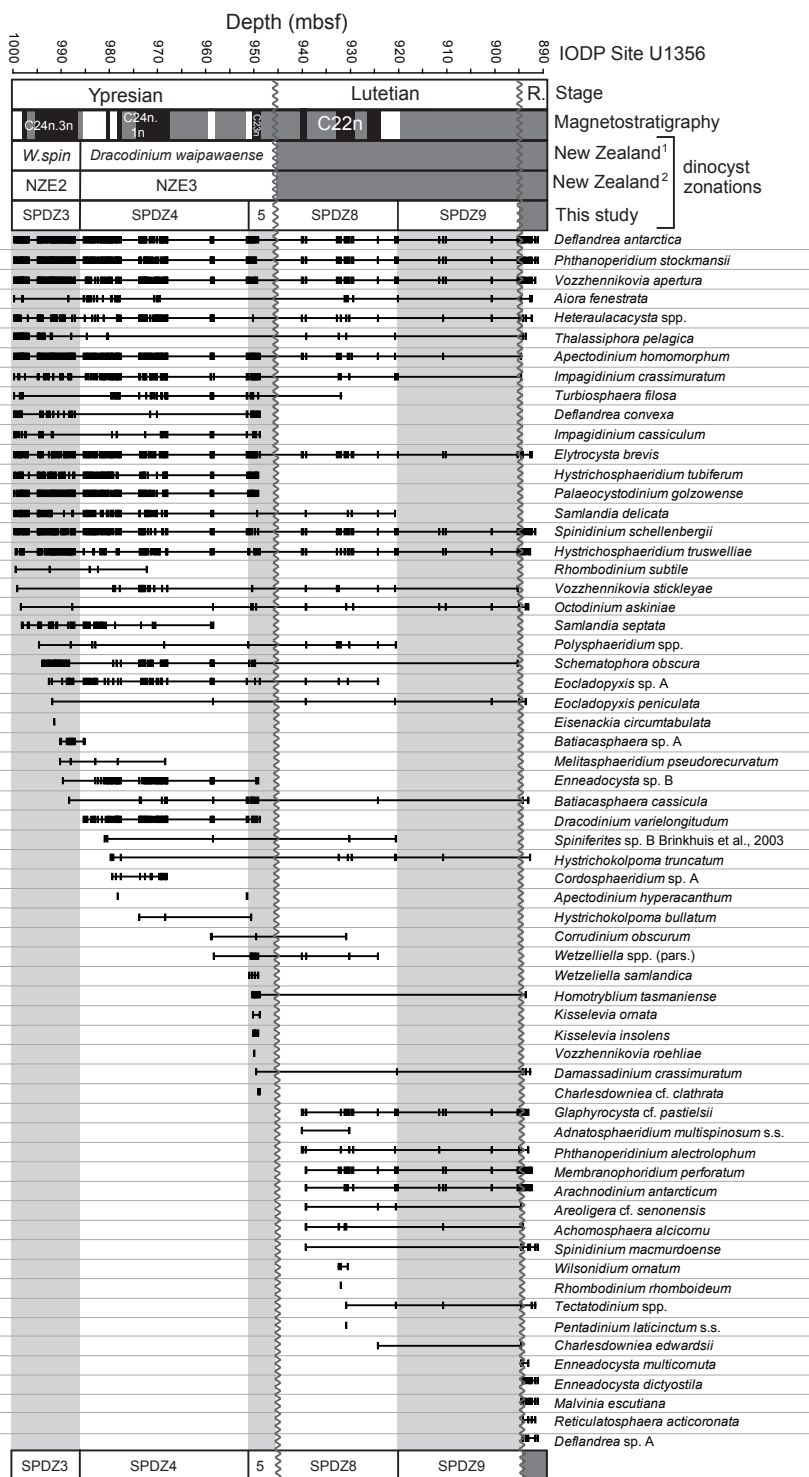




Figure 5 (previous page). Ranges of dinocyst taxa for Site U1356. The stages are indicated, where R. stands for Rupelian. The shipboard magnetostratigraphy is plotted, with grey areas indicating intervals with no magnetostratigraphic information due to disturbed core or core gaps. Dinocyst zonations are shown from Wilson (1988)(1) and Crouch and Brinkhuis (2005)(2).

### 2.3.2 Age model Hole 1171D

Site 1171 has been less intensively studied than Site 1172. Despite earlier claims (Exon et al., 2001; Exon et al., 2003) the PETM was not recovered at this site (Röhl et al., 2004b): oldest recovered sediments are correlated to Subchron C24n. Furthermore, many and large core gaps in the mid-middle Eocene interval compromise proper investigations of the expression of the MECO at this site. An integrated magneto- biostratigraphic age model was published in the Scientific Results Volume (Stickley et al., 2004a), combining dinocyst and few calcareous nannoplankton events with magnetostratigraphy. Higher resolution dinocyst analyses since then has increased confidence in the chronology at this site (Fig. 4). Sedimentation rates in the lower Eocene are much higher (12 cm/kyr) compared to Site 1172. Importantly, the record at Site 1171 does cover the interval from mid-Subchron C24n to mid Subchron C23n, an interval truncated in a hiatus at Site 1172 (Chapter 2, 6).

## 2.4 Site U1356

### 2.4.1 Site and lithology description Hole U1356A

Site U1356 is located on the Wilkes Land Margin at the transition between the continental rise and the abyssal plain at 4003 meters below sea level. Eocene sediments were recovered between 890 and 1000 mbsf, and consist of of dark green bioturbated claystone that is faintly stratified (millimeter to meter scale) as defined by color variations (light to dark bands), followed by interbedded stratified and massive sandstones, diamictites, silty claystones, and siltstones with graded bedding and parallel lamination (Escutia et al., 2010). While the drill site is now at abyssal depths, it was located on the Antarctic continental shelf in the Eocene, when the Wilkes Land shelf was much broader than at present (Close et al., 2009). The outer shelf submerged during the late Eocene-early Oligocene when rapid spreading widened the Australo-Antarctic Gulf.

### 2.4.2 Age model Hole U1356A

Shore-based high-resolution dinocyst analyses (Fig. 5; Chapter 5) have increased confidence in the shipboard integrated dinocyst- and magneto-stratigraphic age model for the Eocene section at Site U1356 (Escutia et al., 2011). The succession covers Subchrons C24n to C23n, followed by strata of middle Eocene age (Magnetochron C22/C21).



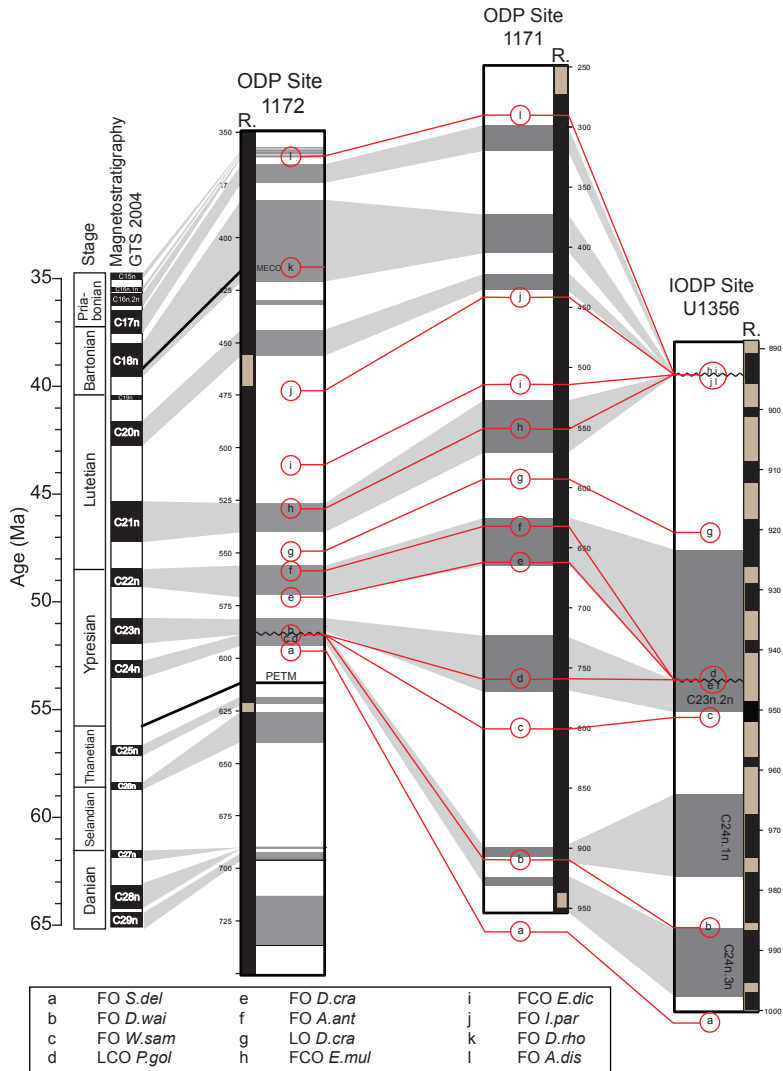


Figure 6. Correlation of Eocene dinocyst events between ODP Sites 1171 and 1172, and IODP Site U1356, and magnetostratigraphic calibration. In red the dinocyst bioevents are indicated: First Occurrence (FO) of *Samlandia delicata* (*S.del*), *Dracodinium waipawaense/varielongitutum* (*D.wai*), *Wetzeliella samlandica* (*W.sam*), *Damassadinium crassimuratum* (*D.cra*), *Arachnodinium antarcticum* (*A.ant*), *Impagidinium parvireticulatum* (*I.par*), *Dracodinium rhomboideum* (*D.rho*) and *Alterbidinium distinctum* (*A.dis*); Last Common Occurrence (LCO) of *Paleocystodinium golzowense* (*P.gol*); Last Occurrence (LO) of *Damassadinium crassimuratum* (*D.cra*); First Common Occurrence (FCO) of *Enneadocysta multicornuta* (*E.mul*) and *Enneadocysta dictyostila* (*E.dic*). Grey bars indicate intervals with normal magnetic polarity; white indicates reversed polarity. Magnetochrons are correlated between the sites based on the dinocyst events in red. Identification of the K-Pg boundary (Schellenberg et al., 2004) and chemostratigraphic correlations to the Paleocene-Eocene Thermal Maximum (PETM; Chapter 4), and Middle Eocene Climatic Optimum (MECO; Chapter 6) further ties ODP Site 1172 to the Geomagnetic Polarity Time Scale of Gradstein et al., (2004).



### 3. Methods

#### 3.1 Palynology

Sediments were processed for palynology using standard palynological processing techniques at the Laboratory of Palaeobotany and Palynology (LPP) of Utrecht University. About 10 grams of sediment was collected, freeze dried, and weighed. Processing involved an initial watering with Agepon detergent, followed by addition of hydrochloric acid (10%) to dissolve carbonates and a treatment of hydrofluoric acid (38%) to dissolve silicates. After each acid step samples were washed by decanting after 24 hours (hrs) of settling, followed by filling up with water, centrifuging and decanting again. The hydrofluoric step included 2 hrs shaking at ~250 rotations per minute (rpm) and adding 30% hydrochloric acid to remove fluoride gels. Subsequently, samples were repeatedly washed in water and finally sieved through a 250-micrometer ( $\mu\text{m}$ ) nylon mesh sieve to remove large palynodebris and pyrite particles. The  $<250\text{-}\mu\text{m}$  fraction was then sieved using a 15- $\mu\text{m}$  nylon mesh sieve. To break up clumps of residue, samples were placed in an ultrasonic bath for 5 minutes. The residue was transferred to a glass tube and centrifuged for 5 minutes at 2000 rpm. For slide preparation, residues were transferred to vials, homogenized and mounted on a slide with glycerine jelly and sealed. All material is stored in the collection of the LPP. Dinocyst taxonomy follows that cited in Fensome and Williams (2004). Recent additions to the latter include dinocyst species that were described or emended by (Levy and Harwood 2000; Clowes and Wilson 2006; Fensome et al., 2009; Sluijs and Brinkhuis 2009; Sluijs et al., 2009b; Houben et al., 2011).

### 4. South Pacific Dinocyst zonation

We recognized many key dinocyst events that allow for detailed correlation between Holes 1172A/D and Hole 1171D (Fig. 6; Table 1). These dinocyst events correlate well to the lower Eocene succession of the Wilkes Land Margin (Fig. 6). For the upper Paleocene - lower Eocene succession in Holes 1172A/D and 1171D, key dinocyst events were recognized that allow to correlate to the dinocyst stratigraphy of New Zealand (Crouch and Brinkhuis 2005). Younger sediments at the Tasmanian sector do not have a calibrated reference frame in New Zealand, but can be correlated to an uncalibrated dinocyst zonal scheme (Wilson 1988). The combined information allows for the recognition of inter-regional dinocyst index-events, which define thirteen formal dinocyst zones for the late Paleocene - late Eocene South Pacific Ocean (Fig. 1; Table 1). Many of our dinocyst index events are recognized in New Zealand dinocyst chronologies (Wilson 1988) and stratigraphies (Crouch and Brinkhuis 2005) as well. This means that those dinocyst events have supra-regional significance in the South Pacific Ocean. Where possible, we maintain the events that were used to define zones in New Zealand for our zonation. The top of each zone is defined by a dinocyst event, which also defines the base of the overlying zone. First occurrences (FO), last occurrences (LO), first common (~25%) occurrences (FCO) and last common (~25%) occurrences (LCO) of dinocyst taxa are used as zonal boundaries. We assign a type locality for each dinocyst zone and a base- and top sample for that zone is assigned at the type locality. In addition, the base and top samples in the paratype locality are



assigned where applicable. The age calibration of the top of each zone is given to the Geomagnetic Polarity Time Scale of Gradstein et al. (2004), including the associated magneto (sub-) chron. The dinocyst zonation is correlated to stages, with ages according to Gradstein et al. (2004). A comparison of our dinocyst zonation to those from previous studies is presented in Fig. 7.

Dinocyst zone	Type section	bottom sample	top sample	bottom depth	top depth	bottom uncertainty	top uncertainty
SPDZ1	1172D	17R-6W, 70-72 cm	15R-5W, 120-122 cm	633.17	612.7	0.895	0.1
SPDZ2	1172D	15R-5W, 100-102 cm	14R-6W, 40-42 cm	612.5	604.44	0.1	0.15
SPDZ3	1172D	14R-6W, 10-12 cm	13R-2W, 60-62 cm	604.14	587.85	0.15	0.1
SPDZ4	1171D	71R-2W, 630-62 cm	59R-CCW, 10-12 cm	912.6	805.32	1.35	2.61
SPDZ5	1171D	59R-4W, 10-12 cm	55R-1W, 10-12 cm	800.1	757.3	2.61	0.025
SPDZ6	1171D	54R-CCW, 9-11 cm	47R-CCW, 17-19 cm	757.25	690.24	0.025	1.865
SPDZ7	1172D	12R-2W, 40-42 cm	10R-3W, 110-112 cm	575.84	559.2	0.61	0.35
SPDZ8	1172D	10R-3W, 40-42 cm	9R-2W, 40-42 cm	558.5	547.3	0.35	0.4
SPDZ9	1172D	9R-1W, 105-107 cm	6R-4W, 135-137 cm	546.5	522.55	0.4	0.535
SPDZ10	1172D	6R-4W, 38-40 cm	5R-3W, 54-56 cm	521.48	510.5	0.535	1.62
SPDZ11	1172A/D	5R-2W, 38-40 cm	51X-4W, 85-87 cm	508.88	475.15	1.62	0.75
SPDZ12	1172A	51X-3W, 85-87 cm	45X-2W, 32-34 cm	473.65	414.02	0.75	0.4
SPDZ13	1172A	45X-1W, 102-104 cm	39R-7W, 45-47 cm	413.22	364.05	0.4	0.07

Table 1. Samples and depths for the zone boundaries in the type locality of the proposed dinocyst zone. SPDZ = South Pacific Dinocyst Zone. The top and bottom depths are in meters below sea floor (mbsf); uncertainties indicate the depth uncertainty ( $\pm$ ) in meters.

### 1. South Pacific Dinocyst Zone (SPDZ) 1

Base definition: LCO *Palaeoperidinium pyrophorum*

Top definition: FCO *Apectodinium homomorphum*

Type locality: ODP Site 1172

Base sample: 1172D-18R-1W, 40-42 cm (634.98 mbsf)

Top sample: 1172D-15R-5W, 120-122 cm (612.7 mbsf)

Calibration: the base is correlated to the base of Subchron C26n. The top of this zone is correlated to just prior to the Paleocene- Eocene boundary, Subchron C24r.

Age: late Thanetian (58.7 Ma to 55.8 Ma)

Characteristic species: *Elytrocysta brevis*, *Senegalinium cpx.*, *Cerebrocysta bartonensis*

Significant bioevents: LO *Eisenackia reticulata*, FO *Cleistosphaeridium placacanthum*, FO *Deflandrea antarctica*, FO *Glapyrocysta delicata*, FO *Phthanoperidinium stockmansii*

Remarks: this zone equates to New Zealand Paleocene Zone 5 of Crouch and Brinkhuis (2005).

### 2. Zone SPDZ2

Base definition: FCO *Apectodinium homomorphum*

Top definition: FO *Samlandia delicata*

Type locality: ODP Site 1172

Base sample: 1172D-15R-5W, 100-102 cm (612.5 mbsf)



Top sample: 1172D-14R-6W, 40-42 cm (604.44 mbsf)

Calibration: at the type locality (ODP Site 1172), bulk carbon isotope analyses have revealed the stratigraphic position of the Paleocene-Eocene boundary within this dinocyst zone (at 611.8 mbsf). This calibrates the oldest strata within this dinocyst zone to the latest Thanetian. The top of this zone is correlated to the top of Subchron C24r

Age: latest Thanetian- early Ypresian (55.8 to 54.0 Ma)

Characteristic species: *Apectodinium homomorphum*, *Senegalinium* sp., *Cordosphaeridium fibrospinosum*, *Elytrocysta brevis*, *Deflandrea antarctica*, *Glaphyrocysta retiintexta*, *Deflandrea convexa*, *Hystrichosphaeridium tubiferum*

Significant bioevents: ACME *Apectodinium homomorphum*, FO *Spinidinium macmurdoense*

Remarks: This dinocyst zone includes the quasi-globally recorded dominance of the genus *Apectodinium* associated with the PETM, calibrated with high accuracy using the negative excursion in stable carbon isotopes ( $\delta^{13}\text{C}$ ) of the exogenic carbon pool (Crouch et al., 2001; Sluijs et al., 2007a). Regionally, this zone is equivalent to Zone New Zealand Eocene zone 1 (NZE1) of (Crouch and Brinkhuis 2005). Centimeter-scale dinocyst and stable carbon isotope studies of expanded PETM sections have revealed that the *Apectodinium* acme precedes the carbon isotope excursion by several thousands of years in New Jersey, in the North Sea and perhaps at Tawanui, New Zealand (Sluijs et al., 2007b), and in the Arctic Ocean (Harding et al., 2011). At Site 1172, the type section of this dinocyst zone, the acme of *Apectodinium* at the CIE is preceded by a separate latest Paleocene acme, prior to the carbon isotope excursion of the PETM (Chapter 4). Because of the limited constraints on sedimentation rates, it remains uncertain if that early acme correlates to the pre-CIE acmes at other sites or if regional environmental forcing caused some degree of diachronism (Chapter 4). Either way, the resulting maximum uncertainty is in the order of  $10^3$  or  $10^4$  years, much smaller than the uncertainty related to the other zones described here. An acme of *Deflandrea* spp. in sample 1172D-15R-1, 10-12 cm (605.6 mbsf) likely correlates to a subzone proposed for New Zealand.

### 3. Zone SPDZ3

Base definition: FO *Samlandia delicata*

Top definition: FO *Dracodinium waipawaense*

Type locality: ODP Site 1172

Base sample: 1172D-14R-6W, 10-12 cm (604.14 mbsf)

Top sample: 1172D-13R-2W, 60-62 cm (587.85 mbsf); 1171D-71R-4W, 30-32 cm (915.3 mbsf)

Calibration: the top of this zone is truncated by a hiatus at ODP Site 1172; ODP Site 1171 indicates a tentative correlation to the top of Subchron C24n for this zone. At the Wilkes Land Margin, the top of this dinocyst zone is correlated to the top of Subchron C24n.3n

Age: mid-Ypresian (54.0 Ma to 53.3 Ma)



Characteristic species: *Apectodinium homomorphum*, *Areoligera* spp., *Deflandrea antarctica*, *Membranosphaera* spp., *Thalassiphora pelagica*, *Cordosphaeridium fibrospinosum*, *Palaeocystodinium golzowense*

Significant bioevents: FO *Enneadocysta* sp. B, LO *Eisenackia circumtabulata*

Remarks: This zone equates to dinocyst zone NZE2 of Crouch and Brinkhuis (2005), indicating the supra-regional stratigraphic significance of the dinocyst species that define the zone. These species have also been recognized in the Australo-Antarctic Gulf. However, on that side of the Tasmanian Gateway, *Dracodinium varielongitudum*, a taxon characteristic for the Northern Hemisphere, has been identified rather than *D. waipawaense*. The differences between the two species are subtle at most, and the stratigraphic ranges are identical. Hence it can be debated whether the subtle differences are eco-phenotypical in nature or have evolutionary significance. We consider these species as interchangeable with respect to the zonation.

#### 4. Zone SPDZ4

Base definition: FO *Dracodinium waipawaense*

Top definition: FO *Wetzeliella samlandica*

Type locality: ODP Site 1171

Base sample: 1171D-71R-2W, 60-62 cm (912.6 mbsf); 1172D-13R-2W, 60-62 cm (587.85 mbsf)

Top sample: 1171D-59R-CCW, 10-12 cm (805.32 mbsf); 1172D-13R-2W, 40-42 cm (587.65 mbsf)

Calibration: At ODP Site 1171 and IODP Site U1356 the top of this zone correlates to the onset of Subchron C23n. This zone is within a core gap at ODP Site 1172

Age: mid-Ypresian (53.3 Ma to 51.9 Ma)

Characteristic species: *Senegalinium* cpx., *Phthanoperidinium stockmansii*, *Deflandrea antarctica*, *Palaeocystodinium golzowense*, *Spinidinium/Vozzhennikovia* cpx.

Significant bioevents: FO *Polysphaeridium subtile*, FO *Corrudinium obscurum*

Remarks: The base of this dinocyst zone equates to the base of NZE3 of Crouch and Brinkhuis (2005), of which the top is defined by the FO of *Wilsonidium ornatum*. While this species is recognized at both Site 1171 and 1172, our calibration against magnetostratigraphy shows that this species apparently has a diachronous first occurrence in the region. We prefer *Wetzeliella samlandica* as a zonal boundary definition because this species apparently has a synchronous first occurrence, also in Wilkes Land. Unfortunately, *Wetzeliella samlandica* has not been reported from New Zealand thus far.

#### 5. Zone SPDZ5

Base definition: FO *Wetzeliella samlandica*

Top definition: LCO *Palaeocystodinium golzowense*

Type locality: ODP Site 1171

Base sample: 1171D-59R-4W, 10-12 cm (800.1 mbsf); 1172D-13R-2W, 60-62 cm (587.85 mbsf)



Top sample: 1171D-55R-1W, 10-12 cm (757.3 mbsf); 1172D-13R-2W, 40-42 cm (587.65 mbsf)

Calibration: at ODP Site 1171 the top of this zone correlates to the top of Subchron C23n. This zone is within a hiatus at ODP Site 1172

Age: mid-Ypresian (51.9 Ma to 50.7 Ma)

Characteristic species: *Senegalinium* cpx., *Phthanoperidinium stockmansii*, *Deflandrea antarctica*, *Palaeocystodinium golzowense*, *Wetzeliella samlandica*, *W. articulata*

Significant bioevents: FO *Polysphaeridium subtile*, FO *Membranophoridium perforatum*,

LO *Samlandia septata*, FO *Ynezidinium waipawaense*

Remarks: The last common occurrence of *Palaeocystodinium golzowense* correlates well between the Tasmanian sector, uncalibrated records from New Zealand sections and tentatively to Wilkes Land.

#### 6. Zone SPDZ6

Base definition: LCO *Palaeocystodinium golzowense*

Top definition: FO *Damassadinium crassimuratum*

Type locality: ODP Site 1171

Base sample: 1171D-54R-CCW, 9-11 cm (757.25 mbsf); 1172D-13R-2W, 40-42 cm (587.65 mbsf)

Top sample: 1171D-47R-CCW, 17-19 cm (690.24 mbsf); 1172D-12R-3W, 10-12 cm (577.06 mbsf)

Calibration: the base of this zone is truncated by a hiatus at ODP Site 1172. At ODP Site 1171 and 1172 the top of this zone is correlated to the onset of Subchron C22n

Characteristic species: *Polysphaeridium subtile*, *Wetzeliella samlandica*, *Wilsonidium ornatum*, *Membranophoridium perforatum*, *Hystrichokolpoma* spp.

Age: late Ypresian (50.7 Ma to 49.4 Ma)

Significant bioevents: FO *Selenopemphix* spp., FO *Hystrichokolpoma truncatum*

Remarks: The base of the youngest dinocyst zone of Crouch and Brinkhuis (2005) is defined by the FO of *Wilsonidium ornatum*. The FO of this species is diachronous between ODP Sites 1171 and 1172. The FO of other key species for the late Ypresian of New Zealand, such as *Charlesdowniea coleothrypta* (as *Kisselovia coleothrypta*) and *Charlesdowniea edwardsii* (as *Kisselovia edwardsii*) (Wilson 1988) were recognized at ODP Sites 1171 and 1172, but are not synchronous. The FO of *Damassadinium crassimuratum*, however, correlates well between 1171 and 1172 is also reported from the uncalibrated sections in New Zealand (as *Danea crassimurata* (Wilson 1988)). We hence consider this the best-suited key dinocyst event to employ for our zonation.

#### 7. Zone SPDZ7

Base definition: FO *Damassadinium crassimuratum*

Top definition: FO *Arachnodinium antarcticum*

Type locality: ODP Site 1172





Base sample: 1172D-12R-2W, 40-42 cm (575.84 mbsf); 1171D-47R-6W, 10-12 cm (686.51 mbsf)

Top sample: 1172D-10R-3W, 40-42 cm (558.5 mbsf); 1171D-42R-5W, 10-12 cm (638.1 mbsf)

Calibration: the top of this zone is correlated to the top of Subchron C22n

Age: late Ypresian (49.7 Ma to 48.6 Ma)

Characteristic species: *Cleistosphaeridium diversispinosum*, *Deflandrea antarctica*, *D. convexa*, *Damassadinium crassimuratum*

Significant bioevents: LO *Apectodinium homomorphum*, FO *Charlesdowniea coleothrypta*, FO *C. edwardsii*, LO *Samlandia delicata*

Remarks: *Arachnodinium antarcticum* is a distinct dinocyst species that is found as a characteristic element of the transantarctic flora (Wrenn and Beckman 1982) from basal middle Eocene sediments upwards on the Antarctic shelf (Wrenn and Hart 1988). However, this species has not been found in New Zealand. One dinocyst event that roughly coincides with the FO of *Arachnodinium antarcticum* and that does allow for correlation to New Zealand is the LO of *Apectodinium homomorphum* (Hollis et al., 2009). We however do not consider this dinocyst event to be a useful zone definition, because this species reaches high abundance in the lower Eocene and hence is very likely to be found reworked in younger sediments.

#### 8. Zone SPDZ8

Base definition: FO *Arachnodinium antarcticum*

Top definition: LO *Damassadinium crassimuratum*

Type locality: ODP Site 1172

Base sample: 1172D-10R-3W, 40-42 cm (558.5 mbsf); 1171D-42R-2W, 10-12 cm (633.6 mbsf)

Top sample: 1172D-9R-2W, 40-42 cm (547.3 mbsf); 1171D-38R-1W, 10-12 cm (593.7 mbsf)

Calibration: the top of this zone is correlated to mid-Subchron C21r

Age: early Lutetian (48.6 Ma to 47.9 Ma)

Characteristic species: *Arachnodinium antarcticum*, *Damassadinium crassimuratum*, *Deflandrea antarctica*, *Vozzhennikovia/Spinidinium* cpx., *Phthanoperidinium* spp.

Significant bioevents: LO *Batiacasphaera cassicula*, LO *Polysphaeridium subtile*, FCO *Octodinium askinae*, LO *Charlesdowniea edwardsii*

Remarks: Also the LO of *Damassadinium crassimuratum* correlates well between ODP Sites 1171 and 1172. Because the range of this species is relatively short, the likelihood of reworking is small. Therefore, this LO is a robust zonal boundary criterion.

#### 9. Zone SPDZ9

Base definition: LO *Damassadinium crassimuratum*

Top definition: FCO *Enneadocysta multicornuta*

Type locality: ODP Site 1172

Base sample: 1172D-9R-1W, 105-107 cm (547.3 mbsf); 1171D-37R-CCW, 17-19 cm (593.56 mbsf)





Top sample: 1172D-6R-4W, 135-137 cm (522.55 mbsf); 1171D-33R-CCW, 0-2 cm (555.02 mbsf)

Calibration: the top of this zone is correlated to mid-to top Subchron C21n

Age: early Lutetian (47.9 Ma to 46.8 Ma)

Characteristic species: *Arachnodinium antarcticum*, *Deflandrea antarctica*, *Membranophoridium perforatum*, *Vozzhennikovia apertura*

Significant bioevents: FO *Enneadocysta multicornuta*

Remarks: The FO of *Enneadocysta multicornuta* is near the top of the previous zone, and subsequently increases in abundance. We prefer to use the FCO of this species as a zone definition rather than its first occurrence because that has a more robust FO compared to the FO.

#### 10. Zone SPDZ10

Base definition: FCO *Enneadocysta multicornuta*

Top definition: FCO *Enneadocysta dictyostila*

Type locality: ODP Site 1172

Base sample: 1172D-6R-4W, 38-40 cm (521.48 mbsf); 1171D-33R-3W, 10-12 cm (548.6 mbsf)

Top sample: 1172D-5R-3W, 54-56 cm (510.5 mbsf); 1171D-30R-CCW, 12-14 cm (524.58 mbsf)

Calibration: the top of this zone is correlated to early Subchron C20r

Age: mid- Lutetian (46.8 Ma to 45.8 Ma)

Characteristic species: *Enneadocysta multicornuta*, *Deflandrea convexa*

Significant bioevents: FO *Enneadocysta dictyostila*, LO *Membranophoridium perforatum*

Remarks: This zone and all overlying zones are characterized by monotypic assemblages of dinocysts, alternating by *Deflandrea antarctica*, *Enneadocysta multicornuta* and *E. dictyostila*. Because of the low diversity of the samples, few dinocyst events are recognized.

#### 11. Zone SPDZ11

Base definition: FCO *Enneadocysta dictyostila*

Top definition: FO *Impagidinium parvireticulatum*

Type locality: ODP Site 1172

Base sample: 1172D-5R-2W, 38-40 cm (508.88 mbsf); 1171D-28R-CCW, 5-7 cm (505.73 mbsf)

Top sample: 1172A-51X-4W, 85-87 cm (475.15 mbsf); 1171D-22R-CCW, 12-14 cm (448.84 mbsf)

Calibration: the top of this zone is correlated to the top of Subchron C20r

Age: mid-Lutetian (45.8 Ma to 42.8 Ma)

Characteristic species: *Enneadocysta dictyostila*, *Deflandrea antarctica*, *Eocladopyxis peniculata*, *Thalassiphora pelagica*

Significant bioevents: LCO *Deflandrea convexa*

Remarks: Similar to *Enneadocysta multicornuta*, *E. dictyostila* has a first occurrence in the underlying zone, followed by rapid increase in abundance. We hence prefer to use the FCO of *E. dictyostila* rather than its FO.



## 12. Zone SPDZ12

Base definition: FO *Impagidinium parvireticulatum*

Top definition: FO *Dracodinium rhomboideum*

Type locality: ODP Site 1172

Base sample: 1172A-51X-3W, 85-87 cm (473.65 mbsf); 1171D-22R-3W, 10-12 cm (442.7 mbsf)

Top sample: 1172A-45X-2W, 32-34 cm (414.02 mbsf); 1171D: not found

Calibration: the top of this zone is calibrated to the onset of Subchron C18n, also with use of isotope stratigraphy around the Middle Eocene Climatic Optimum

Age: mid-Lutetian to early Bartonian (42.8 Ma to 39.4 Ma)

Characteristic species: *Thalassiphora pelagica*, *Arachnodinium antarcticum*, *Deflandrea antarctica*, *Enneadocysta dictyostila*, *E. multicornuta*

Significant bioevents: LO *Cleistosphaeridium diversispinosum*

Remarks: The LO of *Dracodinium rhomboideum* is also calibrated to the onset of Magnetochron C18n in Northern Hemisphere sites (Eldrett and Harding 2009). That allows for correlation of the top of this zone to global dinocyst stratigraphies.

## 13. Zone SPDZ13

Base definition: FO *Dracodinium rhomboideum*

Top definition: FO *Alterbidinium distinctum*

Type locality: ODP Site 1172

Base sample: 1172A-45X-1W, 102-104 cm (413.22 mbsf); 1171D: not found

Top sample: 1172A-39X-7W, 45-47 cm (364.05 mbsf); 1171D-4R-2W, 55-57 cm (278.26 mbsf)

Calibration: the top of this zone is correlated to the onset of C16n.2n

Age: Bartonian-Priabonian (39.4 Ma to 36.3 Ma)

Characteristic species: *Spinidinium macmurdoense*, *Phthanoperidinium stockmansii*, *Vozzhennikovia apertura*, *Enneadocysta* spp., *Glaphyrocysta pastielsii*

Significant bioevents: FO *Deflandrea cygniformis*, FCO *Spinidinium macmurdoense*

Remarks: This zone is characterized by the first occurrence of several transantarctic floral elements with short ranges such as *Deflandrea cygniformis*.

## 5. Concluding remarks

The combined magneto-, isotope- and biostratigraphically calibrated sediment records from ODP Sites 1172 and 1171 in the Tasmanian sector and IODP Site U1356 from the Wilkes Land Margin, Antarctica now provide a solid framework for dinocyst stratigraphy in the Southern Ocean. It also portrays the evolution of Southern Ocean shelf settings from greenhouse to icehouse conditions. We here provide the calibrated ages for key dinocyst events based on the Geomagnetic Polarity Time Scale of Gradstein et al., (2004) in Table 2, as an update compared to those published earlier (Williams et al., 2004; Escutia et al., 2011). Antarctic-endemic as



## EARLY PALEOGENE DINOCYST ZONATION

well as cosmopolitan species are included, and an error is given for each datum. These errors include those caused by calibration uncertainties, sample spacing and core recovery. Ongoing work on the late Eocene - early Oligocene should allow continuation of the dinocyst stratigraphy upwards. The result will be a proper tool for dating Paleogene sediments from marginal marine settings throughout the Southern Ocean.

Dinocyst species	South Pacific Ocean				Other Oceans				References
	FO	error	LO	error	FO	error	LO	error	
<i>Alterbidinium distinctum</i>	36.40	0.20							transantarctic flora
<i>Apectodinium hamamorphum</i>	58.50	0.20	48.60	0.20					
<i>Arachnodinium antarcticum</i>	48.60	0.20	36.00	0.30					transantarctic flora
<i>Charlesdowniea coleophrypta</i>	49.50	0.10							
<i>Charlesdowniea columna</i>	51.90	0.10			51.90	0.20	49.00	0.40	(Bujak and Mudge 1994)
<i>Charlesdowniea edwardsii</i>	49.00	0.10	48.40	0.10	51.60	0.20	47.20	0.20	(Bujak and Mudge 1994)
<i>Cleistosphaeridium diversispinosum</i>	49.50	0.20	38.50	0.30					
<i>Corrudinium regulare</i>	49.00	0.20							transantarctic flora
<i>Damassadinium crassimuratum</i>	49.50	0.10	48.40	0.10					
<i>Deflandrea antarctica</i>	57.60	0.30							transantarctic flora
<i>Deflandrea convexa</i>	57.60	0.30							transantarctic flora
<i>Dracodinium rhomboideum</i>	39.30	0.10			39.30	0.10			(Eldrett and Harding 2009)
<i>Dracodinium waipawaense</i> / <i>D. varielongitutum</i>	53.30	0.10	51.50	0.40	53.30	0.10	51.40	0.10	(Bujak and Mudge 1994)
<i>Elytrocysta brevis</i>	65.50	0.30	33.6	0.30					
<i>Enneadocysta dicyostila</i>	44.60	0.30	33.30	0.30					transantarctic flora
<i>Enneadocysta multicornuta</i>	47.80	0.20	35.20	0.20					
<i>Enneadocysta</i> sp. B	53.10	0.10	51.90	0.10					
<i>Eoaladiopsis penicillata</i>	47.20	0.10							
<i>Glyphrocysta intricata</i>	39.20	0.20	38.50	0.20					
<i>Glyphrocysta ordinata</i>	64.40	0.20	55.80	0.20					
<i>Histiocysta palla</i>	44.70	0.20							
<i>Homotryblum tasmaniense</i>	51.50	0.40	45.30	0.10					
<i>Hystrichokolpoma bullatum</i>	51.00	0.20	48.30	0.20					
<i>Hystrichokolpoma rigaudiae</i>	53.80	0.20							
<i>Hystrichokolpoma spinosum</i>	51.00	0.20							
<i>Hystrichokolpoma truncatum</i>	51.00	0.20	45.30	0.20					
<i>Hystrichostrogylon membraniphorum</i>	50.00	0.20							
<i>Impagidinium cassiculum</i>	53.90	0.10	53.40	0.10					
<i>Impagidinium parvireticulatum</i>	43.70	0.20	35.50	0.10					
<i>Kisselevia insolens</i>	51.90	0.20							
<i>Lingulodinium machaerophorum</i>	57.20	0.20							
<i>Lophocysta</i> spp.	40.40	0.10	38.50	0.20					
<i>Membranophoridium perforatum</i>	53.50	0.20	45.10	0.20					
<i>Nematosphaeropsis labyrinthus</i>	49.40	0.20							
<i>Octodinium askinia</i>	53.80	0.10							transantarctic flora
<i>Palaeocystodinium golzowense</i>			51.10	0.20					
<i>Palaeoperidinium pyrrophorum</i>	68.20	0.30	58.50	0.20	73.60	0.10	58.80	0.10	(Bujak and Mudge 1994)
<i>Phthanoperidinium comatum</i>	45.30	0.20							
<i>Phthanoperidinium stockmansii</i>	56.70	0.20							
<i>Polysphaeridium subtle</i>	59.00	0.30	38.50	0.30					
<i>Samlandia delicata</i>	54.20	0.20	48.40	0.30					
<i>Schematophara obscura</i>	53.60	0.10	51.90	0.10					
<i>Selenopemphix</i> spp.	43.50	3.00							
<i>Spinidinium macmurdoense</i>	55.50	0.20							transantarctic flora
<i>Spinidinium schellenbergii</i>	62.10	0.20							transantarctic flora
<i>Spiniferites</i> sp. B Brinkhuis et al., 2003	62.50	0.20							
<i>Stoveracysta ornata</i>	35.20	0.20							
<i>Thalassiphora delicata</i>	62.50	0.20			58.90	0.10	38.40	0.10	(Bujak et al., 1980; Köthe 1990)
<i>Thalassiphora pelagica</i>	55.80	0.20							
<i>Vozzhennikovia apertura</i>	65.10	0.40							transantarctic flora
<i>Vozzhennikovia cf. roehllae</i>	53.50	0.20							transantarctic flora
<i>Vozzhennikovia stickleyae</i>	53.80	0.10							transantarctic flora
<i>Wetzelhella articulata</i>	51.50	0.50	51.40	0.50					
<i>Wetzelhella samlandica</i>	52.30	0.10	51.80	0.10					
<i>Wilsonidium echinosuturatum</i>	44.90	0.20	39.90	0.20					
<i>Wilsonidium ornatum</i>	50.40	0.20	49.70	0.20					

Table 2. Magnetostratigraphically calibrated ages of key dinocyst species in the Southern Ocean, compared to calibrations from other sections in the world. Ages are calibrated to the geomagnetic polarity time scale of Gradstein et al. (2004). The errors refer to age uncertainty caused by correlation error, core recovery issues and/or sample spacing.



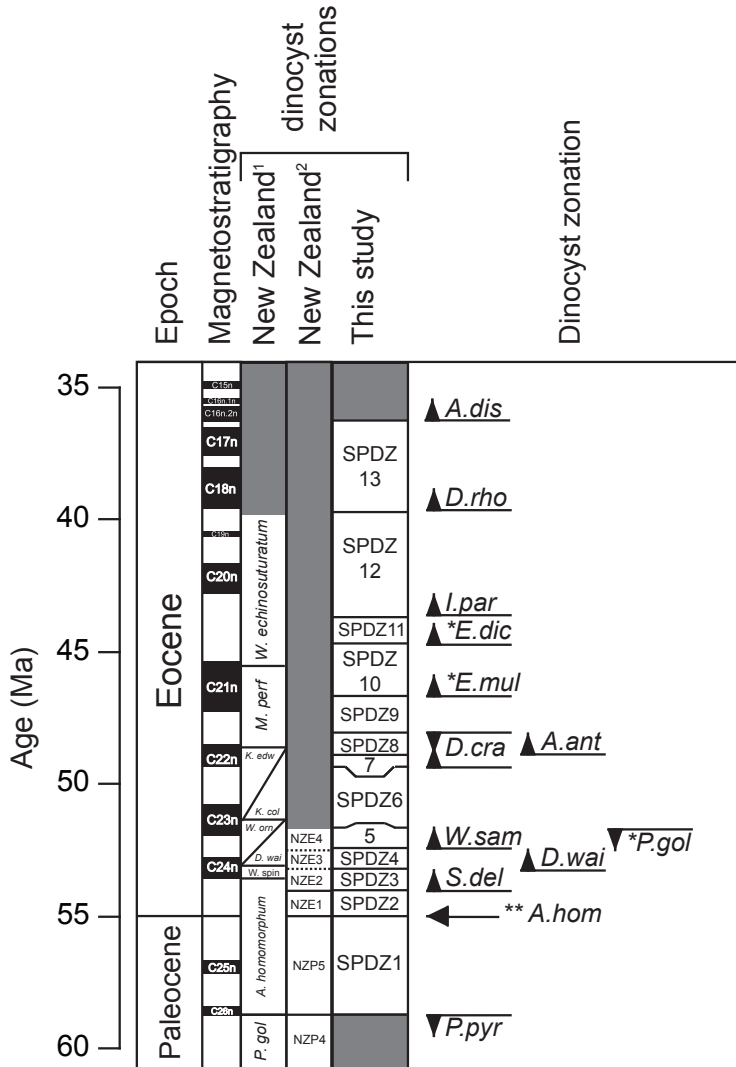


Figure 7. South Pacific dinocyst zonation scheme, with zonal definitions and Southern Ocean dinocyst events within the transantarctic flora. Also indicated are dinocyst zonations from Wilson (1988) (1) and Crouch and Brinkhuis (2005) (2). Abbreviations: *Palaeoperidinium pyrophorum* (*P.pyr*), *Apectodinium homomorphum* (*A.hom*; \*\* indicates acme), *Samlandia delicata* (*S.del*), *Dracodinium waipawaense/varielongitudum* (*D.wai*), *Wetzeliella samlandica* (*W.sam*), *Palaeocystodinium golzowense* (*P.gol*), *Damassadinium crassimuratum* (*D.cra*), *Arachnodinium antarcticum* (*A.ant*), *Enneadocysta multicornuta* (*E.mul*), *Enneadocysta dictyostila* (*E.dic*), *Impagidinium parvireticulatum* (*I.par*), *Dracodinium rhomboideum* (*D.rho*) and *Alterbidinium distinctum* (*A.dis*).



**Dinoflagellate cyst species list**

*Achilleodinium biformoides*

*Achomosphaera crassipellis*

*Achomosphaera alcicornu*

*Achomosphaera ramulifera* [Plate I; a]

*Adnatosphaeridium multispinosum*

*Adnatosphaeridium* sp. A [Plate I; b, c]

Remarks: this species of *Adnatosphaeridium* is characterized by having processes that are united by trabeculae connecting perforate distal platforms.

*Aiora fenestrata*

*Aireiana* spp.

*Alterbidinium acutulum* [Plate I; d]

*Alterbidinium distinctum*

*Apectodinium homomorphum* [Plate I; e, f, Plate VII; j]

*Apectodinium hyperacanthum* [Plate I; g, h, Plate VII; k]

*Apectodinium parvum*

*Apectodinium quinquelatum*

*Apteodinium australiense*

*Arachnodinium antarcticum* [Plate I; i, j]

*Areoligera senonensis*

*Areoligera sentosa*

*Areoligera* spp. [Plate I; k]

*Areosphaeridium arcuatum*

*Batiacasphaera cassicula* [Plate I; l]

*Brigantedinium* spp.

*Cannosphaeropsis* spp.

*Cassidium filosum*

*Cassidium fragile*

*Cerebrocysta bartonensis*

*Cerebrocysta delicata* comb. nov. [Plate I; m]



Remarks: Fensome et al. (2009) stated that the genus *Cerebrocysta* is “...very difficult to differentiate from *Pyxidinospis*, originally described by Habib (1976)”. Since the species assigned to *Pyxidinospis* can be divided into a Jurassic and Neocomian group and a Cenozoic group, and *Cerebrocysta* only occurs in the Cenozoic, they preferred to assign the Cenozoic species of *Pyxidinospis* to *Cerebrocysta*. In their paper, Fensome et al. (2009) only relocated *Pyxidinospis waipawaensis* to *Cerebrocysta*. In agreement with their emendation of *P. waipawaensis*, we hereby transfer the mid-Late Eocene *Pyxidinospis delicata* to *Cerebrocysta*.

*Cerebrocysta waipawaensis* comb. nov. [Plate I; n]

Remarks: this species has been assigned to *Cerebrocysta* following (Fensome et al., 2009). For explanation see remarks under *Cerebrocysta delicata*.

*Charlesdowniea clathrata*

*Charlesdowniea clathrata* [Plate I; o]

*Charlesdowniea coleothrypta* [Plate II; a, b]

*Charlesdowniea columna*

*Charlesdowniea edwardsii* [Plate II; c]

*Cleistosphaeridium diversispinosum* [Plate II; d]

*Cleistosphaeridium placacanthum*

*Cordosphaeridium fibrospinosum* [Plate II; e, Plate VII; l]

*Cordosphaeridium gracile*

*Cordosphaeridium minimum*

*Cordosphaeridium?* sp. A [Plate VII; m]

Remarks: this species is characterized by having, fibrous, sponge-like antapical processes, of which the antapical is elongate and slim. This species is tentatively assigned to *Cordosphaeridium*, and will be formally described elsewhere.

*Corrudinium incompositum*

*Corrudinium obscurum*

*Corrudinium regulare* (Clowes and Wilson 2006) [Plate II; f]

*Criproperidinium* sp. A [Plate II; g]

Remarks: this species of *Criproperidinium* is characterized by having a dark, thick shagreenate to scabrate wall.

*Criproperidinium* spp.

*Damassadinium crassimuratum* [Plate II; h, i]

*Dapsilidinium pastielsii*

*Deflandrea antarctica* [Plate II; j]

*Deflandrea convexa* [Plate III; k]

*Deflandrea cygniformis*



*Deflandrea phosphoritica*

*Deflandrea* sp. A (Brinkhuis et al., 2003a)

*Diphyes colligerum* [Plate II; l]

*Distatodinium paradoxum*

*Dracodinium rhomboideum*

*Dracodinium varielongitudum* [Plate II; m]

*Dracodinium waipawaense* [Plate II; n]

*Eisenackia circumtabulata* [Plate II; o]

*Eisenackia reticulata*

*Elytrocysta brevis* [Plate III; a, Plate VII; n]

*Enneadocysta brevistila*

*Enneadocysta dictyostila* [Plate III; b, c]

*Enneadocysta multicornuta* [Plate III; d]

*Enneadocysta pectiniformis*

*Enneadocysta* sp. A (Brinkhuis et al., 2003a)

Remarks: this species resembles *Enneadocysta dictyostila*, with the exception of the two, rather than one antapical processes that are distally connected into a perforate platform (see Brinkhuis et al., 2003a).

*Enneadocysta* sp. B [Plate III; e, f]

Remarks: This species resembles *E. multicornuta*, but differs in having bifurcations on many larger processes mid-way the process. The stratigraphic occurrence of this species (Magnetochron C24) is also much older than that reported for *E. multicornuta* (Magnetochron C21).

*Eocladopyxis peniculata* [Plate III; g]

*Eocladopyxis?* sp. A [Plate III; h, i]

Remarks: This dinocyst is questionably assigned to *Eocladopyxis*. The archeopyle seems to involve the apical plates and occasionally the precingular plates as well. It has a coarsely perforate surface, but lacks the processes typical for *E. peniculata*.

*Fibrocysta bipolaris*

*Florentinia reichartii* (Sluijs and Brinkhuis 2009)

*Gelatia inflata*

*Glaphyrocysta delicata* [Plate III; j]

*Glaphyrocysta divaricata*

*Glaphyrocysta exuberans*

*Glaphyrocysta ordinata*



*Glaphyrocysta pastielsii* [Plate III; k]  
*Glaphyrocysta retiintexta*

*Hafniasphaera septata*

*Hemiplaciphora semilunifera*

*Heteraulacacysta porosa*  
*Histiocysta palla* [Plate III; l]

*Homotryblium tasmaniense* [Plate III; m, n]

*Hystrichokolpoma bullatum* [Plate III; o, Plate IV; a]  
*Hystrichokolpoma pusillum*  
*Hystrichokolpoma rigaudiae* [Plate IV; b]  
*Hystrichokolpoma salacia*  
*Hystrichokolpoma spinosum*  
*Hystrichokolpoma truncatum* [Plate IV; c]

*Hystrichosphaeridium truswelliae* [Plate IV; d, Plate VII; o]  
*Hystrichosphaeridium tubiferum* [Plate IV; e]

Remarks: *Hystrichosphaeridium truswelliae* is distinguished *H. tubiferum* in having hollow open infundibular processes that forms distally fenestrate, edged platforms, whereas the processes of *H. tubiferum* are tubiform. Occasionally, poor preservation of the distal ends of the processes compromises proper speciation.

*Hystrichosphaeropsis* spp.

*Hystrichostrogylon membraniphorum* [Plate IV; f]

*Impagidinium aculeatum*  
*Impagidinium cassiculum* [Plate IV; g]  
*Impagidinium crassimuratum*  
*Impagidinium dispertitum*  
*Impagidinium maculatum* [Plate IV; h, Plate VIII; a]  
*Impagidinium paradoxum*  
*Impagidinium parvireticulatum* [Plate IV; i]  
*Impagidinium victorianum*

*Kisselevia insolens* [Plate IV; j; Plate VIII; b]  
*Kisselevia ornata* [Plate IV; k]  
*Kisselevia* sp. A [Plate IV; l; Plate VIII; c]

Remarks: This species consists of 2 layers, which assigns it to *Kisselevia* rather than *Charlesdowniea* (following concepts of Lentin and Vozzhennikova (1989)). However, some features, such as the perforate platforms supported





## EARLY PALEOGENE DINOCYST ZONATION

by short processes, are characteristic of *Charlesdowniea*. The absence of a spherical endocyst assigns this species to *Kisselevia*.

*Lejeunecysta hyalina*

*Lingulodinium machaerophorum*

*Lophocysta* spp.

*Mavinia esutiana* (Houben et al., 2011)

*Melitasphaeridium pseudorecurvatum*

*Membranophoridium perforatum* [Plate IV; m, n]

*Nematosphaeropsis labyrinthus*

*Ochetodinium* spp.

*Octodinium askiniae* [Plate V; a]

*Oligosphaeridium* spp.

*Operculodinium centrocarpum*

*Palaeocystodinium golzowense* [Plate V; b]

*Palaeoperidinium pyrophorum* [Plate V; c, d]

*Paucisphaeridium inversibuccinum*

*Paucisphaeridium* spp. (pars.) [Plate IV; o, Plate V; e, f, late VIII; d, e]

Remarks: several new species of *Paucisphaeridium* are identified at this site, but these will be formally described elsewhere.

*Pentadinium laticinctum* [Plate V; g]

*Phthanoperidinium alectrolophum* [Plate V; h]

*Phthanoperidinium comatum*

*Phthanoperidinium crenulatum*

*Phthanoperidinium stockmansii* [Plate V; i, j]

*Phthanoperidinium* sp. A (Goodman and Ford 1983)

*Phthanoperidinium* sp. B (Goodman and Ford 1983)

*Polysphaeridium subtile* [Plate V; k]

*Reticulatosphaera acticoronata*



*Rhombodinium subtile* [Plate V; l]  
*Rhombodinium draco*

*Samlandia delicata* [Plate V; m]  
*Samlandia septata* [Plate VI; a]  
*Samlandia chlamidophora*

*Schematophora obscura* [Plate VI; b, c]  
*Schematophora speciosa*

*Selenopemphix armata*  
*Selenopemphix nephroides*

*Senegalinium* spp. (pars.) [Plate VI; d, e, f, Plate VIII, f, g, h]

*Spinidinium luciae*  
*Spinidinium macmurdoense* [Plate VI; g, Plate VIII; i]  
*Spinidinium schellenbergii* (Sluijs et al., 2009b) [Plate VI; h, i, Plate VIII; j, k]

*Spiniferites pseudofurcatus*  
*Spiniferites ramosus*  
*Spiniferites* sp. B (Brinkhuis et al., 2003a) [Plate VI; j]

*Stoveracysta kakanuiensis*  
*Stoveracysta ornata*

*Tectatodinium pellitum* [Plate VI; k]

*Thalassiphora delicata*  
*Thalassiphora pelagica* [Plate VI; l]

*Turbiosphaera filosa*  
*Turbiosphaera galeata*  
*Turbiosphaera sagena* (Levy and Harwood 2000)

*Vozzhennikovia apertura* [Plate VI; m, n]  
*Vozzhennikovia netrona* (Levy and Harwood 2000)  
*Vozzhennikovia* cf. *roehliae* (Sluijs et al., 2009b) [Plate VI; o, Plate VII; a]

Remarks: this species of *Vozzhennikovia* occurs in Subchron C24n, and shows morphological resemblances to *V. roehliae*. Ornamentation (in the form hollow verrucae) is faintly visible, and the cingulum is slightly indent. However, the outline of the cyst is more rounded compared to *V. roehliae* with no apical or antapical horns. While *V. roehliae* has a consistent 3I archeopyle, the archeopyle of this species is consistent 2a, and the operculum is consistently adnate to 4".

*Vozzhennikovia stickleyae* (Sluijs et al., 2009b) [Plate VII; b]



## EARLY PALEOGENE DINO CYST ZONATION

*Wetzeliella articulata* [Plate VII; c]

*Wetzeliella astra*

*Wetzeliella samlandica* [Plate VII; d, e, Plate VIII; l, m]

*Wilsonidium echinosuturatum* [Plate VII; f]

*Wilsonidium ornatum* [Plate VII; g]

*Ynezidinium waipawaense*

Dinocyst gen. et sp. indet. [Plate VII; h, i; Plate VIII; n, o]

Remarks: this dinocyst species is spherical in polar view, with a clear edged apical archaeopyle. The offset sulcal nodge and occasionally large antapical bulge clearly indicates dorso-ventrally compression. Based on these observations, this species belongs to the *Areoligera* genus. Species within *Areoligera* spp. are characterized by processes or process complexes indicating para-tabulation. The outer wall of this species however is finely rugulate with no expression of para-tabulation.



**Dinocyst plates**

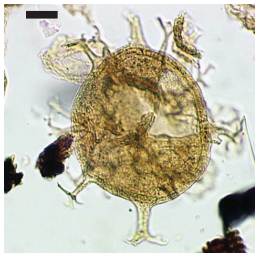


## EARLY PALEOGENE DINOCYST ZONATION

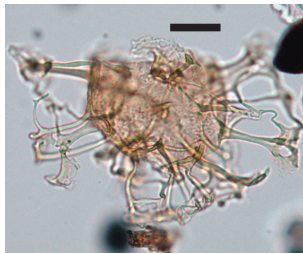
Plate I. a: *Achomospaera ramulifera* 1172D-11R-1W, 113-115 cm b: *Adnatosphaeridium* sp. U1356A-101R-1W, 10-12 cm c: *Adnatosphaeridium* sp. U1356A-101R-1W, 10-12 cm d: *Alterbidinium acutululum* 1172D-10R-2W, 10-12 cm e: *Apectodinium homomorphum* 1172D-13R-3W, 135-137 cm f: *Apectodinium homomorphum* U1356A-103R-4W, 20-22 cm g: *Apectodinium hyperacanthum* 1172D-15R-5W, 100-102 cm h: *Apectodinium hyperacanthum* 1172D-15R-5W, 100-102 cm i: *Arachnodinium antarcticum* 1172D-7R-6W, 135-137 cm j: *Arachnodinium antarcticum* U1356A-97R-1W, 60-63 cm k: *Areoligera* sp. 1172D-14R-1W, 55-57 cm l: *Batiacasphaera* sp. 1172D-12R-4W, 10-12 cm m: *Cerebrocysta delicata* 1172D-5R-3W, 38-40 cm n: *Cerebrocysta waipawaensis* 1172D-11R-3W, 135-137 cm o: *Charlesdowniea clathrata* U1356A- 101R-1W, 10-12 cm.

Scale bar = 25 micrometer ( $\mu\text{m}$ )

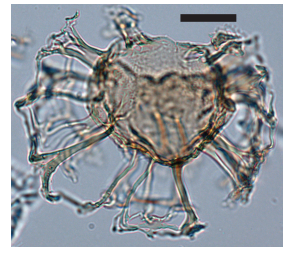




a



b



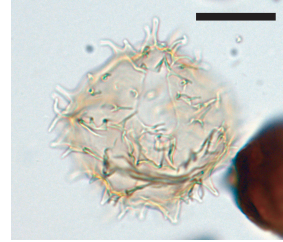
c



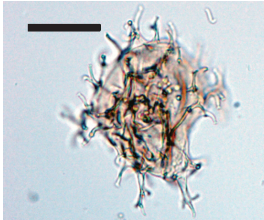
d



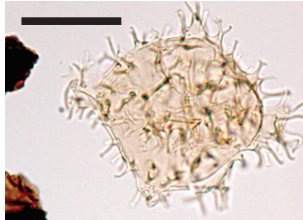
e



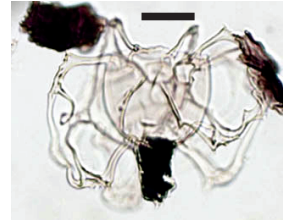
f



g



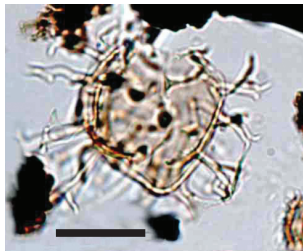
h



i



j



k



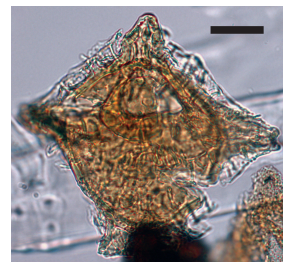
l



m



n



o

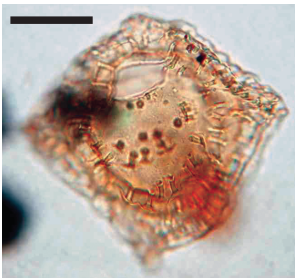


Plate II. a: *Charlesdowniea coleothrypta* 1172D-11R-5W, 40-42 cm b: *Charlesdowniea coleothrypta* U1356A-98R-5W, 0-3 cm c: *Charlesdowniea edwardsii* 1172D-11R-1W, 111-113 cm d: *Cleistosphaeridium diversispinosum* 1172D-11R-2W, 10-12 cm e: *Cordosphaeridium fibrospinosum* 1172D-15R-5W, 100-102 cm f: *Corrudinium regulare* 1172A-42X-1W, 85-87 cm g: *Cribroperidinium* sp. A U1356A-105R-6W, 95-98 cm h: *Damassadinium crassimuratum* 1172D-11R-6W, 40-42 cm i: *Damassadinium crassimuratum* 1172D-10R-2W, 10-12 cm j: *Deflandrea antarctica* 1172D-12R-1W, 10-12 cm k: *Deflandrea convexa* 1172D-5R-1W, 40-42 cm l: *Diphyes colligerum* 1172D-13R-2W, 90-92 cm m: *Dracodinium varielongitudum* U1356A-104R-2W, 120-122 cm n: *Dracodinium waipawaense* 1172D-12R-7W, 10-12 cm o: *Eisenackia circumtabulata* U1356A-105R-4W, 0-2 cm.

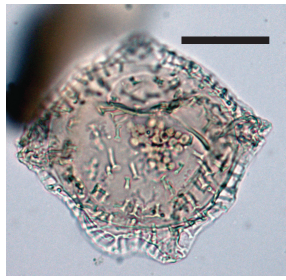
Scale bar = 25  $\mu$ m







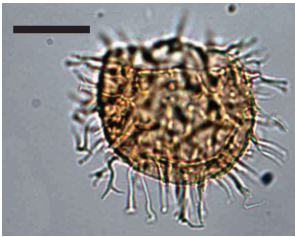
a



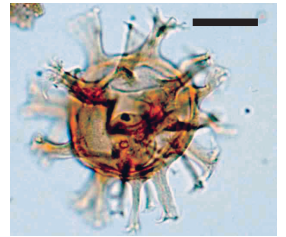
b



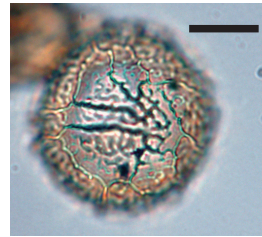
c



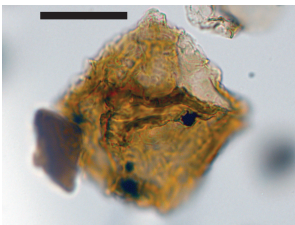
d



e



f



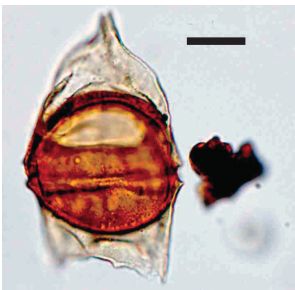
g



h



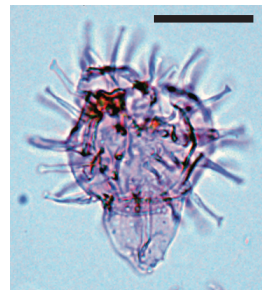
i



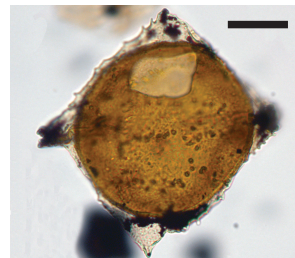
j



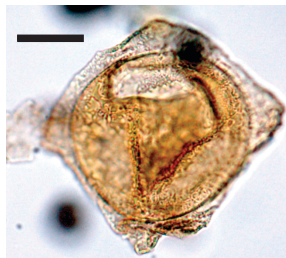
k



l



m



n



o

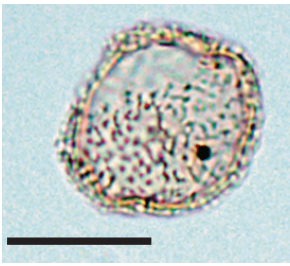




Plate III. a: *Elytrocysta brevis* 1172D-14R-5W, 10-12 cm b: *Enneadocysta dictyostila* 1172D-5R-3W, 38-40 cm c: *Enneadocysta dictyostila* 1172D-5R-1W, 40-42 cm d: *Enneadocysta multicornuta* 1172D-13R-3W, 105-107 cm e: *Enneadocysta* sp. B U1356A-102R-1W, 10-12 cm f: *Enneadocysta* sp. B U1356A-103R-2W, 40-42 cm g: *Eocladopyxis peniculata* 1172D-5R-4W, 38-40 cm h: *Eocladopyxis* sp. A U1356A-101R-1W, 60-62 cm i: *Eocladopyxis* sp. A U1356A-101R-1W, 60-62 cm j: *Glaphyrocysta delicata* 1172D-12R-7W, 10-12 cm k: *Glaphyrocysta pastielsii* U1356A-99R-2W, 40-43 cm l: *Histiocysta palla* U1356A-100R-1W, 10-13 cm m: *Homotryblum tasmaniense* 1172D-10R-2W, 10-12 cm n: *Homotryblum tasmaniense* U1356A-101R-1W, 60-63 cm o: *Hystrichokolpoma bullatum* 1172D-12R-2W, 10-12 cm.

Scale bar = 25  $\mu$ m

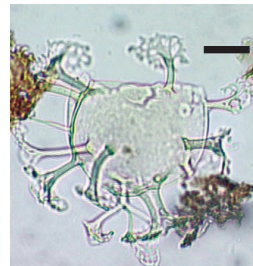




a



b



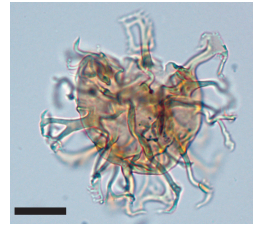
c



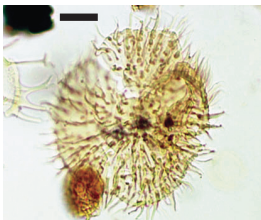
d



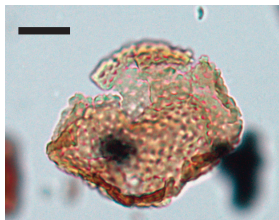
e



f



g



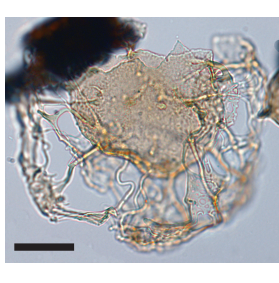
h



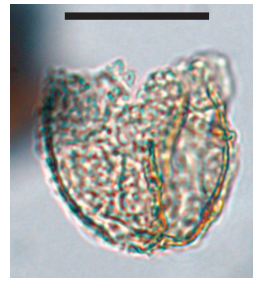
i



j



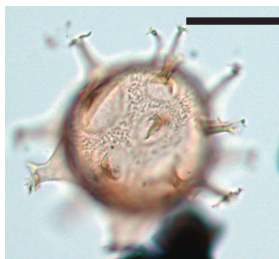
k



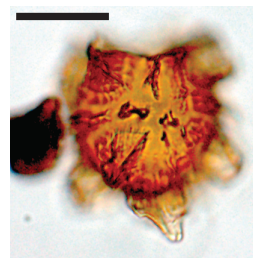
l



m



n



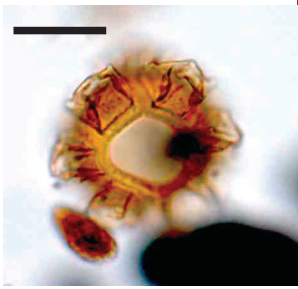
o



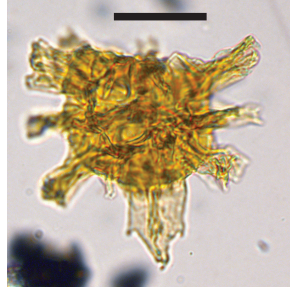
Plate IV. a: *Hystrichokolpoma bullatum* 1172D-12R-7W, 10-12 cm b: *Hystrichokolpoma rigaudiae* U1356A-103R-1W, 10-12 cm c: *Hystrichokolpoma truncatum* U1356A-98R-1W, 100-103 cm d: *Hystrichosphaeridium truswelliae* U1356A-101R-1W, 80-82 cm e: *Hystrichosphaeridium tubiferum* U1356A-98R-1W, 100-103 cm f: *Hystrichostogylon membraniphora* 1172D-11R-5W, 40-42 cm g: *Impagidinium cassiculum* U1356A-104R-2W, 40-42 cm h: *Impagidinium maculatum* 1172D-12R-2W, 10-12 cm i: *Impagidinium parvireticulatum* 1172D-10R-2W, 10-12 cm j: *Kisselovia insolens* 1172D-13R-2W, 90-92 cm k: *Kisselovia ornata* U1356A-101R-1W, 10-12 cm l: *Kisselovia* sp. A 1172D-13R-2W, 40-42 cm m: *Membranophoridium perforatum* 1172D-11R-6W, 104-106 cm n: *Membranophoridium perforatum* 1172D-12R-7W, 65-67 cm o: *Paucisphaeridium* sp. 1172D-14R-1W, 60-62 cm.

Scale bar = 25  $\mu$ m

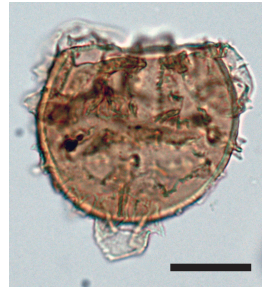




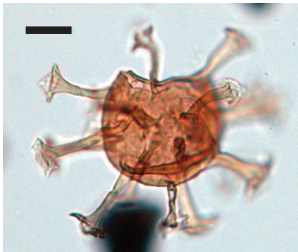
a



b



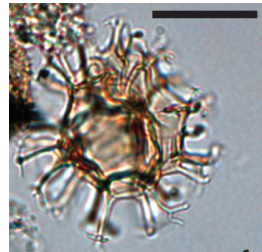
c



d



e



f



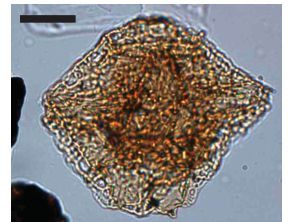
g



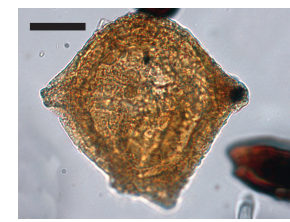
h



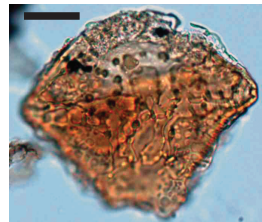
i



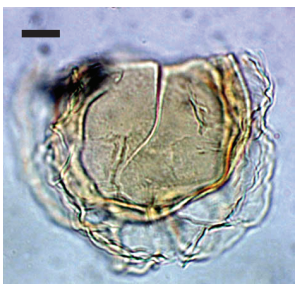
j



k



l



m



n



o



## EARLY PALEOGENE DINOCYST ZONATION

Plate V. a: *Octodinium askinae* 1172D-10R-2W, 10-12 cm b: *Palaeocystodinium golzowense* U1356A- 104R-1W, 50-52 cm c: *Palaeoperidinium pyrophorum* 1172D-24R-5W, 38-40 cm d: 1172D-24R-5W, 20-22 cm e: *Paucisphaeridium* sp. 1172D-14R-2W, 150-152 cm f: *Paucisphaeridium* sp. 1172D-14R-2W, 30-32 cm g: *Pentadinium laticinctum* U1356A-100R-1W, 10-13 cm h: *Phthanoperidinium alectrolohpum* U1356A-100R-1W, 104-107 cm i: *Phthanoperidinium stockmansii* 1172D-9R-6W, 40-42 cm j: *Phthanoperidinium stockmansii* 1172D-9R-6W, 40-42 cm k: *Polysphaeridium subtile* 1172D-12R-4W, 10-12 cm l: *Rhombodinium subtile* U1356A-105R-4W, 99-101 cm m: *Samlandia delicata* U1356A-100R-1W, 104-107 cm.

Scale bar = 25  $\mu$ m







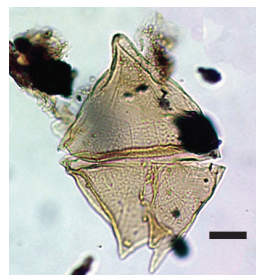
a



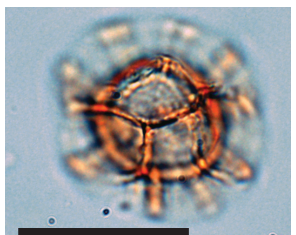
b



c



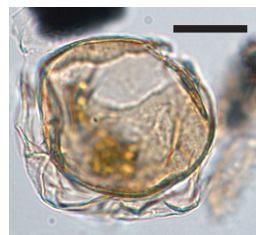
d



e



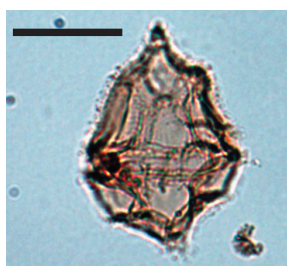
f



g



h



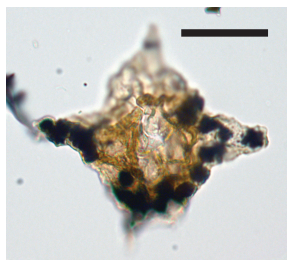
i



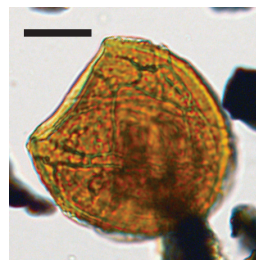
j



k



l



m

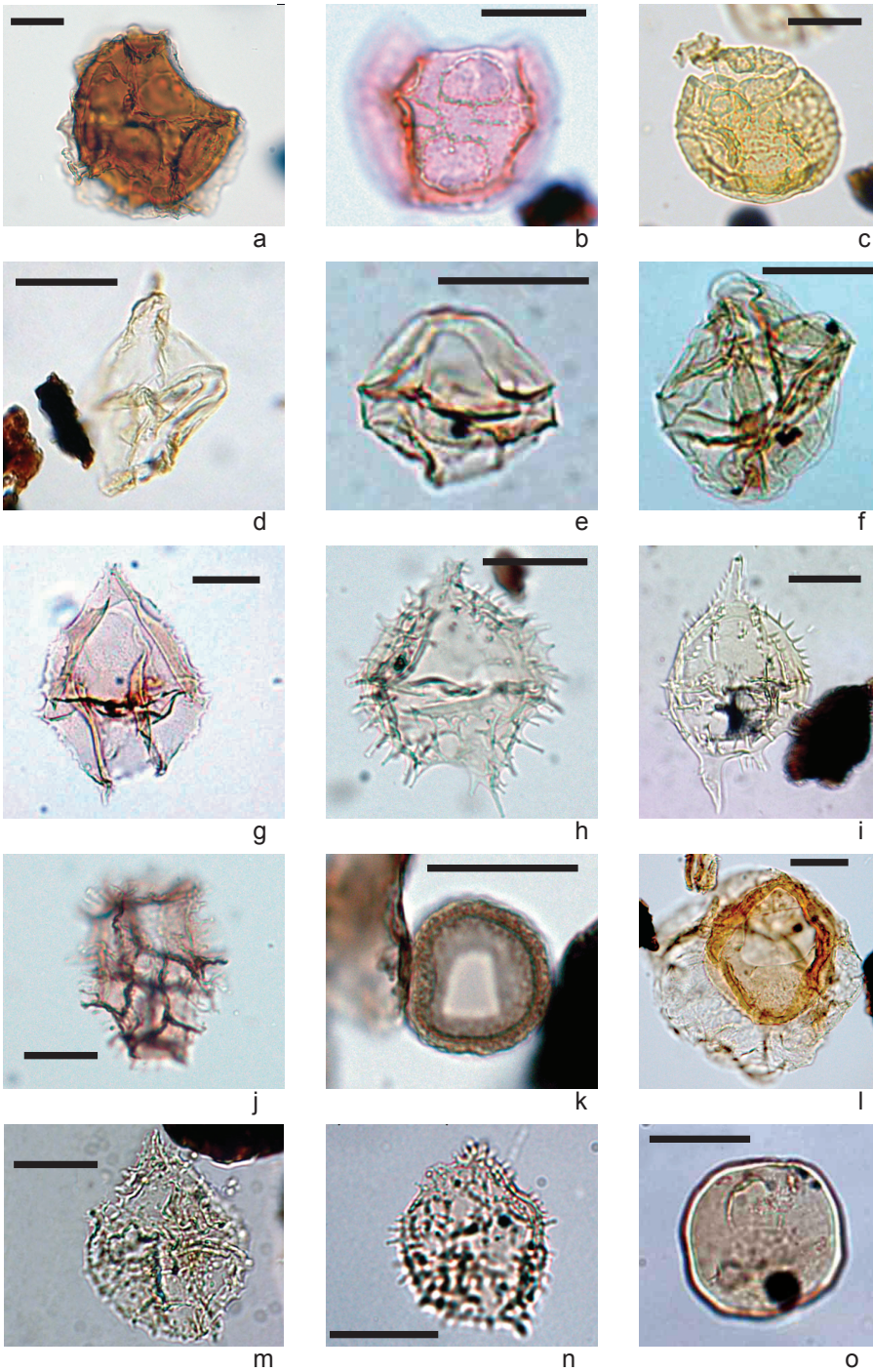


## EARLY PALEOGENE DINOCYST ZONATION

Plate VI. a: *Samlandia septata* U1356A-104R-6W, 70-72 cm b: *Schematophora obscura* 1172D-13R-3W, 105-107 cm c: *Schematophora obscura* U1356A-102R-1W, 30-32 cm d: *Senegalinium* sp. 1172D-15R-7W, 10-12 cm e: *Senegalinium* sp. 1172D-12R-4W, 10-12 cm f: *Senegalinium* sp. 1172D-15R-7W, 10-12 cm g: *Spinidinium macmurdoense* 1172D-13R-7W, 35-37 cm h: *Spinidinium schellenbergii* U1356A-98R-1W, 100-103 cm i: *Spinidinium schellenbergii* 1172D-6R-2W, 38-40 cm j: *Spiniferites* sp. B Brinkhuis et al., 2003 U1356A-101R-1W, 80-82 cm k: *Tectatodinium pellitum* U1356A-99R-2W, 0-3 cm l: *Thalassiphora pelagica* 1172D-12R-2W, 10-12 cm m: *Vozzhennikovia apertura* 1172D-18R-1W, 40-42 cm n: *Vozzhennikovia apertura* 1172D-14R-4W, 10-12 cm o: *Vozzhennikovia* cf. *roehliae* 1172D-13R-3W, 135-137 cm.

Scale bar = 25  $\mu$ m





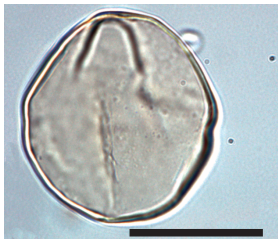


## EARLY PALEOGENE DINOCYST ZONATION

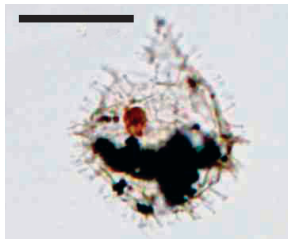
Plate VII. a: *Vozzhennikovia cf. roehliae* 1172D-13R-3W, 135-137 cm b: *Vozzhennikovia stickleyae* 1172D-14R-4W, 10-12 cm c: *Wetziella astra* 1172D-13R-1W, 40-42 cm d: *Wetziella samlandica* 1172D-13R-2W, 40-42 cm e: *Wetziella samlandica* 1172D-13R-2W, 40-42 cm f: *Wilsonidium echinosuturatum* 1172D-5R-4W, 38-40 cm g: *Wilsonidium ornatum* 1172D-12R-5W, 40-42 cm h, i: dinocyst gen. et sp. indet. U1356A-104R-6W, 70-72 cm j: *Apectodinium homomorphum* 1172D-15R-5W, 100-102 cm k: *Apectodinium homomorphum* 1172D-15R-5W, 100-102 cm l: *Cordosphaeridium fibrospinosum* 1172D-15R-5W, 10-12 cm m: *Cordosphaeridium* sp. A U1356A-103R-1W, 90-92 cm n: *Elytrocysta brevis* 1172D-14R-2W, 115-117 cm o: *Hystrichosphaeridium tubiferum* 1172D-15R-5W, 100-102 cm.

Scale bar = 25  $\mu$ m

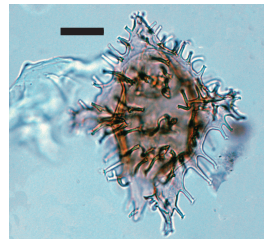




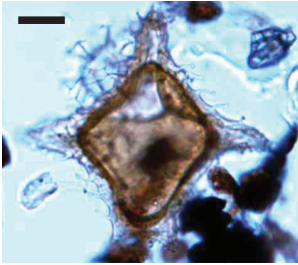
a



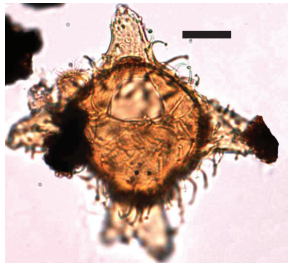
b



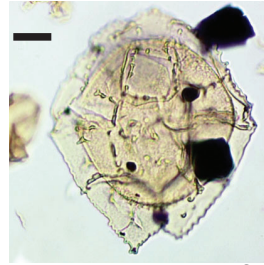
c



d



e



f



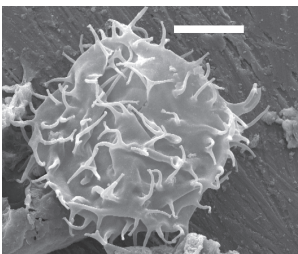
g



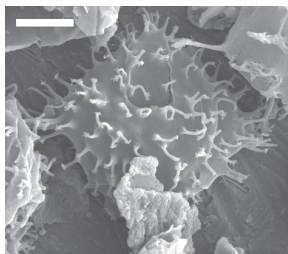
h



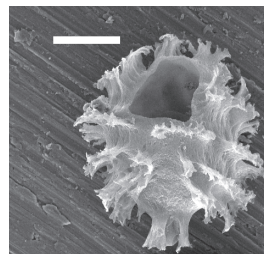
i



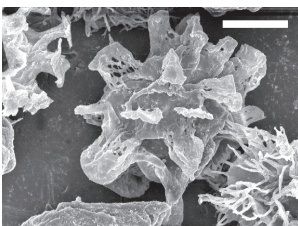
j



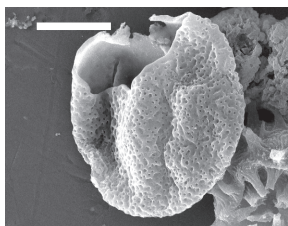
k



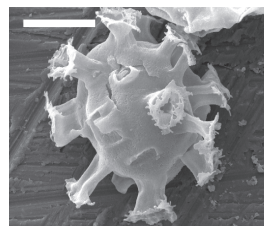
l



m



n



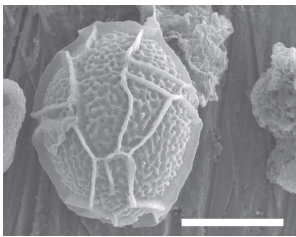
o



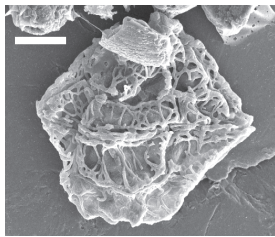
Plate VIII. a: *Impagidinium maculatum* 1172D-14R-4W, 10-12 cm b: *Kisselevia insolens* U1356A-101R-1W, 120-121 cm c: *Kisselevia* sp. A 1172D-13R-2W, 40-42 cm d: *Paucisphaeridium* sp. 1172D-14R-1W, 140-142 cm e: *Paucisphaeridium* sp. 1172D-14R-1W, 140-142 cm f: *Senegalinium* sp. 1172D-14R-4W, 10-12 cm g: *Senegalinium* sp. 1172D-14R-2W, 115-117 cm h: *Senegalinium* sp. 1172D-14R-2W, 115-117 cm i: *Spinidinium macmurdoense* 1172D-14R-4W, 10-12 cm j: *Vozzhennikovia apertura* 1172D-14R-1W, 10-12 cm k: *Vozzhennikovia apertura* 1172D-14R-1W, 10-12 cm l: *Wetzeliella samlandica* 1172D-13R-2W, 40-42 cm m: *Wetzeliella samlandica* 1172D-13R-2W, 40-42 cm n: dinocyst gen. et sp. indet. U1356A-105R-1W, 75-77 cm o: dinocyst gen. et sp. indet. U1356A-104R- 6W, 70-72 cm.

Scale bar = 25  $\mu$ m

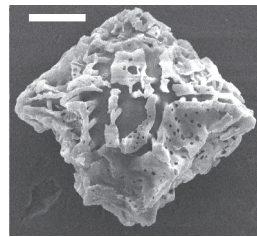




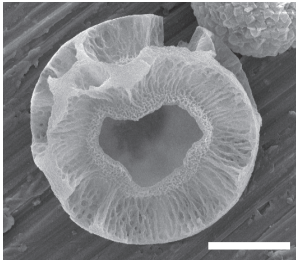
a



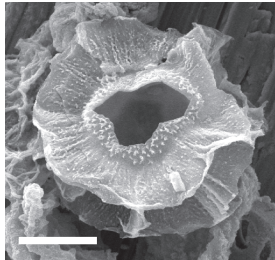
b



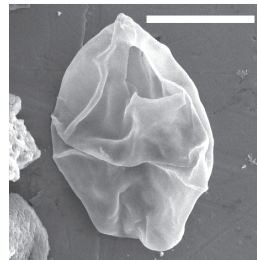
c



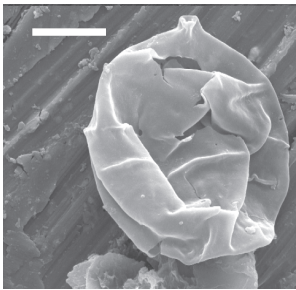
d



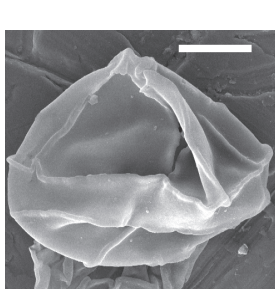
e



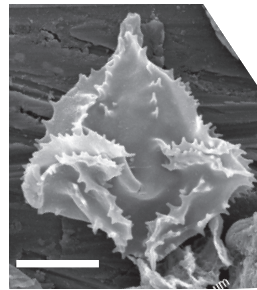
f



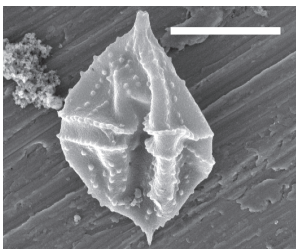
g



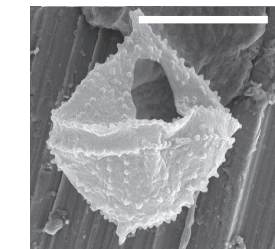
h



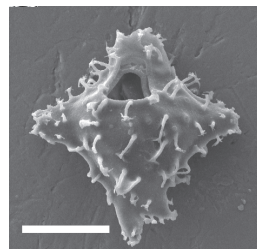
i



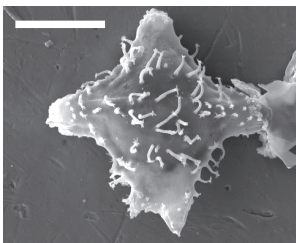
j



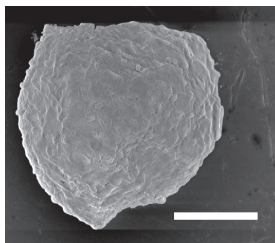
k



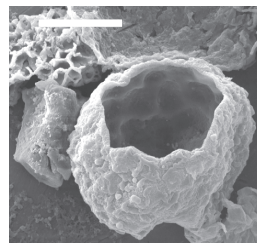
l



m



n



o









Relative to the present day, meridional temperature gradients in the early Eocene age (~56–53 million years ago (Ma)) were unusually low, with slightly warmer equatorial regions (Pearson et al., 2007) but with much warmer subtropical Arctic (Sluijs et al., 2006) and mid-latitude (Sluijs et al., 2007b) climates. By the end of the Eocene epoch (34 Ma), the first major Antarctic ice sheets had appeared (Barker et al., 2007; Zachos et al., 1992), suggesting that major cooling had taken place. Yet the global transition into this icehouse climate remains poorly constrained, as only a few temperature records are available portraying the Cenozoic climatic evolution of the high southern latitudes. Here we present a uniquely continuous and chronostratigraphically well-calibrated  $\text{TEX}_{86}$  record of sea surface temperature (SST) from an ocean sediment core in the East Tasman Plateau (paleolatitude  $\sim 65^\circ\text{S}$ ). We show that southwest Pacific SSTs rose above present-day tropical values (to  $34^\circ\text{C}$ ) during the early Eocene age (53 Ma) and had gradually decreased to about  $21^\circ\text{C}$  by the early late Eocene (36 Ma). Our results imply that there was almost no latitudinal SST gradient between sub-equatorial and sub-polar regions during the early Eocene ( $\sim 55$ –50 Ma). Thereafter, the latitudinal gradient markedly increased. In theory, if Eocene cooling was largely driven by a decrease in atmospheric greenhouse gas concentration (Zachos et al., 2008), additional processes are required to explain the relative stability of tropical SSTs given that there was more significant cooling at higher latitudes.





The Paleogene temperature evolution of the Antarctic margin, particularly the Pacific sector, is still poorly resolved. One difficulty with obtaining relevant records close to the Antarctic continent is the general absence of biogenic carbonate in most marine facies, which hampers traditional  $\delta^{18}\text{O}$  and/or Mg/Ca-based reconstructions of the subpolar temperature evolution. In the absence of biogenic carbonates, organic sea-surface-temperature proxies such as the tetraether index of lipids consisting of 86 carbon atoms ( $\text{TEX}_{86}$ ; Schouten et al., 2002) and the alkenone unsaturation index ( $\text{U}_{37}^{\text{K}}$ ; Müller, 1998) are required for reconstructing high-latitude climatic evolution (Liu et al., 2009; Sluijs et al., 2006).

We apply  $\text{TEX}_{86}$  and  $\text{U}_{37}^{\text{K}}$  on a stratigraphically continuous sedimentary section from the southwest Pacific Ocean, drilled by the Ocean Drilling Program (ODP) Leg 189 Site 1172, paleolatitude  $65^\circ\text{S}$  (Exon et al., 2004; Fig. 1). A full methodological description is available in the Supplements. The record contains an expanded succession of marginal marine sediments from the lower Paleocene epoch to the upper Eocene ( $\sim 64\text{--}36$  Ma), with tight chronostratigraphic control, including magnetostratigraphy (Stickley et al., 2004a; Supplements; Fig. S2). The presence of typical transantarctic organic-walled dinoflagellate cysts in the Tasmanian region indicates an Antarctic-derived northward-flowing Tasman Current throughout the Paleogene, which is verified by experiments based on a general circulation model (Huber et al., 2004; Fig. 1). This Antarctic influence at the East Tasman Plateau (ETP) persisted until at least the early late Eocene ( $\sim 35.5$  Ma), when deepening of the Tasmanian Gateway lead to a reorganization of the Tasman and proto-Leeuwin ocean currents (Stickley et al., 2004b).

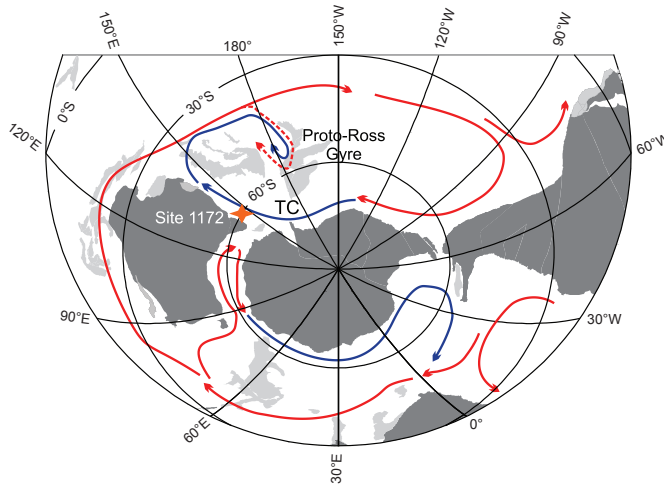


Figure 1. Paleogeographic reconstruction for the South Pacific Ocean at early–middle Eocene times. Surface circulation (Huber et al., 2004) indicates the Antarctic-derived Tasman Current (TC) over the East Tasman Plateau. Paleogeographic charts obtained from the Ocean Drilling Stratigraphic Network (ODSN); after Hay et al. (1999). The dashed red arrow around New Zealand indicates potential mixing of low-latitude surface waters (from the East Australian Current) with the TC.



According to the oldest part of the record, TEX<sub>86</sub>-derived SSTs at the ETP gradually decreased from ~25°C around 63 Ma to a minimum of ~20°C around 58 Ma (Fig. 2a). During the late Paleocene and early Eocene, Tasmanian SSTs gradually rose to tropical values of ~34°C during the early Eocene climatic optimum (EECO; Zachos et al., 2008), between 53 and 49 Ma (Fig. 2a). A gradual cooling trend throughout the middle Eocene (starting at the termination of the EECO ~49 Ma) arrived at temperatures of ~23°C 42 Ma, which is still relatively warm. Subsequently, an interruption of the cooling trend occurred at the middle Eocene climatic optimum (MECO; ~40 Ma; Bohaty and Zachos 2003), followed by a relatively rapid SST decrease to ~21°C in the early late Eocene (Fig. 2a). The late middle and late Eocene TEX<sub>86</sub>-based SSTs are supported by U<sub>37</sub><sup>K'</sup> SST estimates derived from the same samples (Supplements; Fig. S3). Both SST estimates also compare well with those for other late Eocene (Southern Ocean) sites (Liu et al., 2009). Unfortunately, sediments from the ETP older than the MECO did not contain alkenones for U<sub>37</sub><sup>K'</sup> SST reconstructions.

The middle Eocene SSTs correspond closely to those from sections in New Zealand (Burgess et al., 2008; Hollis et al., 2009), according to records based on TEX<sub>86</sub> (Fig. 2a), Mg/Ca and δ<sup>18</sup>O, indicating regional consistency of our reconstructed SSTs. Also, trends in our Tasmanian SST record are remarkably similar to those in the global stack of benthic foraminiferal oxygen isotopes (Zachos et al., 2008; Fig. 2b), which we updated and augmented with recently published data (Supplements). This correspondence between the two records (Supplements; Fig. S4) indicates that the regional SSTs co-varied with the SSTs where 'global' deep water was sourced. It has previously been suggested that the Southern Ocean was the main region of deep-water formation during the Paleogene (Thomas et al., 2003). In contrast, absolute SST estimates from the Tasmanian region are much higher than those inferred from the benthic foraminiferal oxygen isotopes (Fig. 2). Part of this discrepancy might be due to seasonality, with TEX<sub>86</sub> being slightly skewed towards summer temperatures and benthic foraminiferal δ<sup>18</sup>O towards winter temperatures (Supplements). Another possibility is that deep-water formation occurred in areas that were cooler than the Tasmanian sector.

Sea surface temperature reconstructions based on bivalve-shell oxygen isotopes from Seymour Island on the Antarctic shelf, for example, yield much lower SSTs (Ivany et al., 2008). It is possible that the Antarctic margin was more susceptible to winter cooling than the open ocean, or that portions of the coast along the Antarctic sector were somehow isolated from the southern edges of the Southern Ocean gyres. Another possibility is that the aragonite bivalve shells integrate temperature over a greater portion of the year. Regardless, the large SST difference between the Weddell Sea and the ETP would suggest a relatively steep gradient within a few degrees of latitude. Antarctica, being a polar continent, would most likely have experienced extremes in temperature, in particular having cool winters. Such conditions might have been recorded in the bivalves from the Weddell Sea but not in the more distal ETP. In turn, deep-water formation might have been restricted to the Antarctic shelf areas, such as the Weddell Sea.



EARLY PALEOGENE TEMPERATURE EVOLUTION

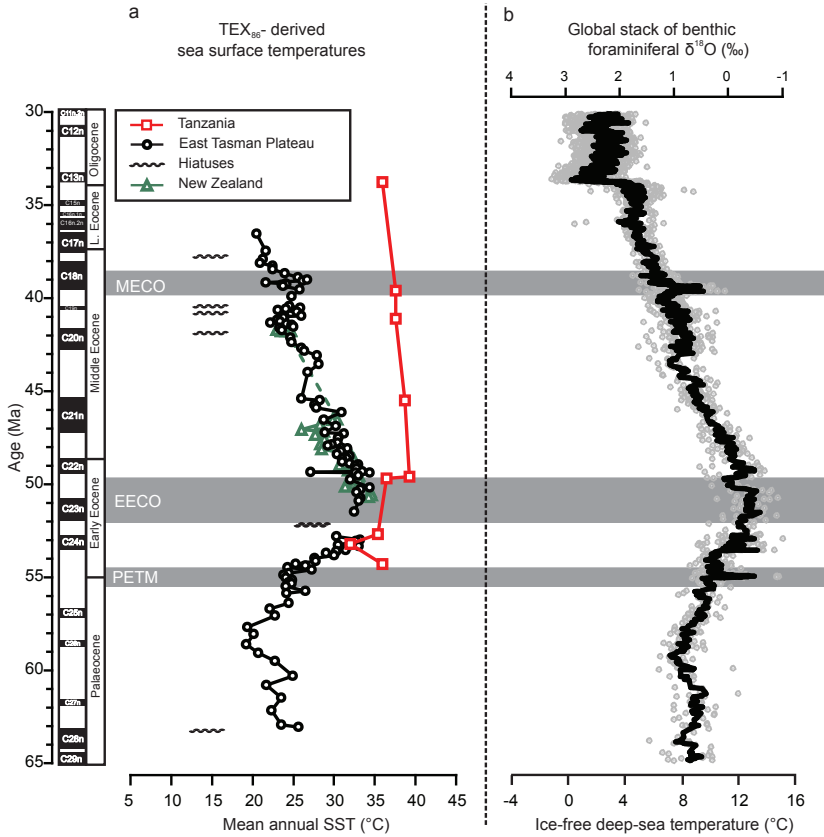


Figure 2. a,  $TEX_{86}$  SST reconstructions from ODP Site 1172, New Zealand (Burgess et al., 2008; Hollis et al., 2009) and Tanzania (Pearson et al., 2007) (all according to the same calibration; see Supplements). The black wiggly lines are short ( $\sim 100$  kyr; Röhl et al., 2004a) and longer hiatuses at Site 1172. b, Global stack of benthic foraminiferal oxygen isotopes (grey data; Supplements). The temperature scale assumes ice-free conditions ( $\delta^{18}O_{SMOW} = -1.2\%$ , where  $\delta^{18}O_{SMOW} = (^{18}O/^{16}O)_{sample} / (^{18}O/^{16}O)_{SMOW} - 1$ ; SMOW, standard mean ocean water), and indicates deep-sea temperatures. The black solid line reflects a five-point running average. PETM, Paleocene–Eocene thermal maximum; EECO, Early Eocene Climatic Optimum; MECO, Middle Eocene Climatic Optimum.

Planktonic foraminiferal  $\delta^{18}O$  analyses from equatorial regions previously indicated that Paleogene low-latitude SSTs were the same, or even lower, than those of today (Barron 1987), a problem that puzzled paleoclimate scientists for decades. The oxygen isotopic composition of planktonic foraminiferal tests in porous carbonate-rich pelagic facies were later found to be partially altered owing to recrystallization primarily during early diagenesis (Pearson et al., 2001; Schrag et al., 1995). In contrast, carbonate-poor and clay-rich facies typically found on the continental margins contain calcite shells without major diagenetic overprint (Pearson et al., 2007). For the Eocene, such well-preserved planktonic foraminifera indicate near equatorial SSTs that were greater than those of the present day, and



agree with  $\text{TEX}_{86}$ -derived SSTs (Pearson et al., 2001, 2007). Another observation from well-preserved foraminifera and  $\text{TEX}_{86}$  is that (sub-) equatorial SSTs were remarkably stable throughout the Eocene (Pearson et al., 2007; Fig. 2). Stable low-latitude SSTs concomitant with high-latitude Eocene cooling thus suggests that there were increasing SST gradients during the Eocene. Although SST trends are often reconstructed using multi-proxy studies, the difference in absolute SSTs between various proxy reconstructions can be considerably large (Hollis et al., 2009; Huber 2008; Liu et al., 2009), even when measured on the same sediments. Despite the fact that multi-proxy approaches are generally encouraged in paleoclimate studies, exclusion of such inter-proxy biases in latitudinal gradient reconstructions requires single-proxy SST records from around the world. Traditional calcite-based SST reconstructions are less suitable for this because calcite is only sparsely available in high-latitude sediments. The organic  $\text{TEX}_{86}$  and  $\text{U}_{37}^{\text{K}'}$  SST proxies, however, can be used independently of latitude and are, hence, suitable for single-proxy SST gradient reconstructions. Moreover, they do not require critical assumptions about ancient seawater chemistry, unlike  $\delta^{18}\text{O}$  and  $\text{Mg}/\text{Ca}$ .

We compiled Eocene  $\text{TEX}_{86}$  and  $\text{U}_{37}^{\text{K}'}$  SST reconstructions from a suite of sedimentary records from localities worldwide and noted increased middle Eocene latitudinal SST gradients in both hemispheres (Fig. 3), relative to the early Eocene. These SST gradients are in general agreement with those found for terrestrial mean annual temperatures, based on early–middle Eocene fossil leaves (Greenwood and Wing 1995). Adding the bivalve-based SST reconstructions from Seymour Island (Ivany et al., 2008) to our organic proxy data suggests a strong gradient between  $60^\circ$  and  $70^\circ\text{S}$ , which contrasts with the small gradient between  $60^\circ\text{S}$  and the equator (Fig. 3). A part of this large Southern Ocean SST gradient might be due to biases between organic and calcite proxies. A large part, however, may realistically reflect the influence of the cool Antarctic interior, which cooled the Antarctic shelf. In contrast to the continental South Pole, the Arctic region is an oceanic basin. Instead of amplifying the seasonal cycle, the Arctic Ocean probably moderated seasonal extremes in the northern high-latitude greenhouse. Hence, Paleogene latitudinal temperature gradients, like those of today, would have exhibited a high degree of asymmetry between the two hemispheres.

It has been suggested that the general warmth that characterized early Paleogene climates was forced by high atmospheric greenhouse gas concentrations (Zachos et al., 2008). Concomitantly, the absence of polar ice sheets eliminated ice-albedo feedbacks in the Paleogene greenhouse. The middle–late Eocene global cooling has been related to long-term atmospheric  $\text{CO}_2$  decline, eventually resulting in the onset of major Antarctic glaciation around the Eocene/Oligocene boundary (Zachos et al., 2008). Our results imply that meridional temperature gradients markedly increased together with deep-sea cooling (Fig. 2; Zachos et al., 2008). Although high-latitudes cooled, tropical temperatures seem to have remained fairly stable throughout the Eocene (Fig. 3; Pearson et al., 2007). This observation raises questions concerning the precise role of decreasing atmospheric greenhouse gas concentrations in cooling the Eocene poles, as in theory (Huber and Sloan 2001) they should have cooled tropical regions as well. The role of potential high-latitude climate feedbacks



involving, for example, differences in cloud/water vapour distribution (Abbot and Tziperman 2008) might have been much more instrumental in the middle Eocene climatic deterioration than previously thought. Another potential positive-feedback mechanism for high-latitude cooling would be ice–albedo feedback. However, the presence of substantial middle Eocene continental ice is still equivocal given the general warmth and overall absence of conclusive physical evidence.

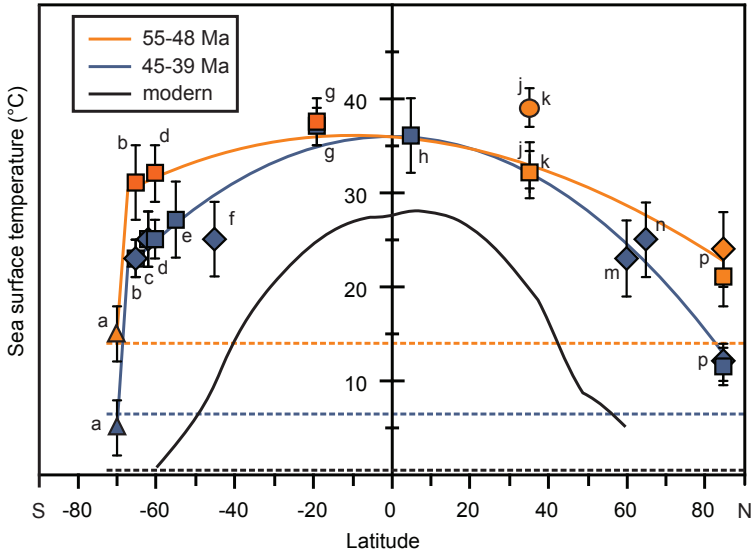


Figure 3. Bivalve-shell  $\delta^{18}O$  (triangles),  $TEX_{86}$  (squares) and  $U_{37}^{K'}$  (diamonds) SST reconstructions for the early (orange) and mid-middle (blue) Eocene. Data are from Seymour Island (Ivany et al., 2008) (a), the East Tasman Plateau (b), Deep Sea Drilling Project (DSDP) Site 277 (Liu et al., 2009) (c), New Zealand (Burgess et al., 2008; Hollis et al., 2009) (d), DSDP Site 511 (Liu et al., 2009) (e), ODP Site 1090 (Liu et al., 2009) (f), Tanzania (Pearson et al., 2007) (g), ODP Site 925 (Liu et al., 2009) (h), New Jersey (Sluijs et al., 2007b) (j, k; circle represents peak PETM SSTs (Sluijs et al., 2007b)), ODP Site 336 (Liu et al., 2009) (m), ODP Site 913 (Liu et al., 2009) (n) and the Arctic Ocean (Sangiorgi et al., 2008; Sluijs et al., 2006; Weller and Stein 2008) (p) (Supplements; Fig. S1). Error bars indicate the range of variation. Gradients represent second-order polynomials, excluding bivalve-shell data. Black and dashed lines represent the present-day zonally averaged latitudinal temperature gradient (Shea et al., 1992) and age-specific deep-sea temperatures, respectively (Fig. 2b; Zachos et al., 2008).



## Supplements to Chapter 2

### 1. Site description, lithology and depositional setting

The East Tasman Plateau (ETP) is located at 45° Southern latitude (Slat.), in the Southwest Pacific. ODP Site 1172 is situated on the flat western side of the (now) submerged ETP, at ~2620 m water depth (Exon et al., 2001). Paleogene sediments were drilled in two holes, 1172A and D, which penetrated ~766 meters of Quaternary to upper Maastrichtian sediments (Stickley et al., 2004a). Paleogene sediments at ODP Site 1172 are olive grey, with some variations to greyish brown and to greenish grey, with abundant bioturbation. Late Paleocene and early Eocene sediments are darker grey, and turn lighter further up section. In the studied section, carbonate content in the sediments is minimal (Exon et al., 2001; Röhl et al., 2004a).

During the early Paleogene, the ETP was at 65°Slat., much closer to Antarctica than it is today (Fig. S1a; Exon et al., 2004). Northward rifting of the ETP (including the Australian continent) started close to the middle- late Eocene boundary (~35.5 Ma) with deepening of the Tasmanian Gateway (Stickley et al., 2004b) and this caused submersion of the ETP. Tectonic movements of the ETP prior to the latest Eocene were confined to slight eastward rifting from the Tasmanian continent (Exon et al., 2004). Prior to the submersion of the ETP, the depositional setting at ODP Site 1172 is interpreted as a shallow marine, tranquil shelf (Exon et al., 2004). During the upper middle Eocene, orbitally forced climatic cycles superimposed on third order sea level changes were identified in ETP sediments (Röhl et al., 2004a). These sea level cycles caused hiatuses in the record (Röhl et al., 2004a), correlated to sea level low stands. It is unknown whether these sea level cycles also influenced the ETP paleo-environments prior to 43 Ma. However, the complete magnetic profile (Stickley et al., 2004a) indicates that hiatuses are relatively small (~100kyr). Microfossil analyses in combination with surface-ocean General Circulation Models (GCMs) indicate that the ETP is under influence of northward flowing surface currents (Huber et al., 2004), bringing Antarctic- derived surface waters over the ETP (Fig. S1b). Therefore, the recorded climate signal at ODP Site 1172 is at least in part Antarctic-derived.

### 2. Revised age model of ODP Leg 189 Site 1172

For the age model, tie points are based solely on magnetic reversals and PETM isotope events (Bijl et al., 2007). The depths of the magnetic reversals were obtained from Fuller and Touchard (2004) and Stickley et al. (2004a). High-resolution organic walled dinoflagellate cyst (dinocyst) chronology comparison between ODP Site 1172 and Site 1171 resulted in the identification of a hiatus spanning from mid-Subchron C24n to mid- Subchron C23n, which resulted in a revision of the published magnetostratigraphy for ODP Site 1172 (Fuller and Touchard 2004). The PETM was previously interpreted to be missing from the record (Röhl et al., 2004b), however we identified the PETM slightly further up section (Bijl et al., 2007; Chapter 4). The identification of the PETM led to a revised interpretation of the paleomagnetic data of Fuller and Touchard (2004). All these re-interpretations resulted in an adapted age



## EARLY PALEOGENE TEMPERATURE EVOLUTION

model for ODP Site 1172 (Table S1 and Fig. S2). To line the deep sea oxygen isotope data up with the data of Site 1172, the onset of the PETM in the deep sea oxygen isotope data was set at 55 Ma, although an older age of the PETM had recently been suggested (Westerhold et al., 2007). Ages for the magnetic reversals were derived from the Gradstein et al. timescale (2004), except for the Subchrons C24n and C25n, which were from Westerhold et al. (2007).

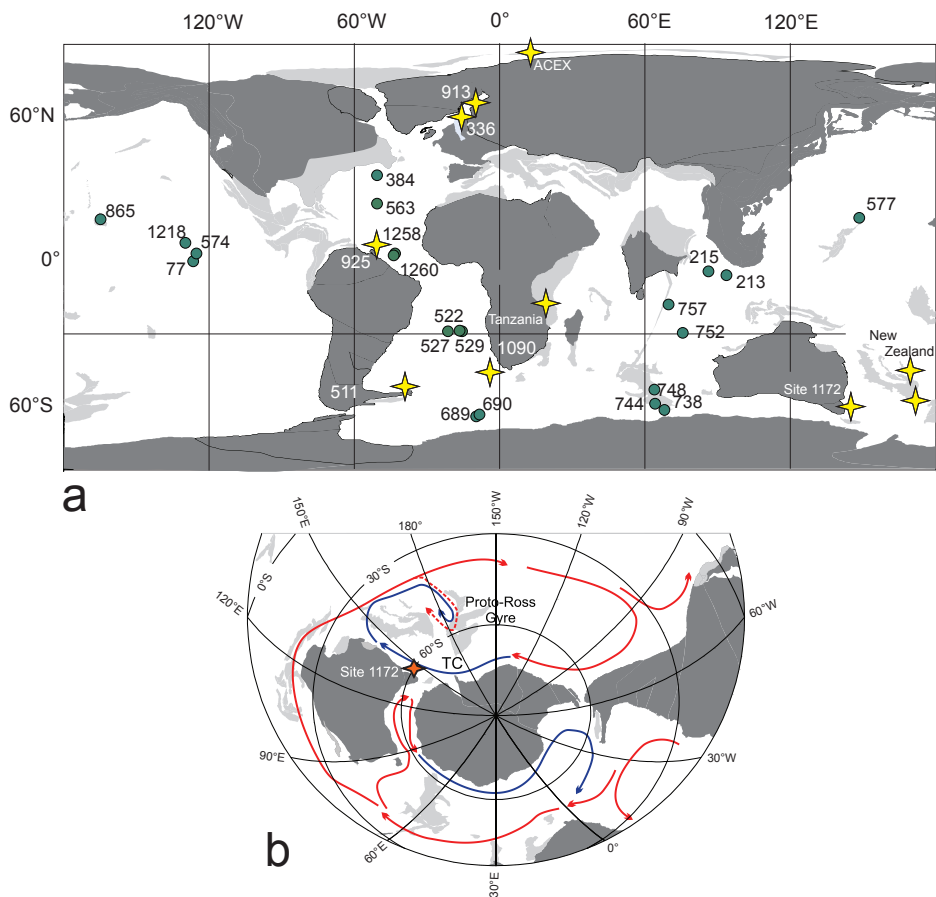


Figure S1. a): Site locations of the records used in this study. The stars represent those sites with  $TEX_{86}$  and/or  $U_{37}^K$  SST reconstructions, circles represent records in the herein updated global stack of benthic foraminiferal oxygen isotopes. The numbers in the graph refer to the site codes as assigned by the different ocean drilling programs DSDP, ODP and IODP. The paleogeographic reconstruction represents early- middle Eocene times (~50 Ma). Paleogeographic chart was obtained from the Ocean Drilling Stratigraphic Network, after Hay et al. (1999). b): South Pacific paleogeographic reconstruction, with GCM- derived ocean current model. Paleogeographic chart was obtained from the Ocean Drilling Stratigraphic Network, after Hay et al. (1999). Reconstructed ocean currents from Huber et al. (2004). TC: Tasman Current.



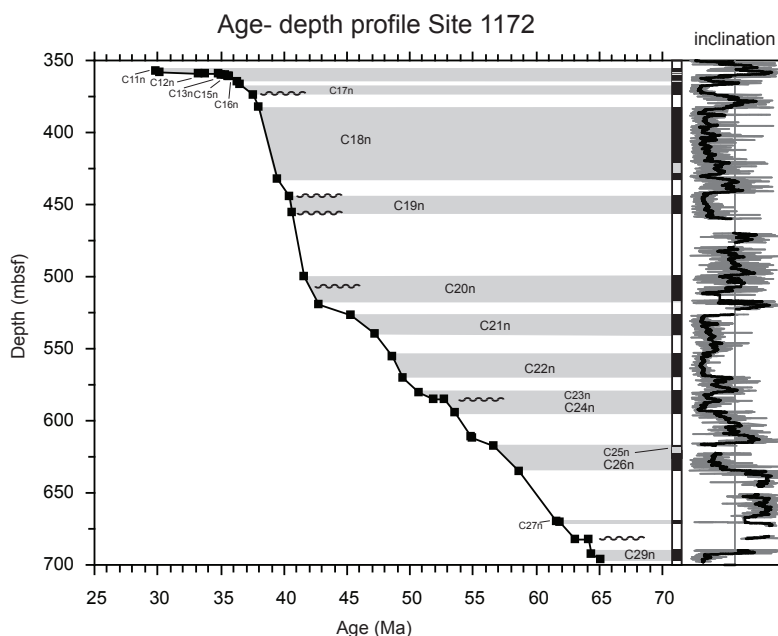


Figure S2. Age- depth profile for ODP Site 1172 with the revised age model. Also plotted are the inclination data, obtained from the Ocean Drilling Program database ([www-odp.tamu.edu](http://www-odp.tamu.edu)). The black line in the inclination curve represents a 25-point running mean through the inclination data. Note the hiatus in the early Paleocene (Schellenberg et al., 2004), the increase in sedimentation rates after the PETM, the small hiatus in the late early Eocene and the drop in sedimentation rates during the late Eocene (Stickley et al., 2004a, b; Sluijs et al., 2003). For more information on the late Eocene to early Oligocene stratigraphy see Sluijs et al. (2003).

### 3. Methods: $\text{TEX}_{86}$ and $\text{U}_{37}^{\text{K}'}$

Organic compounds were extracted from powdered and freeze-dried sediments with dichloromethane (DCM)/ methanol (MeOH) (9:1) by using accelerated solvent extraction technique (Dionex). Excess solvent was removed using rotary evaporation with vacuum. The total extracts were separated in polar and apolar fractions over an activated  $\text{Al}_2\text{O}_3$  column using Hexane:DCM (1:1) and DCM:MeOH (1:1), respectively. The polar fraction was then dissolved in a 99:1 hexane/propanol solvent, and filtered using a  $0.45 \mu\text{m}$ , 4 mm diameter polytetrafluoroethylene (PTFE) filter, before being analyzed using a high performance liquid chromatography/atmospheric pressure positive ion chemical ionization mass spectrometry (HPLC/APCI-MS). HPLC/APCIMS analyses were done according to Schouten et al. (2007a) using an Agilent 1100 series LC/MSD SL and separation and a Prevail Cyano column ( $2.1 \times 150 \text{ mm}$ ,  $36\text{mm}$ ; Alltech), maintained at  $30^\circ\text{C}$ . The glycerol dialkyl glycerol tetraethers (GDGTs) were eluted using a changing mixture of hexane and propanol as follows, 99% hexane: 1% propanol for 5 minutes, then a linear gradient to 1.8% propanol in 45 minutes. Flow rate was  $0.2 \text{ ml per minute}$ . Single ion monitoring was set to scan the  $5 [\text{M}+\text{H}]^+$  ions of the GDGTs with a dwell time of 237 ms for each ion.





We applied the core top calibration equation from Kim et al. (2008) to translate  $\text{TEX}_{86}$  values to an estimation of mean annual sea surface temperature:

$$T = -10.78 + 56.2 \times \text{TEX}_{86} \quad (2.1)$$

About half of the analyzed samples were run in duplicate, to estimate the reproducibility. In all these samples, the reproducibility is better than  $0.5^{\circ}\text{C}$ , and in most cases better than  $0.25^{\circ}\text{C}$ . Recently, Liu et al. (2009) used in their calibration the same core top data set as Kim et al. (2008), but included data that Kim et al. (2008) discarded. However, Kim et al. discarded core top data from cold (Arctic and Antarctic) or hypersaline (Red Sea) regions for a reason: in those special settings, crenarchaeota appear to behave differently to SST (see e.g., Turich et al., 2007). Kim et al. (2008) postulated that the near invariance of high-latitude  $\text{TEX}_{86}$  index values to SST was due to changed membrane adaptation of low temperature crenarchaeotal communities. The good correlation in trends between our  $\text{TEX}_{86}$  SSTs and benthic foraminiferal  $\delta^{18}\text{O}$  suggests that  $\text{TEX}_{86}$  confidently records ancient SST trends and the correlation between polar SSTs and  $\text{TEX}_{86}$  index values in ancient greenhouse climates seems not to be invariant like at present day conditions (Fig. S3).

Therefore, present day  $\text{TEX}_{86}$  issues at polar regions appear to be specific for the present day polar climates, and did not affect the relation between  $\text{TEX}_{86}$  and SST in ancient polar greenhouse climates. In fact, the high-latitude SSTs inferred in our study (Fig. 2) are obviously well above modern day high-latitude SST range. Therefore, addition of polar SST data points to the core top calibration (as was done by Liu et al. (2009)) is not valid for our purpose, but only skews the calibration towards conditions that were not even present in the Paleogene greenhouse. Furthermore, incubation studies show that at the high temperature end (i.e., above modern day temperature range) there is a continued linear relation between  $\text{TEX}_{86}$  and SST at least until  $40^{\circ}\text{C}$  (Schouten et al., 2007b). Hence there is a prior no reason to assume a decreased sensitivity of  $\text{TEX}_{86}$  to SST at above modern day temperatures. Thus, while Liu et al. (2009) may have provided a good  $\text{TEX}_{86}$  calibration for icehouse conditions with low polar temperatures, in ancient greenhouse climates we prefer the linear calibration equation by Kim et al. (2008) instead of the reciprocal calibration of Liu et al. (2009).

To analyze the alkenones, the apolar fractions were separated in 3 fractions by  $\text{Al}_2\text{O}_3$  column chromatography using Hexane:DCM (9:1, v/v); Hexane:DCM (1:1, v/v; the ketone fraction with the alkenones) and DCM. The ketone fractions were analyzed for alkenones by gas chromatography (GC) using an Agilent 6890 equipped with an on column injector. Separation was achieved using a 50m CPSil 5CB column (0.32 mm internal diameter, 0.12 micrometer film thickness). The values calculated from the C37:2 and C37:3 alkenones were converted into temperature values by applying the core-top calibration of Müller et al. (1998):

$$T = (U_{37}^K - 0.033)/0.044 \quad (2.2)$$



The reproducibility of the analysis is better than 0.5°C. Selected fractions were analyzed by GC/mass spectrometry (GC/MS) using a TRACE DSQ to confirm the presence of the alkenones and the absence of co-eluting compounds. Alkenones could only be detected in sufficient quantities in late Eocene sediments.

Type	Event	Reversal	Depth (mbsf)	Age (Ma)
m	T	C11n.2n	357.300	29.853
m	O	C11n.2n	358.600	30.217
m	T	C13n	358.800	33.270
m	O	C13n	358.900	33.740
m	T	C15n	359.700	34.780
m	O	C15n	359.900	35.040
m	T	C16n.1n	360.100	35.400
m	O	C16n.1n	361.300	35.570
m	T	C16n.2n	361.500	35.710
m	O	C16n.2n	365.000	36.280
m	T	C17n	367.100	36.510
m	O	C17n	373.900	37.550
m	T	C18n.1n	382.100	38.032
m	O	C18n.2n	432.000	39.460
m	T	C19n	444.000	40.440
m	O	C19n	456.000	40.670
m	T	C20n	500.000	41.590
m	O	C20n	519.000	42.770
m	T	C21n	526.400	45.350
m	O	C21n	540.000	47.240
m	T	C22n	555.900	48.600
m	O	C22n	570.000	49.430
m	T	C23n	581.000	50.730
m	O	C23n	585.000	51.900
m	T	C24n	585.010	52.730
m	O	C24n	594.200	53.530
i	T	PETM	610.800	54.850
i	O	PETM	611.800	55.000
m	T	C25n	618.000	56.650
m	O	C26n	634.800	58.700
m	T	C27n	670.000	61.650
m	O	C27n	670.750	61.983
m	T	C28n	685.000	63.104
m	O	C28n	685.010	64.128
m	T	C29n	692.600	64.432
m	O	C29n	695.990	65.118
m	T	C30n	695.991	65.861
m	O	C30n	709.100	67.696
m	T	C31n	713.300	67.809
m	O	C31n	736.600	68.732

Table S1. Ages and depths for the magnetic reversals and the PETM as used in the age model. m: magnetic reversal, i: isotope event, O: onset, T: termination.



#### 4. The updated global stack of benthic foraminiferal oxygen isotopes

The previously published global stack of benthic foraminiferal oxygen isotopes (Zachos et al., 2008) (see Fig. S1 for site locations) had been modified for the purpose of this paper. First of all, the entire dataset had been converted to the timescale of Gradstein et al. (2004). Subsequently, data from Site 748B and 1218 had been adjusted to the latest age model for the MECO (Bohaty et al., 2009). Isotope data from Demerara Rise (Site 1258 and 1260; Sexton et al., 2006) were added, after adjustment to the Gradstein timescale (Gradstein et al., 2004). The MECO data of Site 1260 were previously plotted on a predated MECO time scale, and were adjusted according to Bohaty et al. (2009). Figure 2 shows the updated global stack of benthic foraminiferal oxygen isotopes, with a 5 point running mean through the entire dataset. Especially the Paleocene part of the stack is notoriously scattered.

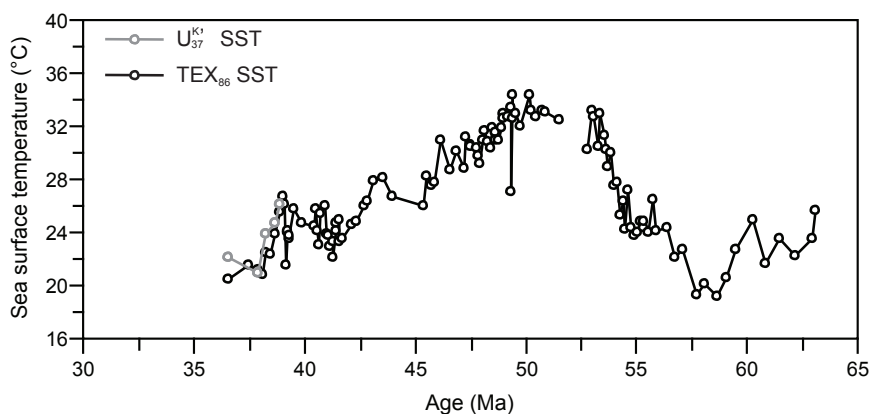


Figure S3. The Tasmanian  $\text{TEX}_{86}$  (black) and  $\text{U}_{37}^{\text{K}'}$  (red) SST record for the early Paleogene.

#### 5. Correlation of benthic foraminiferal $\delta^{18}\text{O}$ and Tasmanian SSTs

In order to make a more detailed comparison between Tasmanian SSTs and the global stack of benthic foraminiferal oxygen isotopes, we re-sampled the global stack. Using Analyseries software (Paillard et al., 1996), we interpolated the oxygen isotope data for each data point of  $\text{TEX}_{86}$ , in order to obtain contemporaneous Tasmanian SST and 'global' benthic foraminiferal oxygen isotope values. Correlation between ETP SSTs and the resampled updated benthic  $\delta^{18}\text{O}$  stack is good for the entire interval between 64 and 36 Ma ( $R^2=0.64$ ; Fig. S4).  $R^2$  values are even higher if Paleocene and early Eocene values are separated from middle and late Eocene values ( $R^2 = 0.76$  and  $0.74$ , respectively). In these two time intervals, SSTs correlate with a different slope to benthic  $\delta^{18}\text{O}$ . This could imply regional SST warming in the Southwest Pacific. Alternatively, it could indicate an increase in the benthic  $\delta^{18}\text{O}$  stack values through an increase in the basin-to-basin  $\delta^{18}\text{O}$  gradient (Fig. S3), changes in deep water source area, or the build up of continental ice. The high  $R^2$  values indicate that the Southwest Pacific SST trend mirrored that of the deep ocean, and suggests



that the locus of deep-water formation may have been in the Southwest Pacific. While overall trends in both records match closely, absolute deep-sea temperatures are much cooler than southwest Pacific SSTs throughout the Paleogene. One explanation for the large discrepancy in absolute temperatures in both records might be seasonality.

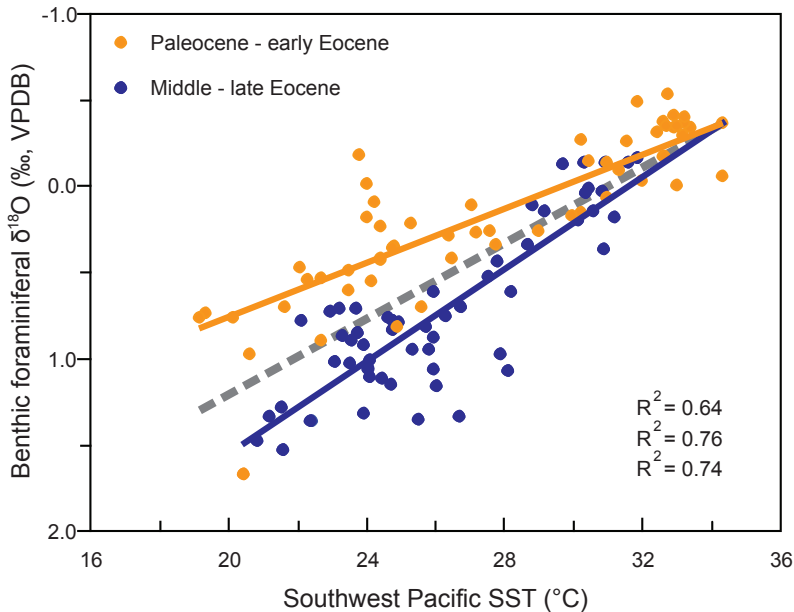


Figure S4. Correlation between Tasmanian SSTs (x-axis) and the re-sampled updated global stack of benthic foraminiferal oxygen isotopes (y-axis) is good (grey line;  $R^2=0.64$ ). Conspicuously, the correlation coefficient for middle Eocene- late Eocene data is different from that for the Paleocene- early Eocene.

While generally the  $TEX_{86}$  SST proxy reflects mean annual SST (Kim et al., 2008; Schouten et al., 2002) high-latitude  $TEX_{86}$  SST reconstructions might be skewed towards summer, because that is the main period of organic carbon export and thus of fluxes of crenarchaeotal membrane lipids to the sea floor (Sluijs et al., 2006, 2008a). Although ODP Site 1172 was not within the polar circle it may be that the main season of lipid export at  $\sim 65^\circ$ S lat. was during summer. In turn, deep-water formation at high-latitudes mainly occurs during winter, when surface waters reach maximum densities, thereby skewing benthic  $\delta^{18}O$ -based temperature estimates towards winter SSTs of the source regions.

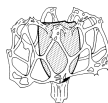








Despite warm polar climates and low meridional temperature gradients, a number of different high-latitude plankton assemblages were, to varying extents, dominated by endemic species during most of the Paleogene. To better understand the evolution of Paleogene plankton endemism in the high southern latitudes, we investigate the spatio-temporal distribution of the fossil remains of dinoflagellates, i.e., organic-walled cysts (dinocysts), and their response to changes in regional sea surface temperature (SST). We show that Paleocene and early Eocene (~65–50 Ma) Southern Ocean dinocyst assemblages were largely cosmopolitan in nature but that a distinct switch from cosmopolitan-dominated to endemic-dominated assemblages (the so-called “transantarctic flora”) occurred around the early-middle Eocene boundary (~50 Ma). The spatial distribution and relative abundance patterns of this transantarctic flora correspond well with surface water circulation patterns as reconstructed through general circulation model experiments throughout the Eocene. We quantitatively compare dinocyst assemblages with previously published  $TEX_{86}$ - based SST reconstructions through the early and middle Eocene from a key locality in the southwest Pacific Ocean, ODP Leg 189 Site 1172 on the East Tasman Plateau. We conclude that the middle Eocene onset of the proliferation of the transantarctic flora is not linearly correlated with regional SST records and that only after the transantarctic flora became fully established later in the middle Eocene, possibly triggered by large-scale changes in surface-ocean nutrient availability, were abundances of endemic dinocysts modulated by regional SST variations.





### 1. Introduction

Early Paleogene temperatures and atmospheric CO<sub>2</sub> concentrations were significantly higher than today (Chapter 2; Pearson and Palmer 2000; Sexton et al., 2006; Sluijs et al., 2006; Zachos et al., 2008). This long-term global warm period peaked during the late early Eocene (~52– 50 Ma; Sexton et al., 2006; Zachos et al., 2001), with high (>30°C) southern high-latitude SSTs and minimal latitudinal temperature gradients (Chapter 2). The subsequent long-term global cooling through the middle and late Eocene (Chapter 2; Sexton et al., 2006; Zachos et al., 2008) culminated in the establishment of large Antarctic ice sheets around the time of the Eocene-Oligocene boundary (~34 Ma; Barker et al., 2007; Coxall et al., 2005; DeConto and Pollard 2003a, b; Miller et al., 1987).

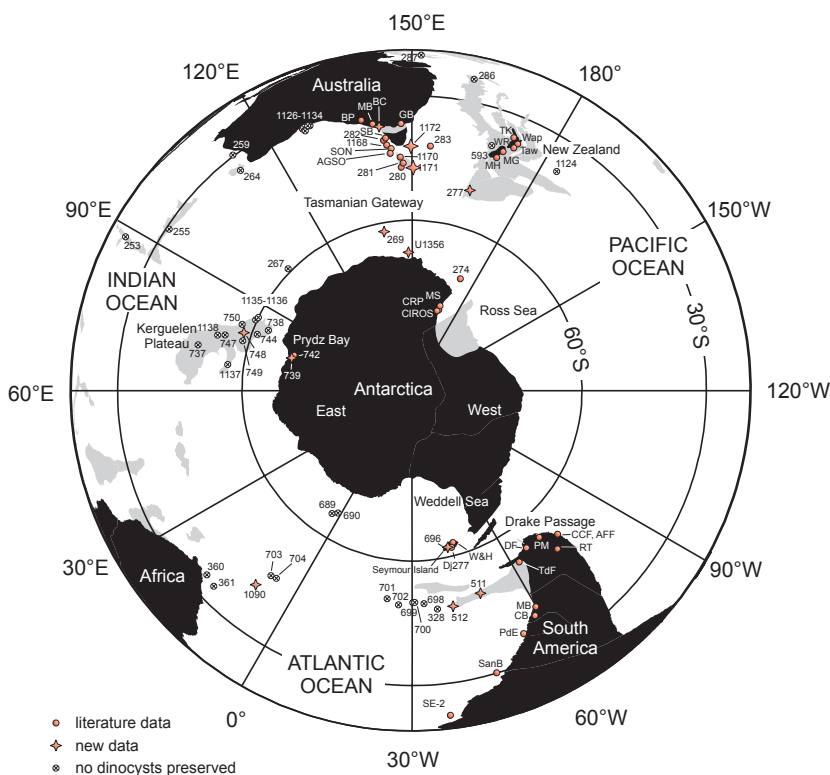
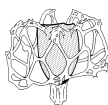


Figure 1. Location map for present-day positions of evaluated sites. Numbers 253–593 refer to Deep Sea Drilling Project (DSDP) sites; numbers 689–1172 refer to Ocean Drilling Program (ODP) sites. IODP Site U1356 refers to a site drilled by the Integrated Ocean Drilling Program. For code legend, see Table S1. The geographic map was derived from the Ocean Drilling Stratigraphic Network (ODSN).



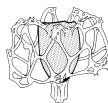
The warm climates and low latitudinal temperature gradients prior to the onset of major Antarctic glaciation facilitated the poleward migration of many biota (Adams et al., 1990; Eberle et al., 2009; Sluijs et al., 2006). Surprisingly, however, Southern Ocean fossil assemblages are distinctly endemic during long intervals of the early Paleogene and become increasingly endemic over time; besides molluscs (Zinsmeister, 1979), this phenomenon has been observed in numerous microfossil groups such as dinocysts (Wrenn and Beckman, 1982; Wrenn and Hart 1988) radiolaria (Lazarus and Caulet, 1993; Lazarus et al., 2008), calcareous nannoplankton and planktonic foraminifera (Nelson and Cooke, 2001; Villa et al., 2008), and diatoms (Harwood, 1991; Stickley et al., 2004b). Dinocysts are abundant in marginal marine sediments, notably at high-latitudes. The early Paleogene Antarctic endemic dinocyst community is taxonomically well documented from outcrops and sediment cores around the Antarctic margin, and it is often referred to as the “transantarctic flora” (cf. Wrenn and Beckman, 1982). However, the evolution and driving forces behind this Paleogene Southern Ocean endemism are largely unknown, although SST is presumed to have been involved (Huber et al., 2004). So far, a lack of reliable SST reconstructions has hampered the evaluation of this hypothesis, and it is only through recently published geochemical data (Chapter 2) that such a test has become possible.

In this study, we aim to elucidate the role of oceanic surface circulation, SST and other environmental changes as a potential selective mechanism for Eocene Antarctic endemism among dinoflagellates. First, we provide an overview of Paleogene dinocyst paleobiogeography, for which we integrate newly generated palynological data with those previously published. Additionally, we statistically examine the relation of SST (using the  $\text{TEX}_{86}$  paleothermometry of Chapter 2) and ocean-wide productivity (using the thallium isotope records of Nielsen et al., 2009) to dinocyst assemblage changes in the southwest Pacific Ocean (Ocean Drilling Program Site 1172).

## 2. Material and Methods

### 2.1. Southern Ocean sites

We generated palynological data on sediments recovered at Ocean Drilling Program (ODP) and Deep Sea Drilling Project (DSDP) Sites 269, 277, 511, 512, 696, 739, 748 and 1090, as well as from the Brown’s Creek section in southeast Australia (Fig. 1). Higher-resolution time series data were obtained from ODP Sites 1172 and 1171, and from outcrop samples from Blanche Point along the Southern Australian Margin. Furthermore, we reviewed published information on Paleogene (~65–25 Ma) Southern Ocean dinocysts from Integrated Ocean Drilling Program (IODP), DSDP and ODP sites, the “Cape Roberts Project” (CRP 1, 2a and 3) and “Cenozoic Investigations of the Ross Sea 1” (CIROS-1) drilling expeditions. In addition, studies of outcrops that flank the Southern Ocean were considered from the southern Australian margin, McMurdo Sound, New Zealand, Tierra del Fuego, Santa Cruz Province, Brunswick Peninsula, and Seymour Island. An inventory of all sites and outcrops considered (including references) is listed in Table S1 at the end of this chapter. An overview on the present-day locations of these sites is provided in Fig. 1.



The age control for these records is based on calcareous nannoplankton stratigraphy and, to a lesser extent, on diatom and/or palynomorph stratigraphies, radiometric dating, and magnetostratigraphy. The approximate tectonic configurations of the continents used in Figs. 2 and 3 were reconstructed using the Ocean Drilling Stratigraphic Network (ODSN) database: <http://www.odsn.de> (after Hay et al. (1999)). The semi-continuous succession recovered at ODP Site 1172 has been magnetostratigraphic calibrated (Stickley et al., 2004a) and extends from the Quaternary to the Maastrichtian (latest Cretaceous). Notably, it represents a reference section for Paleogene Antarctic endemism. ODP Site 1172 is located on the submerged western side of the East Tasman Plateau (ETP) at 45°S and a water depth of 2,620 m (Fig. 1; see Exon et al. (2004) for details). During the early Paleogene, the ETP was located at 65°S, much closer to Antarctica than it is today (Exon et al., 2004). Recovery at Hole 1172A includes Paleogene sediments down to the mid- middle Eocene, while Hole 1172D extends the record from the mid- middle Eocene to the Maastrichtian. Calcite concentrations increase from ~40 Ma onward, which has been linked to a relative sea level rise following basin subsidence (Röhl et al., 2004a). Paleocene and Eocene sediments were recovered from between 350 and 700 meters below seafloor (mbsf; Exon et al., 2003; Stickley et al., 2004a). This part of the section consists of brownish to greenish grey, bioturbated siltstones, that are poor in calcium carbonate, but yield abundant organic matter, including dinocysts (Exon et al., 2004).

## 2.2. Southern Ocean surface-current configurations

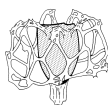
According to modeling experiments and biogeographical data, in the early Paleogene the region was under the influence of the Antarctic-derived, northward flowing Tasman Current (Huber et al., 2004). This current was part of a large gyre system in the South Pacific Ocean, the Proto-Ross Gyre (Stickley et al., 2004b). The tectonic positioning of the continents that prescribe this current system was stable at least until ~35.5 Ma, when the northward movement of Australia from Antarctica deepened the Tasmanian Gateway and much later allowed for the Antarctic Circumpolar Current to establish (Stickley et al., 2004b).

## 2.3. Palynological processing and taxonomy

Processing sediment samples for palynology followed the standardized methods described, e.g., by Sluijs et al. (2003). Briefly, this involves treatment of dried sediment samples with ~30% HCl and ~38% HF. No bleaching and heavy-liquid separation was applied. A 15 micrometer nylon mesh was used for sieving. Residues were mounted on slides for microscope analysis. Approximately 200 dinocysts were counted per sample and identified to the species level at 500× magnification. An inventory of dinocyst species encountered in this study is listed in Table S2 at the end of this chapter; dinocyst nomenclature and taxonomy, unless stated otherwise, are based on the work of Fensome and Williams (2004).

## 2.4. Dinocysts: endemic versus nonendemic taxa

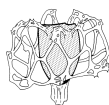
Dinocysts are the remains of unicellular eukaryotic plankton (dinoflagellates) that dwell as motile stages in surface oceans (e.g., Fensome et al., 1993). Dinoflagellates occur in virtually all marine settings, but are most abundant and diverse in shelfal environments (e.g., Dale 1996; Pross and Schmiedl 2002; Pross



and Brinkhuis 2005; Sluijs et al., 2005). The fossil record of dinoflagellates is predominantly based on their resistant organic-walled cysts (dinocysts). The dinocyst record, in turn, is particularly good in shelfal environments where relatively high sedimentation rates lead to a reduced oxygen exposure of the cysts. In contrast, deeper environments with well-ventilated bottom waters exhibit generally lower sedimentation rates and high oxygen concentrations, and in these settings dinocysts oxidize and do not preserve.

<b>Species described by...</b>	<b>Now assigned to transantarctic flora</b>
...prior to Wrenn and Hart (1988)	<i>Alterbidinium distinctum</i>
	<i>Arachnodinium antarcticum</i>
	<i>Deflandrea antarctica</i>
	<i>Deflandrea cygniformis</i>
	<i>Deflandrea granulata</i>
	<i>Deflandrea oebisfeldensis</i>
	<i>Spinidinium macmurdoense</i>
...Wrenn and Hart (1988)	<i>Vozzhennikovia apertura</i>
	<i>Spinidinium colemanii</i>
	<i>Octodinium askiniae</i>
	<i>Hystrichosphaeridium truswelliae</i> : now non-endemic (Sluijs and Brinkhuis, 2009)
	<i>Impletosphaeridium clavus</i>
	<i>Deflandrea webbii</i>
...Wilson (1988)	<i>Spinidinium luciae</i>
...Goodman and Ford (1983)	<i>Membranophoridium perforatum</i>
	<i>Phthanoperidinium</i> sp. A
	<i>Phthanoperidinium</i> sp. B
...Stover and Williams (1987)	<i>Gippslandia extensa</i>
...Mao and Mohr (1995)	<i>Phthanoperidinium antarcticum</i>
...Stover and Williams (1995)	(now) <i>Enneadocysta dictyostila</i>
...Levy and Harwood (2000)	<i>Vozzhennikovia netrona</i>
...Brinkhuis et al. (2003a)	<i>Deflandrea</i> sp. A
...Clowes and Wilson (2006)	<i>Corrudinium regulare</i>
...Sluijs et al. (2009b)	<i>Vozzhennikovia stickleyae</i>
	<i>Vozzhennikovia roehliae</i>
	<i>Spinidinium schellenbergii</i>
	<i>Moria zachosii</i>
<b>Bipolar species assigned by:</b>	<b>Bipolar species</b>
Warnaar (2006)	<i>Phthanoperidinium stockmansii</i>
Wrenn and Hart (1988)	<i>Spinidinium macmurdoense</i>

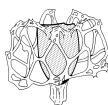
Table 1. Overview of dinocysts herein assigned to the transantarctic flora and the bipolar species.



Dinocyst species are considered to be “endemic to the Southern Ocean” if their empirically established distribution patterns are restricted to this region (i.e., latitudes south of 45°S). The Eocene endemic dinocysts in the Southern Ocean were originally referred to as the “transantarctic flora,” a name derived from their presumed affinity to the inferred Trans-Antarctic Seaway (Wrenn and Beckman 1982). Later studies reported elements of the transantarctic flora from other Southern Ocean sectors (Brinkhuis et al., 2003a; Clowes and Wilson 2006; Levy and Harwood 2000; Macphail and Truswell 2004; Mao and Mohr 1995; Sluijs et al., 2009b; Wrenn and Hart 1988). Some of these reports also described new species, but did not place those within the transantarctic flora. Other species occur in high abundances only in both north and south polar regions, and may therefore be placed in a “bipolar” group (e.g., Wrenn and Hart 1988). For this study, we include the bipolar species in our endemic dinocysts category herein after. Moreover, some taxa that are allegedly endemic to the Southern Ocean are morphologically similar to some cosmopolitan forms. For example, the supposedly endemic species *Dracodinium waipawaense* (Wilson 1967b) and the Northern Hemisphere *D. varielongitudum* (Williams and Downie 1966) have the same stratigraphic range and are taxonomically identical, if one allows for subtle morphological variations in shape, size and number of processes (spines) on the cysts. Hence, it can be debated whether species such as *D. waipawaense* are truly endemic or whether the slight morphological differences are the result of eco-phenotypic variability within a single dinocyst species. Because of these uncertainties, we did not consider such species to be part of the transantarctic flora. On the other hand, the Eocene species *Enneadocysta dictyostila* (Menéndez 1965; Stover and Williams 1995, emend. Fensome et al., 2006) can be classified as endemic, despite its resemblance to the Northern Hemisphere species *Areosphaeridium diktyoplokum* (Klumpp 1953). The two species can be clearly separated based on differing (para-) tabulation, a fundamental structural difference that is highly unlikely to occur within an individual species or genus (Goodman and Ford 1983); see discussions by Fensome et al. (2006). An overview of the dinocyst species we assign herein to the transantarctic flora is provided in Table 1.

### 2.5. Canonical correspondence analyses

We assessed the potential correspondence of the dinocyst data from ODP Site 1172 with four environmental variables reconstructed from the same site as well as other records using Canonical Correspondence Analyses. With this statistical method, quadratic relations between the first and higher axes have been found to cause arch effects in the ordination (ter Braak 1986). To avoid these effects, we applied detrended canonical correspondence analyses (DCCA; see ter Braak 1986). We performed two DCCA analyses, one on the entire investigated record and the second only using middle Eocene data. The TEX<sub>86</sub>-based SST record of ODP Site 1172 from (Chapter 2) was added as the first environmental variable. This SST record comprises ~120 samples for the Paleocene-Eocene (average sample resolution: 250 kyr). As second variable, we used the thallium isotope record from the Pacific Ocean (Nielsen et al., 2009). We averaged two coeval records of thallium isotopes and re-sampled the data to the (lower-resolution) TEX<sub>86</sub> SST data set. The thallium isotope record is interpreted to reflect ocean-wide Pacific Ocean productivity trends (Nielsen et al., 2009). Third, the peridinioid/ gonyaulacoid dinocyst ratio may serve as a measure for



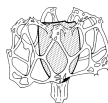
the trophic state of the surface waters (Sluijs et al., 2005). Finally, we added the percentage of endemic dinocysts. We used only those samples that were analyzed for both TEX<sub>86</sub> and palynology, rather than interpolating the TEX<sub>86</sub> data. The DCCA analysis on the entire data set comprises 59 samples. We performed a separate DCCA analysis for the middle Eocene using the same environmental variables, for which the number of samples is 21.

### 3. Results

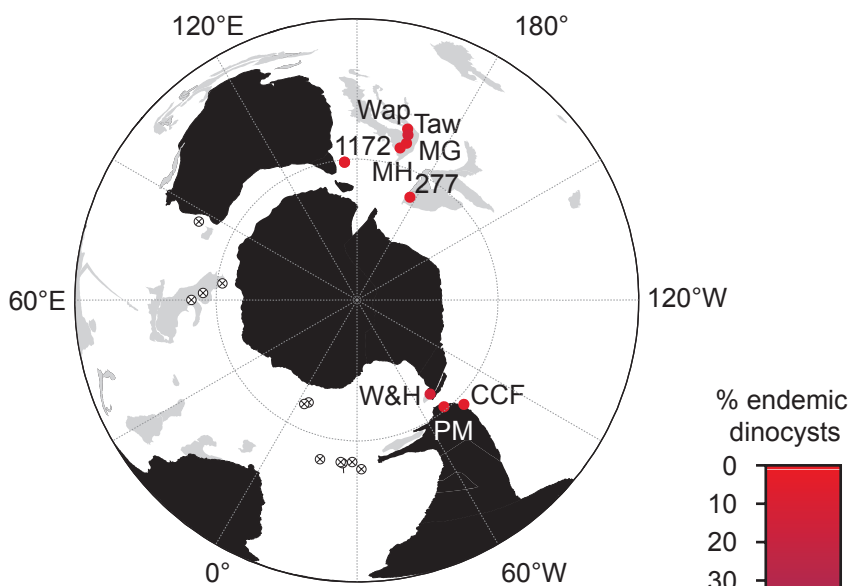
#### 3.1. *Dinocyst biogeography through time*

Distribution maps of the compiled circum-Antarctic dinocyst records for seven time slices spanning ~56 Ma to 36 Ma are presented in Figs. 2a–2g. The distribution patterns for the two oldest time slices (Fig. 2a, 56–54 Ma; Fig. 2b, 53–51 Ma) have limited numbers of dinocyst-bearing sites restricted to the southwest Pacific Ocean and Drake Passage. This limited information shows that endemics are present, but do not numerically dominate the dinocyst assemblages, not even on the Antarctic Margin. During the early middle Eocene, endemic taxa are dominant in the areas east of the Tasman Gateway and Drake Passage (Fig. 2c, 50–48 Ma). From the middle Eocene onward, endemic dinoflagellates consistently and strongly dominate the assemblages along the western boundaries of the Drake Passage and the Tasman Gateway as well as at Prydz Bay (Figs. 2d, 2e, and 2f; 47 Ma to 39 Ma), at least until the mid to late Eocene (Fig. 2g; 38–36 Ma). Many undoubtedly Oligocene and younger records in the south-west Pacific (not presented here; e.g., ODP Leg 28 (Kemp 1975)) and Atlantic (Guerstein et al., 2008) yield some endemic dinocysts. These are most likely reworked from Eocene sediments as a result of Oligocene glacial activity. We have compiled a composite of the generalized distribution of endemic dinocysts during the middle and late Eocene (47–36 Ma) and note that the sectors characterized by dominant endemism are restricted to the Antarctic margins and the eastern sides of the Tasman and Drake conduits (Fig. 3). The Australo-Antarctic Gulf area is characterized by overall low abundances of endemics throughout the Paleogene (Fig. 3).

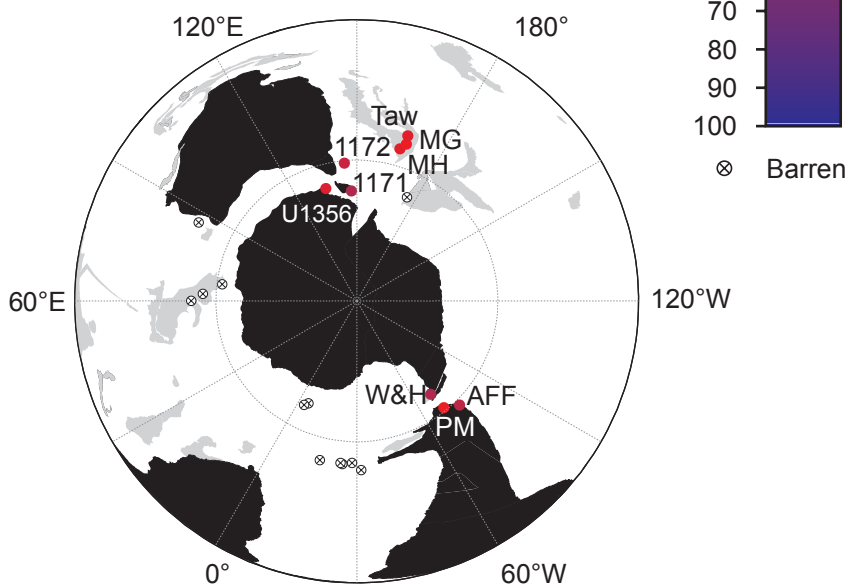
Figure 2 (next pages). Circum-Antarctic geographical distribution maps showing the spatio-temporal evolution of dinocyst endemism for seven different time slices. Color shading of Sites yielding dinocysts indicates relative abundance of transantarctic flora, from red (0%) to blue (100%). (a) Thanetian-Ypresian boundary (56–54 Ma), (b) mid-Ypresian (53–51 Ma), (c) Ypresian- Lutetian boundary (50–48 Ma), (d) early Lutetian (47–45 Ma), (e) late Lutetian (44–42 Ma), (f) Lutetian-Bartonian boundary (41–39 Ma), and (g) Bartonian- Priabonian boundary (38–36 Ma). Maps were derived from the Ocean Drilling Stratigraphic Network (ODSN). Black areas indicate (continental) blocks that are mostly subaerial. Note that several blocks shown in black were partly submerged during the Paleogene (e.g., Ross Sea, southern Australian margin, and parts of Argentina). Shaded areas indicate mostly submerged continental blocks (e.g., Brown et al., 2006). For locality codes, see Table S1.



SOUTHERN OCEAN DINOCYST BIOGEOGRAPHY

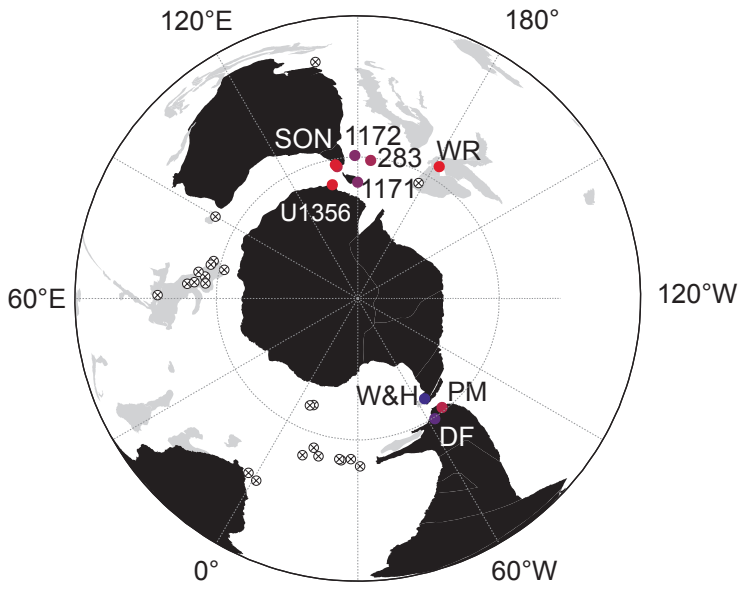


a late Paleocene - early Eocene (56-54 Ma)  
Thanetian - Ypresian

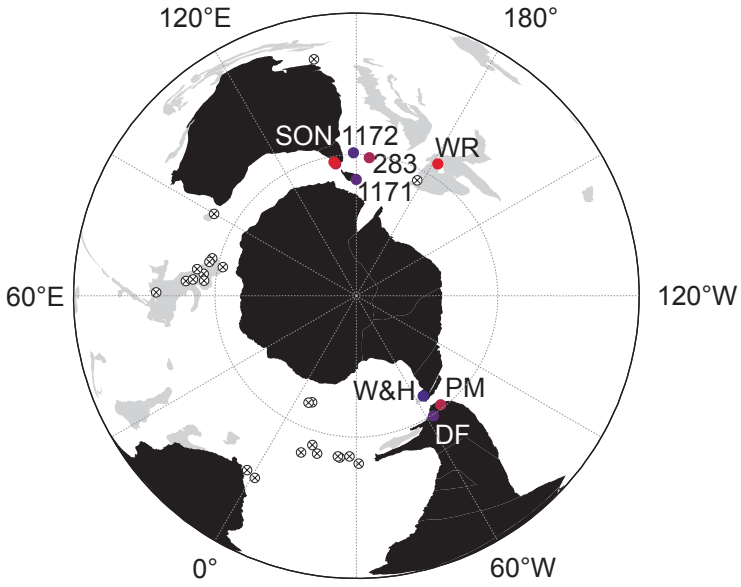


b early Eocene (53-51 Ma)  
Ypresian

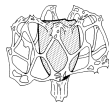




c early - middle Eocene Boundary (50-48 Ma)  
Ypresian - Lutetian

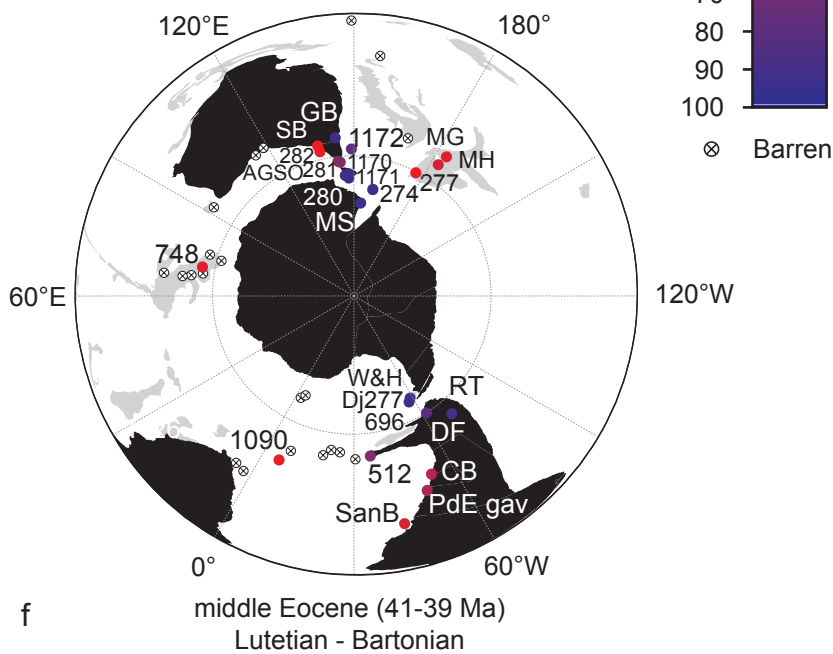
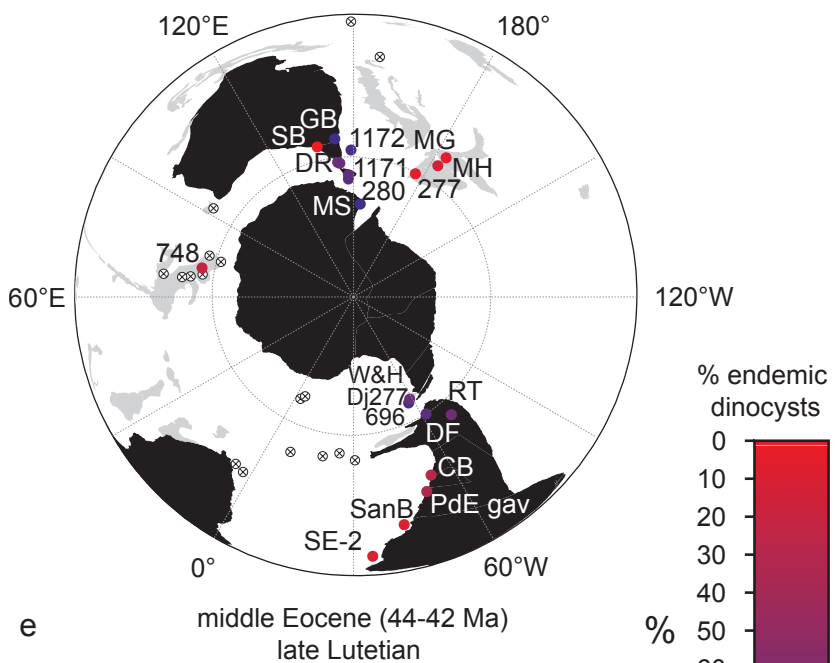


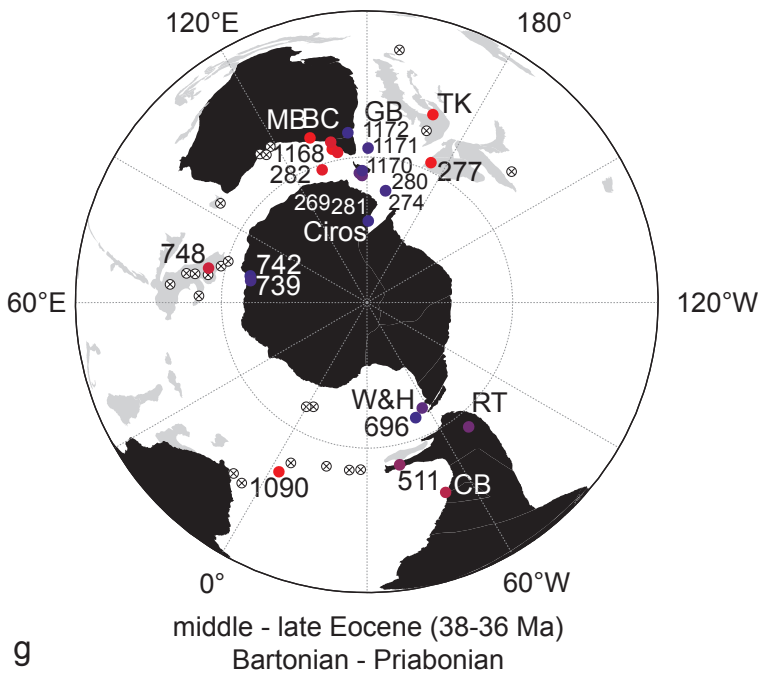
d middle Eocene (47-45 Ma)  
early Lutetian





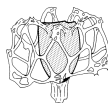
SOUTHERN OCEAN DINOCYST BIOGEOGRAPHY





### 3.2. Statistical analysis

With our DCCA analyses, four canonical axes are established for the four environmental variables. The first axis explains 29% of the dinocyst data, the second axis another 4%. Fig. 4 shows the dinocyst scores for the first two axes with the environmental vectors. The SST vector points to the northeast, whereas the other vectors (i.e., thallium isotopes, % peridinioid dinocysts and % endemic dinocysts) are approximately perpendicular to the temperature vectors. In Fig. 4, the dinocyst groups are divided into endemic (blue triangles) and nonendemic (red circles). The endemic taxa are clearly separated from the nonendemic ones, with high scores on both axes for nonendemic and low scores for endemic dinocysts. The few exceptions include *Membranophoridium perforatum* (Mper) and *Hystrichosphaeridium truswelliae* (Htru). The latter has traditionally been interpreted as being endemic to the Southern Ocean. However, recently *H. truswelliae* was recorded in Paleocene- Eocene strata from New Jersey (northeast North America), clearly disputing its endemic signature (Sluijs and Brinkhuis 2009). 'Outliers' within the nonendemic taxa include the cosmopolitan *Enneadocysta* species (Enne), *Phthanoperidinium comatum* (Pcom) and *Selenopemphix* spp. (Sele). Comparing the scores of the first two axes to the environmental variables, we note that the SST variations correspond with the sample scores of the second axis. This axis explains only 4% of the dinocyst variation (Fig. 5). Patterns in the sample scores of the first axis correspond with the abundance of endemic dinocysts (Fig. 5).



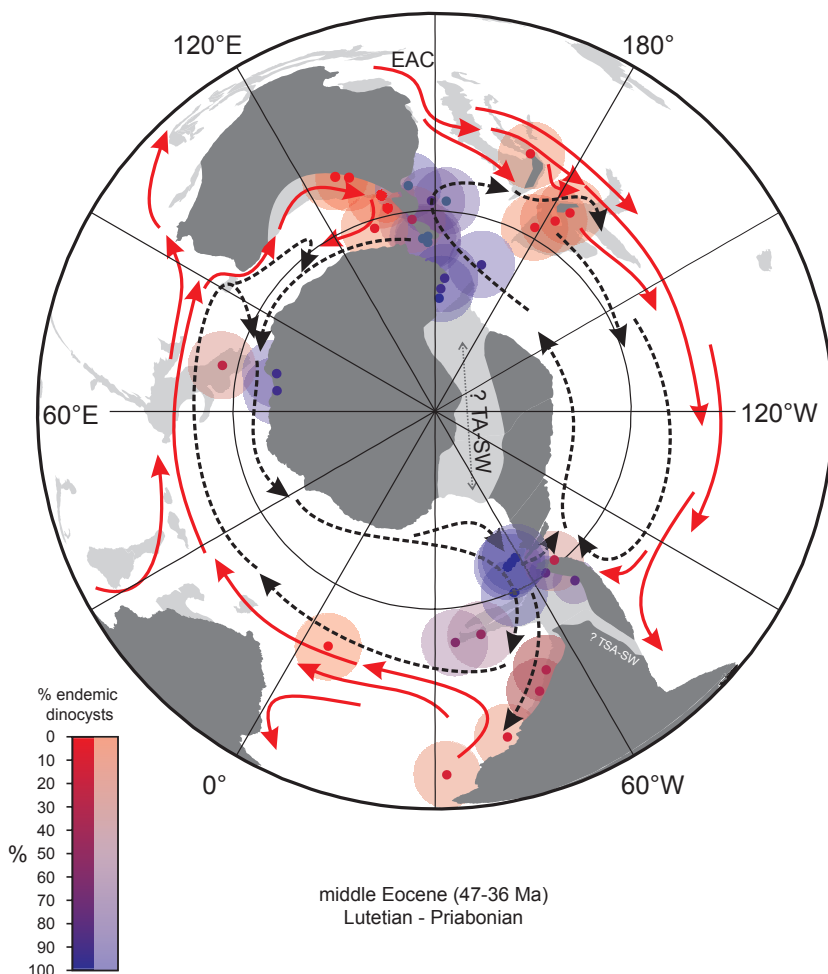


Figure 3. Generalized middle to late Eocene (47-36 Ma) dinocyst geographical distribution map overlain by the ocean circulation pattern inferred from the GCM experiments of (Huber et al., 2004). Maps derived from the Ocean Drilling Stratigraphic Network (ODSN). Shaded areas indicate mostly submerged continental blocks (Brown et al., 2006). Abbreviations: TA-SW, Trans-Antarctic Seaway (hypothetical; see Wrenn and Beckman (1982)); TSA-SW, Trans-South American Seaway (hypothetical; see Kohn et al. (2004) and Lagabrielle et al. (2009)); EAC, East Australian Current (Huber et al., 2004).

Thus, while spatial gradients in % endemic dinocysts appear to be a good indicator of the location of ocean currents, SST appears to have had little effect on the biogeography of endemic dinocysts over the complete record. However, during the interval of long-term cooling which began after the Early Eocene Climatic Optimum (EECO; Chapter 2), abundance changes in endemic dinocysts do now covary with SST. For instance, during the Middle Eocene Climatic Optimum (MECO), a short-lived warming event at ~40 Ma (Bohaty et al., 2009), endemic dinocyst abundances fall again to below 50% (Fig. 5).





After the MECO, the cooling trend continues and endemic dinocysts re-dominate the assemblages (Fig. 5). To test the relation between dinocyst endemism and SST in the post-EECO interval of endemic dinocyst dominance, we performed another DCCA analysis involving only those data within the middle Eocene interval. In this interval, the variation explained by SST is ~20% (Fig. 6).

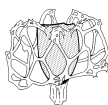
## 4. Discussion

### 4.1. Comparison with other fossil groups

While endemism is recorded within several fossil groups in the Eocene, a direct comparison with the dinocyst record of the southwest Pacific is hampered by a paucity of corresponding records around the Antarctic margin older than ~45 Ma. For instance, although diatomaceous (biosiliceous) sediments of early Cretaceous age and K-T boundary age occur in the western Antarctic margin (Gersonde and Harwood 1990; Harwood 1988; Harwood and Gersonde 1990), these appear to be a rare exception since most known biosiliceous records in Antarctic marginal (shelf) areas are mid Eocene in age (i.e., ODP Site 1172 Stickley et al., 2004a) or commonly much younger (e.g., Lazarus et al., 2008). Calcareous microfossil data from the southern high-latitudes predating 45 Ma are similarly scarce. Nevertheless, the few existing records of microfossils other than dinocysts from that time indeed show an increase in endemism beginning in the mid middle Eocene, as has been shown for radiolarians (Lazarus et al., 2008) and calcareous nannoplankton (Villa et al., 2008). Calcareous nannoplankton also exhibits a decrease in endemism during the MECO (Villa et al., 2008).

### 4.2. Potential driving forces: sea surface temperature, endemism and statistics

The establishment of dominant Antarctic endemic dinocyst assemblages characterizes the early middle Eocene transition (~50 Ma). However, SSTs did not decrease abruptly at that time (Fig. 5). This implies that the increase in abundance of endemic dinocysts was not linearly related to SST. In contrast, during the middle Eocene, abundances of endemic dinocysts are modulated by SST changes (Fig. 6). What then triggered endemic dinocysts to proliferate shortly after ~50 Ma? As stated above, the peak warmth of the EECO at ~50 Ma also marks the transition into the onset of high-latitude and global cooling that, despite an interruption by at least one short warming interval (i.e., the MECO, at ~40 Ma; Fig. 5), culminated in the onset of Antarctic glaciation during the Eocene-Oligocene transition (e.g., Zachos et al., 1992). It may be possible that the endemic dinoflagellate taxa, when they appeared, were capable to sustain in warm subtropical conditions during the EECO, but subsequently evolved to be more specialized to cooler surface waters during middle Eocene cooling. The sudden shift to dominant endemic dinocysts suggests the crossing of an environmental threshold at which cosmopolitan taxa were outcompeted by the endemic taxa. Because the DCCA statistical method identifies linear correspondence between assemblages and environmental data, this threshold may still have been SST.



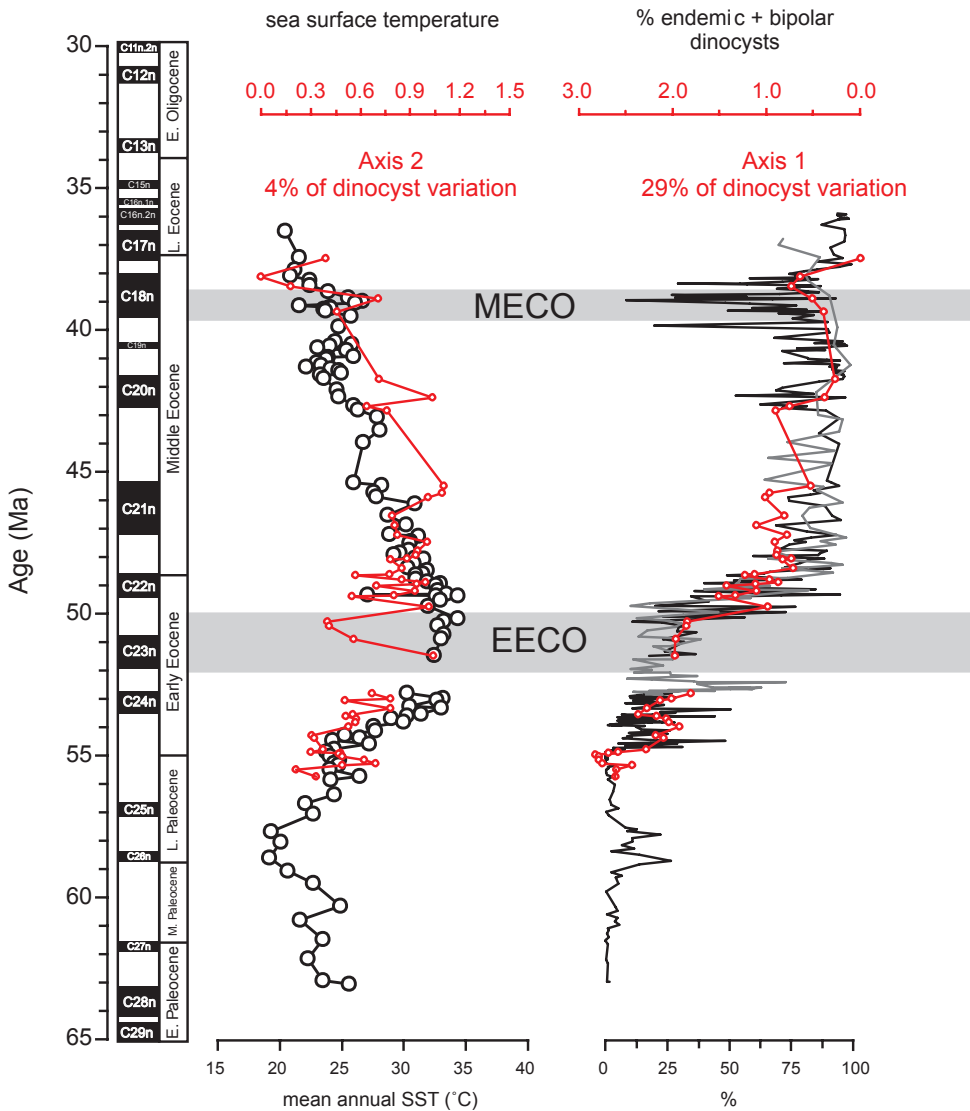
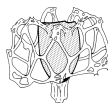


Figure 5. (left) TEX<sub>86</sub>-based SST curve from ODP Site 1172 from Chapter 2 overlain by the second axis scores of the DCCA analysis. Note that the second axis explains only 4% of the total dinocyst assemblage variation. (right) Endemic dinocyst abundances at ODP Sites 1172 (black) and 1171 (grey) overlain by the first axis scores.

The mechanism described above may provide an explanation for the proliferation of endemic dinocysts just after 50 Ma, but it fails to explain the presence, in low abundance, of endemic dinocysts during Paleocene and early Eocene times. The most abundant endemic dinocyst groups, i.e., *Deflandrea antarctica*, *Phthanoperidinium stockmansii* group and *Vozzhennikovia/Spinidinium* spp., are



already present in the Paleocene. Apparently, Paleocene– early Eocene surface waters were not as favourable for endemic species as they were in the middle Eocene. Hence, along with SST changes, other physio-chemical parameters of the surface waters must have changed between the Paleocene and middle Eocene that stimulated Southern Ocean endemism to proliferate just after the early middle Eocene boundary. A possible explanation may lie in the diatom record at ODP Site 1172, where opal-A is preserved from approximately 47 Ma (Stickley et al., 2004a, b) or 45 Ma (Chapter 2) onward (Fig. 7). In the middle Eocene, global cooling enhanced latitudinal gradients (Chapter 2). This cooling stimulated upwelling, bringing silica-enriched waters that characterized Eocene oceans (e.g., McGowran 1989), particularly the Pacific (e.g., Moore 2008), to the surface for utilization by the diatoms. This change apparently brought about significant diatom production and preservation to the region at ODP Site 1172, and coincides with a global evolutionary turnover event within the diatoms and globally enhanced preservation of opal-A associated with global cooling (Baldauf and Barron 1990; Barron and Baldauf 1989; McGowran 1989).

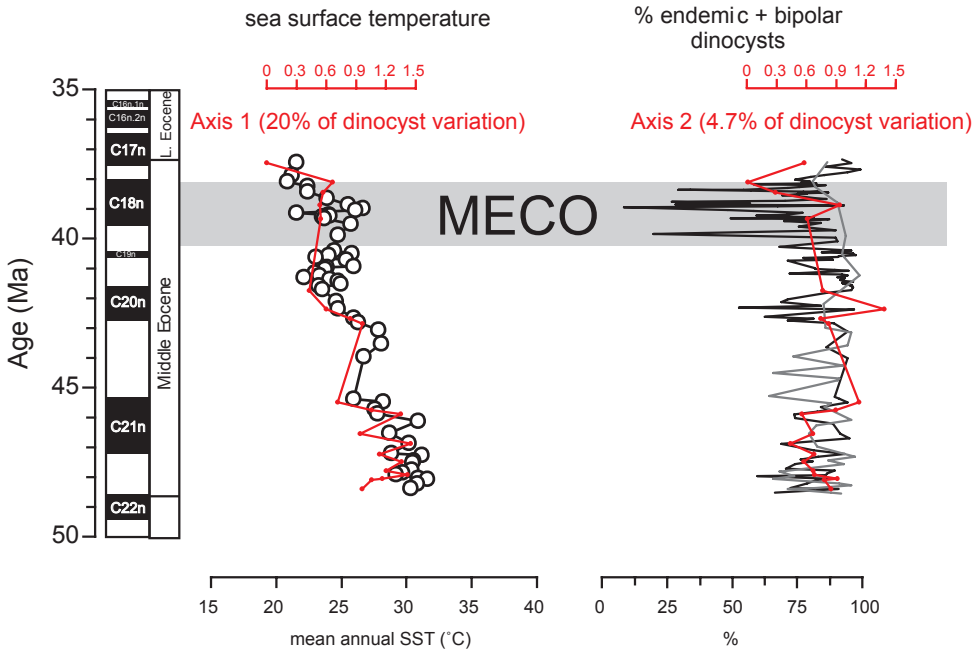


Figure 6. (left) Middle Eocene  $TEX_{86}$ -based SST curve from ODP Site 1172 (Chapter 2) overlain by the first axis scores of the middle Eocene DCCA experiment (in red; 20% of the dinocyst variation). The second axis scores correspond to (right) the % endemic dinocyst curve but explain only 4.7% of the variation in the dinocyst assemblage.

Increased weathering may have led to an additional nutrient supply to the oceans including both Si and the diatom bio-limiting nutrient Fe (Boyd et al., 2000). It appears plausible that the endemic dinocysts that proliferated during the earliest middle Eocene benefited from the same circulation changes and eutrophication phase



that stimulated diatom productivity at that time. Further evidence for changes in ocean-wide surface water fertility comes from thallium isotopes measured on ferromanganese crusts from the Pacific Ocean (Fig. 7; Nielsen et al., 2009). A shift in these isotopes together with a coeval shift in sulphur isotopes suggests a major ocean-wide increase in marine organic carbon export from 55 to 45 Ma. At the same time, deep-water carbon isotopic values between oceanic basins start to diverge, suggesting (among other possibilities) an increase in the biological pump leading to increased water mass aging gradients (Fig. 7; Sexton et al., 2006). The fertilization of the oceanic basins is, as suggested above, likely attributed to increased upwelling and weathering associated with global cooling and ever-increasing latitudinal gradients.

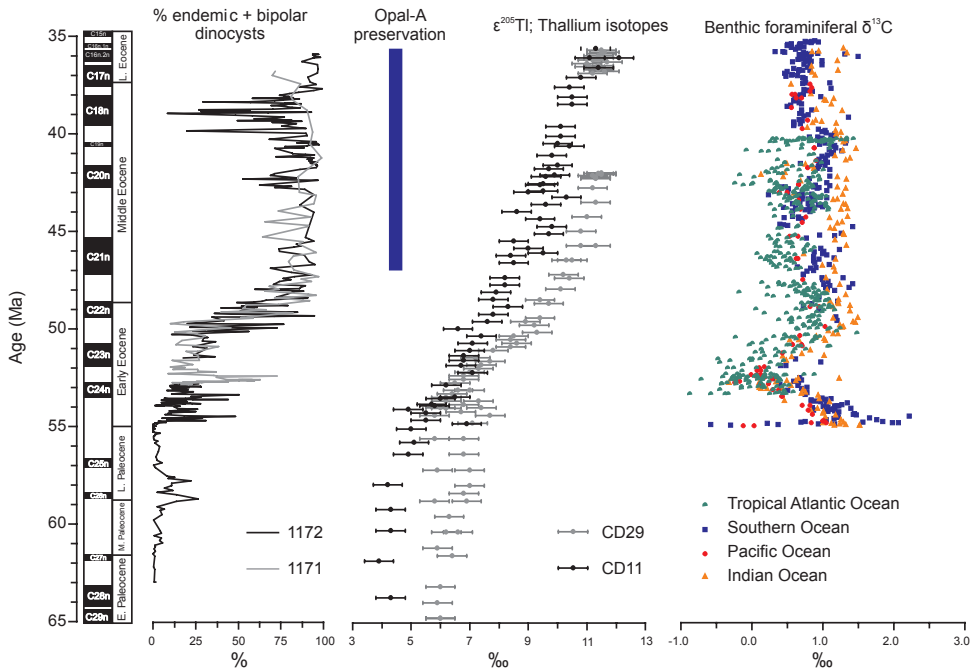
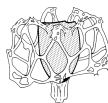


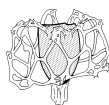
Figure 7. The relative abundance of endemic dinocysts at ODP Site 1172 (black) and Site 1171 (grey) show a major increase at 50 Ma. Opal-A preservation at ODP Site 1172 commenced between 45 Ma (Lazarus et al., 2008) and 47 Ma (Stickley et al., 2004a) probably as a result of increased latitudinal gradients stimulating upwelling and productivity (see text). Thallium isotope records from the Pacific Ocean, measured on two ferromanganese crusts labelled “CD11” (black) and “CD29” (grey), obtained from (Nielsen et al., 2009), show a major increase from 55 to 45 Ma, which has been shown to suggest a permanent increase in marine organic carbon productivity. Benthic foraminiferal carbon isotope data from the tropical Atlantic Ocean (half circles), Southern Ocean (squares), Pacific Ocean (circles), and Indian Ocean (triangles) diverge from ~50 Ma upward, indicating stronger carbon isotope gradients between oceanic basins, which may suggest increased carbon pumping (data from Sexton et al. (2006)).





## 5. Conclusions

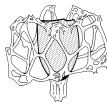
New data and reviews of previous reports allow a considerably improved spatio-temporal reconstruction of Paleogene circum-Antarctic dinocyst distribution patterns. Dinocysts can be divided into Antarctic endemic, bipolar, middle- to low-latitude, and cosmopolitan groups. Their spatial distribution patterns match ocean current patterns generated through GCM experiments (Huber et al., 2004) during the middle to late Eocene. Despite open connections between the Southern Ocean and adjacent mid-latitude oceans, (Exon et al., 2004), circum-Antarctic dinocyst assemblages switched from a cosmopolitan and low-latitude-derived dinoflagellate cyst assemblage to an endemic-dominated assemblage in the early middle Eocene. By numerically evaluating the relation between Southern Ocean dinocyst assemblages and the SST evolution at ODP Site 1172, we identify that SST was not the primary driving factor in the establishment of dominantly endemic dinocyst assemblages. We conjecture that ocean-wide surface water ocean fertility (Nielsen et al., 2009; Sexton et al., 2006) brought about at post-EECO cooling (Chapter 2; Sexton et al., 2006), helped to stimulate diatom production and 'switch on' opal preservation in the area and caused a rapid reorganization of high-latitude dinocyst assemblages. Once the endemic community became the dominant component of the dinocyst assemblages in the early middle Eocene southwest Pacific, the influence of SST variations on the dinocyst assemblage was stronger than during the Paleocene and early Eocene.



## Supplements to Chapter 3

Table S1: Site list

	Leg	Site	type	location	Long	Lat	depth	references	# of samples	bottom age (Ma)	% endemic dinocysts		
<b>Thanetian-Ypresian Boundary 56-54 Ma</b>													
	dspd	29	277	drill	campbell plateau	166.11	-52.13	1214	Kennett and Houtz, 1975; Hollis et al., 1997	2	56	5	
	odp	189	1172	drill	east tasman plateau	149.56	-43.58	2622	Eon et al., 2001/2004; Stujs et al., 2003; Brinkhuis et al., 2003a; Stickle et al., 2004a	>10	66	5	
				CF	brunswick peninsula	-71.33	-53.17	N/A	Quattrocchio and Sarjeant 2003 Quattrocchio, 2009	>10	62	5	
				MC	new zealand	174.00	-42.00	N/A	Strong et al., 1995	8	66	5	
				MH	outer new zealand	45.00	-45.00	N/A	Wilson, 1985; Crouch 2001	>10	56	5	
				PM	southeast tierra del fuego	-68.78	-54.67	N/A	Quattrocchio and Sarjeant, 2003	5	54	5	
				Taw	new zealand	169.53	-46.50	N/A	Crouch 2001	>10	57	5	
				WRH	seymour island	-56.17	-64.17	N/A	Wrenn and Hart, 1988	>10	58	10	
				Wop	new zealand	175.50	-41.40	N/A	Wilson, 1988; Crouch, 2001	>10	56	15	
	dspd	27	259	drill	off west australia	112.42	-29.37	4696	Veevers et al., 1974	N/A	N/A	barren	
	dspd	36	328	drill	east of falkland plateau	-36.40	-49.49	5095	Barker et al., 1976; Gombos (p. 575); Harris (p. 761)	N/A	N/A	barren	
	odp	113	689	drill	maud rise	3.06	-64.31	2080	Barker et al., 1988/1990; Florindo and Roberts, 2005; Diester-Haass and Zahn, 2001	N/A	N/A	barren	
	odp	113	690	drill	maud rise	1.12	-65.10	2914	Barker et al., 1988/1990; Florindo and Roberts, 2005;	N/A	N/A	barren	
	odp	114	698	drill	georgia rise	-33.06	-51.28	2138	Ciesielski et al., 1988/1991; Madlle and Monechi, 1991	N/A	N/A	barren	
	odp	114	699	drill	georgia rise	-30.41	-51.33	3706	Ciesielski et al., 1988/1991; Madlle and Monechi, 1991	N/A	N/A	barren	
	odp	114	700	drill	georgia rise	-30.16	-51.31	3601	Ciesielski et al., 1988/1991; Madlle and Monechi, 1991	N/A	N/A	barren	
	odp	114	698	drill	georgia rise	-33.06	-51.28	2138	Ciesielski et al., 1988/1991	N/A	N/A	barren	
	odp	114	702	drill	mid atlantic ridge	-26.22	-50.57	3083	Ciesielski et al., 1988/1991	N/A	N/A	barren	
	odp	119	738	drill	berquegen plateau	82.47	-62.43	2253	Barron et al., 1989	N/A	N/A	barren	
	odp	120	747	drill	berquegen plateau	76.48	-54.49	1695	Wise et al., 1989/1992	N/A	N/A	barren	
	odp	120	748	drill	berquegen plateau	78.59	-58.26	1288	Wise et al., 1989/1992; Mohr, 1990; Roberts et al., 2003	N/A	N/A	barren	
<b>Ypresian 53-51 Ma</b>													
	odp	189	1171	drill	south tasman rise	149.07	-48.30	2150	Eon et al., 2001/2004; Stujs et al., 2003	>10	54	30	
	odp	189	1172	drill	east tasman plateau	149.56	-43.58	2622	Eon et al., 2001/2004; Stujs et al., 2003; Brinkhuis et al., 2003a; Stickle et al., 2004a	>10	66	20	
				MC	new zealand	174.00	-42.00	N/A	Strong et al., 1995	5	66	5	
				MH	outer new zealand	45.00	-45.00	N/A	Wilson, 1985; Crouch, thesis 2001;	>10	56	5	
				PM	sotheast tierra del fuego	-68.78	-54.67	N/A	Quattrocchio and Sarjeant, 2003	5	54	0	
				Taw	new zealand	169.53	-46.50	N/A	Crouch, thesis 2001	>10	57	5	
				WRH	seymour island	-56.17	-64.17	N/A	Wrenn and Hart, 1988	>10	58	30	
	lodp	318	U1356	drill	wilkes land	136.05	-63.35	4003	Escutia et al., 2010	6	54	10	
				AFI	brunswick peninsula	-71.33	-53.17	N/A	Quattrocchio, 2009	>10	54	25	
	dspd	27	259	drill	off west australia	112.42	-29.37	4696	Veevers et al., 1974	N/A	N/A	barren	
	dspd	29	277	drill	campbell plateau	166.11	-52.13	1214	Kennett and Houtz, 1975; Hollis et al., 1997	N/A	N/A	barren	
	dspd	36	328	drill	east of falkland plateau	-36.40	-49.49	5095	Barker et al., 1976; Gombos (p. 575); Harris (p. 761)	N/A	N/A	barren	
	odp	113	689	drill	maud rise	3.06	-64.31	2080	Barker et al., 1988/1990; Florindo and Roberts, 2005; Diester-Haass and Zahn, 2001	N/A	N/A	barren	
	odp	113	690	drill	maud rise	1.12	-65.10	2914	Barker et al., 1988/1990; Florindo and Roberts, 2005;	N/A	N/A	barren	
	odp	114	698	drill	georgia rise	-33.06	-51.28	2138	Ciesielski et al., 1988/1991	N/A	N/A	barren	
	odp	114	699	drill	georgia rise	-30.41	-51.33	3706	Ciesielski et al., 1988/1991; Madlle and Monechi, 1991	N/A	N/A	barren	
	odp	114	700	drill	georgia rise	-30.16	-51.31	3601	Ciesielski et al., 1988/1991; Madlle and Monechi, 1991	N/A	N/A	barren	
	odp	114	698	drill	georgia rise	-33.06	-51.28	2138	Ciesielski et al., 1988/1991	N/A	N/A	barren	
	odp	114	702	drill	mid atlantic ridge	-26.22	-50.57	3083	Ciesielski et al., 1988/1991	N/A	N/A	barren	
	odp	119	738	drill	berquegen plateau	82.47	-62.43	2253	Barron et al., 1989	N/A	N/A	barren	
	odp	120	747	drill	berquegen plateau	76.48	-54.49	1695	Wise et al., 1989/1992	N/A	N/A	barren	
	odp	120	748	drill	berquegen plateau	78.59	-58.26	1288	Wise et al., 1989/1992; Mohr, 1990; Roberts et al., 2003	N/A	N/A	barren	
<b>Ypresian-Lutetian Boundary (50-48 Ma)</b>													
	dspd	29	283	drill	tasman sea	154.17	-43.55	4729	Kennett and Houtz 1975; Haskell and Wilson (p. 723); Warnar, 2006	>10	65	40	
	odp	189	1171	drill	south tasman rise	149.07	-48.30	2150	Eon et al., 2001/2004; Stujs et al., 2003	>10	54	60	
	odp	189	1172	drill	east tasman plateau	149.56	-43.58	2622	Eon et al., 2001/2004; Stujs et al., 2003; Brinkhuis et al., 2003a; Stickle et al., 2004a	>10	66	60	
				SON	grav	tasman margin (west)	144.25	-43.37	3726	Truswell, 1997	4	50	10
				SON	grav	tasman margin (west)	145.42	-43.47	3755	Truswell, 1997	4	50	25
				DF	outer	southeast tierra del fuego	-68.83	-53.88	N/A	Guxerin et al., 2008	4	48	45
				PM	outer	southeast tierra del fuego	-68.78	-54.67	N/A	Quattrocchio and Sarjeant, 2003	5	54	30
				WRH	outer	seymour island	-56.17	-64.17	N/A	Wrenn and Hart, 1988	>10	58	90
				WR	outer	New Zealand	172.00	-43.04	N/A	Hollis et al., 2009	>10	50	5
	lodp	318	U1356	drill	wilkes land	136.05	-63.35	4003	Escutia et al., 2010	6	54	10	
	dspd	26	255	drill	indian ocean (east)	93.44	-31.08	1144	Davies et al., 1974	N/A	N/A	barren	
	dspd	28	264	drill	offshore sw australia	112.03	-34.58	2873	Hayes et al., 1975	N/A	N/A	barren	
	dspd	29	277	drill	campbell plateau	166.11	-52.13	1214	Kennett and Houtz, 1975; Hollis et al., 1997	N/A	N/A	barren	
	dspd	30	287	drill	coral sea basin	153.16	-15.55	4653	Andrews et al., 1975	N/A	N/A	barren	
	dspd	36	328	drill	east of falkland plateau	-36.40	-49.49	5095	Barker et al., 1976; Gombos (p. 575); Harris (p. 761)	N/A	N/A	barren	
	dspd	40	360	drill	off south africa/aguilhas	18.06	-35.51	2949	Boll et al., 1978; McLachlan & Pieterse (p.857)	N/A	N/A	barren	
	dspd	40	361	drill	off south africa/aguilhas	15.27	-35.04	4549	Boll et al., 1978; McLachlan & Pieterse (p.857)	N/A	N/A	barren	
	odp	113	689	drill	maud rise	3.06	-64.31	2080	Barker et al., 1988/1990; Florindo and Roberts, 2005; Diester-Haass and Zahn, 2001	N/A	N/A	barren	
	odp	113	690	drill	maud rise	1.12	-65.10	2914	Barker et al., 1988/1990; Florindo and Roberts, 2005; Diester-Haass and Zahn, 2001	N/A	N/A	barren	
	odp	114	698	drill	georgia rise	-33.06	-51.28	2138	Ciesielski et al., 1988/1991	N/A	N/A	barren	
	odp	114	699	drill	georgia rise	-30.41	-51.33	3706	Ciesielski et al., 1988/1991; Madlle and Monechi, 1991	N/A	N/A	barren	
	odp	114	700	drill	georgia rise	-30.16	-51.31	3601	Ciesielski et al., 1988/1991; Madlle and Monechi, 1991	N/A	N/A	barren	
	odp	114	701	drill	mid atlantic ridge	-23.13	-51.59	4637	Ciesielski et al., 1988/1991	N/A	N/A	barren	
	odp	114	702	drill	mid atlantic ridge	-26.22	-50.57	3083	Ciesielski et al., 1988/1991	N/A	N/A	barren	
	odp	114	703	drill	meteor rise	7.54	-47.03	1796	Ciesielski et al., 1988/1991; Madlle and Monechi, 1991	N/A	N/A	barren	
	odp	119	737	drill	berquegen heard plateau	73.02	-50.18	344	Barron et al., 1989; Wet and Thierstein, 1991	N/A	N/A	barren	
	odp	119	738	drill	berquegen plateau	82.47	-62.43	2253	Barron et al., 1989	N/A	N/A	barren	
	odp	120	747	drill	berquegen plateau	76.48	-54.49	1695	Wise et al., 1989/1992	N/A	N/A	barren	
	odp	120	748	drill	berquegen plateau	78.59	-58.26	1288	Wise et al., 1989/1992; Mohr, 1990; Roberts et al., 2003	N/A	N/A	barren	
	odp	120	749	drill	berquegen plateau	76.24	-58.43	1071	Wise et al., 1989/1992	N/A	N/A	barren	
	odp	120	750	drill	berquegen plateau	81.14	-57.35	2030	Wise et al., 1989/1992	N/A	N/A	barren	
	odp	183	1135	drill	berquegen plateau (s)	84.16	-59.42	1567	Coffin et al., 2008; 2003	N/A	N/A	barren	
	odp	183	1136	drill	berquegen plateau (s)	84.50	-59.39	1930	Coffin et al., 2008; 2003	N/A	N/A	barren	
	odp	183	1138	drill	berquegen plateau	75.59	-53.33	1141	Coffin et al., 2000; 2003; Bohaty and Zachos, 2003	N/A	N/A	barren	
<b>mid-Lutetian (47-45 Ma)</b>													
	dspd	29	283	drill	tasman sea	154.17	-43.55	4729	Kennett and Houtz, 1975; Hollis et al., 1997	>10	65	40	
	odp	189	1171	drill	south tasman rise	149.07	-48.30	2150	Eon et al., 2001/2004; Stujs et al., 2003	>10	54	80	
	odp	189	1172	drill	east tasman plateau	149.56	-43.58	2622	Eon et al., 2001/2004; Stujs et al., 2003; Brinkhuis et al., 2003a; Stickle et al., 2004a	>10	66	85	



# SOUTHERN OCEAN DINOCCYST BIOGEOGRAPHY

sonne 36, 22d	SON	grav	tasman margin (west)	144.25	-43.37	3726	Truswell, 1997		4	50	10
sonne 36, 30d	SON	grav	tasman margin (west)	145.42	-43.47	1755	Truswell, 1997		4	50	25
la despedida fm.	DF	outer	northeast tierra del fuego	-68.83	-53.88	N/A	Guerstein et al., 2008		6	48	75
península mitre	PM	outer	southeast tierra del fuego	-68.78	-54.67	N/A	Quattrocchio and Sarjeant, 2003		3	54	30
	W&H	outer	seymour island	-56.17	-64.17	N/A	Wrenn and Hart, 1988		>10	58	90
Wajapar river	WR	outer	New Zealand	172.00	-43.04	N/A	Hollis et al., 2009		>10	50	5
<b>mid-Lutetian (44-42 Ma)</b>											
dsdp 29	277	drill	campbell plateau	166.11	-52.13	1214	Kennett and Houtz, 1975; Hollis et al., 1997		3	56	0
dsdp 29	280	drill	tasmania	147.14	-48.57	4176	Kennett and Houtz, 1975; Hasckell and Wilson (p. 723); Perch-Nielsen (p. 873); Crouch & Hollis 1996		6	49	80
dsdp 29	281	drill	tasmania	147.46	-47.60	1591	Kennett and Houtz, 1975; Hasckell and Wilson (p. 723); Perch-Nielsen (p. 873); Crouch & Hollis 1996		2	44	90
oep 113	696	drill	weddell sea	-42.56	-61.51	650	Barker et al., 1988/1990; Mao and Mohr, 1995; Wise et al., 1989/1992		>10	43	90
oep 120	748	drill	herguelen plateau	78.59	-58.26	1288	Wise et al., 1989/1992; Mohr, 1990; Roberts et al., 2003		>10	92	20
oep 189	1171	drill	south tasman rise	149.07	-48.30	2150	Exon et al., 2001/2004; Shajis et al., 2003		>10	54	90
oep 189	1172	drill	east tasman plateau	149.56	-43.58	2622	Exon et al., 2001/2004; Shajis et al., 2003; Brinkhuis et al., 2003a; Stickleby et al., 2004a		>10	66	80
ago 147, dr14	AG20	dred	tasman margin (west)	144.19	-45.02	4100	Truswell, 1997		1	45	75
ago 147, dr13	AG20	dred	south tasman rise	144.57	-45.47	3450	Truswell, 1997		1	45	75
ago 147, gc01	AG20	grav	tasman margin (west)	144.11	-44.10	4264	Truswell, 1997		1	45	75
gaviotin	PdE	drill	off uruguay	-54.75	-36.62	N/A	Daners et al., 2004; Guerstein and Daners, in press		3	44	35
pejerrey	CB	drill	offshore argentina	-55.50	-38.83	N/A	Archangelczyk et al., 1997; Guerstein and Daners, in press		5	44	30
la despedida fm.	DF	outer	northeast tierra del fuego	-68.83	-53.88	N/A	Guerstein et al., 2008		6	48	75
la meseta fm.	Dj27	outer	seymour island	-58.45	-64.10	N/A	Cocozza and Clarke, 1992		10	45	75
muzzle group	MC	outer	new zealand	174.00	-42.00	N/A	Holdgate et al., 1995; 2000; 2003; Macphail, 2001		3	45	90
moeraki-hampden	MS	outer	new zealand	45.00	-45.00	N/A	Wilson, 1967a; Burgess, 2008		>10	43	14
rio turbio	MH	outer	memurdo sound	-166.50	-78.08	N/A	Wilson, 1967a; Cranwell et al., 1960; Cranwell 1964		4	44	90
santos b.	SanB	drill	off brazil	-45.00	-35.00	N/A	Griggs, 1981 in Wrenn and Hart, 1988	unknown	8	46	70
clam-1	SB	drill	sorell basin	144.15	-40.50	N/A	(Esso) Boreham et al., 2002		4	45	0
cape sorell-1	SB	drill	sorell basin	145.02	-42.08	94	Amoco, 1982		4	45	0
serape basin	SE-2	core	serape basin, offshore brazil	-37.80	-11.20	N/A	Ferreira, 2004 in Guerstein and Daners, in press		>10	44	5
	W&H	outer	seymour island	-56.17	-64.17	N/A	Wrenn and Hart, 1988		>10	58	90
<b>Bartonian (41-39 Ma)</b>											
dsdp 29	277	drill	campbell plateau	166.11	-52.13	1214	Kennett and Houtz, 1975; Hollis et al., 1997		1	56	0
dsdp 29	280	drill	tasmania	147.14	-48.57	4176	Kennett and Houtz, 1975; Hasckell and Wilson (p. 723); Perch-Nielsen (p. 873); Crouch & Hollis 1996		6	49	95
dsdp 71	512	drill	north of weddell sea	-40.52	-49.52	1846	Ludwig et al., 1983; Goodman & Ford (p. 859)		10	42	60
oep 113	696	drill	weddell sea	-42.56	-61.51	650	Barker et al., 1988/1990; Mao and Mohr, 1995; Wise et al., 1989/1992		>10	43	95
oep 120	748	drill	herguelen plateau	78.59	-58.26	1288	Wise et al., 1989/1992; Mohr, 1990; Roberts et al., 2003		>10	92	5
oep 177	1090	drill	agulhas ridge	8.54	-42.55	3710	Gersonde et al., 1999; 2001; Latimer and Filippelli, 2002		>10	42	0
oep 189	1170	drill	south tasman rise	146.03	-47.09	2704	Exon et al., 2001/2004; Shajis et al., 2003		>10	41	90
oep 189	1171	drill	south tasman rise	149.07	-48.30	2150	Exon et al., 2001/2004; Shajis et al., 2003		>10	54	93
oep 189	1172	drill	east tasman plateau	149.56	-43.58	2622	Exon et al., 2001/2004; Shajis et al., 2003; Brinkhuis et al., 2003a; Stickleby et al., 2004a		>10	66	80
gaviotin	PdE	drill	off uruguay	-54.75	-36.62	N/A	Daners et al., 2004; Guerstein and Daners, in press		3	44	35
pejerrey	CB	drill	offshore argentina	-55.50	-38.83	N/A	Archangelczyk et al., 1997; Guerstein and Daners, in press		5	44	30
la despedida fm.	DF	outer	northeast tierra del fuego	-68.83	-53.88	N/A	Guerstein et al., 2008		6	48	75
la meseta fm.	Dj27	outer	seymour island	-58.45	-64.10	N/A	Cocozza and Clarke, 1992		10	45	90
muzzle group	MC	outer	new zealand	174.00	-42.00	N/A	Strong et al., 1995		4	46	5
Hampden section	MS	outer	new zealand	45.00	-45.00	N/A	Burgess et al., 2008		>10	42	15
rio turbio	MH	outer	memurdo sound	-166.50	-78.08	N/A	Wilson, 1967a; Cranwell et al., 1960; Cranwell 1964		4	44	95
santos b.	SanB	drill	southwest santa cruz	-72.30	-35.50	N/A	Archangelczyk, 1969; Guerstein, pers. obs.		7	45	35
santos b.	SanB	drill	off brazil	-45.00	-35.00	N/A	Griggs, 1981 in Wrenn and Hart, 1988	unknown	4	45	0
clam-1	SB	drill	sorell basin	144.15	-40.50	102	(Esso) Boreham et al., 2002		4	45	0
cape sorell-1	SB	drill	sorell basin	145.02	-42.08	94	Amoco, 1982		4	45	0
ago 147, dr14	AG20	grav	tasman margin (west)	144.11	-44.10	4264	Truswell, 1997		1	45	60



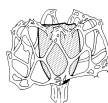
agso 147, dr18	AGZO	dred	tasman margin (west)	144.19	-45.02	4100	Truswell, 1997	1	45	60	
agso 147, geo1	AGZO	dred	south tasman rise	144.57	-46.47	3450	Truswell, 1997	1	45	60	
	W&H	outcr	seymour island	-56.17	-64.17	N/A	Wrenn and Hart, 1988	>10	58	95	
dmdp	26	255	drill	indian ocean (east)	93.44	-31.08	1144	Davies et al., 1974	N/A	N/A	barren
dmdp	28	264	drill	offshore sw australia	112.03	-34.58	2873	Hayes et al., 1975	N/A	N/A	barren
dmdp	28	274	drill	ross sea (nw)	173.26	-68.60	3305	Hayes et al., 1975; Kemp, 1975	N/A	N/A	barren
dmdp	29	281	drill	tasmania	147.46	-47.60	1591	Kennett and Houtz, 1975; Haskell and Wilson (p. 723); Perch-Nielsen (p. 875); Crouch & Hollis 1996	N/A	N/A	barren
dmdp	29	282	drill	tasmania	143.29	-42.15	4202	Kennett and Houtz, 1975; Haskell and Wilson (p. 723)	N/A	N/A	barren
dmdp	30	286	drill	south new hebrides trench	166.22	-16.32	4465	Andrews et al., 1975	N/A	N/A	barren
dmdp	30	289	drill	Ontong-Java Plateau	158.30	0.29	2206	Andrews et al., 1975	N/A	N/A	barren
dmdp	36	328	drill	east of fallland plateau	-36.40	-49.49	5095	Barker et al., 1976; Gombos (p. 575); Harris (p. 761)	N/A	N/A	barren
dmdp	40	360	drill	off south africa/aguhas	18.06	-35.51	2949	Boll et al., 1978; McLachlan & Pieterse (p.857)	N/A	N/A	barren
dmdp	40	361	drill	off south africa/aguhas	15.27	-35.04	4549	Boll et al., 1978; McLachlan & Pieterse (p.857)	N/A	N/A	barren
dmdp	90	593	drill	tasman sea	167.40	-40.30	1068	Kennett et al., 1986	N/A	N/A	barren
odp	113	689	drill	maud rise	3.06	-64.31	2080	Barker et al., 1988/1990; Florindo and Roberts, 2005;	N/A	N/A	barren
odp	113	690	drill	maud rise	1.12	-65.10	2914	Barker et al., 1988/1990; Florindo and Roberts, 2005;	N/A	N/A	barren
odp	114	698	drill	georgia rise	-33.06	-51.28	2138	Ciesielski et al., 1988/1991	N/A	N/A	barren
odp	114	699	drill	georgia rise	-30.41	-51.33	3706	Ciesielski et al., 1988/1991; Madlle and Monechi, 1991	N/A	N/A	barren
odp	114	701	drill	mid atlantic ridge	-23.13	-51.59	4637	Ciesielski et al., 1988/1991	N/A	N/A	barren
odp	114	702	drill	mid atlantic ridge	-26.22	-50.57	3083	Ciesielski et al., 1988/1991	N/A	N/A	barren
odp	114	703	drill	metoor rise	7.54	-47.03	1796	Ciesielski et al., 1988/1991; Madlle and Monechi, 1991	N/A	N/A	barren
odp	119	738	drill	kerguelen plateau	82.47	-62.43	2253	Barron et al., 1989	N/A	N/A	barren
odp	120	747	drill	kerguelen plateau	76.48	-54.49	1695	Wise et al., 1989/1992	N/A	N/A	barren
odp	120	749	drill	kerguelen plateau	76.24	-58.43	1071	Wise et al., 1989/1992	N/A	N/A	barren
odp	182	1124	drill	eye terrace	128.04	-33.31	784	Feary et al., 2000; Li et al., 2003a, 2003b	N/A	N/A	barren
odp	182	1128	drill	great australian hight	127.70	-34.50	3874	Feary et al., 2000; Li et al., 2003a, 2003b	N/A	N/A	barren
odp	183	1135	drill	kerguelen plateau (e)	84.16	-59.42	1567	Coffin et al., 2000; 2003	N/A	N/A	barren
odp	183	1136	drill	kerguelen plateau (s)	84.50	-59.39	1930	Coffin et al., 2000; 2003	N/A	N/A	barren
odp	183	1138	drill	kerguelen plateau	75.59	-53.33	1141	Coffin et al., 2000; 2003; Bohaty and Zachos, 2003	N/A	N/A	barren
<b>Bartonian-Präbian Boundary (38-36 Ma)</b>											
ciros	1	CIROS	drill	ross sea	164.30	-77.05	200	Barrett, 1989; Hannah, 1994; 1997; Coccioni and Galeotti, 1997; Hannah et al., 1997; Wilson et al., 1998	10	37	90
dmdp	28	269	drill	antarctic margin	140.04	-61.41	4282	Hayes et al., 1975	>10	37	5
dmdp	28	274	drill	ross sea (nw)	173.26	-68.60	3305	Hayes et al., 1975; Kemp, 1975	>10	40	90
dmdp	29	277	drill	campbell plateau	166.11	-52.13	1214	Unpublished data: Bijl, Houben Stuijs, Brinkhuis, pers. obs.	>10	56	0
dmdp	29	280	drill	tasmania	147.14	-48.57	4176	Kennett and Houtz, 1975; Haskell and Wilson (p. 723); Perch-Nielsen (p. 875); Crouch & Hollis 1996	6	49	90
dmdp	29	281	drill	tasmania	147.46	-47.60	1591	Kennett and Houtz, 1975; Haskell and Wilson (p. 723); Perch-Nielsen (p. 875); Crouch & Hollis 1996	8	44	90
dmdp	29	282	drill	tasmania	143.29	-42.15	4202	Kennett and Houtz, 1975; Haskell and Wilson (p. 723)	>10	40	10
dmdp	29	283	drill	tasman sea	154.17	-43.55	4729	Kennett and Houtz, 1975; Haskell and Wilson (p. 723)	>10	65	80
dmdp	71	511	drill	north of weddell sea	-46.58	-51.00	2589	Ludwig et al., 1983; Goodman & Ford (p. 859); Wise, 1983	3	37	50
odp	113	696	drill	weddell sea	-42.56	-61.51	650	Barker et al., 1988/1990; Mao and Mohr, 1995;	>10	43	90
odp	119	739	drill	prydz bay	75.05	-67.17	412	Barron et al., 1989; Truswell, 1991; Wei and Thierstein, 1991	>10	37	80
odp	119	742	drill	prydz bay	75.24	-67.33	416	Barron et al., 1989; Truswell, 1991	>10	37	90
odp	120	748	drill	kerguelen plateau	78.59	-58.26	1288	Wise et al., 1989/1992; Mohr, 1990; Roberts et al., 2003	>10	92	18
odp	177	1090	drill	aguhas ridge	8.54	-42.55	3710	Gersonde et al., 1999; 2001; Latimer and Fillipelli, 2002;	>10	42	0
odp	189	1168	drill	tasman margin (west)	144.25	-42.37	2463	Exon et al., 2001/2004; Stuijs et al., 2003; Brinkhuis et al., 2003b	>10	37	10
odp	189	1170	drill	south tasman rise	146.03	-47.09	2704	Exon et al., 2001/2004; Stuijs et al., 2003	>10	41	90
odp	189	1171	drill	south tasman rise	149.07	-48.30	2150	Exon et al., 2001/2004; Stuijs et al., 2003	>10	54	76
odp	189	1172	drill	east tasman plateau	149.56	-43.58	2622	Exon et al., 2001/2004; Stuijs et al., 2003; Brinkhuis et al., 2003a; Stickley et al., 2004a	>10	66	93
pejerrey	pejerrey	CB	drill	offshore argentina	-55.50	-38.83	N/A	Archangelsky et al., 1997	7	44	5
brown's creek	BC	outcr	drill	south australian margin	138.65	-34.59	N/A	Cookson and Eisenack, 1965; Shafik, 1996; Shafik and Idnurn, 1997	2	37	0
	GB	drill	gippsland basin	136.70	-38.30	N/A	Holdgate et al., 1995; 2000; 2003; Macphail, 2001	10	45	90	
	MB	drill	murray basin	141.00	-34.00	N/A	Martin, 1991; 1992	4	37	0	
ria turbida	RT	core	drill	southwest santa cruz	72.30	-51.50	N/A	Archangelsky, 1969; Garstein, pers. obs.	7	45	35
te kniit group	TK	outcr	drill	new zealand	174.00	-37.00	N/A	Pocknall, 1991; Edbrokke et al., 1998	6	37	10
	W&H	outcr	drill	seymour island	-56.17	-64.17	N/A	Wrenn and Hart, 1988	>10	58	80
dmdp	26	253	drill	ninetyeast drill	87.22	-24.53	1962	Davies et al., 1974	N/A	N/A	barren
dmdp	28	264	drill	offshore sw australia	112.03	-34.58	2873	Hayes et al., 1975	N/A	N/A	barren
dmdp	28	267	drill	antarctic margin	104.29	-59.16	4522	Hayes et al., 1975	N/A	N/A	barren
dmdp	29	277	drill	campbell plateau	166.11	-52.13	1214	Kennett and Houtz, 1975; Hollis et al., 1997	N/A	N/A	barren
dmdp	30	286	drill	south new hebrides trench	166.22	-16.32	4465	Andrews et al., 1975	N/A	N/A	barren
dmdp	40	360	drill	off south africa/aguhas	18.06	-35.51	2949	Boll et al., 1978; McLachlan & Pieterse (p.857)	N/A	N/A	barren
dmdp	40	361	drill	off south africa/aguhas	15.27	-35.04	4549	Boll et al., 1978; McLachlan & Pieterse (p.857)	N/A	N/A	barren
dmdp	90	593	drill	tasman sea	167.40	-40.30	1068	Kennett et al., 1986	N/A	N/A	barren
odp	113	689	drill	maud rise	3.06	-64.31	2080	Barker et al., 1988/1990; Florindo and Roberts, 2005;	N/A	N/A	barren
odp	113	690	drill	maud rise	1.12	-65.10	2914	Barker et al., 1988/1990; Florindo and Roberts, 2005;	N/A	N/A	barren
odp	114	699	drill	georgia rise	-30.41	-51.33	3706	Ciesielski et al., 1988/1991; Madlle and Monechi, 1991	N/A	N/A	barren
odp	114	700	drill	georgia rise	-30.16	-51.31	3601	Ciesielski et al., 1988/1991; Madlle and Monechi, 1991	N/A	N/A	barren
odp	114	701	drill	mid atlantic ridge	-23.13	-51.59	4637	Ciesielski et al., 1988/1991	N/A	N/A	barren
odp	114	702	drill	mid atlantic ridge	-26.22	-50.57	3083	Ciesielski et al., 1988/1991	N/A	N/A	barren
odp	114	703	drill	metoor rise	7.54	-47.03	1796	Ciesielski et al., 1988/1991; Madlle and Monechi, 1991	N/A	N/A	barren
odp	114	704	drill	metoor rise	7.25	-46.52	2532	Ciesielski et al., 1988/1991	N/A	N/A	barren
odp	119	737	drill	kerguelen-beard plateau	73.02	-50.14	564	Barron et al., 1989; Wei and Thierstein, 1991	N/A	N/A	barren
odp	119	738	drill	kerguelen plateau	82.47	-62.43	2253	Barron et al., 1989	N/A	N/A	barren
odp	119	744	drill	kerguelen plateau	80.35	-61.35	2307	Barron et al., 1989; Wei and Thierstein, 1991; Robert et al., 2003	N/A	N/A	barren
odp	120	747	drill	kerguelen plateau	76.48	-54.49	1695	Wise et al., 1989/1992	N/A	N/A	barren
odp	120	749	drill	kerguelen plateau	76.24	-58.43	1071	Wise et al., 1989/1992	N/A	N/A	barren
odp	181	1124	drill	esholo drift	176.53	-39.50	3978	Carter et al., 1999; 2002; McConigal and di Stefano, 2002	N/A	N/A	barren
odp	182	1126	drill	eye terrace	128.04	-33.31	784	Feary et al., 2000; Li et al., 2003a, 2003b	N/A	N/A	barren
odp	182	1128	drill	great australian hight	127.70	-34.50	3874	Feary et al., 2000; Li et al., 2003a, 2003b	N/A	N/A	barren
odp	182	1134	drill	eye terrace	127.16	-33.32	701	Feary et al., 2000; Li et al., 2003a, 2003b	N/A	N/A	barren
odp	183	1137	drill	slan bank	68.06	-56.50	1005	Coffin et al., 2000; 2003	N/A	N/A	barren
odp	183	1138	drill	kerguelen plateau	75.59	-53.33	1141	Coffin et al., 2000; 2003; Bohaty and Zachos, 2003	N/A	N/A	barren



SOUTHERN OCEAN DINOCYST BIOGEOGRAPHY

Table S2: Dinocyst species

taxon	type	first decided from	
<i>Achomospaera ramulifera</i>	cosmopolitan	Europe	
<i>Adnatosphaeridium multispinosum</i>	cosmopolitan	North Sea Basin	
<i>Aiorea fenestrata</i>	endemic	South Australian Magin	
<i>Alterbidinium acutulum</i>	endemic SO	New Zealand	
<i>Alterbidinium distinctum</i>	endemic "TF"	McMurdo Sound	
<i>Apectodinium homomorphum</i>	(mid)-low Lat	South Australian Magin	
<i>Aptodinium australiense</i>	mid-low Lat	South Australian Magin	
<i>Arachnodinium antarcticum</i>	endemic "TF"	Antarctica	
<i>Areoligera</i> spp.	mid-low Lat	Europe	
<i>Batiacasphaera cassicola</i>	endemic SO	New Zealand	
<i>Batiacasphaera compta</i>	mid-low Lat	USA	
<i>Batiacasphaera</i> sp. A, B, C, D	endemic SO	East Tasman Plateau	Brinkhuis et al., 2003a, b
<i>Batiacasphaera</i> spp.	mid-low Lat	USA	
<i>Brigantedinium pynei</i>	Antarctic	Ross Sea	
<i>Brigantedinium</i> spp.	mid-low Lat	UK	
<i>Caligodinium</i> spp.	mid-low Lat	USA	
<i>Carpatella</i> spp.	mid-low Lat	Middle Europe	
<i>Cassidium filosum</i>	mid-low Lat	New Zealand	
<i>Cassidium fragile</i>	mid-low Lat	Australia	
<i>Cerebrocysta bartonensis</i>	mid-low Lat	North Sea Basin	
<i>Cerebrocysta</i> sp. A, B, C	endemic SO	East Tasman Plateau	Brinkhuis et al., 2003a, b
<i>Cerebrocysta</i> spp.	mid-low Lat	North Sea Basin	
<i>Cerodinium dartmoorium</i>	mid-low Lat	South Australian Magin	
<i>Cerodinium depressum</i>	mid-low Lat	Northwest Europe	
<i>Cerodinium</i> sp. A	endemic SO	East Tasman Plateau	Brinkhuis et al., 2003a
<i>Cerodinium speciosum</i>	mid-low Lat	Europe	
<i>Cerodinium striatum</i>	mid-low Lat	USA	
<i>Charlesdowniea coleothrypta</i>	mid-low Lat	UK	
<i>Charlesdowniea edwardsii</i>	mid-low Lat	New Zealand	
<i>Cleistosphaeridium ancyreum</i>	mid-low Lat	South Australian Magin	
<i>Cleistosphaeridium diversispinosum</i>	mid-low Lat	Europe	
<i>Cleistosphaeridium placacanthum</i>	mid-low Lat	South Australian Magin	
<i>Cleistosphaeridium</i> spp.	mid-low Lat	Middle Europe	
<i>Cordosphaeridium fibrospinosum</i>	mid-low Lat	Europe	
<i>Cordosphaeridium minimum</i>	mid-low Lat	Northwest Europe	
<i>Corrudinium incompositum</i>	mid-low Lat	USA	
<i>Corrudinium obscurum</i>	endemic SO	New Zealand	
<i>Corrudinium regulare</i>	endemic "TF"	Falkland Plateau	
<i>Cribroperidinium</i> spp.	cosmopolitan	UK	
<i>Damassadinium crassimuratum</i>	cosmopolitan	New Zealand	
<i>Dapsilidinium</i> spp.	mid-low Lat	North Sea Basin	
<i>Deflandrea antarctica</i>	endemic "TF"	McMurdo Sound	
<i>Deflandrea convexa</i>	endemic "TF"	New Zealand	
<i>Deflandrea cygniformis</i>	endemic "TF"	Southern Argentina	
<i>Deflandrea granulata</i>	mid-low Lat	Southern Argentina	
<i>Deflandrea phosphoritica</i> complex	mid-low Lat	Europe	
<i>Deflandrea scabrata</i>	endemic SO	New Zealand	
<i>Deflandrea</i> sp. A	endemic "TF"	East Tasman Plateau	Brinkhuis et al., 2003a
<i>Dinopterygium</i> sp. A	endemic SO	East Tasman Plateau	Brinkhuis et al., 2003a
<i>Dinopterygium</i> spp.	mid-low Lat	Europe	
<i>Diphyes colligerum</i>	cosmopolitan	South Australian Magin	
<i>Distatodinium paradoxum</i>	mid-low Lat	Europe	
<i>Dracodinium wai-pawaense</i>	endemic SO	New Zealand	
<i>Elytrocysta brevis</i> ( <i>Membranosphaera</i> spp.)	mid-low Lat	North Sea Basin	
<i>Enneadocysta dictyostila</i>	endemic "TF"	McMurdo Sound	
<i>Enneadocysta multicornuta</i>	mid-low Lat	North Sea Basin	
<i>Enneadocysta pectiniformis</i>	mid-low Lat	North Sea Basin	
<i>Eacludopyxis peniculata</i>	mid-low Lat	Northwest Europe	
<i>Gelatia inflata</i>	bipolar	North Sea Basin	
<i>Gippslandia extensa</i>	endemic "TF"	Southeast Australia	
<i>Glaphrocysta delicata</i>	mid-low Lat	New Zealand	
<i>Glaphrocysta divaricata</i>	mid-low Lat	North Sea Basin	
<i>Glaphrocysta intricata</i>	mid-low Lat	North Sea Basin	
<i>Glaphrocysta ordinata</i>	mid-low Lat	North Sea Basin	
<i>Glaphrocysta pastelsii</i>	mid-low Lat	South Australian Magin	
<i>Glaphrocysta retintexta</i>	mid-low Lat	South Australian Magin	
<i>Hemiplacophora semilumifera</i>	mid-low Lat	South Australian Magin	
<i>Histiocysta</i> spp.	mid-low Lat	Europe, USA	
<i>Homotryblum tasmaniense</i>	mid-low Lat	South Australian Magin	
<i>Hystrichokolpoma bullatum</i>	mid-low Lat	New Zealand	
<i>Hystrichokolpoma pusillum</i>	mid-low Lat	Europe	
<i>Hystrichokolpoma rigaudae</i>	mid-low Lat	South Australian Magin	
<i>Hystrichokolpoma spinosum</i>	mid-low Lat	New Zealand	
<i>Hystrichokolpoma truncatum</i>	mid-low Lat	Europe	
<i>Hystrichosphaeridium truswelliae</i>	endemic "TF"	Seymour Island	
<i>Hystrichosphaeridium tubiferum</i>	mid-low Lat	Middle Europe	
<i>Hystrichosphaeropsis</i> spp.	mid-low Lat	Europe	
<i>Hystrichostrogylon membraniphora</i>	cosmopolitan	Europe	
<i>Impagidinium aculeatum</i>	mid-low Lat	Australia	
<i>Impagidinium cassiculum</i>	mid-low Lat	New Zealand	
<i>Impagidinium crassimuratum</i>	mid-low Lat	New Zealand	
<i>Impagidinium dispersitum</i>	mid-low Lat	South Australian Magin	
<i>Impagidinium maculatum</i>	mid-low Lat	South Australian Magin	
<i>Impagidinium parvireticulatum</i>	mid-low Lat	New Zealand	
<i>Impagidinium velorum</i>	mid-low Lat	North Sea Basin	



<i>Impagidinium victorianum</i>	mid-low Lat	South Australian Magin	
<i>Impletosphaeridium clavus</i>	endemic SO	Seymour Island	
<i>Impletosphaeridium</i> spp.	mid-low Lat	Northwest Europe	
<i>Lejeuneocysta cowiei</i>	Antarctic	Ross Sea	
<i>Lejeuneocysta fallax</i>	mid-low Lat	Northwest Europe	
<i>Lejeuneocysta hyalina</i>	mid-low Lat	North Sea Basin	
<i>Lejeuneocysta</i> spp.	mid-low Lat	Europe	
<i>Lingulodinium bergmannii</i>	mid-low Lat	Argentina	
<i>Lingulodinium machaerophorum</i>	cosmopolitan	South Australian Magin	
<i>Lophocysta</i> spp.	mid-low Lat	Northern Europe	
<i>Membranophoridium perforatum</i>	endemic SO	New Zealand	
<i>Moria zachosi</i>	endemic "TF"	East Tasman Plateau	
<i>Nematospaeropsis</i> spp. (most)	cosmopolitan	South Australian Magin	
<i>Octodinium askinae</i>	endemic "TF"	Seymour Island	
<i>Operculodinium centrocarpum</i> complex	cosmopolitan	South Australian Magin	
<i>Operculodinium</i> sp. A	endemic SO	East Tasman Plateau	Brinkhuis et al., 2003a
<i>Operculodinium</i> sp. B	endemic SO	East Tasman Plateau	Brinkhuis et al., 2003a
<i>Palaeocystodinium australinum</i>	mid-low Lat	South Australian Magin	
<i>Palaeocystodinium golzowense</i>	mid-low Lat	North Sea Basin	
<i>Palaeoperidinium pyrophorum</i>	mid-low Lat	Middle Europe	
<i>Palaeotetradinium minisculum</i>	mid-low Lat	North Sea Basin	
<i>Paucisphaeridium</i> sp. A	cosmopolitan	East Tasman Plateau	new species
<i>Paucisphaeridium inversibuccinum</i>	mid-low Lat	Europe	
<i>Pentadinium laticinctum</i>	mid-low Lat	North Sea Basin	
<i>Phelodinium cranwelliae</i>	Antarctic	Ross Sea	
<i>Phelodinium harringtonii</i>	Antarctic	McMurdo Sound	
<i>Phthanoperidinium alectrolaphum</i>	mid-low Lat	North Sea Basin	
<i>Phthanoperidinium antarcticum</i>	endemic "TF"	Scotia Sea, Antarctica	
<i>Phthanoperidinium comatum</i>	mid-low Lat	Northwest Europe	
<i>Phthanoperidinium crenulatum</i>	mid-low Lat	Europe	
<i>Phthanoperidinium</i> sp. A	endemic "TF"	Falkland Plateau	new species
<i>Phthanoperidinium</i> sp. B	endemic "TF"	Falkland Plateau	new species
<i>Phthanoperidinium</i> sp. C	endemic "TF"	Kerguelen, Antarctica	new species
<i>Phthanoperidinium stockmansii</i>	bipolar	Southern England	
<i>Polyosphaeridium subtile</i>	mid-low Lat	Europe	
<i>Pxydinopsis</i> spp. (most)	mid-low Lat	Northern Europe	
<i>Pxydinopsis waiapawaensis</i> group	endemic SO	New Zealand	
<i>Rhombodinium rhomboidesum</i>	mid-low Lat	North Sea Basin	
<i>Saetodinium tasmanense</i>	endemic "TF"	Southeast Australia	
<i>Samlandia chlamydophora</i>	mid-low Lat	Europe	
<i>Samlandia delicata</i>	mid-low Lat	New Zealand	
<i>Samlandia septata</i>	mid-low Lat	New Zealand	
<i>Schematophora obscura</i>	endemic SO	New Zealand	
<i>Schematophora speciosa</i>	mid-low Lat	South Australian Magin	
<i>Selenopemphix nephroides</i>	mid-low Lat	Europe	
<i>Selenopemphix prionata</i>	Antarctic	McMurdo Sound	
<i>Selenopemphix selenoides</i>	mid-low Lat	Europe	
<i>Senegalinium asymmetricum</i>	mid-low Lat	McMurdo Sound	
<i>Senegalinium bicavatium</i>	mid-low Lat	Africa	
<i>Senegalinium dibovense</i>	mid-low Lat	South Australian Magin	
<i>Senegalinium</i> spp. (pars)	mid-low Lat	Africa	
<i>Spindinium colemanii</i>	mid-low Lat	Seymour Island	
<i>Spindinium luciae</i>	endemic "TF"	Seymour Island	
<i>Spindinium macmurdoense</i>	bipolar	McMurdo Sound	
<i>Spindinium schellenbergii</i>	endemic "TF"	Tasman region	Sluis et al., 2009b
<i>Spiniferites ramosus</i> complex	cosmopolitan	Middle Europe	
<i>Spiniferites</i> sp. A Brinkhuis et al., 2003a	endemic SO	East Tasman Plateau	Brinkhuis et al., 2003a
<i>Stoveracysta kakanuiensis</i>	endemic SO	New Zealand	
<i>Stoveracysta ornata</i>	cosmopolitan	South Australian Magin	
<i>Tanyosphaeridium</i> spp.	cosmopolitan	Europe	
<i>Tectatodinium pellitum</i>	mid-low Lat	Australia	
<i>Thalassiphora delicata</i>	mid-low Lat	North Sea Basin	
<i>Thalassiphora pelagica</i>	cosmopolitan	Europe	
<i>Turbiosphaera filosa</i>	mid-low Lat	McMurdo Sound	
<i>Turbiosphaera sajana</i>	mid-low Lat	McMurdo Sound	
<i>Vozzhennikovia apertura</i>	bipolar	McMurdo Sound	Levy and Harwood, 2000
<i>Vozzhennikovia minuta</i>	endemic SO	Weddell Sea	Sluis et al., 2009b
<i>Vozzhennikovia netrona</i>	endemic "TF"	McMurdo Sound	
<i>Vozzhennikovia roehliae</i>	endemic "TF"	Tasman region	Sluis et al., 2009b
<i>Vozzhennikovia rotunda</i>	bipolar	McMurdo Sound	
<i>Vozzhennikovia stickleyae</i>	endemic "TF"	Tasman region	Sluis et al., 2009b
<i>Wetzeliella articulata</i>	mid-low Lat	Europe	
<i>Wetzeliella astra</i>	mid-low Lat	Europe	
<i>Wetzeliella samlandica</i>	mid-low Lat	Europe	
<i>Wilsonidium echinosaturatum</i>	endemic "TF"	New Zealand	
<i>Wilsonidium ornatum</i>	mid-low Lat	New Zealand	
<i>Ynezdinium waiapawaense</i>	endemic SO	New Zealand	

Taxonomy based on those cited in Fensome et al., 2004, unless stated otherwise

Legend:	
Mid-low Lat	Species that originate from middle and low latitudes
Cosmopolitan	Species not particularly restricted to any latitude
Endemic SO	Species that are endemic to the Southern Ocean, but most likely represent regional dimorphism within dinoflagellate lineages
Endemic "TF"	Species included in the transantarctic flora
Antarctic	Dinoflagellate cyst species with heterotrophic affinities, and likely associated with sea ice conditions around Antarctica. This group replaces the transantarctic flora in the early Oligocene at numerous places.











A brief (~150 kyr) period of global average surface warming marks the transition between the Paleocene and Eocene Epochs, ~56 million years ago. This so-called “Paleocene-Eocene Thermal Maximum” (PETM) is associated with the massive injection of  $^{13}\text{C}$ -depleted carbon, reflected in a negative carbon isotope excursion (CIE). Biotic responses include a global abundance peak (acme) of the subtropical dinoflagellate *Apectodinium*. Here we identify the PETM in a marine sedimentary sequence deposited on the East Tasman Plateau at Ocean Drilling Program (ODP) Site 1172 and show, based on the organic paleothermometer  $\text{TEX}_{86}$ , that southwest Pacific sea surface temperatures increased from ~26°C to ~33°C during the PETM. Such temperatures before, during and after the PETM are >10°C warmer than predicted by paleoclimate model simulations for this latitude. In part, this discrepancy may be explained by potential seasonal biases in the  $\text{TEX}_{86}$  proxy in polar oceans. Additionally, the data suggest that not only Arctic, but also Antarctic temperatures may be underestimated in simulations of ancient greenhouse climates by current generation fully coupled climate models. An early influx of abundant *Apectodinium* confirms that environmental change preceded the CIE on a global scale. Organic dinoflagellate cyst assemblages suggest a local decrease in the amount of river run off reaching the core site during the PETM, possibly in concert with eustatic rise. Moreover, the assemblages suggest changes in seasonality of the regional hydrological system and storm activity. Finally, significant variation in dinoflagellate cyst assemblages during the PETM indicates that southwest Pacific climates varied significantly over time scales of  $10^3 - 10^4$  years during this event, a finding comparable to similar studies of PETM successions from the New Jersey Shelf.



## 1. Introduction

Gradual widespread warming initiated in the late Paleocene (~59 Ma) and culminated in the Early Eocene Climatic Optimum (EECO; 52–50 Ma; e.g., Chapter 2; Adams et al., 1990; Zachos et al., 2001). Superimposed on this long-term warming trend, at least four “hyperthermals” occurred, which represent relatively brief (<200 kyr) intervals characterized by anomalously high temperatures (e.g., Bowen et al., 2006; Sluijs et al., 2007a). The Paleocene-Eocene Thermal Maximum (PETM) is the most prominent and best-studied hyperthermal and is marked by a negative carbon isotope excursion (CIE) in sedimentary components of 2.5–8‰, depending on analyzed substrate, location and completeness of the section (Kennett and Stott 1991; Koch et al., 1992; Schouten et al., 2007c). Moreover, massive dissolution of biogenic carbonates occurred in deep ocean basins (e.g., Zachos et al., 2005; Zeebe and Zachos 2007). The CIE and carbonate dissolution are consistent with geologically rapid, massive injections of <sup>13</sup>C-depleted carbon into the ocean-atmosphere system (Dickens et al., 1997; Panchuk et al., 2008; Zeebe et al., 2009), although the mechanism for such release remains controversial (Dickens et al., 1995; Kurtz et al., 2003; Svensen et al., 2004).

Stable oxygen isotope ( $\delta^{18}\text{O}$ ) and Mg/Ca studies on planktonic foraminifera from deep-sea sediments indicate a 5–8°C surface warming during the PETM (Kennett and Stott 1991; Thomas et al., 2002; Zachos et al., 2003). Reconstruction of absolute sea surface temperatures (SST) from such sections has been problematic because of post-sedimentary recrystallization of planktonic foraminifera (Pearson et al., 2001; Schrag et al., 1995). Additionally, reduced pH may have dampened foraminifer  $\delta^{18}\text{O}$  excursions, potentially resulting in too low estimates of PETM warming (Uchikawa and Zeebe 2010). More recently, the application of organic paleothermometers, such as TEX<sub>86</sub> and MBT/CBT in marginal marine sequences provided estimates of absolute temperature evolution across the PETM and other hyperthermals in the Northern Hemisphere (e.g., Sluijs et al., 2006; Weijers et al., 2007a; Zachos et al., 2006). This work showed exceptionally high Arctic temperatures during this time interval, suggesting very low meridional temperature gradients (Sluijs et al., 2006). The marginal marine sections used in these studies have also revealed significant increases in river discharge and sediment input (e.g., Crouch et al., 2003; Giusberti et al., 2007; John et al., 2008; Sluijs et al., 2008a; for an overview see Sluijs et al., 2008b), changes in trophic level (e.g., Crouch et al., 2001; Gibbs et al., 2006; Speijer and Wagner 2002), as well as a globally recorded rise in sea level (Sluijs et al., 2008b). However, temperature and paleo-ecological data from marginal marine PETM sections from the Southern Hemisphere are rare (Crouch and Brinkhuis 2005; Crouch et al., 2001), and none are available from the southern high-latitudes, hampering thorough evaluation of climatic change in the sub-Antarctic realm.

We have generated geochemical and palynological data through upper Paleocene – lower Eocene sediments recovered during Ocean Drilling Program (ODP) Leg 189 at Site 1172 on the East Tasman Plateau, deposited at ~65°S paleolatitude (Exon et al., 2004; Fig. 1). Micropaleontological information from the southwest Pacific showed that this site was located within the Antarctic-derived, northward



flowing Tasman Current throughout the Paleogene, which is consistent with general circulation model experiments (Hollis et al., 2009; Huber et al., 2004). In an earlier study, based on initial shipboard samples we suggested that the PETM might not have been recovered at this site (Röhl et al., 2004b). Here, we identify a condensed PETM section on the basis of a negative CIE in organic matter within Subchron C24r. We perform TEX<sub>86</sub>, dinoflagellate cyst assemblage analyses and X-ray fluorescence (XRF) core scanning in order to reconstruct paleoenvironmental conditions at southern high-latitudes across the PETM.

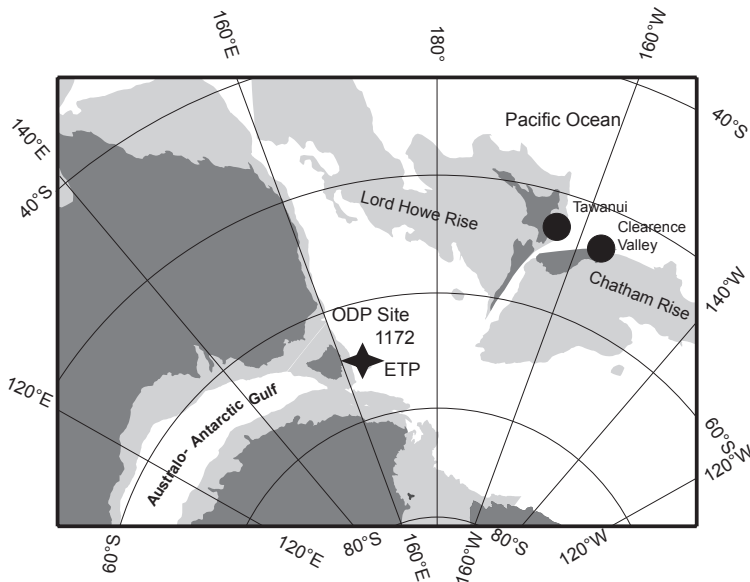


Figure 1. Tectonic reconstruction of the southwest Pacific region for the earliest Eocene, with East Antarctica held fixed, illustrating modern continents (dark grey), areas shallower than 3000m (light grey) and locations of ODP Site 1172 and other sites discussed in the text. ETP = East Tasman Plateau, STR = South Tasman Rise. The figure is modified from Cande and Stock (2004).

## 2. Material and methods

### 2.1. Material

Sediments of late Paleocene and early Eocene age at ODP Site 1172, Hole 1172D, consist mainly of organic-rich green and grey clay- and siltstones with low abundance of calcareous and siliceous microfossils, but high abundance of palynomorphs (notably dinocysts but also terrestrial pollen and spores). Glauconite and accessory minerals are recorded in varying abundance (Exon et al., 2001), with the glauconite grains being irregular and angular, which indicates that glauconite was formed in situ (based on thin sections, data not shown). Lithological and palynological information suggests an overall very shallow marine depositional setting with marked runoff from the nearby shores (Exon et al., 2001; Röhl et al., 2004b). Integrated dinoflagellate cyst and magnetostratigraphic studies identified Subchrons C25n, C24r



and C24n, with the top of Subchron C25n at 618.00 rmbfsf and the onset of Subchron C24n at 594.2 rmbfsf (Fuller and Touchard 2004; Stickley et al., 2004a). Average sedimentation rates implied by this age model are 5.7 m/Myr, when assuming a duration of 3.1 Ma for Subchron C24r (Westerhold et al., 2007).

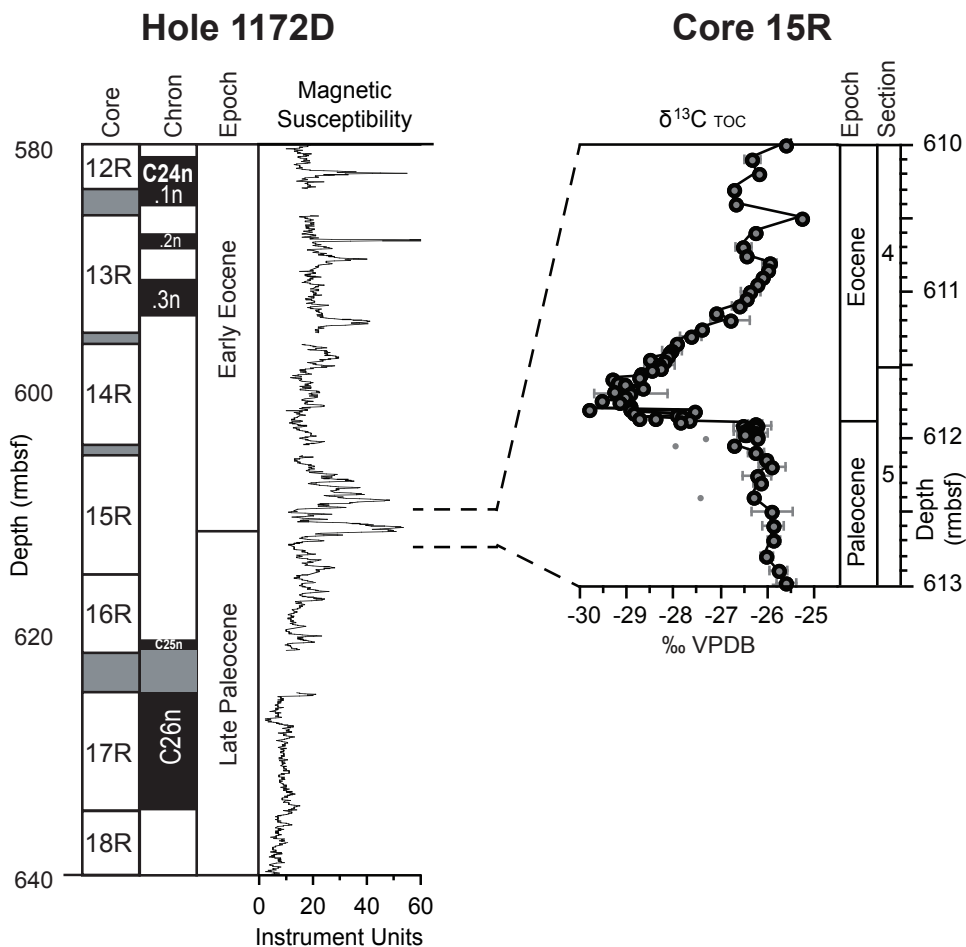


Figure 2. Core recovery and stratigraphic summary of the latest Paleocene to earliest Eocene at ODP Site 1172. Note that the core depths are in revised meters below sea floor (rmbfsf; see text). Magnetostratigraphic interpretation is from Chapter 1, which differs from the interpretations published in the first post-cruise papers (Fuller and Touchard 2004; Röhl et al., 2004b) in the assignment of normal polarity intervals to Subchrons C25n and C26n. Magnetic susceptibility record represents shipboard data (Exon et al., 2001). Stable carbon isotope ( $\delta^{13}\text{C}$ ) values of total organic carbon (TOC) across the PETM are expressed relative to the Vienna Pee Dee Belemnite standard. Error bars reflect duplicate based standard deviations and three grey data points are considered outliers because duplicate analyses indicated values consistent with surrounding samples.



## 2.2. Methods

The archive halves of Core 189-1172D-15R were subject to XRF Core Scanning. Subsequently, half-splits of these archive halves were sampled on a resolution of 1 to 2 cm, after which samples were freeze-dried. Splits of samples were then taken for palynology and organic geochemistry.

### 2.2.1. X-ray fluorescence (XRF) core scanning

We measured the elemental composition of sediments from Cores ODP Leg 189 Site 1172D-15R to -17R at the MARUM, Bremen University, Germany, using the XRF core scanner (Richter et al., 2006; Tjallingii et al., 2007). The XRF core scanner acquires bulk-sediment chemical data from split core surfaces. Although measured elemental intensities are predominantly proportional to concentration, they are also influenced by the energy level of the X-ray source, count time, and physical properties of the sediment (Röhl and Abrams 2000; Tjallingii et al., 2007). XRF data were collected every cm down-core over a 1 cm<sup>2</sup> area using 30 s count time. We used a generator setting of 20 kV and an X-ray current of 0.15 mA.

### 2.2.2. Palynology

Samples of 1–2 cm stratigraphic thickness were freeze-dried and a known amount of *Lycopodium* spores was added to ~4 g of material. Samples were then treated with 30% HCl and twice with 38% HF for carbonate and silicate removal, respectively. Residues were sieved using a 15- $\mu$ m nylon mesh to remove small particles. To break up clumps of residue, the sample was placed in an ultrasonic bath for a maximum of 5 min, sieved again, and subsequently concentrated into 1 ml of glycerine water, of which 10  $\mu$ l was mounted on microscope slides. Slides were counted for marine (e.g., dinocysts) and terrestrial palynomorphs (e.g., pollen and spores) to a minimum of 200 dinocysts. Marine and terrestrial palynomorph preservation was excellent for all samples. We generally follow dinocyst taxonomy of Fensome and Williams (2004), but follow Sluijs et al. (2009b) for the various spiny peridinioid taxa. Absolute quantitative numbers were counted using the relative abundance of *Lycopodium* spores (Stockmarr 1972).

### 2.2.3. Organic geochemistry

For stable carbon isotope analyses of total organic carbon ( $\delta^{13}\text{C}_{\text{TOC}}$ ), freeze-dried samples were powdered, treated with 1M HCl to remove carbonate, centrifuged and the supernatant decanted, followed by two rinses with demineralised water and freeze-dried again. Residues were analyzed with a Fison NA 1500 CNS analyzer coupled to a Finnigan Delta Plus isotope ratio mass spectrometer. Analytical precision and accuracy were determined by replicate analyses and by comparison with in-house standards, and were better than 0.1‰ and 0.1‰, respectively. For biomarker analyses, freeze-dried sediment samples (~3.5 g dry mass) were extracted with dichloromethane (DCM)/methanol (2:1) using accelerated solvent extraction (Dionex ACE). The extracts were separated by Al<sub>2</sub>O<sub>3</sub> column chromatography using hexane/DCM (9:1, v/v) and DCM/methanol (1:1, v/v) to yield the apolar and polar fractions, respectively. The polar fractions were analyzed using high performance liquid chromatography/atmospheric pressure chemical ionization-mass spectrometry, according to Schouten et al. (2007a). Single ion monitoring was used to



quantify the abundance of the Glycerol Dialkyl Glycerol Tetraether (GDGT) lipids. The relative abundance of GDGTs was used to calculate  $TEX_{86}$  (Schouten et al., 2002).  $TEX_{86}$  is converted to mean annual SST by means of quasi-global core top calibrations. A new calibration with a logarithmic function was recently published (Kim et al., 2010), which is based on the currently available core-top data and thorough statistical analyses between GDGTs abundances and SST. An earlier calibration assumes a different logarithmic relation (Liu et al., 2009) that produces particularly different SSTs for high  $TEX_{86}$  values. We also determined the Branched and Isoprenoid Tetraether (BIT) index. This is a ratio between soil bacteria-derived and marine crenarchaeota-derived membrane lipids, and serves as a proxy for the relative amount of river transported soil organic matter versus marine organic matter (Hopmans et al., 2004).

#### 2.2.4. Core depth adjustments

Based on correlations between physical properties data generated on core material and down hole logging, we have slightly changed the meters below sea floor (mbsf) depth of the core sediments in a recent paper (Chapter 2). We use revised mbsf (rmbfsf) for these revised depths throughout. Relative to mbsf, Core 189-1172D-12R was shifted up by 0.36 m, -13R down by 1.87m, -14R down by 2.84 m, -15R down by 2.4 m, -16R down by 2.57m and -17R and -18R down by 2.66m.

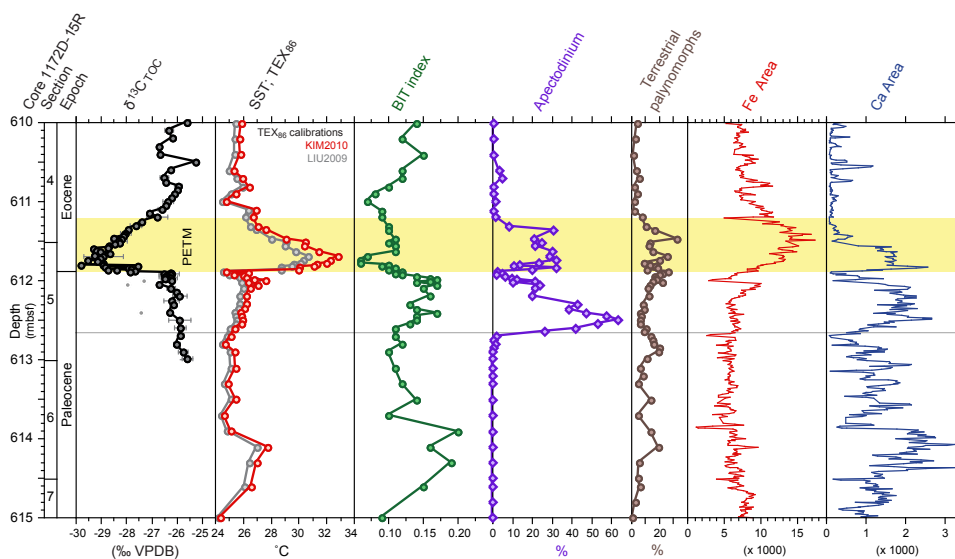


Figure 3. Organic geochemical, palynological and XRF results across the PETM of ODP Site 1172. From left to right: stable carbon isotope ( $\delta^{13}C$ ) values of total organic carbon (TOC) (see caption at Fig. 2 for details); sea surface temperature (SST) based on  $TEX_{86}$  following the calibrations KIM2010 (Kim et al., 2010) and LIU2009 (Liu et al., 2009); BIT index; *Apectodinium* percentage of the dinocyst assemblage; abundance of terrestrially derived palynomorphs as a percentage of total pollen and dinocysts; and XRF intensity data for iron (Fe) and calcium (Ca).



### 3 Results

#### 3.1. Stratigraphy

Between 611.89 and 611.86 rmbsf, the  $\delta^{13}\text{C}_{\text{TOC}}$  curve shows a  $\sim 3\text{‰}$  negative step from  $-26$  to  $-29\text{‰}$ , followed by a  $\sim 20$  cm interval of relatively stable values, and a subsequent exponential recovery that reaches background values between 611.2 and 611.0 rmbsf (Fig. 2). This excursion is located within Subchron C24r. Average sedimentation rates of 5.7 m/Myrs for this Subchron (see Material) imply that this excursion occurred  $\sim 1$  Myr after the termination of Subchron C25n (Fuller and Touchard 2004; Chapter 2) and  $\sim 2$  Myrs between this CIE and the onset of Subchron C24n. The orbitally based age model from Blake Nose (ODP Leg 171B) and Walvis Ridge (ODP Leg 208) also indicates  $\sim 1$  Myr between the top of Subchron C25n and the PETM (Norris and Röhl 1999), and  $\sim 2$  Myrs between the PETM and the onset of Subchron C24n (Westerhold et al., 2007). The onset of Eocene Thermal Maximum 2 occurred  $\sim 150$  kyrs prior to the reversal of Subchron C24r to C24n.3n, which is inconsistent with the location of the recorded CIE. Rather, the overall stratigraphic position of the CIE implies the presence of the PETM in Core 1172D-15R. The thickness of the CIE at ODP Site 1172 is 65–90 cm, depending on the definition of its termination (Röhl et al., 2007). Assuming a 170 kyr duration of the CIE (Abdul Aziz et al., 2008; Röhl et al., 2007), this indicates average PETM sedimentation rates of  $\sim 0.4$ – $0.5$  cm/kyr, although sediment accumulation rates were likely highly variable in this pro-deltaic setting.

#### 3.2. $\text{TEX}_{86}$ and BIT

Late Paleocene SSTs average  $\sim 26^\circ\text{C}$  ( $1\sigma = 0.9$ ) based on  $\text{TEX}_{86}$ , regardless of the applied calibration (Fig. 2). Concomitantly with the onset of the CIE, SSTs rise to average PETM values of  $\sim 31^\circ\text{C}$  ( $1\sigma = 0.7$ ) following KIM2010, or  $\sim 29^\circ\text{C}$  for LIU2009 with peak values of almost  $33^\circ\text{C}$  and  $31^\circ\text{C}$  for the two calibrations, respectively, at 611.70 rmbsf. The magnitude of PETM warming was thus  $\sim 7^\circ\text{C}$  with KIM2010 and  $4^\circ\text{C}$  with LIU2009. SSTs returned to pre-excursion values during the recovery of the CIE. The warming and the CIE are preceded by two samples with relatively low temperatures ( $\sim 25^\circ\text{C}$ ). BIT values are low throughout the analyzed interval, indicating that  $\text{TEX}_{86}$  values are not influenced by soil derived GDGTs (Weijers et al., 2006). The BIT record exhibits some scatter, but values during the PETM ( $0.09 \pm 0.02$ ) are on average somewhat lower than before and after the PETM ( $0.13 \pm 0.03$ ), suggesting increased marine production of isoprenoid GDGTs or a decreased supply of soil organic matter.

#### 3.3. Palynology

Palynological assemblages are rich, well preserved and dominated by dinoflagellate cysts (dinocysts). Terrestrial pollen and spores are common to abundant throughout, with relatively high abundances within the PETM (Figs. 2, 3). Stratigraphically important dinocyst taxa include *Apectodinium* spp., *Eocladopyxis peniculata*, *Deflandrea* spp., *Melitasphaeridium pseudorecurvatum*, *Muratodinium fimbriatum* and the recently described species *Florentinia reichartii* (Sluijs and Brinkhuis 2009). In particular, the oldest abundant occurrence ( $>40\%$  of the





assemblage) of *Apectodinium* in the southwest Pacific Ocean has been calibrated to the PETM (Crouch et al., 2001). At ODP Site 1172 however, the First Occurrence (FO) of abundant *Apectodinium* is at ~612.6 rmbsf, ~75 cm below the onset of the CIE (Fig. 3). *Apectodinium* abundances subsequently decrease to ~2%, followed by a second abundance maximum starting at the onset of the CIE. Along with *Apectodinium* spp., other quantitatively significant taxa in the assemblage mostly comprise cosmopolitan taxa such as *Senegalinium* spp., *Glaphyrocysta* spp., *Eocladopyxis peniculatum*, *Cordosphaeridium fibrospinosum*, *Thalassiphora* spp., *Kenleyia* spp., *Fibrocysta* spp. (and other members of the *Cordosphaeridium fibrospinosum* complex sensu Sluijs and Brinkhuis (2009)), *Diphyes colligerum*, *Paucisphaeridium*, *Deflandrea* (and a few related *Cerodinium*), *Membranosphaera* (often referred to as *Elytrocysta* in the Southern Ocean), and *Spiniferites* spp. *Hystrichosphaeridium truswelliae*, common in certain intervals, was long thought to have been endemic to the Antarctic realm, but was recently recorded in uppermost Paleocene and PETM sediments on the New Jersey Shelf (Sluijs and Brinkhuis 2009). In fact, PETM assemblages as a whole are strikingly similar to those reported from the New Jersey Shelf. Only few aspects of the assemblages are typical for the Antarctic Realm (e.g., Warnaar et al., 2009; Wrenn and Beckman 1982), including rare *Vozzhennikovia* spp., and temporally abundant *Pyxidinopsis* spp. *Senegalinium* spp. dominate assemblages from the base of the studied section (~615 rmbsf) up to ~613 rmbsf, an interval with very stable dinocyst assemblages with common *Pyxidinopsis*, *Spiniferites*, and *Deflandrea* spp. Assemblages are slightly richer above 613 rmbsf, with more abundant *Pyxidinopsis* spp. and common *H. truswelliae* and *Membranosphaera* spp. A peak in *Glaphyrocysta* spp. occurs around 613 rmbsf, directly followed by the first *Apectodinium* acme. Between 612.2 and 611.9 rmbsf, just below the onset of the CIE, successive transient abundances of *Glaphyrocysta*, *Deflandrea*, *Pyxidinopsis*, and *Operculodinium* spp., and *C. fibrospinosum* complex occur. A second acme of *Apectodinium* is recorded concomitant with the CIE. Within the CIE, transient abundances of *Glaphyrocysta* spp. and *Eocladopyxis peniculatum* occur. After the CIE, *Senegalinium* dominates assemblages again, while *Operculodinium* spp., *H. truswelliae* and *Membranosphaera* spp. are common.

### 3.4. XRF

Fe and Ca intensities exhibit a characteristic variability that can be directly attributed to lithology (Fig. 2). The sediments at this site are composed of clay- and siltstones with low abundance of CaCO<sub>3</sub> (<0.3%), between ~0.5–1% TOC, pyritized diatoms, glauconite, accessory minerals in changing abundance, including varying amounts of quartz (Exon et al., 2001). The dominant lithology is expressed as generally low Ca values in the XRF scans, but the Ca in these sediments is related to carbonate (Röhl et al., 2004a, b). Ca values are higher in the lower part of Core -15R, just three meters below the PETM (Fig. 2). These relatively higher carbonate contents, reflecting higher abundance of nannofossils, are in line with a shallow marine environment, but compared to the sediments below and above a relatively deeper depositional environment. The Ca intensities in this interval of Core -15R show regular fluctuations: about four cycles below the onset of the PETM, which may also be present in the BIT index, the TEX<sub>86</sub> sea surface temperature data, and reversely in the percentage of terrestrial palynomorphs. Assuming an average sedimentation rate



of 5.7 m/Myrs these cycles could represent the low eccentricity frequency of the Milankovitch orbital band (100-kyr cycles). Ca values exhibit peak values during the warming of the PETM, followed by the lowest Ca values in the interval (611.56–610.57 rmbsf) (Fig. 2). Ca and Fe are often closely anticorrelated in the pelagic realm, e.g., at ODP Sites 690 and 1263, because abundances of these elements are both forced by carbonate export and preservation (Röhl et al., 2007). Although the Fe and Ca intensities are overall anti-correlated during the PETM at ODP Site 1172 (611.2–611.9 rmbsf) their relation is not as strong as in the deep sea. The Fe record exhibits maximum values (broad peak) in the upper part of the CIE, where the Ca values are lower and the terrestrial palynomorphs show maximum values. This indicates that the abundances of these elements are not controlled by carbonate dissolution, as expected for this shallow marine setting (Röhl et al., 2004a, b), but rather by the sediment supply from land and marine biogeochemical cycling. Indeed, it suggests that the relation of these two main elements Ca and Fe is driven by minor (Milankovitch-driven) variations in clay mineralogy in combination with very low carbonate contents. Ca values stay low above the PETM. In general, for the long-term Site 1172 record including Core -15R, Ca and Fe do not particularly anti-correlate on a larger scale. This is partly caused by the relatively high amount of silica in the sediments in addition to carbonate (Ca) and clay (Fe), which disturbed the perhaps expected anti-correlation of Ca and Fe.

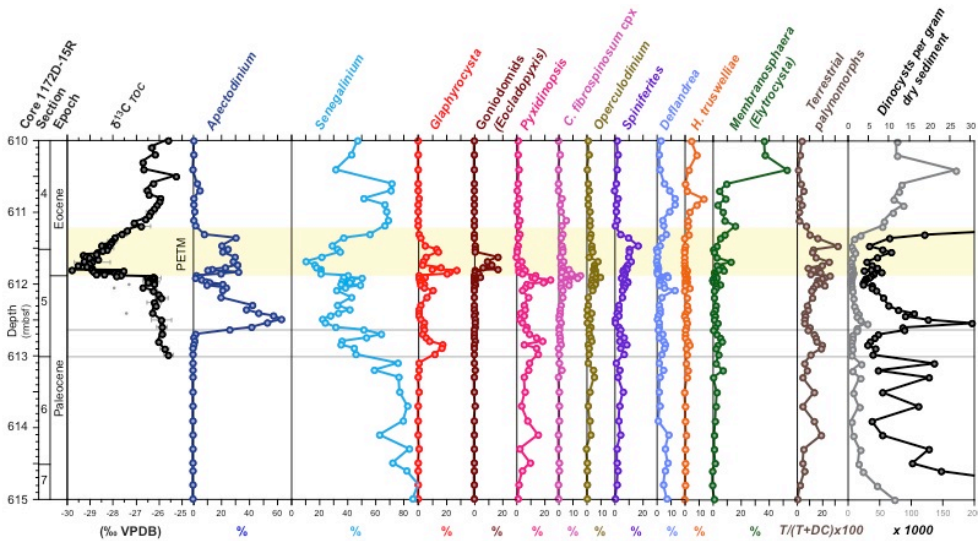


Figure 4. Palynological results across the PETM of ODP Site 1172. Dinocyst abundances are reflected as the percentage of the total dinocyst assemblage and the abundance of terrestrially derived palynomorphs as a percentage of total palynomorph sum. Goniodomids almost exclusively represent *Eoeladopyxis peniculata*. *Membranosphaera* spp. is often referred to as *Elytrocyta* spp. in Southern Ocean literature. Grey and black lines in the absolute quantitative dinocyst abundance panel reflect two different scales for illustration purposes.



## 4 Discussion

### 4.1. The carbon isotope excursion

The magnitude ( $\sim 3\text{‰}$ ) of the CIE recorded at ODP Site 1172 is similar to or slightly smaller than the 4–5‰ often recorded in  $\delta^{13}\text{C}_{\text{TOC}}$  at other marine sites (Bolle et al., 2000; Crouch et al., 2001; Kaiho et al., 1996; Sluijs et al., 2006; Steurbaut et al., 2003). Since the lowest  $\delta^{13}\text{C}$  values for most carbon isotope records across the PETM are located close to the onset of the event (e.g., Bowen et al., 2001; Sluijs et al., 2007a; Thomas et al., 2002), this could imply that the earliest part of the PETM is not represented in our record. Alternatively, the seemingly damped magnitude of the excursion may be caused by changing sources of organic matter as hypothesized for the small CIE at Tawanui, New Zealand (Crouch et al., 2003), but our palynological analyses do not support major changes in organic matter composition (Figs. 2, 3). Globally, most  $\delta^{13}\text{C}$  curves from the PETM show a rapid drop at the onset, which probably took less than 10,000 years. Subsequently, some bulk carbonate and bulk organic carbon records suggest a slower, sometimes stepwise, continued decline that may span several tens of thousands of years (e.g., Bains et al., 1999; Nicolo et al., 2011). In other records, notably those of single specimen foraminifera, the first negative step is directly followed by  $\sim 80$  kyr of stable carbon isotope values and subsequent recovery that is also recorded in the bulk records, often referred to as the “body” of the CIE (e.g., McCarren et al., 2009; Thomas et al., 2002). Our record clearly shows an interval of stable values of around  $-29\text{‰}$  between  $\sim 611.9\text{--}611.7$  rmbfs, implying that at least part of the stable peak phase is represented in the record. In fact, the magnitude of the CIE in our record is very close to the  $-3$  to  $-3.5\text{‰}$  that is generally assumed to have been the excursion in the global exogenic carbon (McCarren et al., 2009; Zachos et al., 2007). Hence, the record at ODP Site 1172 appears to contain at least a large part of the “body” of the CIE as well as the recovery, allowing comparison to other PETM sites.

### 4.2. Sea surface temperature evolution

#### 4.2.1. Magnitude of PETM warming

The range of SST estimates based on  $\text{TEX}_{86}$  is slightly different for the two applied calibrations; LIU2009 gives relatively low temperature estimates and implies a very low sensitivity for  $\text{TEX}_{86}$  values at temperatures  $>30^\circ\text{C}$ . In contrast, KIM2010 implies a higher sensitivity and absolute temperature estimates (Fig. 2). In the New Jersey PETM records for example, the KIM2010 is most consistent with mixed layer planktonic foraminifer stable oxygen isotope ( $\delta^{18}\text{O}$ ) paleothermometry (Kim et al., 2010), also regarding the magnitude of warming. Because the awkwardly low sensitivity of the LIU2009 calibration and decent multi-proxy intercomparison we prefer the magnitude of warming implied by the KIM2010 calibration in this upper range of  $\text{TEX}_{86}$  values. A warming of  $\sim 7^\circ\text{C}$  is similar to or slightly less than the only other Southern Ocean estimates from the Weddell Sea (Sites 689 and 690 at Maud Rise), based on the  $\delta^{18}\text{O}$  excursion in the surface dwelling foraminifer *Acarinina* (Thomas et al., 2002; Zachos et al., 2007). The magnitude of the SST rise is also similar to that recorded at marginal marine sites on the New Jersey Shelf based on foraminiferal  $\delta^{18}\text{O}$  and  $\text{TEX}_{86}$  (John et al., 2008; Sluijs et al., 2007b; Zachos et al., 2006). However, the magnitude of warming was smaller in open-ocean and continental



settings, and in the Arctic (e.g., Sluijs et al., 2006; Thomas and Shackleton 1996; Tripathi and Elderfield 2005; Weijers et al., 2007a; Wing et al., 2005; Zachos et al., 2003). This suggests that, while the Arctic warmed with a magnitude comparable to the global average (Sluijs et al., 2006), some marginal marine regions warmed slightly more and some polar amplification may have occurred in the Southern Hemisphere. If so, this amplification may have been caused by three mechanisms. First, the melting of small ice sheets on high mountains in Antarctica may have reduced albedo and thus amplified Antarctic warming. This would be consistent with the reconstructed PETM eustatic rise (Sluijs et al., 2008b). Secondly, an increase in atmospheric heat transport may have occurred. Indeed, increased precipitation in Southern Hemisphere PETM records would suggest more latent heat transport from tropical regions to the Antarctic (Crouch et al., 2003; Robert and Kennett 1994). However, Arctic sections also exhibit evidence for intensified regional hydrology (Pagani et al., 2006), but no amplification of warming is recorded there (Sluijs et al., 2006). Third, a change in ocean circulation during the PETM may have resulted in regionally enhanced warming in the southwest Pacific Ocean and Weddell Sea.

#### 4.2.2. Absolute temperatures

Late Paleocene SSTs average  $\sim 26^{\circ}\text{C}$  for both the LIU2009 and KIM2010 calibrations (Fig. 2). Average PETM SSTs are  $\sim 31^{\circ}\text{C}$  following KIM2010 and  $\sim 29^{\circ}\text{C}$  for LIU2009, with peak values of almost  $33^{\circ}\text{C}$  and  $31^{\circ}\text{C}$  for the two calibrations, respectively. Because of this calibration difference and as these temperatures are outside the range of modern SSTs, care should be taken in interpreting absolute PETM SST values. Considering the uncertainties of the respective calibrations,  $\text{TEX}_{86}$  indicates that maximum PETM SSTs at ODP Site 1172 were in the range between  $29\text{--}34^{\circ}\text{C}$ . Although  $\text{TEX}_{86}$  is calibrated to mean annual SST in the modern ocean, like other proxies seasonal and depth biases can occur with the  $\text{TEX}_{86}$  paleothermometer (Castañeda et al., 2010; Huguët et al., 2007). The marine Crenarchaeota (recently renamed Thaumarchaeota by Spang et al. (2010)) currently mainly proliferate during winter in both the Arctic and Antarctic oceans (Alonso-Saez et al., 2008; Kalanetra et al., 2009). Likely, this is because most of them are chemoautotrophs (Wuchter et al., 2006a), living on ammonia and being not directly depending on light. Also in the present day North Sea they preferentially grow during winter, low light and no competition with algae for ammonia (Wuchter et al., 2006a). Because Crenarchaeota/Thaumarchaeota have low kinetics for ammonia (Martens-Habbena et al., 2009), they outcompete bacteria and algae at low ammonia concentrations. These microbiological studies would thus imply that the  $\text{TEX}_{86}$  signal may be even skewed towards winter temperatures. However, the export of membrane lipids to the sea floor is not necessarily a function of Thaumarchaeotal cell abundance but rather of export through faecal pelleting (Wakeham et al., 2003; Wuchter et al., 2006b). Because the dominant season of export in Paleogene polar oceans was likely summer, we previously suggested that  $\text{TEX}_{86}$  values in such regions might be skewed towards summer temperatures (Sluijs et al., 2006, 2008a). Multi-proxy comparison has indicated good correspondence between  $\text{TEX}_{86}$  and the molecular MBT/CBT proxy for continental air temperature across the PETM in the Arctic (Weijers et al., 2007a). Although direct comparison to terrestrial reconstructions in the southwest Pacific is complex, our temperatures are qualitatively consistent with dominant angiosperm



pollen in the Site 1172 record. Moreover, records from New Zealand generally exhibit subtropical to tropical floral incursions, including occurrences of the mangrove palm *Nypa* in the Taranaki, East Coast, and Canterbury Basins (e.g., Crouch et al., 2005; Crouch and Visscher 2003). In marine sections from New Zealand,  $\text{TEX}_{86}$  agrees with foraminiferal stable oxygen isotope and Mg/Ca ratios in the Eocene (Creech et al., 2010; Hollis et al., 2009). Moreover,  $\text{TEX}_{86}$  and  $\text{U}_{37}^{\text{K}'}$  yield similar SST estimates across the Middle Eocene Climatic Optimum (~40 Ma) at ODP Site 1172 (Chapter 6). However, it should be noted that seasonal biases cannot be excluded in any of these proxies. Oxygen isotope ratios of reputedly Eocene molluscs from Seymour Island in coastal Antarctica indicate significantly cooler conditions on the Antarctic shelf (Ivany et al., 2008). However, it should be noted that these molluscs are relatively poorly dated and may also be of middle Eocene age. Nevertheless, if the molluscs are early Eocene and their  $\delta^{18}\text{O}$  values yield reliable SST estimates, this might imply that  $\text{TEX}_{86}$  is skewed towards summer temperatures. Moreover, temperature estimates for deep-sea waters, which at time most likely derived from Antarctic surface waters, are 10–15°C cooler than our SST estimates (McCarren et al., 2009; Thomas and Shackleton 1996; Tripathi and Elderfield 2005). Again, part of this discrepancy can result from seasonal biases. The temperature of deep waters most likely represents winter SST along the Antarctic margin. Collectively, although with the available data it remains impossible to exclude that  $\text{TEX}_{86}$  represents MAT, we consider it likely that the proxy is biased towards summer temperatures in the polar oceans of the Paleogene. Even if  $\text{TEX}_{86}$  temperatures are skewed towards summer SST estimates, the values are surprisingly high for this latitude, even with the conservative LIU2009 calibration.

Pre-PETM SSTs of ~26–27°C and maximum PETM SSTs of ~30–34°C are only 3–6°C cooler than on the New Jersey Shelf at a paleolatitude of ~35–40°N (Sluijs et al., 2007b; Zachos et al., 2006), and 8–12°C warmer than those in the Arctic (Sluijs et al., 2006) depending on the applied calibration. Even these reflect maximum summer temperature estimates, the difference with late Paleocene and early Eocene SSTs 30–35°C from Tanzania at ~17°S (Pearson et al., 2007) and northern South America at ~10°N (Jaramillo et al., 2010) is extremely small. Originally, the high temperatures in the southern ocean were explained by the supply of warm water through poleward ocean currents (Kennett 1977; Murphy and Kennett 1986), but more recent work has indicated that the East Tasman Plateau was more likely influenced by an Antarctic-derived Tasman Current (Chapter 3; Hollis et al., 2009; Huber et al., 2004). Although the warmest regions have not been sampled yet (Huber 2008), this supports previous observations (Chapter 2; Hollis et al., 2009) of a significantly reduced temperature gradient between the southwest Pacific and low latitudes. As indicated for the Northern Hemisphere data (Sluijs et al., 2007b; Sluijs et al., 2006; Zachos et al., 2006), and then particularly the high winter temperatures (e.g., Sluijs et al., 2009a), the small meridional gradients remain problematic to reconcile with current generation climate models, although recent modeling work has reduced the discrepancy (Abbot et al., 2009; Heinemann et al., 2009). Interestingly, regardless of the calibration, peak PETM SSTs are similar to those recorded for the EECO at ODP Site 1172 (Chapter 2). Unless Earth's surface temperatures were not sensitive to changing greenhouse forcing at this high temperature end, this suggests that atmospheric greenhouse gas levels were comparable during the peak of the PETM and long-term warmth of the EECO. In fact,





although regional differences exist, peak PETM temperatures were similar to those during ETM2 (Sluijs et al., 2009a; Stap et al., 2010). If so, one may speculate that the long-term late Paleocene – early Eocene warming and associated carbon isotope trend that culminated in the EECO as well as the superimposed hyperthermals, were caused by carbon injection (Hancock et al., 2007) from the same reservoir. Such a scenario requires a source that slowly added carbon to the global exogenic pool during the long-term trend resulting in the EECO. During the hyperthermals, it must have released carbon catastrophically, perhaps when an orbital (Lourens et al., 2005) threshold was surpassed, followed by partial recharge. One reservoir that may behave like this is the methane hydrate reservoir (Dickens 2003). Several potential problems exist with methane hydrates as the only source of  $^{13}\text{C}$ -depleted carbon, such as the volume and residence time of this reservoir during the Paleogene. However, a long-term net leakage from hydrates during late Paleocene – early Eocene warming is qualitatively consistent with a concomitant decrease in deep ocean  $\delta^{13}\text{C}$  as observed in benthic foraminiferal calcite (Zachos et al., 2001) and a long-term deepening of the calcite compensation depth (Hancock et al., 2007).

#### 4.3. Leads and lags

The genus *Apectodinium* originated close to the Danian- Selandian boundary (Brinkhuis 1994; Guasti et al., 2006) but abundant occurrences were restricted to low latitudes until the PETM (Bujak and Brinkhuis 1998; Iakovleva et al., 2001). On a global scale, *Apectodinium* is an important (often dominant) constituent of the dinoflagellate cyst assemblages described from the PETM (Heilmann-Clausen 1985; Steurbaut et al., 2003; Sluijs et al., 2007a; Sluijs et al., 2006). At ODP Site 1172, however, the lowermost acme starts approximately 70 cm below the CIE. An influx of abundant *Apectodinium* has also been shown to lead the CIE on the New Jersey Shelf, the Central North Sea and, perhaps, New Zealand (Sluijs et al., 2007b), by approximately 5 kyrs (perhaps slightly longer if sedimentation rates decreased in response to sea level rise; see Sluijs et al. (2008b)). The early *Apectodinium* acme recorded at ODP Site 1172 can be interpreted in two ways. First, if the uppermost Paleocene record at ODP Site 1172 is relatively expanded, the early acme may actually correlate to the early onset recorded at other sites. Latest Paleocene sedimentation rates of  $\sim 10$  cm/kyr are required to support this hypothesis, which is significantly higher than the average across this part of the section at ODP Site 1172, but quite common for marginal marine settings. If so, the rise in  $\text{TEX}_{86}$  around 612 rmbfsf might comprise the early warming recorded in New Jersey between the onset of the *Apectodinium* acme and the CIE (Sluijs et al., 2007b), although the latter records do not show a subsequent cooling immediately prior to the onset of the CIE. We cannot exclude this hypothesis because of the poor constraints on sedimentation rates in the uppermost Paleocene part of the section. Secondly, average sedimentation rates of 5.7 m/Myr suggest that this acme leads the CIE by some 100 kyr. If so, the early *Apectodinium* acme may imply that conditions at ODP Site 1172 locally became similar to low-latitude equatorial environments  $\sim 100$  kyr prior to the CIE, but unrelated to the PETM. This would imply extremely anomalous environmental change on the East Tasman Plateau, associated with the first and mass occurrence of a typical low-latitude dinoflagellate in the Southern Ocean, which is not accompanied by significant change in other proxies and, critically, not recorded in nearby sections at lower



latitudes in New Zealand (Crouch and Brinkhuis 2005; Crouch et al., 2003; Crouch et al., 2001). Although, this hypothesis seems inconsistent with the strictly low-latitude biogeography of abundant Paleocene *Apectodinium*, we cannot exclude it with the present data.

#### 4.4. Sea level, hydrology and productivity

Low sedimentary Ca values are in line with a shallow marine depositional environment, dominated by siliciclastic input. The Ca record shows a peak during the lower part of the PETM. The persistence of carbonate accumulation in this interval indicates that the calcite compensation depth resided below the shelf at the East Tasman Plateau during the entire event, consistent with other shelf locations (e.g., Bolle et al., 2000; John et al., 2008). Representatives of the genus *Senegalinium* dominate dinocyst assemblages for most of the studied interval (Fig. 3). Dinocysts assignable to this genus have been shown to tolerate very low salinities (Brinkhuis et al., 2006). High *Senegalinium* abundances have been associated with salinity stratification on the New Jersey Shelf during the PETM (Sluijs and Brinkhuis 2009). Moreover, *Senegalinium* likely represents heterotrophic dinoflagellates, thereby thriving in relatively nutrient-rich waters (Sluijs et al., 2005). Accordingly, consistent with lithological information, we interpret high abundances of *Senegalinium* spp. prior to the PETM as to indicate near-shore, relatively high-productive shelf settings, with sustained fresh-water runoff from nearby rivers. This interpretation is corroborated by relatively abundant river-transported terrestrial palynomorphs (Fig. 3). Although the low BIT values suggest a relatively low contribution of riverine transported soil derived organic matter, and relative terrestrial palynomorph abundances are not as high as seen in other shelf settings across the PETM (e.g., Crouch et al., 2003; Sluijs et al., 2006) these aspects most likely rather reflect high burial fluxes of marine organic matter and isoprenoid GDGTs compared to terrestrial organic matter. A decrease in *Senegalinium* abundance at 613.3 rmbfsf is accompanied by a peak in *Glaphyrocysta* spp., a taxon of which abundant occurrences are often associated with transgressive system tracts and sea level rise (Iakovleva et al., 2001; Pross and Brinkhuis 2005), suggesting uppermost Paleocene transgression at ODP Site 1172. Generally increasing abundances of other normal marine taxa, such as *Pyxidinospis* spp., *C. fibrospinosum* cpx., *Spiniferites* spp., and *Operculodinium* spp. support this interpretation. A second peak in *Glaphyrocysta* spp. at the onset of the CIE also suggests renewed sea level rise during the early stages of the PETM, supported by dropping BIT index values and a second drop in *Senegalinium* abundances. This transgression is seen along continental margins on a global scale, including in aspects of dinocyst assemblages in the New Zealand sections (Crouch and Brinkhuis 2005), and has, hence, shown to represent eustatic rise (Sluijs et al., 2008b). A record of sea level rise near the Antarctic margin is particularly interesting regarding the potential contributing role of melting Antarctic ice sheets. If an Antarctic ice sheet would have been present in the Paleocene, its self-gravitation should have increased sea level around the continental margin. If the ice sheet melted during the PETM, the loss of gravity should have led to a decrease in sea level during the PETM close to Antarctica, similar to that projected for the Greenland margin if the Greenland Ice Sheet would melt (Bamber et al., 2009). Hence, the record of sea level rise during the PETM at ODP Site 1172 might imply that no significant ice sheet was present on Antarctica during the Paleocene.



#### 4.5. Hydrology and sediment supply

Most studied marginal marine sites exhibit a vast increase in sediment supply from the continent during the PETM (Sluijs et al., 2008b), including New Jersey (John et al., 2008), Lomonosov Ridge in the Arctic Ocean (Sluijs et al., 2008a), the North Sea (Sluijs et al., 2008b; Steurbaut et al., 2003), the Bay of Biscay (Pujalte and Schmitz 2006; Schmitz et al., 2001), the Central Northern Tethys (Giusberti et al., 2007), California (John et al., 2008), and several sections in the southwest Pacific region, notably in New Zealand, such as Tawanui (Crouch et al., 2003) and the Clarence River Valley (Hollis et al., 2005; Nicolo et al., 2011). This is generally interpreted as an increase in terrestrial weathering and resulting supply of siliciclastic material to the shelf by rivers. At ODP Site 1172, no obvious change in average sedimentation rates was recorded during the PETM. This could mean that the strong hydrological response as recorded elsewhere did not take place in the region of the East Tasman Plateau, which is supported by the decrease in fresh-water tolerant dinocysts (Fig. 2). Alternatively, transgression caused sediment condensation at this proximal site. In addition, during the sampling of the core, we did note that the PETM interval is slightly coarser-grained, although, as yet, no data were generated to quantify this. Hence, potentially the sediment-water interface experienced more intense winnowing, hampering the deposition of large amounts of clay.

#### 4.6. Speculations on salinity and storminess

A peak of *Eocladopyxis* spp., a member of the extant family Goniodomidae that mainly inhabits polysaline, lagoonal environments (Wall et al., 1977), occurs within the PETM. Potentially, SSTs were only warm enough for this species to thrive in the Southern Ocean during peak PETM warmth, which may also seasonally have caused regional hypersaline conditions. The ecology of extant Goniodomids provides room for speculations regarding the conditions for the local environment. Abundant representatives of related species in the modern ocean (e.g., the harmful species *Pyrodinium bahamense*) have been related to hypersaline conditions (Reichart et al., 2004). Critically, however, in many regions, seasonal storm activity appears important to resuspend dormant cysts into the water column to hatch and fulfil their life cycle (Villanoy et al., 1996; Villanoy et al., 2006). In such systems, the subsequent bloom initiates in the wake of the storm when salinities drop due to increased river run off, and when turbulence is minimal (e.g., Dale 2001; Siringan et al., 2008). Increased river runoff and surface ocean stratification might be induced by tropical storms. Hence, storm activity and seasonal river input might have increased in the southwest Pacific region during the PETM, consistent with increased abundances of terrestrial palynomorphs. In any case, a peak in Goniodomids has at ODP Site 1172 only been recorded during the PETM (Fig. 3) and the EECO (Bijl et al., 2007; Brinkhuis et al., 2003a; Sluijs et al., 2003), indicating a very particular environment for this region, likely associated with a change in seasonality of regional hydrology, maximum temperatures and perhaps storm activity.

#### 4.7. Highly variable assemblages within the PETM

The dinocyst record suggests relatively stable conditions through the latest Paleocene and some more variation close to the onset of the CIE and within the PETM, with short-lived abundances of *Glaphyrocysta*, *Eocladopyxis*, *Pyxidinospis*,





*Cordosphaeridium fibrospinosum* complex, *Spiniferites*, *Operculodinium*, and *Membranosphaera*. Such intra-PETM variability has also been recorded in continental deposits from Wyoming (Bowen et al., 2004; Kraus and Riggins 2007; Wing et al., 2005) and on the New Jersey Shelf (Sluijs and Brinkhuis 2009). Although at the moment the cause of these variations are unknown, they do suggest that climate during the PETM may have been much more variable and dynamic on time scales of  $10^3$ – $10^4$  years, perhaps on a global scale.

## 5 Conclusions

A relatively complete PETM record was identified in sediments recovered from the East Tasman Plateau during ODP Leg 189, deposited at a paleolatitude of  $\sim 65^\circ\text{S}$ . Sediments are almost devoid of biogenic calcite but yield rich organic microfossil assemblages.  $\text{TEX}_{86}$  paleothermometry indicates that SSTs warmed by  $\sim 7^\circ\text{C}$  to maximum values of  $33^\circ\text{C}$  during the PETM, with a magnitude similar to or slightly larger than the global estimate of warming. Such surprisingly warm SSTs for this latitude indicate that meridional temperature gradients were very low across the Paleocene- Eocene transition, even though the reconstructed SSTs may be biased towards summer temperatures. Maximum temperatures were similar to those during the EECO, perhaps implying similar greenhouse gas concentrations. If so, one may speculate that long-term late Paleocene to early Eocene warming, carbon isotope trends and superimposed hyperthermals, were associated with carbon release from the same reservoir, perhaps methane hydrates. The globally recorded acme of the taxon *Apectodinium* leads the CIE at ODP Site 1172, which may represent the same early onset as recorded on the New Jersey Shelf and the North Sea. A decrease in the abundance of the fresh water-tolerant dinoflagellate cyst *Senegalinium* suggests a decrease in the influence of river run off at the core site during the PETM, possibly in concert with sea level rise. However, a unique abundance of the euryhaline taxon *Eocladopyxis* may indicate a change in the seasonality of the regional hydrological system and an increase in storm activity. Finally, significant variations in dinocyst assemblages within the PETM indicate that southwest Pacific climates varied much more significantly over time scales of  $10^3$ – $10^4$  years during the event, than during background late Paleocene – early Eocene times, consistent with records from the New Jersey Shelf and continental North America.







The transition from the warm early Paleogene “Greenhouse” climates towards the “Icehouse” initiated at the end of the early Eocene, ~50 million years ago (Ma), when both deep ocean and southern ocean temperatures started cooling (Zachos et al., 2008; Chapter 2). Although recent work argues that cooling was mainly forced by declining atmospheric greenhouse gas concentrations ( $p\text{CO}_2$ ; DeConto and Pollard 2003a, b; DeConto et al., 2008), the role of the opening of critical Southern Ocean gateways in Antarctic climate change (Kennett et al., 1974; Kennett 1977; Lawver and Gahagan 2003; Lagabriele et al., 2009) remains uncertain. Here we present proxy-records from recently recovered sediments from the Wilkes Land Margin, Antarctica (Escutia et al., 2011), deposited west of the Tasmanian Gateway in the Australo-Antarctic Gulf. Integrated marine and terrestrial microfossil and organic geochemical analyses show a strong cooling of east Antarctic surface waters (3-4°C) and adjacent landmasses (~6°C), at ~49 Ma. Critically, this cooling coincides with the first incursion of typical southwest Pacific phytoplankton that migrated across an apparently shallow southern opening of the Tasmanian Gateway at that time. Collectively, this implies that the onset of the relatively cool westward Antarctic Counter Current through the Tasmanian Gateway diminished the influence of the warmer Australo-Antarctic waters. This suggests a significant role of the shallow opening of the Tasmanian Gateway in East Antarctic cooling, presetting this region for massive cryosphere development at the Eocene-Oligocene boundary at ~34 Ma.



## EARLY PALEOGENE TASMANIAN GATEWAY OPENING

Early work suggested that the opening of critical Southern Ocean oceanic conduits, the Drake and Tasmanian gateways, played a major role in Cenozoic Antarctic cooling and cryosphere development (Kennett et al., 1974; Kennett 1977). Recent new field and model evidence from the Tasmanian region essentially led to the rejection of this hypothesis: both the timing of the critical deepening (Stickley et al., 2004b), and reconstructed oceanic circulation patterns (Huber et al., 2004), do not support a direct link between gateway opening and Antarctic glaciation. Rather, ever declining Eocene atmospheric CO<sub>2</sub> levels, although poorly documented (Beerling and Royer 2011), are now regarded as the principal driver (DeConto and Pollard 2003a, b). The role of oceanic gateways may still have been important for regional climate change, particularly along eastern Antarctica. Prior to opening, this region was bounded by a southern derivative of the Proto-Leeuwin Current (PLC) in the Australo-Antarctic Gulf (AAG), which presumably yielded low-latitude Indian Ocean waters (Huber et al., 2004; Fig. 1). Early through flow of relatively cool surface waters from the Pacific should in this region significantly affect bioprovincialism and regional climate. However, very little is known about the timing, dynamics and climatic significance of shallow oceanic connection along the Tasmanian Gateway (Veevers et al., 1991; Woodburne and Case 1996), hampering quantification of the environmental consequences of opening.

Recently, Integrated Ocean Drilling Program (IODP) recovered a relatively complete early - middle Eocene shelf sequence at Site U1356 that yields ample organic matter, suitable to reconstruct the environmental conditions along the east Antarctic margin and hinterland (Fig 1). Combined organic geochemical and marine and terrestrial palynological information portray a near-tropical setting for the early Eocene (~53 Ma; Contreras et al., in prep.; Bendle et al., in prep.), and a sea-ice dominated earliest Oligocene (Escutia et al., 2011), evidencing major middle - late Eocene cooling. To capture the timing and duration of this cooling and assess the potential role of early Tasmanian Gateway opening, we studied assemblages of dinoflagellate cysts for ocean circulation reconstructions (Chapter 3), and biomarkers for continental air temperature (MBT/CBT; Weijers et al., 2007b) and sea surface temperature (TEX<sub>86</sub>; Schouten et al., 2002; Kim et al., 2010; see Supplements for detailed discussions on these proxies).

The MBT/CBT and TEX<sub>86</sub> from the Wilkes Land Margin indicate near-tropical conditions in the early Eocene, with air temperatures of 25-27°C and SSTs of 23°C or 32°C, depending on the applied calibration. In the latest early Eocene, MAAT cooled by ~6°C and SSTs cooled by 3-5°C, regardless of the calibration (see Supplements; Fig. 2). The TEX<sub>86</sub> data from the Pacific side of the Tasmanian Gateway (ODP Site 1172; recalibrated from Chapter 2; see Supplements), show a distinctly different pattern: southwest Pacific Ocean SSTs remain tropically warm or warmed slightly in the same interval (Fig. 2; Chapter 2). Critically, the SST trends in the southwest Pacific Ocean closely track deep-ocean temperatures, as indicated by the global stack of benthic foraminiferal oxygen isotopes (Fig. 2; Chapter 2). This implies that the recorded cooling starting at ~52-49 Ma in the Wilkes Land sector, was regional in nature.



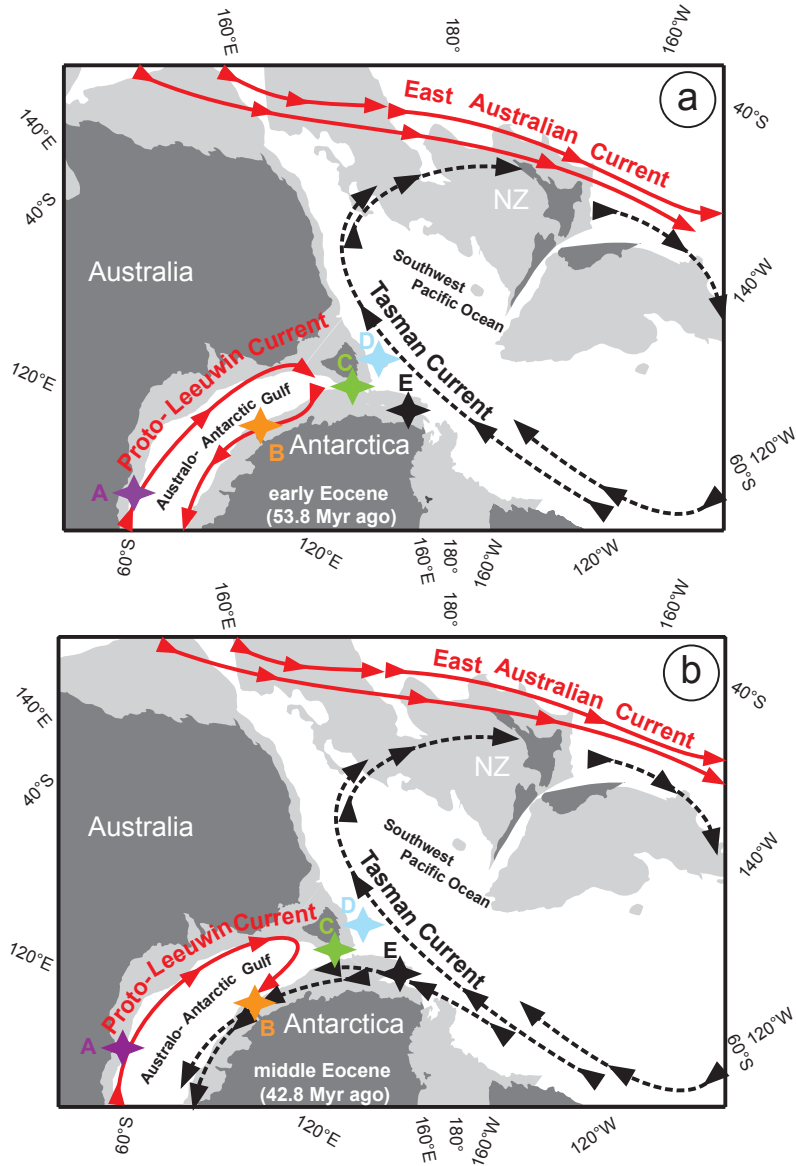


Figure 1. Eocene continental configurations of the Australian sector of the Southern Ocean for the early Eocene (a; Subchron C24n; 53.8 Ma) and middle Eocene (b; Subchron C20n; 42.8 Ma). Maps (modified from Cande and Stock (2004)) show the positions of the sites used in this study: ODP Site 1128 (A); IODP Site U1356 (B); *RV Sonne* and *RV Rig Seismic* gravity core sites (C); ODP Site 1172 (D) and ODP Sites 1171 (E). Dark-grey areas reflect present-day shorelines, light-grey areas are submerged continental blocks above 3000 meters water depth. NZ refers to New Zealand. The maps are overlain by surface currents as interpreted from modeling experiments of Sloan and Rea (1995), later reproduced by Huber et al. (2004). We here present evidence that the Tasmanian Gateway was open from 52-49 Ma onwards, which allowed for the through flow of the Antarctic Counter Current.



# EARLY PALEOGENE TASMANIAN GATEWAY OPENING

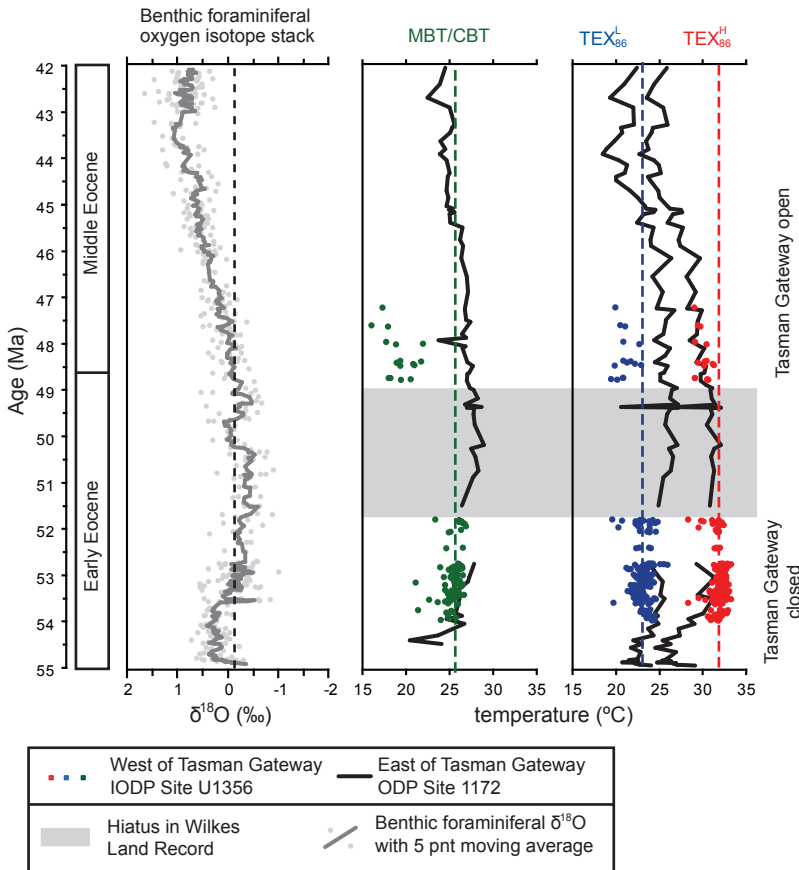


Figure 2. Benthic foraminiferal oxygen isotope stack (from Zachos et al., (2008) with amendments; see Chapter 2) MBT/CBT- (green) and  $\text{TEX}_{86}$ -based reconstructions (in two calibrations:  $\text{TEX}_{86}^{\text{H}}$  (red) and  $\text{TEX}_{86}^{\text{L}}$  (blue); see Supplements) for mean annual air and sea-surface temperature, respectively, from the west side of the Tasmanian Gateway (IODP Site U1356). These data are plotted with the temperature evolution from the east side of the Tasmanian Gateway (black lines; ODP Site 1172). Dashed lines represent average early Eocene temperatures for Wilkes Land as a reference for the lower middle Eocene temperatures.

We reconstruct oceanic surface circulation by tracking assemblages of organic cysts of dinoflagellates (dinocysts), which are highly sensitive recorders of surface ocean properties (Sluijs et al., 2005). Early Paleogene Southern Ocean dinoflagellate cyst (dinocyst) assemblages closely track different water masses (Chapter 3). Typically, assemblages from the southwest Pacific Ocean are dominated by endemic Antarctic dinocysts, while those from the AAG are mainly characterized by cosmopolitan and low- and mid-latitude-derived dinocyst taxa (Chapter 3). These bioprovinces mirror surface currents as projected by modeling experiments: the AAG is characterized by the low-latitude-derived PLC, while the southwest Pacific Ocean receives Antarctic-derived surface waters via the Tasman Current (Sloan and Rea 1995; Huber et al., 2004; Fig. 1a). In addition, middle Eocene dinocyst assemblages



from Ocean Drilling Program (ODP) Site 1128 on the Australian Bight almost entirely consist of cosmopolitan low- and mid-latitude taxa, consistent with the modeled circulation (Fig. 1; 3; see Supplements).

Abundant occurrences of the genus *Apectodinium* are restricted to (sub-) tropical settings in the early Paleogene (Iakovleva et al., 2001; van Roij 2009), apart from during Paleocene-Eocene Thermal Maximum, when it becomes globally abundant (Crouch et al., 2001; Sluijs et al., 2007a). Southern Ocean sediments, including the Southwest Pacific (Fig. 3), are typically devoid of *Apectodinium* even for the warm early Eocene. Uniquely, *Apectodinium* is dominant along the Wilkes Land margin in the early Eocene (50-80% of the dinocyst assemblage throughout; Fig. 3). We consider this dinocyst signal to document the influence of the PLC in the AAG (Fig. 1a). Endemic dinocysts exhibit much higher abundances in the early Eocene on the east side of the Tasmanian Gateway (~30%) as compared to the AAG (<10%; Fig 3), reflecting the influence of the Antarctica-derived Tasman Current in the Southwest Pacific Ocean (Fig. 1a).

The first incursion of Antarctic endemic dinocysts into the AAG is recorded in Wilkes Land in the uppermost early Eocene, at ~49 Ma, while these taxa already dominated South Pacific assemblages from ~50 Ma onwards (Fig. 3). Also in samples obtained from the southern tip of Tasmania (RV *Rig Seismic* and RV *Sonne* cores (Truswell 1997); Fig. 1, 2) endemic dinocysts dominate. Other sites on the Australian side of the AAG (ODP Site 1128; Feary et al., 2000) are consistently dominated by low-mid-latitude dinocysts during the middle Eocene (Fig. 3). Younger sites in that region are typically dominated by low-latitude and/or cosmopolitan taxa as well, with clear affinities to the PLC (Chapter 3). The dominance of endemic dinocysts with Pacific affinities at the Wilkes Land margin is hence unique for the western side of the Tasmanian Gateway. We consider this distinct pattern to reflect the onset of through flow of an Antarctic Counter Current from the southwest Pacific Ocean into the Southern part of the AAG (Fig. 2b). The timing of the onset of dinocyst endemism on the Wilkes Land shelf lies between 52 and 49 Ma, the uncertainty caused by a 2-3 million year long hiatus in Hole U1356A (see age model section in Supplements). The middle Eocene section from the Wilkes Land margin contains dinocyst taxa that are unknown from the southwest Pacific Ocean, such as the Northern Hemisphere *Phthanoperidinium alectrolophum*. This testifies to a persistent influence of the PLC on the AAG. It also implies that the Tasmanian Gateway apparently effectively blocked any eastward flow of the PLC waters. Through flow of this current to the Southwest Pacific Ocean did not occur until 35.5 Ma, when the influx of cosmopolitan and low-latitude dinocysts species to the southwest Pacific sites is documented (Stickley et al., 2004b).

The onset of Antarctic dinoflagellate endemism at the Wilkes Land margin at ~50 Ma coincides with an abrupt increase in spreading rates of oceanic crust in the AAG (Cande and Stock 2004), at least with the present resolution of dinocyst data and tectonic reconstructions. Sedimentary records from the continental blocks surrounding Tasmania suggest a gradual deepening during the middle Eocene (Röhl et al., 2004a). We hypothesize that the increased spreading rates in the AAG initiated a





## EARLY PALEOGENE TASMANIAN GATEWAY OPENING

gradual drowning of the continental blocks of the Tasmanian Gateway. Early stages of opening of the gateway are likely to have occurred between the South Tasman Rise and the Antarctic Margin, via the active Balleny Fracture Zone, south of 60° Slat. (Cande and Stock 2004). Because of the prevailing easterlies, this would be particularly favorable to westward through flow of an Antarctic Counter Current.

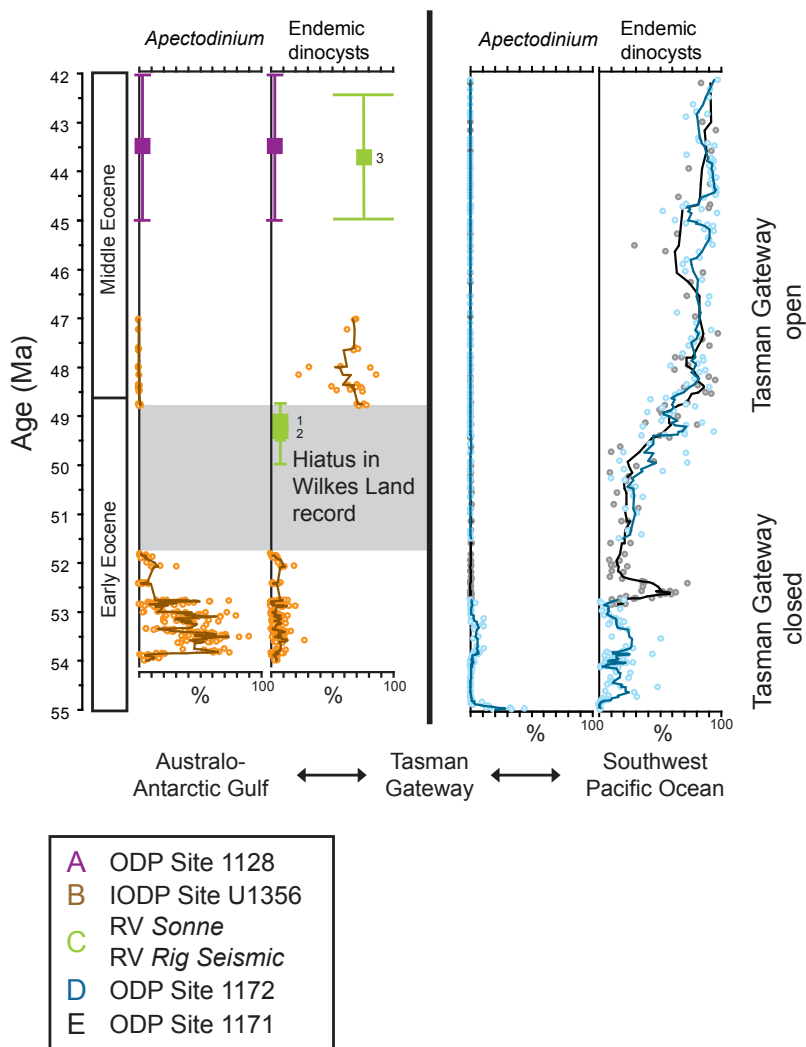


Figure 3. Selected dinocyst data from four investigated localities (letters refer to Fig. 1), combined for both sides of the Tasmanian Gateway: ODP Site 1128 (purple); IODP Site U1356 (orange); RV Sonne and RV Rig Seismic Gravity Core Sites (green; SO36-22SL (1), SO36-30KL (2) and RV Rig Seismic Core 147/GC01 (3) (Truswell 1997); ODP Site 1172 (black) and ODP Site 1171 (blue). Plotted is the relative abundance of *Apectodinium* spp. and endemic dinocysts.



General circulation model (GCM) experiments suggest that the climatic consequences of the late Eocene deepening of the Tasmanian Gateway were limited to a regional scale only and that there was little effect on inter-regional, let alone global climates (Huber et al., 2004; Sijp et al., in press). Deep and wide northern opening of the Tasmanian Gateway (which is the scenario investigated in these models) leads to the initiation of eastward through flow of the subtropical PLC. Eventually, this led to distinct warming of the SE offshore Australian sector by incoming subtropical waters, but only minor cooling along the Antarctic margin according to (Huber et al., 2004). However, a southern opening as reconstructed here, with through flow of just the Antarctic Counter Current, has not yet been investigated with GCM models, because that requires small grid cells and extensive computational time. Other GCM experiments point to declining atmospheric greenhouse gas concentrations as a major forcing for Paleogene global cooling (DeConto et al., 2008), although field data supporting this is little (Zachos et al., 2008). Our data support inferences that the onset of westward through flow of an Antarctic Counter Current invoked regional cooling along the eastern Antarctic margin, and that this process occurred much earlier than previously thought.

The tectonic phase separating the southern Tasmanian continental margin from Antarctica closely coincides with the first steps of global cooling following the warmest time interval of the past 100 million years. Proxy data and climate modeling suggested that greenhouse gas concentration changes were an important global climate forcing element in the greenhouse-icehouse transition. However, ice sheet models suggest that Southern Ocean gateways do modulate the timing and magnitude of continental ice sheet formation with declining atmospheric  $p\text{CO}_2$  (DeConto and Pollard 2003a, b). Hence, the opening of critical ocean gateways may still have provided critical climatic boundary conditions that increased Antarctic sensitivity to greenhouse gas forcing.



## Supplement to Chapter 5

### 1. Material

#### 1.1 Site and lithology descriptions

##### 1.1.1 IODP Site U1356

Integrated Ocean Drilling Program Site U1356 is located at  $\sim 64^\circ$  southern latitudes (Slat.) off Wilkes Land, Antarctica, at the transition between the continental rise and the abyssal plain at 4003 meters below sea level (Escutia et al., 2011). The lowermost 110 meters of core (890-1000 mbsf) are dated as early-middle Eocene based on dinocyst- and magnetostratigraphy. Sediments from 890 to 945 mbsf consist of interbedded stratified and massive sandstones, diamictites, silty claystones, and siltstones with graded bedding and parallel lamination. Abundant intraformational clasts are present in the fining-upward sandstones.

##### 1.1.2 ODP Site 1128

Ocean Drilling Program Leg 182 Site 1128 is located on the upper continental rise at 3875 meters water depth (Feary et al., 2000). The Eocene section (290-452 meters below sea floor (mbsf)) consists of bioturbated clayey siltstone and sandy siltstone with glauconite. Initial results from the expedition suggest that the low concentration of carbonate in the lowermost sediments recovered at the site argues for deposition below the CCD or lysocline (Feary et al., 2000). Dinocyst stratigraphy confirms the age provided by the benthic foraminifer assemblages as late early Eocene (Feary et al., 2000). However, based on dinocyst-derived data we argue for syn-depositional dissolution of carbonate in shelfal environments, because dinocyst assemblages suggest upper shelfal settings in the Eocene. Also, in light of the drowning of the Wilkes Land and Tasmanian continental blocks in the Eocene (Stickley et al., 2004b; Close et al., 2009), the sections in the Australian Bight may have experienced deepening from shelfal settings to continental rise settings in the latter part of the Eocene.

##### 1.1.3 ODP Site 1171

Ocean Drilling Program Leg 189 Site 1171 is located in lower bathyal water depths of about 2150 meters on the southern part of the South Tasman Rise, at  $48^\circ$  Slat. (Fig. S1; Exon et al., 2001). Drilling at ODP Site 1171 penetrated a small north-south oriented rift basin bounded to the east by the Balleny Fracture Zone (Exon et al., 2001). The Eocene part of the succession is cored within Hole 1171D, which penetrated to  $\sim 959$  mbsf. The age model for this site suggests strata from early Eocene (mid Subchron C24n) to early Oligocene times (Stickley et al., 2004b; Chapter 1) in Hole 1171D. Sediments are composed of dark greenish-grey or olive-grey nannofossil-bearing claystones and silty claystones. Carbonate content decreases downhole, evidencing deepening trend going upsection. The bottom  $\sim 40$  m of the sedimentary succession is pervasively laminated. Carbonate content is  $<1$  wt% and organic carbon content (0.9 wt%) is higher than upsection. Sedimentation rates average 4-12 cm/kyr for the entire Eocene section (Exon et al., 2001).



## 1.1.4 ODP Site 1172

Ocean Drilling Program Leg 189 Site 1172 is located on thinned continental crust on the submerged flat western side of the East Tasman Plateau (ETP) at 45° Slat. and at a water depth of 2620 meters (Fig. S1; Exon et al., 2004). The plateau is roughly circular (200 km across), lies in water depths of 2200–2800 m, has late Cretaceous oceanic crust to the east and probably to the southwest and south, and is attached to Tasmania to the northwest (Exon et al., 2001). During the middle Eocene, the ETP was at ~65° Slat. and at much shallower water depths, before its rapid collapse and subsequent northward movement (55 km/m.y.) commenced in the late Eocene (Stickley et al., 2004b). Four holes were drilled in total, of which Hole 1172A extends to the mid-Lutetian (Exon et al., 2001). Hole 1172D contains sediments from mid-Lutetian downwards, with good overlap between the two holes.

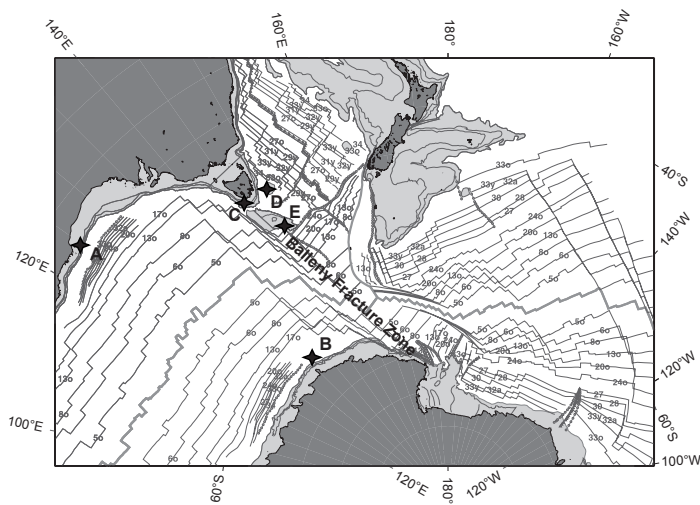


Figure S1. Present-day continental configuration of the Australian Sector of the Southern Ocean (map modified after Cande and Stock (2004)), showing the position of the sites used in this study: ODP Site 1128 (A); IODP Site U1356 (B); *RV Sonne* and *RV Rig Seismic* Gravity Core Sites (C) and ODP Sites 1172 (D) and 1171 (E). Also plotted are magnetic anomalies in the oceanic crust. Dark grey areas are subaerial, light grey areas are submerged continental blocks above 3000 meters water depth, white is below 3000 meters water depth.

Sediments used in this study are from about 500 to 605 mbsf and consist of olive-grey claystone with minor amounts of silty claystone, nannofossil-bearing claystone, and clayey siltstone (Exon et al., 2001). Age control in the section relies on dinocyst biostratigraphy and magnetostratigraphy (Stickley et al., 2004a; Chapter 1). A first inventory of dinocyst species found during ODP Leg 189 is published in the Scientific Results section of the Ocean Drilling Program (Brinkhuis et al., 2003a). The magnetostratigraphy allowed for comparison of the Southern Ocean bio-events found at ODP Site 1172 to global dinocyst events (Williams et al., 2004), and a dinocyst zonation scheme for the early Paleogene was proposed (Chapter 1). The sandstones also contain mica and pyritized shell fragments. Within Core -98R distinctive reddish brown silty claystones are repetitively interbedded at the decimeter- to meter-scale



with greenish grey and brown sandy mudstones with parallel laminae. The lowermost 50 meters of sediment consists of dark green bioturbated claystone that is faintly stratified (millimeter- to meter-scale) as defined by colour variations (light to dark bands; Escutia et al., 2011).

## 2. Methods

### 2.1 Palynology

#### 2.1.1 Sample processing (ODP Site 1128 and IODP Site U1356)

Palynological data from ODP Sites 1171 and 1172 were published in Chapter 1 and 3; we refer to that chapter for processing methodology for samples of those sites. Standard procedures of the Laboratory of Palaeobotany and Palynology of Utrecht University were used to process samples for palynology, with some amendments. Samples were crushed to chips of several millimeters, and oven-dried (60°C) or freeze-dried for several days. Subsequently, samples were weighted and put in 200 ml plastic bottles with screw-on caps. A tablet containing a known amount of *Lycopodium* spores (18,583 ±4.1% spores per tablet) was added to each sample for quantitative analyses. Samples were wetted with a 10% Agepon wetting detergent, and subsequently 10% HCl was added to carbonate-free samples. In case carbonate was present, 30% HCl was added, and samples were settled overnight, decanted, water was added and centrifuged (2000 rpm, 5 minutes). Samples were decanted again. For all samples, silicates were removed by adding 38% HF. Samples were shaken on a shaker table for 2 hours (300 rpm), bottles were filled up with water and samples settled overnight. Subsequently, bottles were decanted, and an overload of 30% HCl was added to remove silica gels. Samples were centrifuged (2000 rpm, 5 minutes), decanted and bottles were filled to halfway with HF. Samples were shaken for 2 hrs on a shaker table (300 rpm), filled up with water and settled overnight. The next day samples were decanted, and removal of silica gels was done again by adding an overload of 30% HCl, samples were centrifuged (2000 rpm, 5 minutes), decanted and subsequently rinsed with water, centrifuged and decanted. The rinsing was done 3 times.

From the organic residue, a small subsample was taken for pyrite analyses. The remainder of the residue was sieved over a 250-micrometer nylon sieve to remove large particles. The filtrate was subsequently sieved over a 10-micrometer sieve. For sieving, an ultrasonic bath was used to disintegrate palynodebris. The organic residue was separated from heavier particles (pyrite and other particles) by placing it into a ceramic bowl in the ultrasonic bath for 5 minutes: the heavy particles settled, and the palynofacies remained suspended. The ceramic bowl was subsequently decanted and the palynofacies were transferred into a glass vial. Heavy particles left over in the ceramic bowl after decanting, were transferred into the vial containing the unsieved residue for pyrite analyses. Palynofacies residues were centrifuged (2000 rpm, 5 minutes), decanted and glycerin water was added. The residue was transferred to microscope slides and slides were sealed using nail polish. Two slides were made for each sample.



### 2.1.2 Dinocyst taxonomy and endemism

Dinocyst taxonomy follows that as cited in Fensome and Williams (2004) and with emended dinocyst species and formally described new species such as Sluijs et al. (2009b) and Clowes and Wilson (2006). We follow the inventory of endemic dinocysts as listed in Chapter 3.

### 2.2 Organic geochemistry IODP Site U1356

Organic compounds were extracted from powdered and freeze-dried sediments of Site U1356 with dichloromethane (DCM)/methanol (MeOH) (9:1, v/v) using the accelerated solvent extraction technique (Dionex). Excess solvent was removed using rotary evaporation under vacuum. The total lipid extracts (TLEs) were dried under nitrogen flow, weighed, and split where possible. An aliquot of the TLE was further separated in an apolar, ketone, ethyl acetate (EtOAc) and polar fractions over an activated Al<sub>2</sub>O<sub>3</sub> column using hexane:DCM (9:1, v/v), hexane:DCM (1:1, v/v), EtOAc:DCM (1:1 v/v) and DCM:MeOH (1:1, v/v), respectively. Aluminum oxide (Al<sub>2</sub>O<sub>3</sub>) was activated by oven-drying for at least 4 hrs at 150°C. All fractions were dried over nitrogen flow and subsequently weighed.

The polar fractions were dissolved in a 99:1 hexane/propanol solvent, and filtered using a 0.45 µm, 4 mm diameter polytetrafluoroethylene (PTFE) filter, before being analyzed using a high performance liquid chromatography/atmospheric pressure positive ion chemical ionization mass spectrometry (HPLC/APCI-MS). HPLC/APCI-MS analyses were done according to Schouten et al. (2007a) using an Agilent 1100 series LC/MSD SL and separation and a Prevail Cyano column (2.1 x 150 mm, 3 mm; Alltech), maintained at 30°C. The GDGTs were eluted using a changing mixture of hexane and propanol as follows: 99% hexane: 1% propanol for 5 minutes, then a linear gradient to 1.8% propanol in 45 minutes. Flow rate was 0.2 ml per minute. Single ion monitoring was set to scan the 5 [M+H]<sup>+</sup> ions of the GDGTs with a dwell time of 237 ms for each ion.

The TEX<sub>86</sub><sup>L</sup> and TEX<sub>86</sub><sup>H</sup> ratios are based on glycerol dialkyl glycerol tetraethers (GDGTs; Fig. S2) and were calculated according to Kim et al. (2010). For conversion to temperature we used the following equations based on core top calibrations of Kim et al. (2010):

$$\text{SST} = 68.4 * \text{TEX}_{86}^{\text{H}} + 38.6 \quad (\text{R}^2 = 0.87; n = 255; p < 0.0001) \quad (5.1)$$

$$\text{SST} = 67.5 * \text{TEX}_{86}^{\text{L}} + 46.9 \quad (\text{R}^2 = 0.86; n = 396; p < 0.0001) \quad (5.2)$$

MBT/CBT ratios were calculated according to Weijers et al. (2007b). They were converted to air temperature using the calibration:

$$\text{MBT} = 0.122 + 0.187 * \text{CBT} + 0.020 * \text{MAT} \quad (\text{R}^2 = 0.77) \quad (5.3)$$



## EARLY PALEOGENE TASMANIAN GATEWAY OPENING



Figure S2. Chemical structure of the glycerol dialkyl glycerol tetraethers that were used to establish the  $TEX_{86}$  proxy for mean annual sea surface temperature.

### 3. Application and uncertainties of $TEX_{86}$ paleothermometry

Soil-derived input of membrane lipids can significantly influence  $TEX_{86}$  SSTs (Weijers et al., 2006). The input of soil-derived membrane lipids relative to the marine is estimated using the Branched versus Isoprenoid Tetraether (BIT) index (Hopmans et al., 2004). We discarded  $TEX_{86}$  SST estimates in those samples with  $BIT > 0.4$ . Consequently, we excluded 25% of  $TEX_{86}$  data points (Fig. S3), but that did not significantly affect average early Eocene or middle Eocene SSTs. The latest core top data set for  $TEX_{86}$  and the statistical evaluation of the relationships between



Crenarchaeal lipids (Fig. S2) abundances and temperature resulted in two separate calibrations for  $\text{TEX}_{86}$ . It was found that the abundance of regional isomer of crenarchaeol (cren'), used in the original  $\text{TEX}_{86}$  calibration (Schouten et al., 2002) was not varying with temperatures in polar oceans (Kim et al., 2010). Therefore the  $\text{TEX}_{86}$  index has a much higher coefficient when the polar core top data (i.e., those with SSTs  $<5^\circ\text{C}$ ) are removed and thus the  $\text{TEX}_{86}^{\text{H}}$  (which is the log of  $\text{TEX}_{86}$ ) was proposed to estimate SSTs  $>15^\circ\text{C}$ :

$$\text{SST} = 68.4 * \text{TEX}_{86}^{\text{H}} + 38.6 \quad (r^2 = 0.87; n = 255; p < 0.0001) \quad (5.4)$$

Where

$$\text{TEX}_{86}^{\text{H}} = \log((\text{II} + \text{III} + \text{cren}') / (\text{I} + \text{II} + \text{III} + \text{cren}')) \quad (5.5)$$

For SSTs below  $15^\circ\text{C}$ , in particular the polar oceans and alternative index was proposed without the crenisomer,  $\text{TEX}_{86}^{\text{L}}$ . These two calibrations provide statistically the best-fit solutions to the core-top dataset (Kim et al., 2010). It is as yet unknown why the relationship between  $\text{TEX}_{86}$  and SST is atypical in colder environments, compared to the rest of the world. One could hypothesize that the archaeal community consists of different species at high latitudes, with different membrane adaptation to SST. Another possibility is that the extreme seasonality at high latitudes, with half a year of darkness, biases the  $\text{TEX}_{86}$  signal. In any case, this difference causes a conundrum when  $\text{TEX}_{86}$  is applied to high latitude settings in the early Paleogene greenhouse world. The Southern high latitudes experienced extreme warmth in the Eocene. Pollen analyses indicate coldest month minimum temperatures approaching  $13^\circ\text{C}$ . This would argue for the use of  $\text{TEX}_{86}^{\text{H}}$ . Yet, like present day, also the Paleogene Southern Ocean experienced extreme seasonal cycles, with several months of darkness each year. Until the mechanism explaining the difference in the two  $\text{TEX}_{86}$ -calibrations is solved, it is uncertain which calibration can be applied. For instance, if the seasonal extremes cause the present-day atypical  $\text{TEX}_{86}$ -SST relationship, then the geographical position of the Southern Ocean suggest the use of  $\text{TEX}_{86}^{\text{L}}$  irrespective of the SSTs being above or below  $15^\circ\text{C}$ . However, if the crenisomer is important in temperature adaptation at higher temperatures, as implied by Kim et al. (2010), then  $\text{TEX}_{86}^{\text{H}}$  should be applied in the Paleogene Southern Ocean. An argument for  $\text{TEX}_{86}^{\text{L}}$  is that it predicts SST  $>15^\circ\text{C}$  just as good as  $\text{TEX}_{86}^{\text{H}}$ : the latter becomes important when extrapolations outside present-day temperature ranges are encountered. On the other hand,  $\text{TEX}_{86}^{\text{H}}$  provides the best fit with  $U_{37}^{\text{K}}$  SSTs in the middle Eocene of the southwest Pacific Ocean (Chapter 6). The calibration error is not plotted in the main text, but is  $\pm 3^\circ\text{C}$  for  $\text{TEX}_{86}^{\text{H}}$  and  $\pm 4^\circ\text{C}$  for  $\text{TEX}_{86}^{\text{L}}$ .





# EARLY PALEOGENE TASMANIAN GATEWAY OPENING

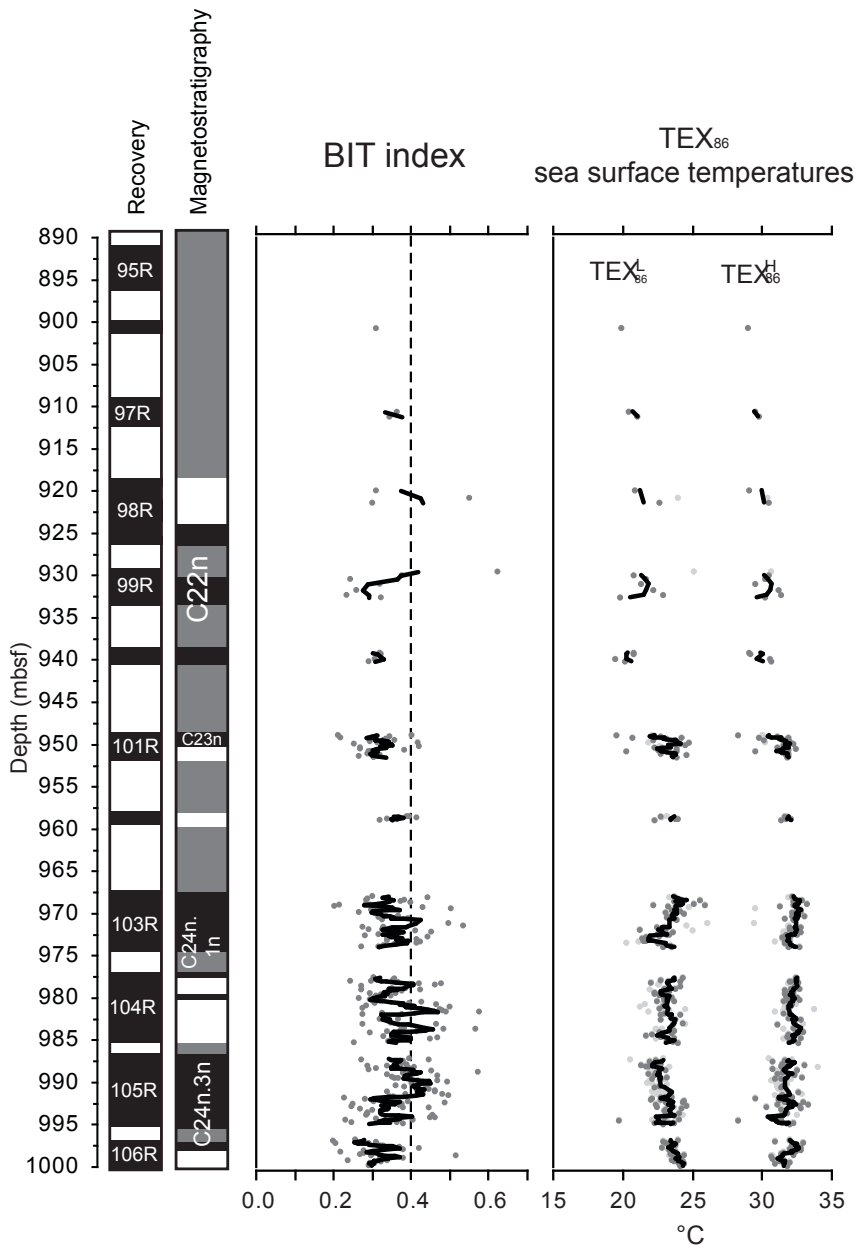


Figure S3. Branched versus isoprenoid tetraether (BIT) index values (left), and  $TEX_{86}$  SST inferences (right; in two calibrations, see text) of IODP Site U1356A. We use a cutoff value for BIT values of 0.4 (black dashed line), above which we discard the  $TEX_{86}$  estimates (grey  $TEX_{86}$  data points). This resulted in the loss of ~25% of the  $TEX_{86}$  data.



#### 4. Constraints on MBT/CBT air temperature proxy

The MBT/CBT proxy for air temperature is a proxy derived from branched glycerol dialkyl glycerol tetraether (GDGT) membrane lipids (Fig. S4) and its relationship to pH. These membrane lipids are produced by a yet unknown group of anaerobic soil bacteria (Weijers et al., 2007b). In marine sedimentary records, notably those in shelf settings, these compounds were recognized as well, and were interpreted to originate from continental soils: soil erosion processes and runoff further transported the molecules to the marine realm (Hopmans et al., 2004; Walsh et al., 2008). The process involved in this transport causes -by definition- that the MBT/CBT air temperature signal is averaged over large areas and long time scales. However, MBT-CBT records of coastal marine sites shows that temperature changes are in phase with known climate events and do not show a considerable time lag (Weijers et al., 2007a; Weijers et al., 2007c).

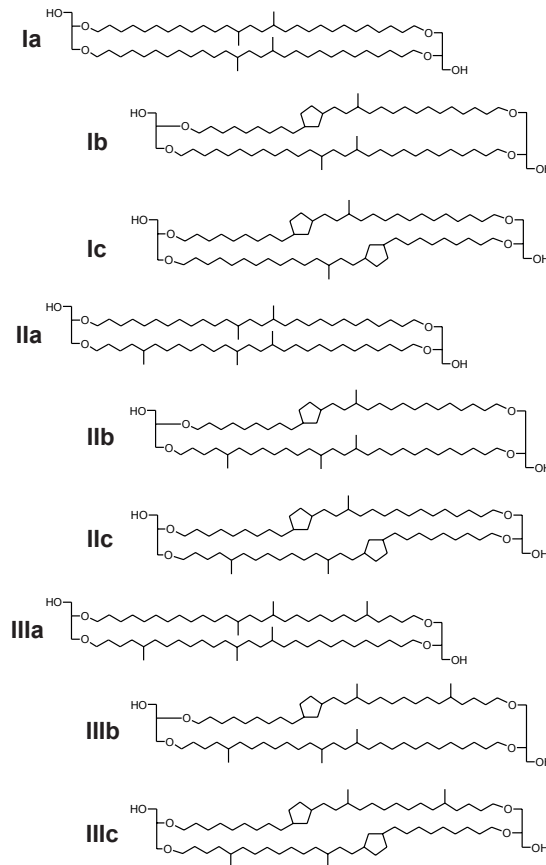


Figure S4. Chemical structure of the branched glycerol dialkyl glycerol tetraethers that were used to establish the MBT/CBT proxy for mean annual air temperature and soil pH.



The MBT/CBT proxy is calibrated against mean annual air temperature and a recent study could not detect a seasonal change in this proxy, although this does not exclude a seasonal bias (Weijers et al., 2011). Indeed, application of this proxy in the Cenozoic suggests that at high latitudes there may be a seasonal bias and that the proxy mainly reflects summer temperatures (Eberle et al., 2010). In contrast, other high latitude applications of this proxy show good matches with MAT records from other proxies (Schouten et al., 2008; Ballantyne et al., 2010). Therefore, it is uncertain to which extent the MBT/CBT proxy will be seasonally biased in Antarctica. The MBT-CBT temperature data fall in the middle of the temperature ranges of the pollen and spores, which suggests that the MBT-CBT proxy indeed reflects mean annual air temperature.

### 3 Age models

#### 3.1 Age model ODP Site 1171 and 1172

An integrated dinocyst-magneto-isotope stratigraphic framework is developed from ODP Sites 1171 and 1172 (Chapter 1). Key dinocyst events were recognized at both sites that could be correlated to New Zealand sections (Crouch 2001; Crouch and Brinkhuis 2005) as well. Both sections were calibrated to magnetostratigraphy, also with additional age constraints from carbon isotope stratigraphy for the Middle Eocene Climatic Optimum (Chapter 6) and the Paleocene-Eocene Thermal Maximum (Chapter 4). The magnetostratigraphic age model from Chapter 1 is applied.

#### 3.2 Age model IODP Site U1356

The coeval presence of *Impagidinium cassiculum* and *Samlandia delicata* in the lowermost samples of the record from IODP Site U1356A correlates to dinocyst zone NZE2b of Crouch and Brinkhuis (2005) and SP4 as described in Chapter 1 (Fig. S5). At ODP Site 1172, this dinozone is correlated to just below the C24r-C24n.3n magnetic reversal. That makes the oldest magnetic reversal in Core U1356A-106R (at 997.80 mbsf) the C24r-C24n.3n reversal (Fig. S5). This dinocyst zone also sees the FO of *Schematophora obscura*. The First Occurrence (FO) of *Dracodinium waipawaense* is tentatively correlated to nannoplankton zone NP11 in New Zealand. At ODP Site 1172, the FO of *D. waipawaense* is within a hiatus spanning the latter half of Subchron C24n and C23r. Therefore, the FO of *D. waipawaense* correlates to Subchron C24n. At ODP Site 1171, the FO of *D. waipawaense* is poorly correlated to magnetostratigraphy, but seems to be correlated to mid-Subchron C24n. Consistently, at Site U1356A we find the FO of *D. varielongitudum*, which is the Northern Hemisphere ecophenotypic morphotype of *D. waipawaense*, correlated to a magnetic reversal between Cores U1356A-105R and -104R (~986 mbsf) that we here assign the C24n.3n-C24n.2r chronboundary to (Fig. S5). The subsequent cores (U1356A-104R and -103R) bear little biostratigraphic datums to allow for a high-resolution correlation to other sites; all dinocyst species present correlate to Subchron C24n. The top of Core U1356A-104R and Core -103R has a normal polarity, which we, based on the presence of *D. varielongitudum*, assign to Subchron C24n.1n. Core U1356A-102R has a reversed polarity and still contains *D. varielongitudum*. This core is correlated to Subchron C23r. The first occurrence of *Wetzeliella samlandica* and *Charlesdowniea columna*



within Core U1356A-101R (~951.04 and 948.9 mbsf) correlates to the onset of C23n. In turn, the reversal within Core U1356A-101R (~950 mbsf) is correlated to the C23r-C23n.2n reversal. Dinocyst assemblages within these cores are similar to those found in age-equivalent strata of ODP Sites 1172 and 1171, with high abundances of the Goniodomid and Wetzelielloid complexes. Dinocyst assemblages in Core U1356A-100R are distinctly different from those below. Between Cores U1356A-101R and -100R, the last occurrence of *Wetzeliella samlandica*, *Homotryblidium tasmaniense* and *Palaeocystodinium golzowense* is observed. Within Core -100R, *Arachnodinium antarcticum* has a FO, together with *Phthanoperidinium alectrolophum* and *Membranophoridium perforatum*. The FO of *A. antarcticum* correlates to Subchron C22n. Few specimens of *Damassadinium crassimuratum* were identified, with a LO within Core -98R, that correlates to C22n. The absence of *Enneadocysta multicornuta* and *Enneadocysta dictyostila* in Cores U1356A-100R through -96R correlates this entire section to Subchron C21r or older. The LO of in situ *Membranophoridium perforatum* makes the recovered section in Cores 95R-4 and 100R older than 46 Ma.

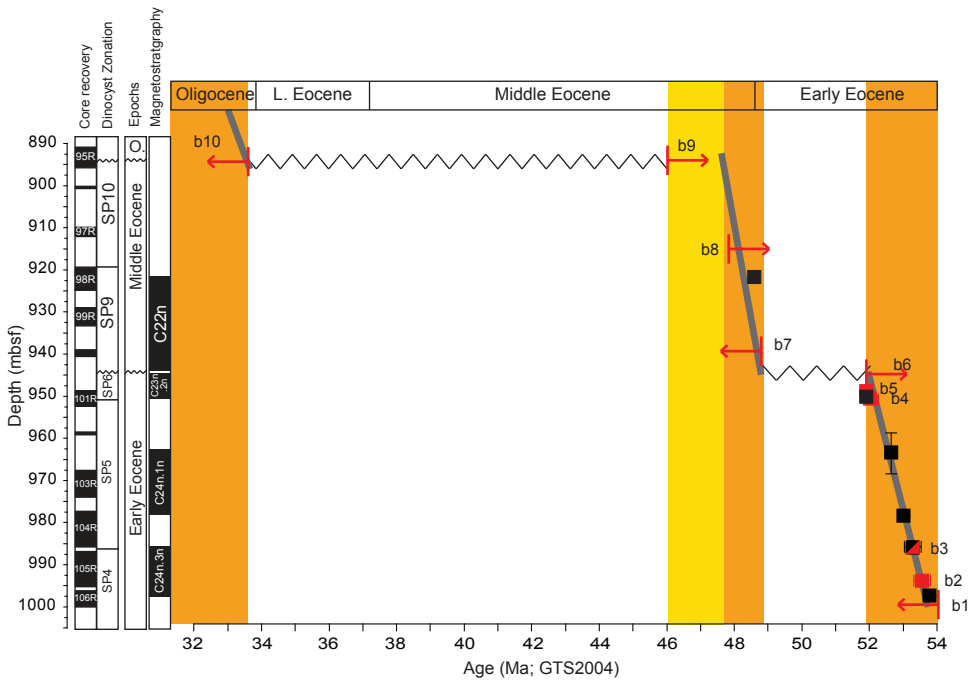


Figure S5. Age-depth plot of the lowermost 110 meters of core of IODP Site U1356. Plotted are dinocyst events (red) and (shipboard) magnetic reversals (black). Orange shading indicates which time intervals are recovered, yellow shaded area is uncertain. Grey line represents best fit through the bio-magnetostratigraphic data points. Biostratigraphic labels are as follows: b1 FO *Impagidinium cassiculum*; b2 FO *Schematophora obscura*; b3 FO *Dracodinium varielongitudum/waipawaense*; b4 FO *Wetzeliella samlandica*; b5 FO *Charlesdowniea columna*; b6 LO *Palaeocystodinium golzowense*; b7 FO *Arachnodinium antarcticum*; b8 LO *Damassadinium crassimuratum*; b9 LO in situ *Membranophoridium perforatum*; b10 FO *Malvinia escutiana*.



## EARLY PALEOGENE TASMANIAN GATEWAY OPENING

Within Core U1356A-95R Section 3 interval 82-85 cm. we recognized the FOs of the Eocene species *Enneadocysta multicornuta*, *E. dictyostila*, *Deflandrea* sp. A sensu Brinkhuis et al., 2003a, *Schematophora speciosa*, *Reticulosphaera acticoronata*, *Turbiosphaera sagena*, and *Stoveracysta kakanuiensis*. All these species have magnetostratigraphically calibrated FOs in the latter part of the Eocene (Subchrons C21n, C20r, C16n.1r, C16n.1r, C15r, C15r, and C13r, respectively). Concomitantly, this sample contains the FO of *Malvinia escutiana* (Houben et al., 2011). The first occurrence of this species has been calibrated to the Oligocene isotope event 1 (Oi-1) in the South Atlantic Ocean (Houben et al., 2011). The LO is not defined at the type locality, but ranges at least to 31.5 Ma (Houben et al., 2011). The coeval FOs of all species mentioned above suggests a hiatus between U1356A-95R section 3 and -95R section 4 that covers at least the time interval correlated to the FO of *Enneadocysta multicornuta* (onset of Subchron C21n) and the Oi-1 isotope event. According to the GTS2004 time scale, this hiatus spans at least from 47.24 Ma to 33.6 Ma. Subsequent strata contain numerous dinocyst species that originate from the time period covered by the hiatus.

### 3.3 Age model ODP Site 1128

We processed 22 samples from Cores 1128C-11H to -26X in Hole C (94-237 mbsf) and from 1128D-2R to -18R of Hole D (232-397 mbsf). Nine samples were barren for dinocysts. Dinocyst-bearing samples contain many taxa that are stratigraphically significant. These suggest a late Eocene age for the interval between 94 and 366 mbsf, with the presence of *Stoveracysta kakanuiensis*, *S. ornata*, *Corrudinium incompositum*, *Reticulosphaera acticoronata* and *Schematophora speciosa* (Sluijs et al., 2003). The two lowermost samples, however, do not yield these species and hence are considered older. The presence of (rare) *Enneadocysta dictyostila* and *Cleistosphaeridium diversispinosum*, and the absence of *Corrudinium incompositum* suggest an age between 45 Ma and 40 Ma for the lowermost sample at Hole 1128D.

### 3.4 Age model RV Sonne and RV Rig Seismic gravity cores

With the Southern Ocean dinocyst stratigraphy being well-calibrated to magnetostratigraphy, we can confidently evaluate the ages for the sediments cored at Site S036-22SL, S036-30KL and 147/GC01. The presence of *Membranophoridium perforatum* (SPDZ7-SPDZ11; Chapter 1) in samples from S036-22SL corresponds to the lower Lower *Nothofagidites asperus* Zone as correlated to by Truswell (1997). The absence of *Arachnodinium antarcticum* places the record time equivalent to Subchron C22n. S036-30KL contains *Charlesdowniea edwardsii*, which has a narrow range in the latest Ypresian (dinocyst zone SPDZ9/SPDZ10 boundary; Subchron C22n; Chapter 1). Core 147/GC01 has a considerable younger age as is suggested by the presence of *Enneadocysta dictyostila* (as *E. partridgei*; Truswell 1997). This species has a first common occurrence in dinocyst zone SPDZ12, at ~45 Ma.







The long-term warmth of the Eocene (~56-34 Ma) is commonly associated with elevated partial pressure of atmospheric carbon dioxide ( $p\text{CO}_2$ ). However, a relationship between the two has not been established for short-term climate perturbations. Here we reconstruct changes in both  $p\text{CO}_2$  and temperature over an episode of transient global warming called the Middle Eocene Climatic Optimum (MECO; ~40 Ma). Organic molecular paleothermometry indicates a 3-6°C warming of southwest Pacific sea surface temperatures (SSTs). Reconstructions of  $p\text{CO}_2$  indicate a concomitant two- to three-fold increase. The marked consistency between SST and  $p\text{CO}_2$  trends during the MECO suggests that elevated  $p\text{CO}_2$  played a major role in global warming during the MECO.





The Middle Eocene Climatic Optimum (MECO;  $\sim 40$  Ma; Bohaty and Zachos 2003) interrupts a long-term middle Eocene cooling trend (Zachos et al., 2001), with a globally uniform 4-6°C warming of both surface and deep oceans within  $\sim 400$  kyrs, as derived from foraminiferal stable oxygen isotope records (Bohaty et al., 2009). A decrease in carbonate mass accumulation rates during the MECO argues for ocean acidification induced by a rise in  $p\text{CO}_2$  (Bohaty et al., 2009). Application of paleo- $p\text{CO}_2$  proxies across the MECO has yet to confirm whether  $p\text{CO}_2$  changes are indeed associated with MECO warming.

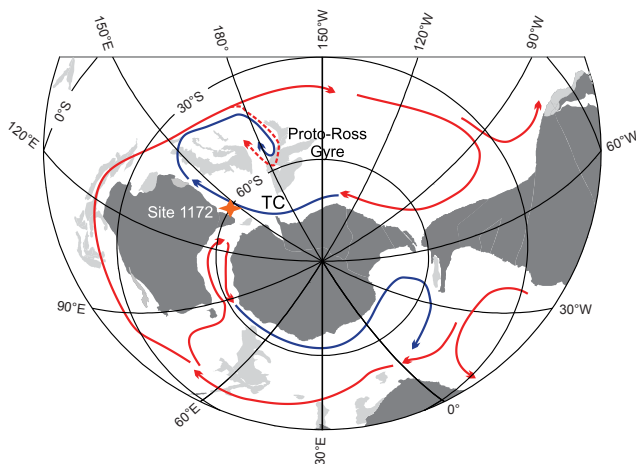


Figure 1. Paleogeographic configuration of the southern high-latitudes during the middle Eocene ( $\sim 49$ -37 Ma; map obtained from [www.ods.n.de](http://www.ods.n.de)) and ocean surface current configurations inferred from general circulation model experiments (Huber et al., 2004). The orange star indicates the paleogeographic location of ODP Site 1172 at 65°S in the southwest Pacific Ocean (Exon et al., 2004), under influence of the Antarctic-derived Tasman Current (TC).

We investigated a sedimentary succession spanning the MECO recovered from the East Tasman Plateau at Ocean Drilling Program (ODP) Site 1172, which at that time was situated on the shelf ( $\sim 65^\circ$  South paleolatitude; Fig. 1; Supplements; Exon et al., 2004). To fully capture the magnitude of the SST change associated with the MECO at this site we applied two independent temperature proxies: the alkenone unsaturation index ( $U_{37}^K$ ; Brassell et al., 1986) and the index of tetraethers consisting of 86 carbon atoms ( $\text{TEX}_{86}$ ; Schouten et al., 2002; Supplements). At the onset of the MECO,  $U_{37}^K$  and  $\text{TEX}_{86}$  indicate a rise in SST of 3°C or 6°C, respectively, which, also at this location, stands out as an interruption of long-term middle Eocene cooling (Fig. 2). Bulk carbonate oxygen isotope values ( $\delta^{18}\text{O}$ ) decrease by 1.0-1.2‰, which, if forced by SST only, also indicates a  $\sim 4$ -5°C SST rise. Additional evidence of warming is derived from assemblages of hypnozygotic organic cysts of surface dwelling dinoflagellates (dinocysts). While the middle Eocene dinocyst record at ODP Site 1172 is dominated by taxa that are endemic to the Southern Ocean (Brinkhuis et al., 2003a), an incursion of low-latitude dinocyst taxa characterizes the MECO (Fig. 2; Fig. S4). A 3-6°C SST increase is consistent with inferences from benthic foraminiferal and fine



fraction carbonate oxygen isotope records at other sites (Bohaty and Zachos 2003; Bohaty et al., 2009). The  $U_{37}^{K'}$  and  $TEX_{86}$  proxies are independent of seawater  $\delta^{18}O$ . Hence, the consistent magnitude of warming between the proxies suggests that the carbonate  $\delta^{18}O$  records were not affected by a change in  $\delta^{18}O$  of seawater, and that global ice-volume did not change significantly during MECO.

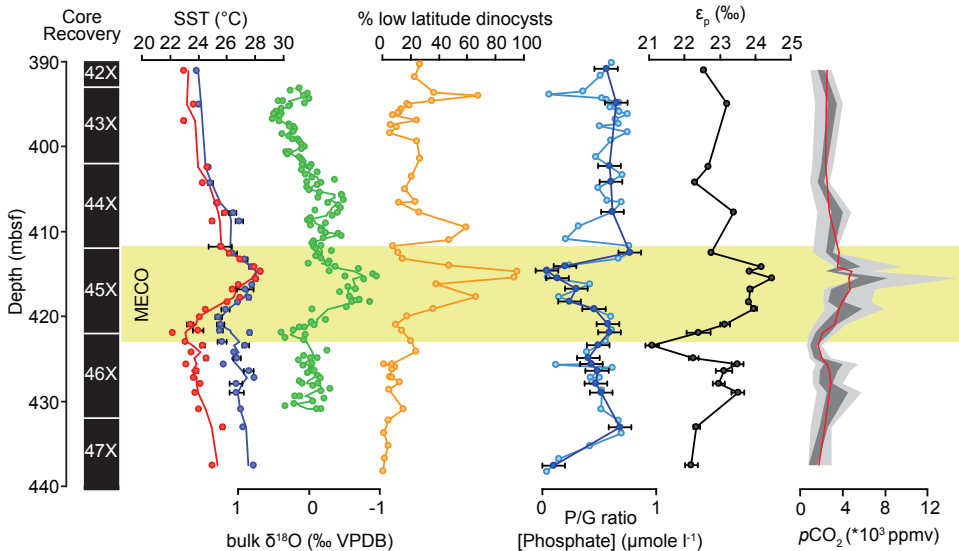


Figure 2. Geochemical and palynological results across the MECO at ODP Site 1172, Hole A, Cores 42X-47X. The MECO is identified by integrating magneto- (Stickley et al., 2004a), bio- (Stickley et al., 2004a) and isotope stratigraphy (Bohaty et al., 2009; see Fig. S2). The  $U_{37}^{K'}$  (purple),  $TEX_{86}$  (red) and bulk  $\delta^{18}O$  (green) SST reconstructions show a 3°C to 6°C warming. The yellow shaded area delimits the MECO interval. The increase in % low latitude dinocysts (in orange) at the expense of endemic dinocysts during MECO illustrates biotic response to warming. We estimated  $pCO_2$  from carbon isotopic fractionation during carbon fixation ( $\epsilon_p$ ; black) by haptophyte algae with a phosphate concentration bandwidth of 0 and 1  $\mu\text{mol l}^{-1}$  (light grey band). We further constrained phosphate estimates (dark blue line) by allowing phosphate concentrations to vary between  $0.1 \pm 0.1 \mu\text{mol l}^{-1}$  and  $0.9 \pm 0.1 \mu\text{mol l}^{-1}$  as a function of the ratio of peridinioid over gonyaulacoid dinocysts (P/G ratio; light blue line). This results in further constrained  $pCO_2$  estimates (dark grey band).  $TEX_{86}$ ,  $U_{37}^{K'}$ , oxygen isotope and  $pCO_2$  data are plotted with a 3-point running mean (solid orange, purple, green and red lines, respectively). The error bars on  $TEX_{86}$  and  $U_{37}^{K'}$  represent analytical error, and on  $\epsilon_p$  the difference between  $TEX_{86}$  and  $U_{37}^{K'}$  to calculate  $\epsilon_p$ .

Absolute SSTs as indicated by  $U_{37}^{K'}$  and  $TEX_{86}$  are consistent, with 26°C or 24°C just below the onset of MECO for the two proxies, respectively, and peak MECO SSTs exceeding 28°C. These values are much ( $\sim 10^\circ\text{C}$ ) higher than those derived from fine fraction carbonate oxygen isotope measurements from elsewhere in the Southern Ocean (Bohaty and Zachos 2003; Bohaty et al., 2009). At least part of this large discrepancy is the result of diagenetic alteration of calcite (Pearson et al., 2001). We assessed  $pCO_2$  changes by determining the stable carbon isotopic composition ( $\delta^{13}C$ ) of alkenones – long-chained ketones exclusively synthesized by specific haptophyte



algae. Carbon isotopic fractionation during carbon fixation ( $\epsilon_p$ ) by haptophyte algae varies as a function of dissolved  $\text{CO}_2$  [ $\text{CO}_{2(\text{aq})}$ ] (Pagani 2002) specific cell-physiological parameters (which show good correspondence to the surface-water concentrations of soluble phosphate), and other environmental parameters, primarily light intensity. Surface ocean [ $\text{CO}_{2(\text{aq})}$ ] originates from atmospheric  $p\text{CO}_2$  and deep waters, of which the latter is of major importance in marginal marine upwelling areas. Changes in upwelling through time may substantially change [ $\text{CO}_{2(\text{aq})}$ ] and hence would skew the reconstructed  $p\text{CO}_2$  record. At Site 1172 we argue that a change in upwelling is not responsible for the signal we recorded in the alkenones, because that would have led to prominent shifts in the bulk carbonate carbon isotope profile (Supplements).

The carbon isotopic composition of diunsaturated alkenones ( $\delta^{13}\text{C}_{37:2}$ ) ranges between -32.5 and -35.5‰ (Supplements). We used bulk carbonate  $\delta^{13}\text{C}$  to estimate the  $\delta^{13}\text{C}$  value of the dissolved inorganic carbon pool (DIC) in seawater to determine  $\epsilon_p$ . The data show background  $\epsilon_p$  values of 21-22‰ rising up to 24.5‰ during MECO (Figs. 2, 3, Supplements). The relationship between  $\epsilon_p$  and  $p\text{CO}_2$  is exponential, which results in a relatively large uncertainty in reconstructed  $p\text{CO}_2$  levels with high  $\epsilon_p$  values (Fig. 3). Temperature variations, however, play a minor role in the range of temperatures indicated by  $\text{TEX}_{86}$  and  $\text{U}_{37}^{\text{K}}$  (Fig. 2) and cannot explain the high  $\epsilon_p$  values (Fig. 3). It seems unlikely that changes in light intensity influenced  $\epsilon_p$  substantially at ODP Site 1172 (Supplements). The soluble phosphate concentration exerts a strong influence on the relation between  $\epsilon_p$  and  $p\text{CO}_2$ , particularly if  $\epsilon_p$  values are high.

To evaluate all possible absolute  $p\text{CO}_2$  estimates from our record, we applied the full range of present-day surface water phosphate concentrations. These vary between  $0 \mu\text{mol l}^{-1}$  in the oligotrophic gyres to  $>2 \mu\text{mol l}^{-1}$  in the Southern Ocean (Supplements). Yet, even when phosphate concentrations of  $0 \mu\text{mol l}^{-1}$  are assumed,  $\epsilon_p$  values between 21.2‰ and 24.5‰ yield  $p\text{CO}_2$  estimates between 600 ppmv prior to MECO and 6,400 ppmv for the MECO (Fig. 2, 3). Hence, elevated levels of  $p\text{CO}_2$  must in part be responsible for the high  $\epsilon_p$  values, with middle Eocene  $p\text{CO}_2$  being more than two times the pre-industrial value. When we assume maximal phosphate concentrations of  $2 \mu\text{mol l}^{-1}$ ,  $p\text{CO}_2$  ranges between  $\sim 2,500$  and  $\sim 24,000$  ppmv (Fig. 2, 3). The marginal marine Eocene East Tasman Plateau (Exon et al., 2004) likely experienced phosphate concentrations that were higher than  $0 \mu\text{mol l}^{-1}$  but smaller than  $2 \mu\text{mol l}^{-1}$ , because closed oceanic gateways during the Eocene (Huber et al., 2004) prevented mixing associated with the Antarctic Circumpolar Current (ACC) that causes high phosphate levels in the present Southern Ocean. Eocene southwest Pacific surface water phosphate concentrations unlikely exceeded  $1 \mu\text{mole l}^{-1}$ , which implies maximum  $p\text{CO}_2$  estimates of 1,600 ppmv just prior to MECO and 15,000 ppmv for the MECO (Fig. 2, 3). With a realistic range of phosphate concentrations,  $p\text{CO}_2$  values were between 600 and 1,600 ppmv just prior to MECO, which is in line with previous estimates of middle Eocene  $p\text{CO}_2$  values using the same proxy (Pagani et al., 2005), and rose to between 6,400 and 15,000 ppmv during MECO (Fig. 2; light grey band). Critically, MECO values exceed any previous Eocene alkenone-based estimate even when we assume phosphate concentrations of  $0 \mu\text{mol l}^{-1}$ . Despite uncertainties



regarding absolute  $p\text{CO}_2$  values, we note that the trends in  $p\text{CO}_2$  follow those in the SST records remarkably well (Fig. 2).

Surface water phosphate concentrations, however, may have varied in a marginal marine setting at ODP Site 1172. In fact, remains of dinoflagellates, which are known as extremely sensitive to surface-water nutrient availability changes, suggest a decrease in nutrient concentrations. The ratio between peridinioid and gonyaulacoid dinocyst groups (the P/G ratio) is often employed to reconstruct changes in relative nutrient abundance (Sluijs et al., 2005). The MECO at ODP Site 1172 shows a significant decrease in the P/G ratio (Röhl et al., 2004a; Fig. 2), suggesting a decrease in nutrient concentrations (Röhl et al., 2004a). As an experiment, we allowed phosphate to linearly vary as a function of the P/G ratio (Fig. 2). The most prominent shift towards low P/G ratio values occurs at MECO warming, resulting in lower phosphate concentration estimates. Also when this drop in phosphate is taken into account,  $p\text{CO}_2$  rises during MECO and follows the SST trends (Fig. 2; dark grey band). Hence, regardless of the constraints on phosphate concentrations and other environmental parameters,  $p\text{CO}_2$  levels must have been substantially higher during the MECO compared to the middle Eocene background.

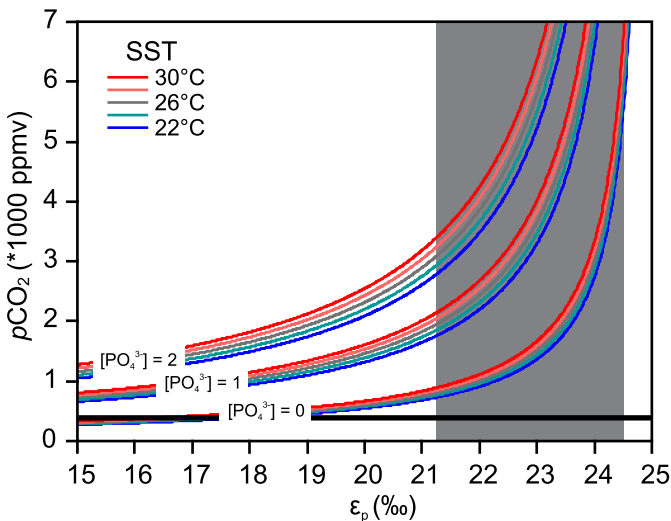


Figure 3. The relationship between  $\epsilon_p$  (in ‰; versus VPDB) and  $p\text{CO}_2$  (in ppmv). The phosphate concentration ranges plotted are those from the present day surface ocean, and the SST ranges (22°C to 30°C) are those inferred from  $\text{TEX}_{86}$  and  $\text{U}_{37}^K$  data presented in Fig. 2 and a suite of Southern Ocean sites (Chapter 2; Burgess et al., 2008; Hollis et al., 2009; Liu et al., 2009). The grey vertical bar indicates the values for  $\epsilon_p$  as reconstructed for the MECO interval at ODP Site 1172, with use of  $\text{TEX}_{86}$ - and  $\text{U}_{37}^K$ -based SST reconstructions for these same levels, and bulk carbonate  $\delta^{13}\text{C}$  measurements on the same section. Black horizontal line represents present day  $p\text{CO}_2$ . Figure is modified from Pagani et al. (2002).

One outstanding issue is the source of carbon responsible for the increase in middle Eocene atmospheric  $\text{CO}_2$ . The rise in  $p\text{CO}_2$  by 2,000 to 3,000 ppmv emerging from our data requires a carbon source capable of injecting vast amounts of carbon



into the atmosphere. Moreover, the absence of a significant negative carbon isotope excursion excludes reservoirs with  $\delta^{13}\text{C}$  signatures significantly below that of marine DIC (Bohaty et al., 2009). One mechanism capable of emanating carbon with such a geochemical signature is the metamorphic alteration of carbonates (decarbonation; Bohaty and Zachos 2003). Massive decarbonation occurred until the late Eocene, with the subduction of vast amounts of Tethyan Ocean pelagic carbonates under Asia as India drifted northwards (Aitchison et al., 2007; Dupont-Nivet et al., 2008; Kent and Muttoni 2008). However, the flux of carbon required to increase  $p\text{CO}_2$  by 2,000 to 3,000 ppmv within  $\sim 400$  kyrs, appears high to invoke metamorphic (volcanic) outgassing as the sole mechanism.

Our  $p\text{CO}_2$  and SST reconstructions allow for a tentative assessment of high-latitude climate sensitivity to  $\text{CO}_2$  forcing on  $\sim 100$  kyr time scales, assuming that all MECO warming was caused by  $p\text{CO}_2$  and associated feedbacks. With an average  $5^\circ\text{C}$  SST increase and a two- to three-fold increase in  $p\text{CO}_2$  we arrive at a climate sensitivity of  $\sim 2\text{-}5^\circ\text{C}$  per  $p\text{CO}_2$  doubling. When we consider the  $p\text{CO}_2$  decline from the middle Eocene ( $\sim 2,000$  ppmv; this study) to the latest Eocene ( $\sim 1,000$  ppmv; Pearson et al., 2009) and the coeval high-latitude temperature decline ( $\sim 3.5^\circ\text{C}$ ; Liu et al., 2009; Zachos et al., 2008) we derive similar values. Thus, long-term climate sensitivity to  $p\text{CO}_2$  forcing in a world without the amplifying effects of ice-albedo feedbacks (Pagani et al., 2010) may have been larger than previously anticipated.



## Supplements to Chapter 6

### 1. Material

The middle Eocene section at ODP Site 1172 is represented by Lithological Unit IIIA as described in the Initial Reports volume of Ocean Drilling Program Leg 189 (Exon et al., 2001). This unit consists of greenish grey and dark brownish grey diatom- and nannofossil-bearing claystones. Increasing calcium carbonate content, as well as the gradual up-section trend towards more offshore, oligotrophic organic walled dinoflagellate cyst (dinocyst) and diatom assemblages indicate a gradual deepening, starting ~42 Ma, and is probably related to the earliest stages of subsidence of the East Tasman Plateau (ETP; Röhl et al., 2004a). Low carbonate concentrations, however, still suggests marginal marine depositional settings; dinocyst assemblages confirm that the site was still located on the ancient shelf (Brinkhuis et al., 2003a). Subsidence rates of the ETP vastly increased due to Tasmanian Gateway deepening during the latest Eocene (starting around 35.5 Ma), leading to the deposition of carbonate oozes (Stickley et al., 2004b). The carbonate content is generally low (~0 to 15%) throughout the study interval, but increases somewhat up-section (Röhl et al., 2004a). The carbonate is mainly derived calcareous nannofossils (Exon et al., 2001).

### 2. Magneto-chemostratigraphic age model

The inclination data at ODP Site 1172 are characterized by a strong normal overprint (Exon et al., 2001). Fuller and Touchard (2004) used the z-intensity to interpret normal polarities, and with use of the available biostratigraphic datums, a bio-magnetostratigraphic age model was developed (Stickley et al., 2004a; Fig. S1; Column A). However, Bijl et al. (Chapter 1, 2) reinterpreted the magnetostratigraphy after the identification of the Paleocene-Eocene Thermal Maximum (PETM) and a hiatus spanning Magnetosubchron C23r (Bijl et al., 2007; Chapter 1). Following this interpretation, all normal polarity intervals up to C18n had to represent a younger Magnetochron, which was consistent with the available biostratigraphic information (Fig. S1; Column B).

Carbon isotope stratigraphy provides another calibration tool to correlate middle Eocene paleomagnetic signal to the Geomagnetic Polarity Time Scale. We assigned 9 tie points in the bulk carbonate carbon isotopes of ODP Site 1172 and correlated those to the calibrated carbon isotope records from ODP Site 748, 738 and 702 (Bohaty et al., 2009; Fig. S2). This shows that the original magnetostratigraphic interpretation by Stickley et al., (2004a) for Subchrons C18n to C20n was correct, which we incorporate in our age model (Fig. S1C). Because of the large uncertainties in the age model at high sample resolution we have decided to plot the data in the depth domain in this paper.



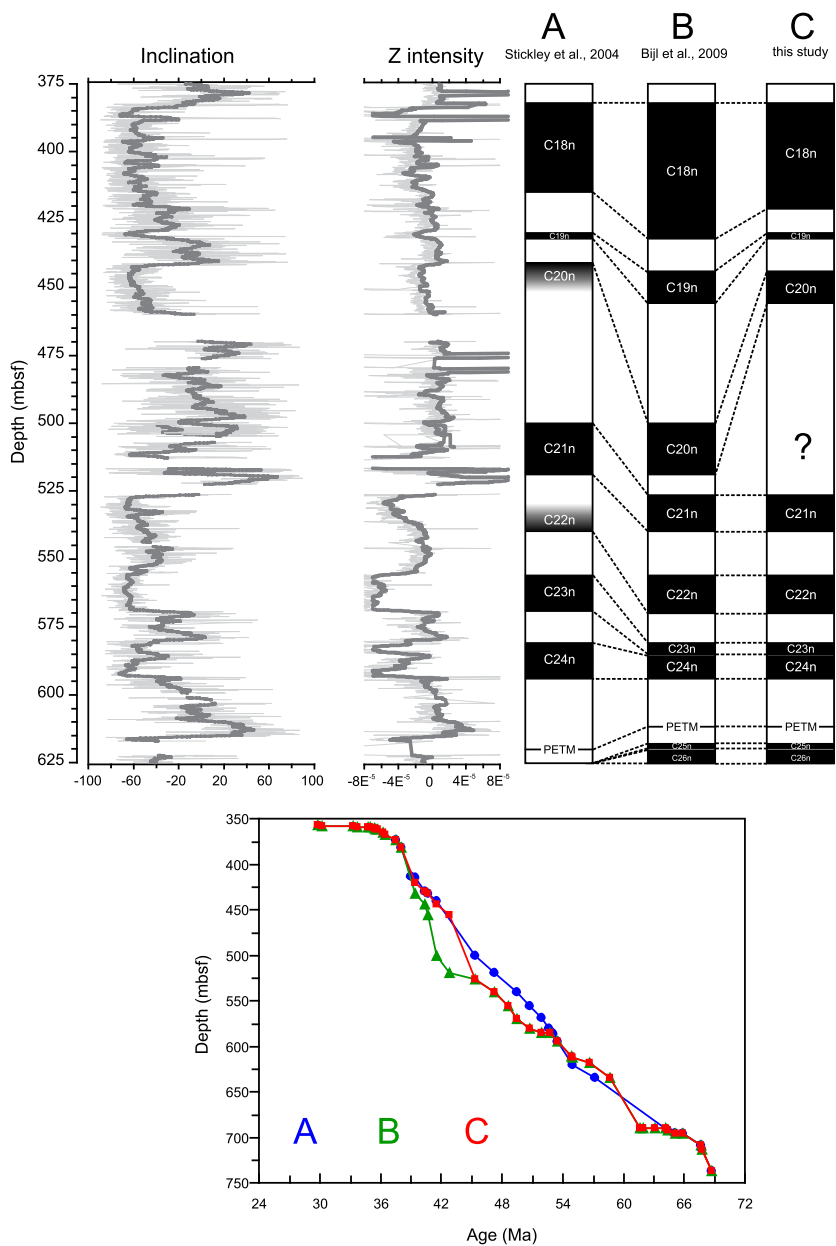


Figure S1. Magnetostratigraphy option A is published by Stickley et al. (2004a) in the Scientific Results section of the Ocean Drilling Program. Subsequently, the identification of the PETM and a hiatus spanning magnetosubchron C23n results in a revised magnetostratigraphic interpretation (Chapter 2) (B). Now, with carbon isotope stratigraphy for the MECO the magnetostratigraphic interpretation was revised again (C). All stratigraphies are (re-) calibrated to the time scale of Gradstein et al. (2004).



### 3. Methods

#### 3.1. Palynology

Palynological processing followed the standardized quantitative methods used at the Laboratory of Palaeobotany and Palynology, Utrecht University, the Netherlands (Sluijs et al., 2003). Briefly, this involves reaction with ~30% HCl and ~38% HF, and ultrasonic separation. A 15 $\mu$ m nylon mesh was used for sieving. Residues were mounted on slides for microscope analysis. At least 200 dinocysts were counted per sample and identified to the species level at 500x magnification. Taxonomy is according to that cited in the Lentin and Williams Index of Fossil Dinoflagellates, 2004 (Fensome and Williams 2004), unless stated otherwise. We follow Chapter 3 (see Table S1) for groupings of endemic, cosmopolitan and low-latitude taxa. All samples and slides are stored in the collection of the Laboratory of Palaeobotany and Palynology, Utrecht University, the Netherlands.

#### 3.2. Stable isotope analysis on bulk carbonate and inferred SSTs

Bulk-sediment stable isotope analyses of samples from the MECO interval of ODP Hole 1172A were performed using a VG Optima dual-inlet isotope-ratio mass spectrometer at the University of California, Santa Cruz, USA. The samples were first freeze-dried, and subsamples (~1.0 g) were then ground with an agate mortar and pestle in order to fully homogenize the sediment.

#### 3.3. Organic geochemical analysis

Organic compounds were extracted from powdered and freeze-dried sediments with dichloromethane (DCM)/methanol (MeOH; 9:1, v/v) using the accelerated solvent extraction technique (Dionex). Excess solvent was removed using rotary evaporation under vacuum. The total extracts were separated in apolar and polar fractions over an activated Al<sub>2</sub>O<sub>3</sub> column using hexane:dichloromethane (DCM; 1:1, v/v) and DCM:MeOH (1:1, v/v), respectively. Approximately 200-500  $\mu$ g of sample was reacted at 90°C in a common acid bath using an automated carbonate preparation system with a carousel device. NBS-19, an in-house Carrara marble standard, and a bulk-sediment consistency standard were included in all sample runs. All values are reported in standard delta notation ( $\delta$ ) in parts per mill (‰) relative to VPDB (Vienna Pee Dee Belemnite), and analytical precision is estimated at 0.04‰ (1 $\sigma$ ) for  $\delta^{13}\text{C}$  and 0.06‰ (1 $\sigma$ ) for  $\delta^{18}\text{O}$ . Several samples with extremely low carbonate concentrations (<0.5%) have been excluded from the Hole 1172A dataset. We used the equation of Bemis et al. (1998) to interpret SST changes from bulk carbonate  $\delta^{18}\text{O}$ , where we assume no change in  $\delta^{18}\text{O}_{\text{sw}}$ .

##### 3.3.1 TEX<sub>86</sub> paleothermometry

The polar fraction was dissolved in a 99:1 hexane/propanol solvent, and filtered using a 0.45  $\mu$ m, 4 mm diameter polytetrafluoroethylene (PTFE) filter, before being analyzed using a high performance liquid chromatography/ atmospheric pressure positive ion chemical ionization mass spectrometry (HPLC/ APCI-MS). HPLC/APCI-MS analyses were done according to Schouten et al. (2007a) using an Agilent 1100 series LC/MSD SL and separation and a Prevail Cyano column (2.1 x 150 mm, 3 mm; Alltech), maintained at 30°C.





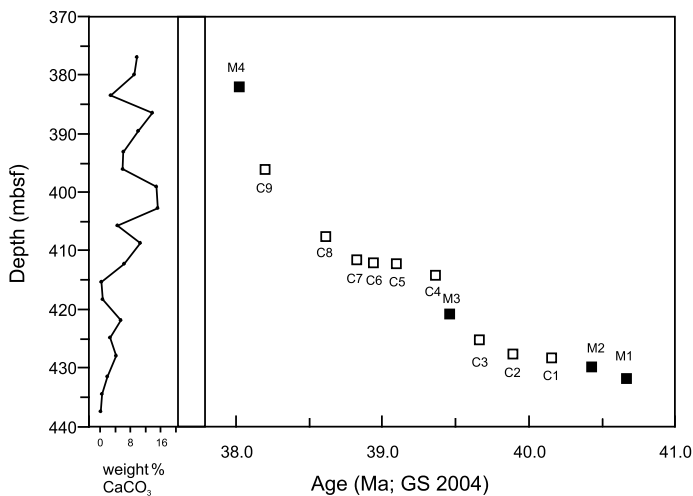
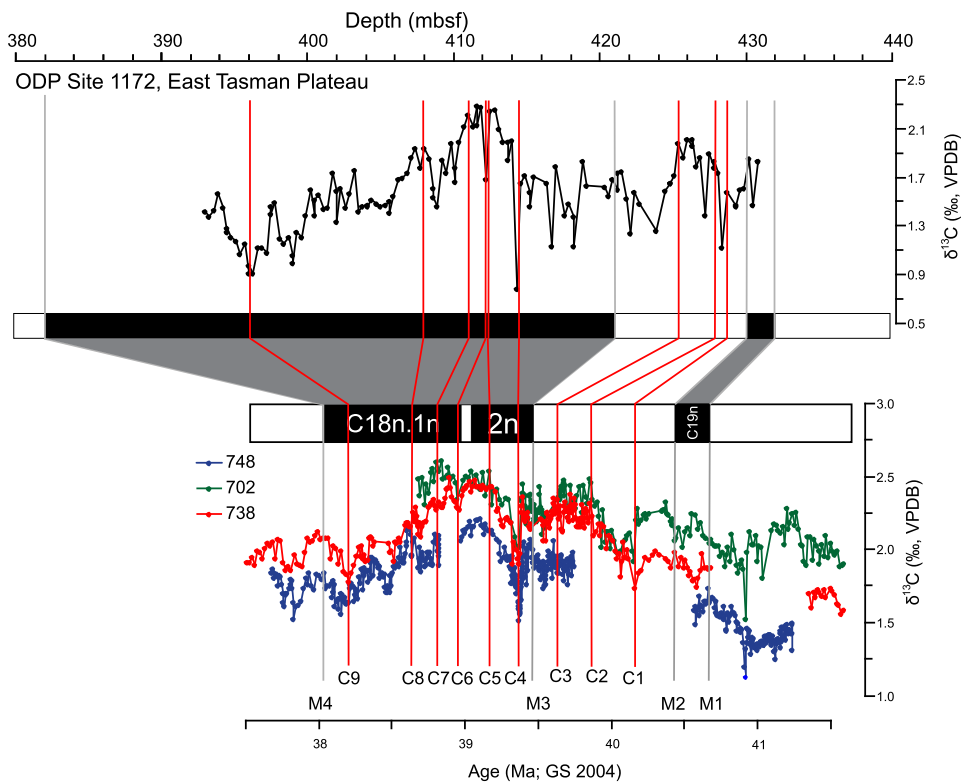


Figure S2. The bulk carbonate carbon isotope record from ODP Site 1172 was correlated to the magnetostratigraphically calibrated MECO records from ODP Site 702 (green) and the two Southern Ocean records ODP Sites 748 (blue) and 738 (red). C1-9: carbon isotope tie points, M1-4: magnetostratigraphic tie points.



Endemic and bipolar cysts	Low-latitude cysts	Protopteridinioid cysts	Cosmopolitan cysts	Unknown/other cysts
<i>Alterbidinium distinctum</i>	<i>Phthanoperidinium comatum</i>	<i>Brigantedinium</i> spp.	<i>Achomospaera alaicornu</i>	<i>Batiacasphaera</i> spp. (pars)
<i>Deflandrea antarctica</i>	<i>Dracodinium rhomboideum</i>	<i>Lejeunecysta</i> spp.	<i>Achomospaera ramulifera</i>	<i>Cerebrocysta</i> spp.
<i>Phthanoperidinium</i> sp. A*	<i>Achilleodinium biformoides</i>	<i>Octodinium askinia</i>	<i>Lingulodinium machaerophorum</i>	<i>Membranosphaera</i> spp.
<i>Phthanoperidinium</i> sp. C*	<i>Batiacasphaera compta</i>	<i>Selenopemphix armata</i>	<i>Spiniferites</i> spp.	<i>Eocladopyxis</i> spp.
<i>Phthanoperidinium stockmansii</i>	<i>Cleistosphaeridium</i> spp.	<i>Selenopemphix nephroides</i>	<i>Thalassiphora pelagica</i>	<i>Paucisphaeridium</i> spp.
<i>Spinidinium macmurdoense</i>	<i>Corrudinium incompositum</i>		<i>Senegalinium</i> spp.	
<i>Spinidinium schellenbergii</i> **	<i>Cribroperidinium</i> spp.			
<i>Vozzhennikovia roehliae</i> **	<i>Cordosphaeridium fibrospinusum</i>			
<i>Corrudinium regulare</i> ***	<i>Dapsilidinium</i> spp.			
<i>Vozzhennikovia stickleyae</i> **	<i>Enneadocysta multicornutum</i> group			
<i>Vozzhennikovia apertura</i>	<i>Enneadocysta pectiniformis</i>			
<i>Arachnodinium antarcticum</i>	<i>Glaphyrocysta</i> spp.			
<i>Enneadocysta dictyostila</i> group****	<i>Heteraulacacysta porosa</i>			
	<i>Histiocysta</i> spp.			
	<i>Hystrichokolpoma rigaudiae</i>			
	<i>Hystrichosphaeridium tubiferum</i>			
	<i>Impagidinium</i> spp.			
	<i>Melitasphaeridium pseudorecurvatum</i>			
	<i>Hemiplacophora semilunifera</i>			
	<i>Hystrichosphaeridium truswelliae</i>			
	<i>Operculodinium</i> spp.			
	<i>Pentadinium</i> spp.			
	<i>Tectatodinium</i> spp.			

Table S1. Dinocyst species encountered throughout the MECO record at ODP Site 1172 and their biogeographic affinity following Chapter 3. Taxonomy is based on that cited in the Lentin and Williams Index of Fossil Dinoflagellates, 2004 (Fensome and Williams 2004) apart from those indicated with an asterix: \* undescribed species sensu Goodman and Ford (1983); \*\* species described by Sluijs et al. (2009b); \*\*\* species described by Clowes and Wilson (2006); \*\*\*\* species emended by Fensome et al. (2006).

The GDGTs were eluted using a changing mixture of hexane and propanol as follows, 99% hexane: 1% propanol for 5 minutes, then a linear gradient to 1.8% propanol in 45 minutes. Flow rate was 0.2 ml per minute. Single ion monitoring was set to scan the 5 [M+H]<sup>+</sup> ions of the GDGTs with a dwell time of 237 ms for each ion. We applied the core top calibration equation from Kim et al. (2010) to translate TEX<sub>86</sub> index values (Fig. S3; Table S2) to mean annual sea surface temperature:

$$\text{SST} = 68.4 \cdot \text{TEX}_{86}^{\text{H}} + 38.6 \quad (6.1)$$



Where

$$\text{TEX}_{86}^{\text{H}} = \log(\text{TEX}_{86}) \quad (6.2)$$

About half of the analyzed samples were run in duplicate, to estimate the reproducibility. In all of these samples, the reproducibility is better than  $0.5^\circ\text{C}$  and in most cases better than  $0.25^\circ\text{C}$ .

### 3.3.2. Alkenone $\text{U}_{37}^{\text{K}}$ paleothermometry

To purify the alkenones, the apolar fractions were separated into three fractions by activated  $\text{Al}_2\text{O}_3$  column chromatography using hexane:DCM (9:1, v/v); hexane:DCM (1:1, v/v; the ketone fraction) and DCM. The ketone fractions were analyzed for alkenones by gas chromatography (GC) using an Agilent 6890 equipped with an on column injector. Separation was achieved using a 50m CPSil 5CB column (0.32 mm internal diameter, 0.12 micrometer film thickness). The ratio of  $\text{C}_{37:2}$  and  $\text{C}_{37:3}$  alkenones (Fig. S3; Table S2) were converted into temperature values by applying the core-top calibration of Müller et al. (1998):

$$T = (\text{U}_{37}^{\text{K}} - 0.033)/0.044 \quad (6.3)$$

All samples were analyzed in duplicate and the reproducibility of the analysis is better than  $0.5^\circ\text{C}$ . Selected fractions were analyzed by GC/mass spectrometry (GC/MS) using a TRACE DSQ to confirm the presence of the alkenones and the absence of co-eluting compounds.

### 3.3.3. Alkenone stable carbon isotope analyses

The stable carbon isotopic composition of the  $\text{C}_{37}$  di-unsaturated alkenone ( $\delta^{13}\text{C}_{\text{C}_{37:2}}$ ) was measured in duplicate using GC-isotope ratio monitoring (IRM) MS using a Agilent 6890 GC coupled to a Thermo Science Delta V isotope mass spectrometer. GC conditions were as described above. The isotopic compositions of the compounds were calibrated against external reference  $\text{CO}_2$  gas (in per mill versus VPDB) and the performance of the GC-IRMMS was checked by daily injections of two perdeuterated n-alkanes and comparison to off-line measured values. Average reproducibility was  $\pm 0.2$  (see Fig. S3; Table S3).

### 3.4 Alkenone $p\text{CO}_2$ estimates

Estimation of  $p\text{CO}_2$  from  $\delta^{13}\text{C}_{37:2}$  requires three steps: calculation of  $\epsilon_p$ ,  $[\text{CO}_{2(\text{aq})}]$  and, ultimately,  $p\text{CO}_2$ .

#### 3.4.1 Calculation of $\epsilon_p$

From the stable carbon isotope ratio in alkenones ( $\delta^{13}\text{C}_{37:2}$ ), the fractionation factor during photosynthesis ( $\epsilon_p$ ) of haptophyte algae (Fig. S3; Table S3) is expressed in the following equation (Pagani 2002):

$$\epsilon_p = [(\delta_d + 1000/\delta_p + 1000) - 1] * 1000 \quad (6.4)$$



Site (Hole)	Core (type)	Section (type)	Interval (cm)	Depth (mbsf)	Average $TEX_{86}^H$ index	Average $TEX_{86}^H$ SST	$TEX_{86}^H$ SST error	Average $U_{37}^K$ index	Average $U_{37}^K$ SST	$U_{37}^K$ SST error
1172A	42X	6W	10-12	391.00	-0.223	22.97		0.832	23.86	0.000
1172A	43X	2W	42-44	394.92	-0.224	23.62	0.035	0.837	24.02	0.063
1172A	43X	3W	85-87	396.85	-0.217	22.99	0.041			
1172A	43X	5W	37-39	402.37	-0.205	24.59	0.006	0.859	24.68	0.041
1172A	44X	2W	10-12	404.20	-0.209	24.29		0.864	24.84	0.121
1172A	44X	3W	102-104	406.62	-0.191	25.32		0.878	25.28	0.017
1172A	44X	4W	62-64	407.72	-0.191	25.90	0.158	0.918	26.47	0.139
1172A	44X	5W	10-12	408.70	-0.201	24.96	0.095	0.931	26.87	0.187
1172A	44X	7W	10-12	411.70	-0.190	25.60		0.887	25.54	0.576
1172A	45X	1W	32-34	412.52	-0.181	26.21		0.915	26.40	0.242
1172A	45X	1W	102-104	413.22	-0.163	26.91		0.944	27.27	0.141
1172A	45X	2W	32-34	414.12	-0.152	27.93	0.022	0.960	27.76	0.145
1172A	45X	2W	98-100	414.68	-0.151	28.36	0.074	0.979	28.35	0.037
1172A	45X	3W	22-24	415.52	-0.155	28.02		0.969	28.03	0.088
1172A	45X	3W	102-104	416.22	-0.176	26.84		0.961	27.78	0.048
1172A	45X	4W	10-12	416.80	-0.176	26.43	0.129	0.945	27.30	0.395
1172A	45X	4W	102-104	417.72	-0.171	26.93		0.953	27.55	0.105
1172A	45X	5W	10-12	418.30	-0.183	26.06		0.928	26.80	0.033
1172A	45X	5W	92-94	419.12	-0.206	24.48		0.899	25.91	0.202
1172A	45X	6W	32-34	420.02	-0.216	24.07		0.882	25.40	0.171
1172A	45X	6W	122-124	420.92	-0.221	23.41	0.160	0.887	25.54	0.190
1172A	45X	7W	42-44	421.62	-0.225	23.96	0.268	0.886	25.52	0.132
1172A	46X	1W	10-12	421.90	-0.240	22.18		0.956	27.63	0.076
1172A	46X	1W	112-114	422.92	-0.219	23.07		0.891	25.66	0.231
1172A	46X	2W	10-12	423.40	-0.208	24.28	0.106	0.945	27.31	0.174
1172A	46X	2W	92-94	424.22	-0.212	23.50		0.919	26.51	0.075
1172A	46X	3W	10-12	424.90	-0.207	24.53	0.097	0.926	26.72	0.173
1172A	46X	3W	82-84	425.62	-0.221	23.13		0.893	25.74	0.001
1172A	46X	4W	10-12	426.40	-0.214	23.87	0.062	0.953	27.55	0.255
1172A	46X	4W	92-94	427.22	-0.219	23.62		0.967	27.96	0.004
1172A	46X	5W	10-12	427.90	-0.212	24.11		0.923	26.64	0.306
1172A	46X	5W	114-116	428.96	-0.217	23.78		0.925	26.69	0.351
1172A	46X	7W	10-12	430.90	-0.201	24.04		0.934	26.98	0.052
1172A	47X	2W	10-12	433.00	-0.187	25.70	0.088	0.939	27.13	0.000
1172A	47X	5W	10-12	437.50	-0.199	24.97		0.965	27.89	0.015

Table S2.  $TEX_{86}^H$  and  $U_{37}^K$  index values and inferred SSTs for ODP Site 1172.

For this calculation, two unknowns need to be constrained:

- $\delta_p$  is the carbon isotopic composition of haptophyte organic matter, which is enriched in  $^{13}\text{C}$  by 4.2‰ relative to  $\delta^{13}\text{C}_{37:2}$  (Laws et al., 2000).
- $\delta_d$  is  $\delta^{13}\text{C}$  of dissolved  $\text{CO}_2$  ( $\delta^{13}\text{C}_{\text{aq}}$ ), which we can derive from the  $\delta^{13}\text{C}$  of bulk carbonate.

We interpolated the bulk carbonate carbon isotope record (Fig. S3) using the Analyseries (Paillard et al., 1996) software to fit the resolution of the carbon isotope record to that of the alkenone record. The equation to estimate  $\epsilon_p$  with use of carbonate  $\delta^{13}\text{C}$  uses foraminiferal  $\delta^{13}\text{C}$ . Unfortunately, only bulk  $\delta^{13}\text{C}$  was available at our site, which composes of calcareous nannoplankton. We added 0.5‰ to bulk carbonate  $\delta^{13}\text{C}$  to correct for differential biotic fractionation between foraminiferal calcite and calcareous nannoplankton calcite (Pagani 2002). The carbon isotopic fractionation factors of from biogenic calcite ( $\delta^{13}\text{C}_{\text{calc}}$ ) to gaseous  $\text{CO}_2$  ( $\delta^{13}\text{C}_{\text{CO}_2(\text{g})}$ ) are required to calculate  $\delta^{13}\text{C}_{\text{aq}}$ .

$$\epsilon_{\text{calc}-\text{CO}_2(\text{g})} = 11.98 - (0.12 * \text{SST}) \quad (6.5)$$

And that from  $\text{CO}_2(\text{g})$  to  $\text{CO}_2(\text{aq})$ :

$$\epsilon_{\text{CO}_2(\text{g})-\text{CO}_2(\text{aq})} = -373 / (273.15 + \text{SST}) + 0.19 \quad (6.6)$$

SST was obtained from the organic paleothermometer proxies  $\text{TEX}_{86}$  and  $\text{U}_{37}^K$ . Differences in absolute SST reconstructions derived from these proxies are included as error bars (Fig. 2; Fig. S3; Table S3).

To calculate  $\delta^{13}\text{C}_{\text{CO}_2(\text{g})}$  from  $\delta^{13}\text{C}_{\text{calc}}$  we use;

$$\delta^{13}\text{C}_{\text{CO}_2(\text{g})} = ((\delta^{13}\text{C}_{\text{calc}} + 1000) / (1 + \epsilon_{\text{calc}-\text{CO}_2(\text{g})} * 0.001)) - 1000 \quad (6.7)$$

This  $\delta^{13}\text{C}_{\text{CO}_2(\text{g})}$  is then used to calculate the  $\delta^{13}\text{C}_{\text{CO}_2(\text{aq})}$  following;

$$\delta^{13}\text{C}_{\text{aq}} = ((0.001 * \epsilon_{\text{CO}_2(\text{g})-\text{CO}_2(\text{aq})} + 1) * (\delta^{13}\text{C}_{\text{CO}_2(\text{g})} + 1000)) - 1000 \quad (6.8)$$

### 3.4.2. Calculation of $[\text{CO}_2(\text{aq})]$

The estimation of  $[\text{CO}_2(\text{aq})]$  from  $\epsilon_p$  follows that of Pagani et al. (2005):

$$\epsilon_p = \epsilon_f - b / [\text{CO}_2(\text{aq})] \quad (6.9)$$

where  $\epsilon_f$  represents the carbon isotopic fractionation due to carboxylation (which is  $\sim 25\text{‰}$  in the modern day ocean (Pagani et al., 2002; Popp et al., 1998)), and  $b$  represents the sum of all physiological factors, such as growth rate and cell geometry. These physiological factors are strongly correlated to surface water  $[\text{PO}_4^{3-}]$  because this is one of the limiting nutrients, or it serves as a proxy for other limiting nutrients.



The simplified term  $b$  is related to phosphate via the following equation (Pagani et al., 2005):

$$b = [(118.52[\text{PO}_4^{3-}]) + 84.07] / (25 - \varepsilon_p) \quad (6.10)$$

In our experiment, to assess the influence of varying phosphate concentrations, we allowed  $[\text{PO}_4^{3-}]$  to vary throughout the record as a function of the abundance of peridinioid organic walled dinoflagellate cyst taxa in the same samples. The middle Eocene record at ODP Site 1172 shows large fluctuations in the abundance of peridinioid cysts (Röhl et al., 2004a; Fig. 2), and we therefore allow  $[\text{PO}_4^{3-}]$  to vary between  $0.1 \pm 0.1$  and  $0.9 \pm 0.1$  as a function of the percentage peridinioid cysts (see discussion under Section 4).

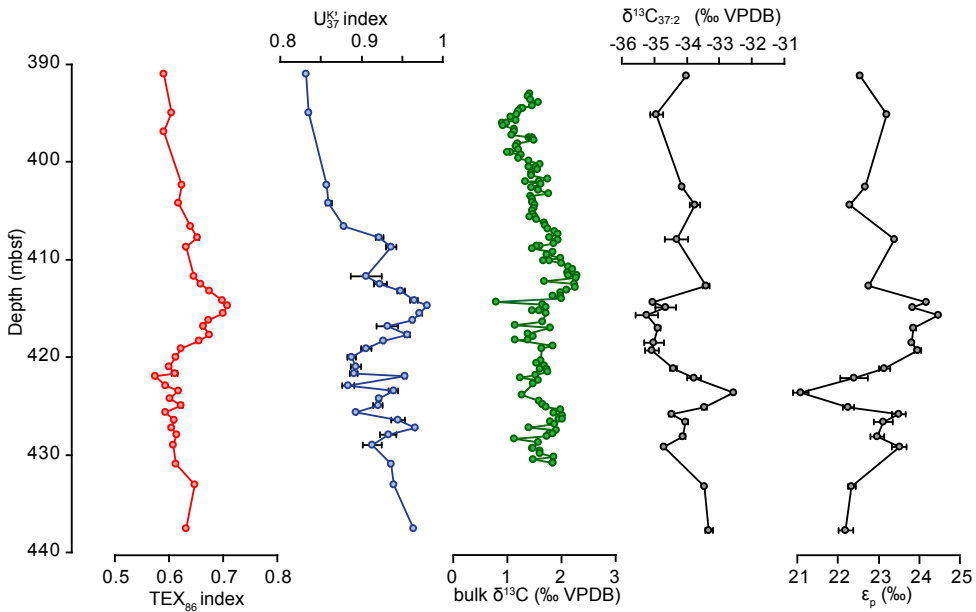


Figure S3. Index values for  $\text{TEX}_{86}$  and  $U_{37}^{K'}$ , carbon isotope values for the bulk carbonate at ODP Site 1172 and for the 37:2 di-unsaturated alkenones, fractionation factor  $\varepsilon_p$ , all in per mill and versus Vienna Pee Dee Belemnite.

### 3.4.3. Calculation of $p\text{CO}_2$

The conversion of  $[\text{CO}_{2(\text{aq})}]$  to  $p\text{CO}_2$  uses Henry's Law (Weiss 1974):

$$p\text{CO}_2 = [\text{CO}_{2(\text{aq})}] / 10^{[-60.2409 + 93.4517 \cdot (100/\text{SST}) + 23.3585 \cdot \ln(\text{SST}/100) + \text{SSS} \cdot (0.023517 - 0.023656 \cdot (\text{SST}/100) + 0.0047036 \cdot ((\text{SST}/100) \cdot (\text{SST}/100))]} \quad (6.11)$$



We assume a sea surface salinity (SSS) of 35 p.s.u. (Pagani 2002) and SSTs derived from  $\text{TEX}_{86}$  and  $U_{37}^{\text{K}}$  (converted to the Kelvin scale). Because the temperature proxies disagree on absolute SSTs prior to the MECO, the error for reconstructed  $p\text{CO}_2$  is higher in that interval (Fig. 2).

## 4. Discussions

### 4.1. *Dinoflagellate response to MECO warming*

Dinocyst assemblages in the middle- and late Eocene Southern Ocean are characterized by dominance of taxa that are biogeographically restricted (endemic) to the circum-Antarctic region (Chapter 3; Wrenn and Beckman 1982). In this time period, the relative abundance and distribution of endemic dinocysts is found to closely relate to SST changes as reconstructed by  $\text{TEX}_{86}$  (Chapter 3). This is now particularly well recognized in the MECO record at ODP Site 1172, where we find that endemic dinocyst assemblages declined in abundance at peak MECO warming (Fig. S4). Biogeographically cosmopolitan taxa (with no apparent relation with temperature) show no large variation in abundance associated to MECO. However, a marked increase in low latitude taxa (Fig. 2; Fig. S4, Table S1) provides evidence for biotic response in consequence of MECO warming. Apparently, when the Southern Ocean surface waters warmed, conditions began to approach those of lower latitudes. The protoperidinioid dinocyst taxa dominate Southern Ocean assemblages from the Oligocene onwards (Kemp 1975; Mohr 1990), but are only present in low abundance during MECO times (see also discussions under section 4.3).

### 4.2. *The effect of light-limited growth on $p\text{CO}_2$ estimates*

An important factor that influences  $\epsilon_p$  in alkenones from the main modern alkenone producer *Emiliania huxleyi* grown in incubation studies and chemostat experiments is light intensity (Rost et al., 2002). In these experiments, the carbon isotopic fractionation of alkenones varies up to 2 per mille when light intensity acts a growth-limiting factor during carbon fixation (Rost et al., 2002). In incubation studies, this effect is more pronounced under nutrient-repleted conditions (Rost et al., 2002). In theory, natural environments with eutrophic surface waters would particularly experience light limitation, as high surface-water productivity causes limitations for light-penetration. A modeling experiment suggested that the effect of coccolith blooms on light penetration is considerable, particularly because the white surfaces of the coccolith platelets act as a reflective surface (Tyrrell et al., 1999). Following this model, the light intensities used in the experiments of Rost et al. (2002); 15 to 150  $\mu\text{mole m}^{-2} \text{s}^{-1}$ ) assume that coccolith concentrations increased from 0 to 300  $\text{mg CaCO}_3 \text{m}^{-3}$ . Critically, this is equivalent to a transition from no coccoliths to a full bloom, and may be considered an extreme situation. Along with the notion that the above experiment describes an extreme case, several other points compromise the hypothesis that changes in the magnitude of light-limited growth forced the recorded changes in  $\epsilon_p$ . First of all, the magnitude of light-limited growth as recorded in the laboratory is not easily extrapolated to the natural environment. The relation between  $\epsilon_p$ , phosphate/nutrients and  $p\text{CO}_2$  has been shown in a number of environments (Benthien et al., 2002; 2005), and in more recent geological times (Palmer et al., 2010;



Seki et al., 2010) while no relation with light limitation and  $\epsilon_p$  has, at this point, been reported for the natural environment.

Site (Hole)	Core (type)	Section (type)	Interval (cm)	Depth (mbsf)	$\delta^{13}\text{C}_{37:2}$ measurement 1	$\delta^{13}\text{C}_{37:2}$ measurement 2	Average $\delta^{13}\text{C}_{37:2}$	$\delta^{13}\text{C}_{37:2}$ error	$\delta^{13}\text{C}_{\text{calc}}$	TEX <sub>86</sub> <sup>H</sup> SST	U <sub>37</sub> <sup>K'</sup> SST	$\epsilon_p$ TEX <sub>86</sub> <sup>H</sup>	$\epsilon_p$ U <sub>37</sub> <sup>K'</sup>	$\epsilon_p$ average	$\epsilon_p$ error	[PO <sub>4</sub> <sup>3-</sup> ] (±0.1)	pCO <sub>2</sub> average	pCO <sub>2</sub> upper	pCO <sub>2</sub> lower
1172A	42X	6W	10-12 cm	391.00	-34.005	-34.026	-34.016	0.015	2.090	22.97	23.86	22.48	22.60	22.54	0.06	0.56	2022	2357	1709
1172A	43X	2W	42-44 cm	394.92	-35.076	-34.791	-34.934	0.202	1.739	23.62	24.02	23.18	23.23	23.21	0.03	0.65	3000	3423	2598
1172A	43X	5W	37-39 cm	402.37	-34.123	-34.149	-34.136	0.018	1.947	24.59	24.68	22.67	22.68	22.68	0.01	0.59	2259	2549	1976
1172A	44X	2W	10-12 cm	404.20	-33.644	-33.865	-33.755	0.156	1.983	24.29	24.84	22.26	22.33	22.30	0.03	0.60	1956	2241	1685
1172A	44X	4W	62-64 cm	407.72	-34.073	-34.566	-34.320	0.349	2.260	25.90	26.47	23.35	23.42	23.38	0.04	0.62	3449	3985	2947
1172A	45X	1W	32-34 cm	412.52	-33.489	-33.324	-33.407	0.117	2.578	26.21	26.40	22.75	22.77	22.76	0.01	0.77	2779	3115	2458
1172A	45X	2W	32-34 cm	414.12	-35.055	-35.033	-35.044	0.016	2.071	27.93	27.76	24.18	24.16	24.17	-0.01	0.20	4762	5680	3857
1172A	45X	2W	98-100 cm	414.68	-34.876	-34.431	-34.654	0.315	2.089	28.36	28.35	23.84	23.84	23.84	0.00	0.04	2950	3451	2438
1172A	45X	3W	22-24 cm	415.52	-35.480	-34.981	-35.231	0.353	2.150	28.02	28.03	24.47	24.47	24.47	0.00	0.13	6918	8251	5560
1172A	45X	4W	10-12 cm	416.80	-34.842	-34.948	-34.895	0.075	2.040	26.43	27.30	23.80	23.91	23.86	0.06	0.30	3763	4611	2981
1172A	45X	5W	10-12 cm	418.30	-35.225	-34.804	-35.015	0.298	1.932	26.06	26.80	23.77	23.86	23.82	0.05	0.24	3384	4142	2674
1172A	45X	5W	92-94 cm	419.12	-34.926	-35.225	-35.076	0.211	2.168	24.48	25.91	23.88	24.06	23.97	0.09	0.45	4652	5845	3597
1172A	45X	6W	122-124 cm	420.92	-34.494	-34.338	-34.416	0.110	2.136	23.41	25.54	23.01	23.28	23.15	0.13	0.58	2808	3473	2217
1172A	46X	1W	10-12 cm	421.90	-33.922	-33.628	-33.775	0.208	2.012	22.18	27.63	22.05	22.74	22.39	0.34	0.59	2082	2806	1465
1172A	46X	2W	10-12 cm	423.40	-32.548	-32.576	-32.562	0.020	1.867	24.28	27.31	20.88	21.27	21.08	0.19	0.49	1273	1568	1010
1172A	46X	3W	10-12 cm	424.90	-33.395	-33.512	-33.454	0.083	2.124	24.53	26.72	22.12	22.40	22.26	0.14	0.41	1690	2080	1337
1172A	46X	3W	82-84 cm	425.62	-34.417	-34.518	-34.468	0.071	2.427	23.13	25.74	23.33	23.66	23.49	0.16	0.43	3087	4017	2282
1172A	46X	4W	10-12 cm	426.40	-33.990	-34.087	-34.039	0.069	2.353	23.87	27.55	22.89	23.35	23.12	0.23	0.48	2682	3553	1935
1172A	46X	5W	10-12 cm	427.90	-34.185	-34.067	-34.126	0.083	2.153	24.11	26.64	22.81	23.13	22.97	0.16	0.47	2406	3032	1854
1172A	46X	5W	114-116 cm	428.96	-34.747	-34.661	-34.704	0.061	2.103	23.78	26.69	23.33	23.70	23.51	0.18	0.52	3445	4514	2524
1172A	47X	2W	10-12 cm	433.00	-33.455	-33.472	-33.464	0.012	2.100	25.70	27.13	22.25	22.43	22.34	0.09	0.68	2214	2602	1860
1172A	47X	5W	10-12 cm	437.50	-33.239	-33.319	-33.319	0.113	2.100	24.97	27.89	22.01	22.38	22.19	0.18	0.10	1219	1608	873

Table S3.  $\delta^{13}\text{C}_{37:2}$ ,  $\delta^{13}\text{C}_{\text{calc}}$ ,  $\epsilon_p$ , phosphate assumptions and inferred pCO<sub>2</sub> values.  $\delta^{13}\text{C}_{\text{calc}}$  was interpolated from the bulk organic carbon isotope data presented in Fig. S3.





Second, coccolithophores generally occur in blooms, and hence always produce their ‘own’ light-limitation. The change in light penetration throughout our record thus should result from the abundance of other particles in the surface ocean.

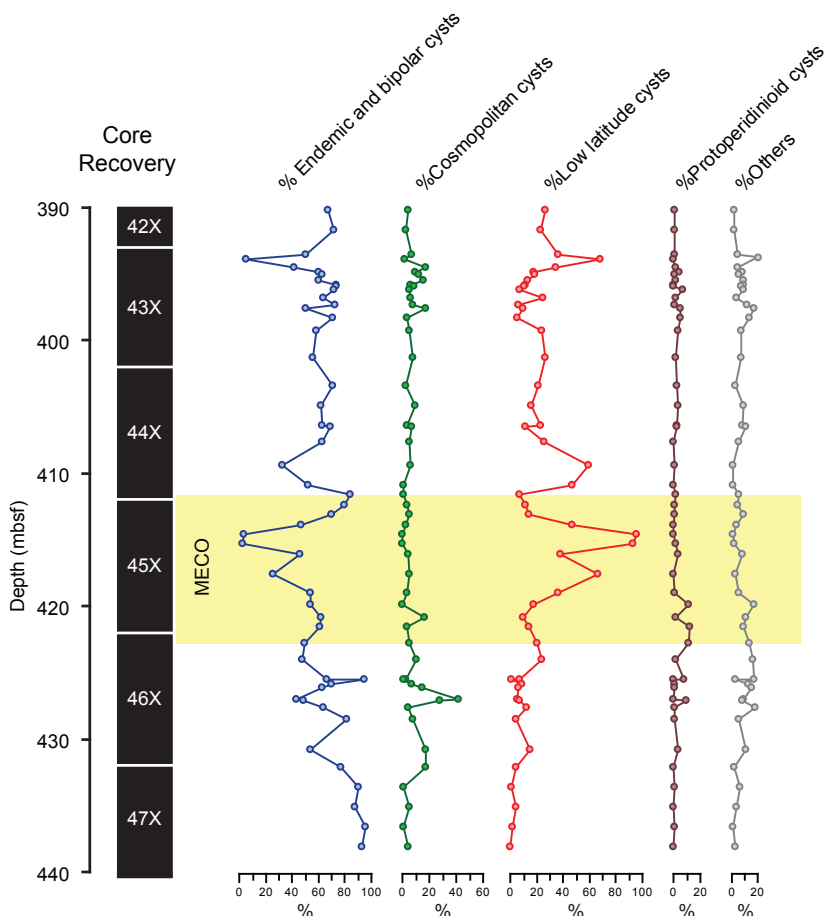


Figure S4. Dinoflagellate cyst assemblages grouped as follows (see Table S1): endemic and bipolar cysts; cosmopolitan (in terms of latitude) cysts, low latitude cysts; protoperidinioid cysts and others.

The only indications we have for changes affecting surface water turbidity are relative nutrient changes, based on e.g., dinocyst assemblages (Fig. 2; Röhl et al., 2004a); the more nutrients are available in the surface waters, the more particles reside in the water, and the higher the light limitation. A shift towards more oligotrophic settings is interpreted at the MECO. That would prescribe a decrease of the effect of light limitation on the  $\epsilon_p$  values (Rost et al., 2002). Although this effect might explain part of the increased  $\epsilon_p$  values at the MECO, we argue that it cannot explain the total change we observe. ODP Site 1172 is not comparable to an oligotrophic gyral system but was situated on an extended flat shelf, with a proximal-



distal nutrient gradient. Diatoms, abundant dinocysts and calcareous nannofossils are present in MECO sediments (Exon et al., 2001; Röhl et al., 2004a; Exon et al., 2004), and indicate more eutrophic conditions than central gyres. Compared to pre-MECO environments, however, nutrient concentrations decreased as interpreted from the dinocysts (Fig. 2). Light penetration in these settings strongly depends on the amount of particulate matter dwelling in the surface waters. It is unlikely that this factor changed dramatically throughout MECO times at the ETP, certainly not to the extent simulated in the incubation experiments. Hence the effect can only explain a minor part of the 3‰ change we observe associated with the MECO. Third, ODP Site 1172 was situated at a paleolatitude of 65°S. The growing season (i.e. austral summer) of this site experiences conditions with near-continuous light. Rost et al. (2002) showed that under these conditions, the effect of light limited growth was smaller compared to experiments with a light-dark cycle.

In summary, the effect of light-limited growth has not been shown to have a major effect on  $\epsilon_p$  values in environments similar to the paleo-setting at ODP Site 1172 as much as in incubation experiments. Although we cannot exclude an effect of light limited growth in our  $p\text{CO}_2$  record, it is likely that the effect is relatively minor, and cannot be held responsible for the large magnitude of the  $\epsilon_p$  change.

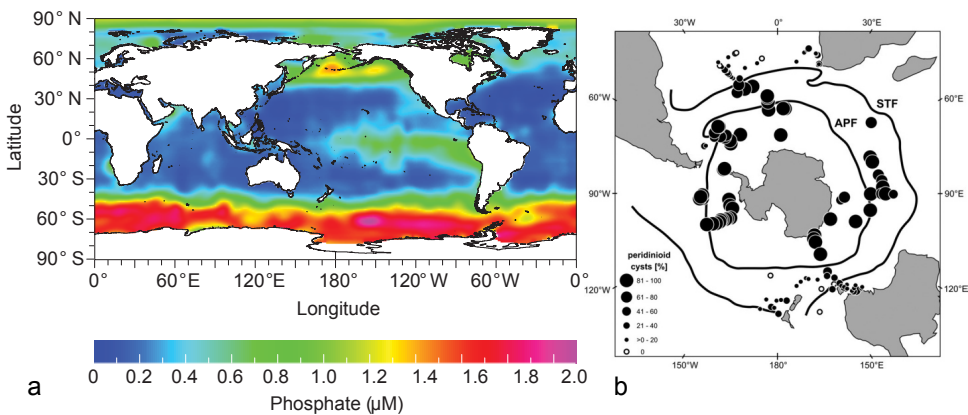


Figure S5. a: the mean annual concentration of surface water soluble phosphate from the World Ocean Database (Garcia et al., 2006) modified from Pagani et al., (2010). b: The relative abundance of peridinioid dinocysts in surface sediments. Figure obtained from Esper and Zonneveld (2007).

#### 4.3. Phosphate concentrations and dinocysts

In our study, we derive concentration changes of sea surface soluble phosphate by using dinocysts preserved in sediments. The present day Southern Ocean has a steep lateral gradient of phosphate in the surface waters (Fig. S5A). Strong Antarctic circumpolar currents (the ACC) promote mixing of surface waters with deeper water, thereby constantly replenishing the photic zone with phosphate. Dinocyst assemblages within the ACC almost exclusively consist of proto-peridinioid



taxa, which are produced by heterotrophic dinoflagellates. Outside the ACC, phosphate concentrations are significantly lower (Fig. S5a), and dinocyst assemblages are dominated by gonyaulacoid taxa. Esper and Zonneveld (2007) made a survey of the distribution of peridinioid dinocysts versus gonyaulacoid dinocysts (P/G ratio) within surface samples throughout the Southern Ocean, and identified the coherence between the ACC and the percentage of peridinioid dinocysts (Esper and Zonneveld 2007; Fig. S5b). The relationship between the abundance of protoperidinioid dinocysts and nutrients was also recognized in Holocene sediment cores from the Arabian Sea (Reichart and Brinkhuis 2003). Present day Southern Ocean protoperidinioid dinocysts share the same lineage with the Eocene peridinioid dinocysts (Fensome et al., 1993). Furthermore, a wealth of multi-proxy investigations suggests a relation between the abundance of peridinioid dinocysts and nutrient availability throughout the Cenozoic (Sluijs et al., 2005) With use of the Analyseries (Paillard et al., 1996) software, we interpolated the P/G ratio record to fit the resolution with the alkenone record.







- Abbot, D.S. and E. Tziperman (2008). "Sea ice, high-latitude convection, and equable climates." Geophysical Research Letters **35**: L03702.
- Abbot, D.S., M. Huber, G. Bousquet and C.C. Walker (2009). "High-CO<sub>2</sub> cloud radiative forcing feedback over both land and ocean in a global climate model." Geophysical Research Letters **36**: L05702.
- Abdul Aziz, H., F.J. Hilgen, G.M. van Luijk, A. Sluijs, M.J. Kraus, J.M. Pares and P.D. Gingerich (2008). "Astronomical climate control on paleosol stacking patterns in the upper Paleocene - lower Eocene Willwood Formation, Bighorn Basin, Wyoming." Geology **36**: 531-534.
- Adams, C.G., D.E. Lee and B.R. Rosen (1990). "Conflicting isotopic and biotic evidence for tropical sea-surface temperatures during the Tertiary." Palaeogeography, Palaeoclimatology, Palaeoecology **77**: 289-313.
- Aitchison, J.C., J.R. Ali and A.M. Davis (2007). "When and where did India and Asia collide?" Journal of Geophysical Research **112**: doi:10.1029/2006JB004706.
- Alonso-Saez, L., O. Sanchez, J.M. Gasol, V. Balague and C. Pedros-Alio (2008). "Winter-to-summer changes in the composition and single-cell activity of near-surface Arctic prokaryotes." Environmental Microbiology **10**: 2444-2454.
- Amoko (1982). "Cape Sorell No. 1. Geological completion report, Exploration Permit T-12-P, offshore west Tasmania, Australia". Amoco Australia Petroleum Company.
- Andrews, J.E. and G. Packham (1975). Initial Reports of the Deep Sea Drilling Project, volume 30. Washington, U.S. Government Printing Office.
- Archangelsky, S. (1969). "Estudio del paleomicroplancton de la Formación Río Turbio (Eocene), provincia de Santa Cruz." Ameghiniana **3**: 181-218.
- Archangelsky, S., G.R. Guerin and M.E. Quattrocchio (1997). "Pejerrey x-1 offshore well, Palynological report. Buenos Aires." Shell Capsa: **19**.
- Archer, D. (2005). "Fate of fossil fuel CO<sub>2</sub> in geologic time." Journal of Geophysical Research **110**: C09S05.
- Bains, S., R.M. Corfield and R.D. Norris (1999). "Mechanisms of climate warming at the end of the Paleocene." Science **285**: 724-727.
- Baldauf, J.G. and J.A. Barron (1990). "Evolution of biosiliceous sedimentation patterns - Eocene through Quaternary: paleoceanographic response to polar cooling." Geological history of the polar oceans: Arctic versus Antarctic. U. Bleil and J. T. J. Dordrecht, Kluwer Academic: 575-607.
- Ballantyne, A.P., D.R. Greenwood, J.S. Sinninghe Damsté, A.Z. Csank, J.J. Eberle and N. Rycbczynski (2010). "Significantly warmer Arctic surface temperatures during the Pliocene indicated by multiple independent proxies." Geology **38**: 603-606.
- Bamber, J.L., R.E.M. Riva, B.L.A. Vermeersen and A.M. LeBrocq (2009). "Reassessment of the Potential Sea-Level Rise from a Collapse of the West Antarctic Ice Sheet." Science **324**: 901-903.
- Barke, J., H.A. Abels, F. Sangiorgi, D.R. Greenwood, A.R. Sweet, T. Donders, G.-J. Reichart, A.F. Lotter and H. Brinkhuis (2011). "Orbitally forced Azolla blooms and middle Eocene Arctic hydrology: Clues from palynology." Geology **39**: 427-430.
- Barker, P. and I.W.D. Dalziel (1976). Initial Reports of the Deep Sea Drilling Project, volume 36. Washington, U.S. Government Printing Office.
- Barker, P.F. and J.P. Kennett (1988). Proceedings of the Ocean Drilling Program, Initial Reports, volume 113. College Station, Texas, U.S. Government Printing Office.
- Barker, P.F. and J.P. Kennett (1990). Proceedings of the Ocean Drilling Program, Scientific Results, volume 113. College Station, Texas, U.S. Government Printing Office.
- Barker, P.F., B. Dieckmann and C. Escutia (2007). "Onset of Cenozoic Antarctic Glaciation." Deep-Sea Research II **54**: 2293-2307.
- Barrett, P.J. (1989). "Antarctic Cenozoic history from the CIROS-1 drillhole, McMurdo Sound." Wellington, Science Information Publishing Centre. DSIR Bulletin, volume 245.
- Barron, E.J. (1987). "Eocene equator-to-pole surface ocean temperatures: a significant climate problem?" Paleoceanography **2**(6): 729-739.
- Barron, J. and B. Larsen (1989). Proceedings of the Ocean Drilling Program, Initial Reports, volume 119. College Station, Texas, U.S. Government Printing Office.
- Barron, J.A. and J.G. Baldauf (1989). "Tertiary cooling steps and paleoproductivity as reflected by diatoms and biosiliceous sediments." Productivity of the oceans: Present and Past. W. H. Berger, et al. New York, Dahlem Workshop Reports: 341-354.
- Beerling, D.J. and D.L. Royer (2011). "Convergent Cenozoic CO<sub>2</sub> history." Nature Geoscience **4**: 418-420.
- Bemis, B.E., H.J. Spero, J. Bijma and D.W. Lea (1998). "Reevaluation of the oxygen isotope composition of planktonic foraminifera: Experimental results and revised paleotemperature equations." Paleoceanography **13**(2): 150-160.



## REFERENCES

- Bendle, J., P.K. Bijl, J. Pross, S. Schouten, L. Contreras, U. Röhl, S. Bohaty, H. Brinkhuis, C. Escutia, A. Klaus and E. Scientists (in prep.). "Early Eocene warmth from marine proxies: results from IODP Leg 318."
- Benthien, A., N. Andersen, S. Schulte, P.J. Müller, R.R. Schneider and G. Wefer (2002). "Carbon isotopic composition of the C37:2 alkenone in core top sediments of the South Atlantic Ocean: Effects of CO<sub>2</sub> and nutrient concentrations." *Global Biogeochemical Cycles* **16**(1) 1012.
- Benthien, A., N. Andersen, S. Schulte, P.J. Müller, R.R. Schneider and G. Wefer (2005). "The carbon isotopic record of the C37:2 alkenone in the South Atlantic: Last Glacial Maximum (LGM) vs. Holocene." *Palaeogeography, Palaeoclimatology, Palaeoecology* **221** 123–140.
- Bijl, P.K., H. Brinkhuis, A. Sluijs, G.-J. Reichart, S. Schouten and U. Röhl (2007). "Late Paleocene- Early Eocene paleoenvironments in the Southwest Pacific (ODP Leg 189): Revised Stratigraphy of an Antarctic PETM Record." American Geophysical Union Fall Meeting, San Francisco, U.S.A.
- Bohaty, S.M. and J.C. Zachos (2003). "Significant Southern Ocean warming event in the late middle Eocene." *Geology* **31**(11): 1017-1020.
- Bohaty, S.M., J.C. Zachos, F. Florindo and M.L. Delaney (2009). "Coupled greenhouse warming and deep-sea acidification in the Middle Eocene." *Paleoceanography* **24**: PA2207: doi:10.1029/2008PA001676.
- Bolle, M.-P., A. Pardo, K.-U. Hinrichs, T. Adatte, K. von Salis, S. Burns, G. Keller and N. Muzylev (2000). "The Paleocene-Eocene transition in the marginal northeastern Tethys (Kazakhstan and Uzbekistan)." *International Journal of Earth Sciences* **89**: 390–414.
- Bolli, H.M. and W.B.F. Ryan (1978). *Initial Reports of the Deep Sea Drilling Project, volume 40*. Washington, U.S. Government Printing Office.
- Boreham, C.J., J.E. Blevin, I. Duddy, J. Newman, K. Liu, H. Middleton, M.K. Macphail and A.C. Cook (2002). "Exploring the potential for oil generation migration and accumulation in cape Sorell-I, Sorell Basin, offshore West Tasmania." *Appea Journal*: 405-435.
- Bowen, G.J., P.L. Koch, P.D. Gingerich, R.D. Norris, S. Bains and R.M. Corfield (2001). "Refined isotope stratigraphy across the continental Paleocene-Eocene boundary on Polecat Bench in the Northern Bighorn Basin." *Paleocene-Eocene Stratigraphy and Biotic Change in the Bighorn and Clarks Fork Basins, Wyoming*. P. D. Gingerich, University of Michigan Papers on Paleontology **33**: 73–88.
- Bowen, G.J., D.J. Beerling, P.L. Koch, J.C. Zachos and T. Quattlebaum (2004). "A humid climate state during the Palaeocene/Eocene thermal maximum." *Nature* **432**: 495–499.
- Bowen, G.J., T.J. Bralower, M.L. Delaney, G.R. Dickens, D.C. Kelly, P.L. Koch, L.R. Kump, J. Meng, L.C. Sloan, E. Thomas, S.L. Wing and J.C. Zachos (2006). "Eocene Hyperthermal Event Offers Insight Into Greenhouse Warming." *EOS, Transactions, American Geophysical Union* **87**: 165-169.
- Boyd, P.W., A.J. Watson, C.S. Law, E.R. Abraham, T. Trull, R. Murdoch, D.C.E. Bakker, A.R. Bowie, K.O. Buesseler, H. Chang, M. Charette, P. Croot, K. Downing, R. Frew, M. Gall, M. Hadfield, J. Hall, M. Harvey, G. Jameson, J. LaRoche, M. Liddicoat, R. Ling, M.T. Maldonado, R.M. McKay, S. Nodder, S. Pickmere, R. Pridmore, S. Rintoul, K. Safi, P. Sutton, R. Strzpek, K. Tanneberger, S. Turner, A. Waite and J. Zeldis (2000). "A mesoscale phytoplankton bloom in the polar Southern Ocean stimulated by iron fertilization." *Nature* **407**: 695-702.
- Braak, C.J.F., ter (1986). "Canonical Correspondence Analysis: A new eigenvector technique for multivariate direct gradient analysis." *Ecology* **67**(5): 1167-1179.
- Brassell, S.C., G. Eglinton, I.T. Marlowe, U. Pflaumann and M. Sarnthein (1986). "Molecular stratigraphy: a new tool for climatic assessment." *Nature* **320**: 129-133.
- Brinkhuis, H. (1994). "Late Eocene to Early Oligocene dinoflagellate cysts from the Priabonian type-area (northeast Italy); biostratigraphy and palaeoenvironmental interpretation." *Palaeogeography, Palaeoclimatology, Palaeoecology* **107**: 121-163.
- Brinkhuis, H., S. Sengers, A. Sluijs, J. Warnaar and G.L. Williams (2003a). "Latest Cretaceous to earliest Oligocene, and Quaternary dinoflagellates from ODP Site 1172, East Tasman Plateau." *Proceedings of the Ocean Drilling Program, Scientific Results, volume 189*. N. Exon and J. P. Kennett. College Station, Texas, U.S. Government Printing Office.
- Brinkhuis, H., D.M. Munsterman, S. Sengers, A. Sluijs, J. Warnaar and G.L. Williams (2003b). "Late Eocene to Quaternary dinoflagellate cysts from ODP Site 1168, off western Tasmania." *Proceedings of the Ocean Drilling Program, Scientific Results, volume 189*. N. Exon and J. P. Kennett. College Station, Texas, U.S. Government Printing Office.



- Brinkhuis, H., S. Schouten, M.E. Collinson, A. Sluijs, J.S. Sinninghe Damsté, G.R. Dickens, M. Huber, T.M. Cronin, J. Onodera, K. Takahashi, J.P. Bujak, R. Stein, J.v.d. Burg, J.S. Eldrett, I.C. Harding, A.F. Lotter, F. Sangiorgi, H.v. Konijnenburg-Cittert, J.W.d. Leeuw, J. Matthiessen, J. Backman, K. Moran and Expedition 302 Scientists (2006). "Episodic fresh surface waters in the Eocene Arctic Ocean." *Nature* **441**: 606-609.
- Brown, B., C. Gaina and R.D. Müller (2006). "Circum-Antarctic palaeobathymetry: Illustrated examples from Cenozoic to recent times." *Palaeogeography, Palaeoclimatology, Palaeoecology* **231**: 158-168.
- Bujak, J.P., C. Downie, G.L. Eaton and G.L. Williams (1980). "Dinoflagellate cysts and acritarchs from the Eocene of southern England." *Special papers in Paleontology* **24**: 100
- Bujak, J.P. and D.C. Mudge (1994). "A high-resolution North Sea Eocene dinocyst zonation." *Journal of the Geological Society London* **151**: 449-462.
- Bujak, J.P. and H. Brinkhuis (1998). "Global warming and dinocyst changes across the Paleocene/Eocene boundary." *Late Paleocene - Early Eocene Climatic and Biotic Events in the Marine and Terrestrial Records*. M. P. Aubry. New York, Columbia University Press: 277-295.
- Burgess, C.E., P.N. Pearson, C.H. Lear, H.E.G. Morgans, L. Handley, R.D. Pancost and S. Schouten (2008). "Middle Eocene climate cyclicity in the southern Pacific: Implications for global ice volume." *Geology* **36**(8): 651-654.
- Cande, S.C. and J.M. Stock (2004). "Cenozoic Reconstructions of the Australia-New Zealand-South Pacific Sector of Antarctica." *The Cenozoic Southern Ocean: Tectonics, Sedimentation and Climate Change Between Australia and Antarctica*. N. F. Exon, J. P. Kennett and M. Malone, Geophysical Monograph Series, American Geophysical Union. **151**: 5-18.
- Carter, R.M., I.N. McCave, C. Richter and L. Carter (1999). *Proceedings of the Ocean Drilling Program, Initial Reports, volume 181*. College Station, Texas, U.S. Government Printing Office.
- Carter, R.M., I.N. McCave, C. Richter and L. Carter (2002). *Proceedings of the Ocean Drilling Program, Scientific Results, volume 181*. College Station, Texas, U.S. Government Printing Office.
- Castañeda, I.S., E. Scheffuß, J. Patzold, J.S. Sinninghe Damsté, S. Weldeab and S. Schouten (2010). "Millennial-scale sea surface temperature changes in the eastern Mediterranean (Nile River Delta region) over the last 27,000 years." *Paleoceanography* **25**: PA1208.
- Ciesielski, P.F., Y. Kristoffersen and B. Clement (1988). *Proceedings of the Ocean Drilling Program, Initial Reports, volume 114*. College Station, Texas, U.S. Government Printing Office.
- Ciesielski, P.F., Y. Kristoffersen, B. Clement and T. Moore (1991). *Proceedings of the Ocean Drilling Program, Scientific Results, volume 114*. College Station, Texas, U.S. Government Printing Office.
- Close, D.I., A.B. Watts and H.M.J. Stagg (2009). "A marine geophysical study of the Wilkes Land rifted continental margin, Antarctica." *Geophysical Journal International* **177**: 430-450.
- Clowes, C.D. and G.J. Wilson (2006). "Some new species of *Corrudinium* Stover and Evitt, 1978 (Dinophyceae) from the Eocene of New Zealand." *New Zealand Journal of Geology and Geophysics* **49**: 399-408.
- Coccioni, R. and S. Galeotti (1997). "Foraminiferal biostratigraphy and palaeoecology of the CIROS-1 core from McMurdo Sound (Ross Sea, Antarctica)." *Terra Antarctica* **4**(2): 103-117.
- Cocozza, C.C. and C.M. Clarke (1992). "Eocene microplankton from La Meseta Formation, northern Seymour Island." *Antarctic Science* **4**(3): 355-362.
- Coffin, M.F., F.A. Frey and P.J. Wallace (2000). *Proceedings of the Ocean Drilling Program, Initial Reports, volume 183*. College Station, Texas, U.S. Government Printing Office.
- Coffin, M.F., F.A. Frey and P.J. Wallace (2003). *Proceedings of the Ocean Drilling Program, Scientific Results, volume 183*. College Station, Texas, U.S. Government Printing Office.
- Collinson, M.E., J. Barke, J. v.d. Burgh, J.H.A. v. Konijnenburg-v. Cittert, C. Heilmann-Clausen, L.E. Howard and H. Brinkhuis (2010). "Did a single species of Eocene *Azolla* spread from the Arctic Basin to the southern North Sea?" *Review of Palaeobotany and Palynology* **159**(3-4): 152-165.
- Contreras, L., P.K. Bijl, J. Bendle, J. Pross, H. Brinkhuis, S. Schouten, C. Escutia and A. Klaus (in prep.). "terrestrial palynomorphs from the Wilkes Land Margin, Antarctica." *Nature*.
- Cookson, I.C. and A. Eisenack (1965). "Microplankton from the Browns Creek Clays southwest Victoria." *Proceedings of the Royal Society of Victoria* **79**: 119-131.
- Costa, L.I. and C. Downie (1979). The Wetzeliellaceae; Palaeogene dinoflagellates. *Proceedings of the 4th International Palynological Conference, Lucknow* **2**: 34-46.
- Coxall, H.K., P.A. Wilson, H. Pälike, C.H. Lear and J. Backman (2005). "Rapid stepwise onset of Antarctic glaciation and deeper calcite compensation in the Pacific Ocean." *Nature* **433**: 53-57.





## REFERENCES

- Cramer, B.S., J.D. Wright, D.V. Kent and M.P. Aubry (2003). "Orbital climate forcing of  $\delta^{13}\text{C}$  excursions in the late Paleocene–early Eocene (chrons C24n–C25n)." *Paleoceanography* **18**(4): doi:10.1029/2003PA000909.
- Cranwell, L.M., H.J. Harrington and I.G. Speden (1960). "Lower Tertiary microfossils from McMurdo Sound, Antarctica." *Nature* **186**: 700-702.
- Cranwell, L.M. (1964). "Hystrichospheres as an aid to Antarctic dating with special reference to the recovery of *Cordosphaeridium* in erratics at McMurdo Sound." *Grana Palynologica* **5**(3): 397-405.
- Creech, J.B., J.A. Baker, C.J. Hollis, H.E.G. Morgans and E.G.C. Smith (2010). "Eocene sea temperatures for the mid-latitude southwest Pacific from Mg/Ca ratios in planktonic and benthic foraminifera." *Earth and Planetary Science Letters* **299**: 483–495.
- Crouch, E.M. and C.J. Hollis (1996). "Paleogene palynomorph and radiolarian biostratigraphy of DSDP leg 29, sites 280 and 281." Lower Hutt, New Zealand, *Institute of Geological and Nuclear Sciences internal report* **96/19**.
- Crouch, E.M. (2001). "Environmental Change at the time of the Paleocene-Eocene Biotic Turnover." *LPP Contributions Series no. 14*. Utrecht University, Utrecht, the Netherlands. **PhD thesis**.
- Crouch, E.M., C. Heilmann-Clausen, H. Brinkhuis, H.E.G. Morgans, K.M. Rogers, H. Egger and B. Schmitz (2001). "Global dinoflagellate event associated with the late Paleocene thermal maximum." *Geology* **29**: 315-318.
- Crouch, E.M., G.R. Dickens, H. Brinkhuis, M.-P. Aubry, C.J. Hollis, K.M. Rogers and H. Visscher (2003). "The *Apectodinium* acme and terrestrial discharge during the Paleocene-Eocene thermal maximum: new palynological, geochemical and calcareous nannoplankton observations at Tawanui, New Zealand." *Palaeogeography, Palaeoclimatology, Palaeoecology* **194**: 387–403.
- Crouch, E.M. and H. Visscher (2003). "Terrestrial vegetation record across the initial Eocene thermal maximum at the Tawanui marine section, New Zealand." *Causes and Consequences of Globally Warm Climates in the Early Paleogene*. S. L. Wing, P. D. Gingerich, B. Schmitz and E. Thomas. Boulder, Colorado, Geological Society of America Special Paper. **369**: 351–363.
- Crouch, E.M. and H. Brinkhuis (2005). "Environmental change across the Paleocene–Eocene transition from eastern New Zealand: A marine palynological approach." *Marine Micropaleontology* **56**: 138-160.
- Crouch, E.M., J.I. Raine and E.M. Kennedy (2005). "Vegetation and climate change at the Paleocene-Eocene transition." *Geological Society of New Zealand 50th annual conference*. Wellington, NZ.
- Crouch, E.M. (2010). "Provisional New Zealand Tertiary dinoflagellate cyst zonation scheme." *GNS Science Internal Report* **2010/05**.
- Dale, B. (1996). "Dinoflagellate cyst ecology: Modelling and geological applications." *Palynology: Principles and applications*. J. Jansonius and D. C. McGregor, American Association of Stratigraphic Palynologist Foundation. **3**: 1249-1275.
- Dale, B. (2001). "The sedimentary record of dinoflagellate cysts: looking back into the future of phytoplankton blooms." *Scientia Marina* **65**: 257–272.
- Daners, G., G.R. Guerin, M.V. Guler and G. Veroslavsky (2004). "Las transgresiones del Maastrichtiense - Daniense y Eoceno medio en la cuenca Punta del Este y su correlacion regional basada en dinoflagelados." *unpublished*.
- Davies, T.A. and B.P. Luyendyk (1974). *Initial Reports of the Deep Sea Drilling Project, volume 26*. Washington, U.S. Government Printing Office.
- DeConto, R.M. and D. Pollard (2003a). "A coupled climate-ice sheet modeling approach to the Early Cenozoic history of the Antarctic ice sheet." *Palaeogeography, Palaeoclimatology, Palaeoecology* **198**(1): 39-52.
- DeConto, R.M. and D. Pollard (2003b). "Rapid Cenozoic glaciation of Antarctica induced by declining atmospheric  $\text{CO}_2$ ." *Nature* **421**: 245-249.
- DeConto, R.M., D. Pollard, P.A. Wilson, H. Pälike, C.H. Lear and M. Pagani (2008). "Thresholds for Cenozoic bipolar glaciation." *Nature* **455**: 652-657.
- Deflandre, G. (1935). "Considérations biologiques sur les microorganismes d'origine planctonique conservés dans les silex de la craie." *Bulletin biologique de la France et de la Belgique* **69**: 213-244.
- Deflandre, G. and I.C. Cookson (1955). "Fossil microplankton from Australian Late Mesozoic and Tertiary sediments." *Australian Journal of Marine and Freshwater research* **6**(2): 242-313.
- Dickens, G.R., J.R. O'Neil, D.K. Rea and R.M. Owen (1995). "Dissociation of oceanic methane hydrate as a cause of the carbon isotope excursion at the end of the Paleocene." *Paleoceanography* **10**: 965–971.
- Dickens, G.R., M.M. Castillo and J.C.G. Walker (1997). "A blast of gas in the latest Paleocene: Simulating first order massive dissociation of oceanic methane hydrate." *Geology* **25**(3): 259-262.



- Dickens, G.R. (2003). "Rethinking the global carbon cycle with a large, dynamic and microbially mediated gas hydrate capacitor." *Earth and Planetary Science Letters* **213**: 169-183.
- Diester-Haass, L. and R. Zahn (2001). "Paleoproductivity increase at the Eocene - Oligocene climatic transition: ODP/DSDP sites 763 and 592." *Palaeogeography, Palaeoclimatology, Palaeoecology* **172**: 153-170.
- Dupont-Nivet, G., C. Hoorn and M. Konert (2008). "Tibetan uplift prior to the Eocene-Oligocene climate transition: Evidence from pollen analysis of the Xining Basin." *Geology* **36**: 987-990.
- Eaton, G.L. (1971). "A morphogenetic series of dinoflagellate cysts from the Backlesham Beds of the Isle of Wight, Hampshire, England." *Proceedings of the 2nd Planktonic Conference, Rome, 1970*. A. Farinacci, Rome, Edizioni tecnoscienza: 355-379.
- Eberle, J., H. Fricke and J. Humphrey (2009). "Lower-latitude mammals as year-round residents in Eocene Arctic forests." *Geology* **37**: 499-502.
- Eberle, J.J., H.C. Fricke, J.D. Humphrey, L. Hackett, M.G. Newbrey and J.H. Hutchison (2010). "Seasonal variability in Arctic temperatures during early Eocene time." *Earth and Planetary Science Letters* **296**: 481-486.
- Edbrooke, S.W., E.M. Crouch, H.E.G. Morgans and R. Sykes (1998). "Late Eocene - Oligocene Te Kuiti Group at Mount Roskill, Auckland, New Zealand." *New Zealand Journal of Geology and Geophysics* **41**: 85-93.
- Ehrmann, W. (1998). "Implications of late Eocene to early Miocene clay mineral assemblages in McMurdo Sound (Ross Sea, Antarctica) on paleoclimate and ice dynamics." *Palaeogeography, Palaeoclimatology, Palaeoecology* **139**: 213-231.
- Eldrett, J.S., I.C. Harding, J.V. Firth and A.P. Roberts (2004). "Magnetostratigraphic calibration of Eocene-Oligocene dinoflagellate cyst biostratigraphy from the Norwegian-Greenland Sea." *Marine Geology* **204**(1-2): 91-127.
- Eldrett, J.S., I.C. Harding, P.A. Wilson, E. Butler and A.P. Roberts (2007). "Continental ice in Greenland during the Eocene and Oligocene." *Nature* **446**: 176-179.
- Eldrett, J.S. and I.C. Harding (2009). "Palynological analyses of Eocene to Oligocene sediments from DSDP Site 338, Outer Vøring Plateau." *Marine Micropaleontology* **73**: 226-240.
- Escutia, C., H. Brinkhuis, A. Klaus and Expedition 318 Scientists (2010). "Wilkes Land Glacial History: Cenozoic East Antarctic Ice Sheet evolution from Wilkes Land margin sediments. *Proceedings of the Integrated Ocean Drilling Program, Preliminary Reports, volume 318*.
- Escutia, C., H. Brinkhuis, A. Klaus and Expedition 318 Scientists (2011). *Proceedings of the Integrated Ocean Drilling Program, Initial Results, volume 318*. Tokyo (Integrated Ocean Drilling Program Management International, Inc.). doi:10.2204/iodp.proc.318.101.2011
- Esper, O. and K.A.F. Zonneveld (2007). "The potential of organic-walled dinoflagellate cysts for the reconstruction of past sea-surface conditions in the Southern Ocean." *Marine Micropaleontology* **65**: 185-212.
- Exon, N.J., J.P. Kennett and M. Malone (2001). *Proceedings of the Ocean Drilling Program, Initial Reports, volume 189*. College Station, Texas, U.S. Government Printing Office.
- Exon, N.J., J.P. Kennett and M.J. Malone (2003). *Proceedings of the Ocean Drilling Program, Scientific Results, volume 189*. College Station, Texas, U.S. Government Printing Office.
- Exon, N., J.P. Kennett and M. Malone (2004). *The Cenozoic Southern Ocean. Tectonics, sedimentation and climate change between Australia and Antarctica*. Washington, American Geophysical Union (AGU), Geophysical Monograph **151**.
- Feary, D.A., A.C. Hine and M.J. Malone (2000). *Proceedings of the Ocean Drilling Program, Initial Reports, volume 182*. College Station, Texas, U.S. Government Printing Office.
- Fensome, R.A., F.J.R. Taylor, G. Norris, W.A.S. Sarjeant, D.I. Wharton and G.L. Williams (1993). *A Classification of Modern and Fossil Dinoflagellates*. Salem, Micropalaeontology, Special Paper.
- Fensome, R.A. and G.L. Williams (2004). "The Lentin and Williams index of fossil dinoflagellates (2004 edition)." *American Association of Stratigraphic Palynologists Foundation Contribution Series*.
- Fensome, R.A., G.R. Guerin and G.L. Williams (2006). "New insights on the Paleogene dinoflagellate cyst genera *Enneadocysta* and *Licracysta* gen. nov. based on material from offshore eastern Canada and southern Argentina." *Micropaleontology* **52**(5): 385-410.
- Fensome, R.A., G.L. Williams and R.A. MacRae (2009). "Late Cretaceous and Cenozoic fossil dinoflagellates and other palynomorphs from the Scotian Margin, offshore eastern Canada." *Journal of Systematic Palaeontology* **7**: 1-79.



## REFERENCES

- Ferreira, E.P. (2004). "Palinoestratigrafia e caracterização de paleoambientes da seção paleocênica-eocênica da Bacia de Sergipe." Instituto de Geociências – UFRJ, Dr., Programa de Pós-Graduação em Geologia. Inédita. PhD thesis: 253.
- Florindo, F., S.M. Bohaty, P.S. Erwin, C. Richter, A.P. Roberts, P.A. Whalen and J.M. Whitehead (2003). "Magnetobiostratigraphic chronology and palaeoenvironmental history of Cenozoic sequences from ODP sites 1165 and 1166, Prydz Bay, Antarctica." Palaeogeography, Palaeoclimatology, Palaeoecology **198**: 69-100.
- Florindo, F. and A.P. Roberts (2005). "Eocene - Oligocene magnetobiochronology of ODP sites 689 and 690, Maud Rise, Weddell Sea, Antarctica." Geological Society of America Bulletin **117**(1-2): 46-66.
- Francis, J.E. (1988). "A 50-Million-Year-Old Fossil Forest from Strathcona Fiord, Ellesmere Island, Arctic Canada: Evidence for a Warm Polar Climate." Arctic **41**(4): 314-318.
- Francis, J.E. and I. Poole (2002). "Cretaceous and early Tertiary climates of Antarctica: Evidence from fossil wood." Palaeogeography, Palaeoclimatology, Palaeoecology **182**: 47-64.
- Fuller, M. and Y. Touchard (2004). "On the magnetostratigraphy of the East Tasman Plateau, timing of the opening of the Tasmanian Gateway and paleoenvironmental changes." The Cenozoic Southern Ocean. Tectonics, sedimentation and climate change between Australia and Antarctica. N. Exon, J. P. Kennett and M. Malone. Washington, American Geophysical Union (AGU) Geophysical Monograph series. **151**: 127-151.
- Garcia, H.E., R.A. Locarnini, T.P. Boyer and J.I. Antonov (2006). "Nutrients (phosphate, nitrate, silicate)." World Ocean Atlas 2005. Washington, D.C., U.S. Government Printing Office **4**.
- Gersonde, R. and D.M. Harwood (1990). "Lower Cretaceous Diatoms from ODP LEG 113 Site 693 (Weddell Sea). Part 1: Vegetative Cells." Proceedings of the Ocean Drilling Program, Scientific Results, volume 113. P. R. Barker and J. P. Kennett. College Station, TX, Ocean Drilling Program.
- Gersonde, R., D.A. Hodell and P. Blum (1999). Proceedings of the Ocean Drilling Program, Initial Reports, volume 177. College Station, Texas, U.S. Government Printing Office.
- Gersonde, R., D.A. Hodell and P. Blum (2001). Proceedings of the Ocean Drilling Program, Scientific Results, volume 177. College Station, Texas, U.S. Government Printing Office.
- Gibbs, S.J., T.J. Bralower, P.R. Bown, J.C. Zachos and L.M. Bybell (2006). "Shelf and open-ocean calcareous phytoplankton assemblages across the Paleocene-Eocene Thermal Maximum: Implications for global productivity gradients." Geology **34**: 233-236.
- Giusberti, L., D. Rio, C. Agnini, J. Backman, E. Fornaciari, F. Tateo and M. Oddone (2007). "Mode and tempo of the Paleocene-Eocene thermal maximum in an expanded section from the Venetian pre-Alps." Geological Society of America Bulletin **119**: 391-412.
- Goodman, D.K. and L.N. Ford jr. (1983). "Preliminary dinoflagellate biostratigraphy for the middle Eocene to lower Oligocene from the Southwest Atlantic Ocean." Ludwig, W.J., Krasheninnikov, V.A., et al., Initial Reports of the Deep Sea Drilling Project, volume 71: Washington, U.S. Government Printing Office: 859-977.
- Gradstein, F.M., J.G. Ogg and A.G. Smith (2004). A Geologic Timescale 2004. Cambridge, Cambridge University Press.
- Greenwood, D.R. and S.L. Wing (1995). "Eocene continental climates and latitudinal temperature gradients." Geology **23**: 1044-1048.
- Guasti, E., R.P. Speijer, H. Brinkhuis, J. Smit and E. Steurbaut (2006). "Paleoenvironmental change at the Danian-Selandian transition in Tunisia: Foraminifera, organic-walled dinoflagellate cyst and calcareous nannofossil records." Marine Micropaleontology **59**: 210-229.
- Guerstein, G.R., M.V. Guler, G.L. Williams, R.A. Fensome and J.O. Chiesa (2008). "Middle Palaeogene dinoflagellate cysts from Tierra del Fuego, Argentina: biostratigraphy and palaeoenvironments." Journal of Micropalaeontology **27**: 75-94.
- Guerstein, G.R., M.V. Guler, H. Brinkhuis and J. Warnaar (2010). "Mid-Cenozoic Paleoclimatic and Paleoceanographic trends in the southwestern Atlantic Basins: a dinoflagellate view." The Paleontology of Gran Barranca: Evolution and Environmental Change through the Middle Cenozoic of Patagonia. R. H. Madden, A. A. Carlini, M. G. Vucetich and R. F. Kay, Cambridge University Press.
- Habib, D. (1976). "Neocomian dinoflagellate zonation in the Western North Atlantic." Micropaleontology **21**(4): 373-392.
- Hancock, H.J.L., G.R. Dickens, E. Thomas and K. Blake (2007). "Reappraisal of early Paleogene CCD curves: foraminiferal assemblages and stable carbon isotopes across the carbonate facies of Perth Abyssal Plain." International Journal of Earth Sciences **96**: 925-946.



- Hannah, M.J. (1994). "Eocene dinoflagellates from CIROS-1 drill hole, McMurdo Sound, Antarctica." *Terra Antarctica* **1**(2): 3.
- Hannah, M.J. (1997). "Climate controlled dinoflagellate distribution in late Eocene - earliest Oligocene strata from CIROS-1 drillhole, McMurdo Sound, Antarctica." *Terra Antarctica* **4**(2): 73-78.
- Hannah, M.J., M.B. Cita, R. Coccioni and S. Monechi (1997). "The Eocene/Oligocene boundary at 70 degrees South, McMurdo Sound, Antarctica." *Terra Antarctica* **4**(2): 79-87.
- Harding, I.C., A.J. Charles, J.E.A. Marshall, H. Pälike, A.P. Roberts, P.A. Wilson, E. Jarvis, R. Thorne, E. Morris, R. Moremon, R.B. Pearce and S. Akbari (2011). "Sea-level and salinity fluctuations during the Paleocene–Eocene thermal maximum in Arctic Spitsbergen." *Earth and Planetary Science Letters* **303**: 97–107.
- Hartwich, S.J., J.G. Conran, J.M. Bannister, J.K. Lindqvist and D.E. Lee (2010). "Calamoid fossil palm leaves and its fruits (Arecaceae: Calamoideae from late Eocene Southland, New Zealand." *Australian Systematic Botany* **23**: 131-140.
- Harwood, D.M. (1988). "Upper Cretaceous and lower Paleocene diatom and silicoflagellate biostratigraphy of Seymour Island, eastern Antarctic Peninsula." *Geology and Paleontology of Seymour Island*. R. Feldman and M. O. Woodburne, Geological Society of America Memoir Series **169**: 55-129.
- Harwood, D.M. and R. Gersonde (1990). "Lower Cretaceous Diatoms from ODP Leg 113 Site 693 (Weddell Sea). Part 2: Resting Spores, Chrysophycean Cysts, an endoskeletal dinoflagellate and notes on the origin of diatoms." *Proceedings of the Ocean Drilling Program, Scientific Results, volume 113*. P. F. Barker and J. P. Kennett. College Station, Texas, U.S. Government Printing Office.
- Harwood, D.M. (1991). "Cenozoic diatom biogeography in the southern high latitudes: Inferred biogeographical barriers and progressive endemism." *Geological Evolution of Antarctica*. M. R. A. Thompson, J. A. Crame and J. W. Thomson. Cambridge, Proceedings of the Fifth International Symposium on Antarctic Earth Sciences: 667-673.
- Hay, W.W., R. DeConto, C.N. Wold, K.M. Wilson, S. Voigt, M. Schulz and A. Wold-Rosby (1999). "Alternative global Cretaceous paleogeography." *The evolution of Cretaceous ocean/climate systems*. E. Barrera and C. Johnson, Geological Society of America Special Paper. **332**: 1-47.
- Hayes, D.E. and L.A. Frakes (1975). *Initial Reports of the Deep Sea Drilling Project, volume 28*. Washington, U.S. Government Printing Office.
- Heilmann-Clausen, C. (1985). "Dinoflagellate stratigraphy of the uppermost Danian to Ypresian in the Viborg I borehole, central Jylland, Denmark." *Danmarks Geologiske Undersøgelse, Series A 7*: 1-69.
- Heinemann, M., J.H. Jungclauss and J. Marotzke (2009). "Warm Paleocene/Eocene climate as simulated in ECHAM5/MPI-OM." *Climate of the Past* **5**: 785–802.
- Holdgate, G.R., A.P. Kershaw and I.R.K. Sluiter (1995). "Sequence stratigraphic analysis and the origins of Tertiary brown coal lithotypes, Latrobe Valley, Gippsland Basin, Australia." *International Journal of Coal Geology* **28**: 249-275.
- Holdgate, G.R., M.W. Wallace, S.J. Gallagher and D. Taylor (2000). "A review of the Traralgon Formation in the Gippsland Basin - a world class brown coal resource." *International Journal of Coal Geology* **45**: 55-84.
- Holdgate, G.R., C. Rodriguez, E.M. Johnstone, M.W. Wallace and S.J. Gallagher (2003). "The Gippsland Basin top Latrobe unconformity, and its expression in other SE Australia basins." *Appea Journal*: 149-174.
- Hollis, C.J., D.B. Waghorn, C.P. Strong and E.M. Crouch (1997). Integrated Paleogene biostratigraphy of DSDP Site 277 (Leg 29): "Foraminifera, calcareous nannofossils, radiolaria and palynomorphs." Lower Hutt, New Zealand, *Institute of geological and nuclear sciences* **97/7**.
- Hollis, C.J., G.R. Dickens, B.D. Field, C.M. Jones and P.C. Strong (2005). "The Paleocene-Eocene transition at Mead Stream, New Zealand: A southern Pacific record of early Cenozoic global change." *Palaeogeography, Palaeoclimatology, Palaeoecology* **215**(3-4): 313-343.
- Hollis, C.J., E.M. Crouch, H.E.G. Morgans, L. Handley, J.A. Baker, J. Creech, K.S. Collins, S.J. Gibbs, M. Huber, S. Schouten, J.C. Zachos and R.D. Pancost (2009). "Tropical sea temperatures in the high latitude South Pacific during the Eocene." *Geology* **37**(2): 99-102.
- Hopmans, E.C., J.W.H. Weijers, E. Schefuß, L. Herfort, J.S. Sinninghe Damsté and S. Schouten (2004). "A novel proxy for terrestrial organic matter in sediments based on branched and isoprenoid tetraether lipids." *Earth & Planetary Science Letters* **224**: 107-116.
- Houben, A.J.P., P.K. Bijl, G.R. Guerin, A. Sluijs and H. Brinkhuis (2011). "*Malvinia escutiana*, a new biostratigraphically important Oligocene dinoflagellate cyst from the Southern Ocean." *Review of Palaeobotany and Palynology* **165**(3-4): 175 - 182.



## REFERENCES

- Huber, M. and L.C. Sloan (2001). "Heat transport, deep waters, and thermal gradients: Coupled simulation of an Eocene 'Greenhouse' climate." *Geophysical Research Letters* **28**: 3481–3484.
- Huber, M., H. Brinkhuis, C.E. Stickley, K. Döös, A. Sluijs, J. Warnaar, S.A. Schellenberg and G.L. Williams (2004). "Eocene circulation of the Southern Ocean: Was Antarctica kept warm by subtropical waters?" *Paleoceanography* **19**: PA4026.
- Huber, M. (2008). "A Hotter Greenhouse?" *Science* **321**: 353-354.
- Huguet, C., A. Schimmelmann, R. Thunell, L.J. Lourens, J.S. Sinninghe Damsté and S. Schouten (2007). "A study of the TEX<sub>86</sub> paleothermometer in the water column and sediments of the Santa Barbara Basin, California." *Paleoceanography* **22**: PA3203.
- Iakovleva, A.I., H. Brinkhuis and C. Cavagnetto (2001). "Late Palaeocene-Early Eocene dinoflagellate cysts from the Turgay Strait, Kazakhstan; correlations across ancient seaways." *Palaeogeography, Palaeoclimatology, Palaeoecology* **172**: 243–268.
- IPCC (2007). *Contribution of Working Group I to the Fourth Assessment Report of the Intergovernmental Panel on Climate Change*. Cambridge, United Kingdom and New York, USA, Cambridge University Press.
- Ivany, L.C., K.C. Lohmann, D.B. Blake, A. Glass, R.B. Aronson and R.M. Moody (2008). "Eocene climate record of a high southern latitude continental shelf: Seymour Island, Antarctica." *Geological Society of America Bulletin* **120**(5/6): 659-678.
- Jaramillo, C., D. Ochoa, L. Contreras, M. Pagani, H. Carvajal-Ortiz, L.M. Pratt, S. Krishnan, A. Cardona, M. Romero, L. Quiroz, G. Rodriguez, M.J. Rueda, F. de la Parra, S. Moron, W. Green, G. Bayona, C. Montes, O. Quintero, R. Ramirez, G. Mora, S. Schouten, H. Bermudez, R. Navarrete, F. Parra, M. Alvaran, J. Osorno, J.L. Crowley, V. Valencia and J. Vervoort (2010). "Effects of Rapid Global Warming at the Paleocene-Eocene Boundary on Neotropical Vegetation." *Science* **330**: 957–961.
- John, C.M., S.M. Bohaty, J.C. Zachos, A. Sluijs, S.J. Gibbs, H. Brinkhuis and T.J. Bralower (2008). "North American continental margin records of the Paleocene-Eocene thermal maximum: Implications for global carbon and hydrological cycling." *Paleoceanography* **23**: PA2217.
- Kaiho, K., T. Arinobu, R. Ishiwatari, H.E.G. Morgans, H. Okada, N. Takeda, K. Tazaki, G. Zhou, Y. Kajiwarra, R. Matsumoto, A. Hirai, N. Niitsuma and H. Wada (1996). "Latest Paleocene benthic foraminiferal extinction and environmental change at Tawanui, New Zealand." *Paleoceanography* **11**: 447–465.
- Kalanetra, K.M., N. Bano and J.T. Hollibaugh (2009). "Ammonia oxidizing Archaea in the Arctic Ocean and Antarctic coastal waters." *Environmental Microbiology* **11**: 2434–2445.
- Kemp, E.M. (1975). "Palynology of Leg 28 drill sites, Deep Sea Drilling Project." *Initial Reports of the Deep Sea Drilling Project, volume 28*. D. E. Hayes and L. A. Frakes. Washington, U.S. Government Printing Office.
- Kennett, J.P., R.E. Houtz, P.B. Andrews and A.R. Edwards (1974). "Development of the circum-Antarctic current." *Science* **186**: 144-147.
- Kennett, J.P. and R.E. Houtz (1975). *Initial Reports of the Deep Sea Drilling Project, volume 29*. Washington, U.S. Government Printing Office.
- Kennett, J.P. (1977). "Cenozoic evolution of Antarctic glaciation, the circum-Antarctic Ocean, and their impact on global paleoceanography." *Journal of Geophysical Research* **82**(27): 3843-3860.
- Kennett, J.P. and C.C. v.d. Borch (1986). *Initial Reports of the Deep Sea Drilling Project, volume 90, parts 1&2*. Washington, U.S. Government printing office.
- Kennett, J.P. and L.D. Stott (1991). "Abrupt deep sea warming, paleoceanographic changes and benthic extinctions at the end of the Paleocene." *Nature* **353**: 225-229.
- Kent, D.V. and G. Muttoni (2008). "Equatorial convergence of India and early Cenozoic climate trends." *Proceedings of the National Academy of Sciences of the USA* **105**(42): 16065-16070.
- Kim, J.H., S. Schouten, E.C. Hopmans, B. Donner and J.S. Sinninghe Damsté (2008). "Global sediment core-top calibration of the TEX<sub>86</sub> paleothermometer in the ocean." *Geochimica et Cosmochimica Acta* **72**: 1154–1173.
- Kim, J.-H., J.v.d. Meer, S. Schouten, P. Helmke, V. Willmott, F. Sangiorgi, N. Koç, E.C. Hopmans and J.S. Sinninghe Damsté (2010). "New indices and calibrations derived from the distribution of crenarchaeal isoprenoid tetraether lipids: Implications for past sea surface temperature reconstructions." *Geochimica et Cosmochimica Acta* **74**: 4639-4654.
- Klumpp, B. (1953). "Beitrag zur Kenntnis der Mikrofossilien des mittleren und oberen Eozän." *Paleontographica, Abteilung A* **103**: 377-406.
- Koch, P.L., J.C. Zachos and P.D. Gingerich (1992). "Correlation between isotope records in marine and continental carbon reservoirs near the Paleocene/Eocene boundary." *Nature* **358**: 319-323.



- Kohn, M.J., J.A. Josef, R. Madden, R. Kay, G. Vucetich and A.A. Carlini (2004). "Climate Stability across the Eocene-Oligocene transition, southern Argentina." Geology **32**(7): 621-624.
- Köthe, A. (1990). "Paleogene dinoflagellates from northwest Germany: biostratigraphy and paleoenvironment." Geologischer Jahrbuch, Reihe A **118**: 3-111.
- Kraus, M.J. and S. Riggins (2007). "Transient drying during the Paleocene-Eocene Thermal Maximum (PETM): Analysis of paleosols in the bighorn basin, Wyoming." Palaeogeography, Palaeoclimatology, Palaeoecology **245**: 444-461.
- Kurtz, A., L.R. Kump, M.A. Arthur, J.C. Zachos and A. Paytan (2003). "Early Cenozoic decoupling of the global carbon and sulfur cycles." Paleoceanography **18**: 1090.
- Lagabrielle, Y., Y. Godd ris, Y. Donnadieu, J. Malavieille and M. Suarez (2009). "The tectonic history of Drake Passage and its possible impacts on global climate." Earth and Planetary Science Letters **279**: 197-211.
- Latimer, J.C. and G.M. Filippelli (2002). "Eocene to Miocene terrigenous inputs and export production: geochemical evidence from ODP leg 177, site 1090." Palaeogeography, Palaeoclimatology, Palaeoecology **182**: 151-164.
- Laws, E.A., B.N. Popp and R.R. Bidigare (2000). "Controls on the molecular distribution and carbon isotopic composition of alkenones in certain haptophyte algae." Geochemistry, Geophysics, Geosystems **2**: 2000GC000057.
- Lawver, L.A. and L.C. Gahagan (2003). "Evolution of Cenozoic seaways in the circum-Antarctic region." Palaeogeography, Palaeoclimatology, Palaeoecology **198**: 11-37.
- Lazarus, D. and J.P. Caulet (1993). "Cenozoic Southern Ocean reconstruction from sedimentologic, radiolarian, and other microfossil data." The Antarctic paleoenvironment: A perspective on global change, part 2. J. P. Kennett and D. A. Warnke. Washington, AGU. **60**: 145-174.
- Lazarus, D.B., C.J. Hollis and M. Apel (2008). "Patterns of opal and radiolarian change in the Antarctic mid-Paleogene: clues to the origin of the Southern Ocean." Micropaleontology **54**(1): 41-48.
- Lentin, J.K. and T.F. Vozzhennikova (1989). "The fossil dinoflagellate cyst *Kisselovia* emend. and *Charlesdownia* gen. nov." Review of Palaeobotany and Palynology **58**: 215-229.
- Lentin, J.K. and G.L. Williams (1976). "A monograph of fossil peridinioid dinoflagellate cysts." Bedford Institute of Oceanography, Report Series BI-R-75-16: 237.
- Lentin, J.K. and G.L. Williams (1977). "Fossil dinoflagellates: index to genera and species, 1977 edition." Bedford Institute of Oceanography, Report Series BI-R-77-8: 1-209.
- Lentin, J.K. and G.L. Williams (1985). "Fossil dinoflagellates: index to genera and species, 1985 edition." Canadian technical report hydrography and ocean sciences **60**(451).
- Levy, R.H. and D.M. Harwood (2000). "Tertiary marine palynomorphs from the McMurdo Sound erratics, Antarctica." Paleobiology and Paleoenvironments of Eocene rocks, McMurdo Sound, East Antarctica. J. D. Stilwell and R. M. Feldmann, AGU Antarctic Research Series. **76**: 183-242.
- Li, Q., N.P. James and B. McGowran (2003a). "Middle and late Eocene Great Australian Bight lithobiostratigraphy and stepwise evolution of the southern Australian continental margin." Australian Journal of Earth Sciences **50**: 113-128.
- Li, Q., B. McGowran and N.P. James (2003b). "Eocene-Oligocene planktonic foraminiferal biostratigraphy of sites 1126, 1130, 1132 and 1134, ODP leg 182, Great Australian Bight." Proceedings of the Ocean Drilling Program, Scientific Results, volume 182. A. C. Hine, D. A. Feary and M. J. Malone. College Station, Texas, U.S. Government Printing Office.
- Liu, Z., M. Pagani, D. Zinniker, R. DeConto, M. Huber, H. Brinkhuis, S.R. Shah, M. Leckie and A. Pearson (2009). "Global Cooling During the Eocene-Oligocene Climate Transition." Science **323**: 1187-1190.
- Lourens, L., A. Sluijs, D. Kroon, J.C. Zachos, E. Thomas, U. R hl, J. Bowles and I. Raffi (2005). "Astronomical pacing of late Palaeocene to early Eocene hyperthermal events." Nature **435**: 1083-1087.
- Ludwig, W.J. and V.A. Krashennikov (1983). Initial Reports of the Deep Sea Drilling Project, volume 71. Washington, U.S. Government Printing Office.
- Macphail, M.K. (2001). "The Tasmanian offshore zone: A link between the Gippsland and Taranaki basin petroleum provinces". Canberra, Australian Geological Survey Organization (AGZO/GA): 1-45.
- Macphail, M.K. and E.M. Truswell (2004). "Palynology of Site 1166, Prydz Bay, East Antarctica." Proceedings of the Ocean Drilling Program, Scientific Results, volume 188. P.E. O'Brien, A.K. Cooper and C. Richter. College Station, Texas, U.S. Government Printing Office.





## REFERENCES

- Madile, M. and S. Monechi (1991). "Late Eocene to early Oligocene calcareous nannofossil assemblages from Sites 699 and 703, subantarctic South Atlantic Ocean." Proceedings of the Ocean Drilling Program, Scientific Results, volume 114. P.F. Ciesielski and Y. Kristoffersen. College Station, Texas, U.S. Government Printing Office: 179-192.
- Mao, S. and B. Mohr (1995). "Middle Eocene dinocysts from Bruce Bank (Scotia Sea, Antarctica) and their palaeoenvironmental and palaeogeographic implications." Review of Palaeobotany and Palynology **86**: 235-263.
- Markwick, P.J. (1998). "Fossil crocodilians as indicators of Late Cretaceous and Cenozoic climates: implications for using paleontological data in reconstructing palaeoclimate." Palaeogeography, Palaeoclimatology, Palaeoecology **137**: 205-271.
- Martens-Habbena, W., P.M. Berube, H. Urakawa, J.R. de la Torre and D.A. Stahl (2009). "Ammonia oxidation kinetics determine niche separation of nitrifying Archaea and Bacteria." Nature **461**: 976-979.
- Martin, H.A. (1991). "Dinoflagellate and spore pollen biostratigraphy of SADME MC63 bore, western Murray Basin." Alcheringa **15**: 107-144.
- Martin, H.A. (1993). "Middle Tertiary dinoflagellate and spore/pollen biostratigraphy and palaeoecology of the Mallee Cliffs Bore, central Murray Basin." Alcheringa **17**: 91-124.
- McCarren, H., E. Thomas, T. Hasegawa, U. Röhl and J.C. Zachos (2009). "Depth dependency of the Paleocene-Eocene carbon isotope excursion: Paired benthic and terrestrial biomarker records (Ocean Drilling Program Leg 208, Walvis Ridge)." Geochemistry, Geophysics, Geosystems **9**(Q10008).
- McGonigal, K. and A. DiStefano (2002). "Calcareous nannofossil biostratigraphy of the Eocene - Oligocene transition, ODP Sites 1123 and 1124." Proceedings of the Ocean Drilling Program, Scientific Results, volume 181. C. Richter. College Station, Texas, U.S. Government Printing Office.
- McGowran, B. (1989). "Silica burp in the Eocene ocean." Geology **17**: 857- 860.
- Menéndez, C.A. (1965). "Microplankton fósil de sedimentos Terciarios y Cretácicos del norte de Tierra del Fuego(Argentina)." Ameghiniana **4**(1): 7-18.
- Miller, K.G., R.G. Fairbanks and G.S. Mountain (1987). "Tertiary oxygen isotope synthesis, sea-level history and continental margin erosion." Paleoceanography **2**: 1-19.
- Mohr, B.A.R. (1990). "Eocene and Oligocene Sporomorphs and dinoflagellate cysts from leg 113 drill sites, Weddel Sea, Antarctica." Proceedings of the Ocean Drilling Program, Scientific Results, volume 113. P. F. Barker and J. P. Kennet. College Station, Texas, U.S. Government Printing Office: 595-611.
- Moore, T.C., jr. (2008). "Chert in the Pacific: Biogenic silica and hydrothermal circulation." Palaeogeography, Palaeoclimatology, Palaeoecology **261**: 87-99.
- Moran, K., J. Backman, H. Brinkhuis, S.C. Clemens, T. Cronin, G.R. Dickens, F.D.R. Eynaud, J.R.M. Gattacceca, M. Jakobsson, R.W. Jordan, M. Kaminski, J. King, N. Koç, A. Krylov, N. Martinez, J. Matthiessen, D. McInroy, T.C. Moore, J. Onodera, M. O'Regan, H. Pälike, B. Rea, D. Rio, T. Sakamoto, D.C. Smith, R. Stein, K. St John, I. Suto, N. Suzuki, K. Takahashi, M. Watanabe, M. Yamamoto, J. Farrell, M. Frank, P. Kubik, W. Jokat and Y. Kristoffersen (2006). "The Cenozoic palaeoenvironment of the Arctic Ocean." Nature **441**: 601-605.
- Müller, P.J., Kirst, G., Röhl, U. and, G., von Storch, I., Rosell-Melé, A. (1998). "Calibration of the alkenone paleotemperature index  $U^{K'_{37}}$  based on core-tops from the eastern South Atlantic and the global ocean (60°N-60°S)." Geochimica et Cosmochimica Acta **62**(10): 1757-1772.
- Murphy, M.G. and J.P. Kennett (1986). "Development of latitudinal thermal gradients during the Oligocene: Oxygen-isotope evidence from the southwest Pacific." Initial reports of the Deep Sea Drilling Project, volume 90, part 2. J. P. Kennett and C. C. v. d. Borch. Washington, U.S. Government printing office: 1347-1360.
- Nelson, C.S. and P.J. Cooke (2001). "History of oceanic front development in the New Zealand sector of the Southern Ocean during the Cenozoic: A synthesis." New Zealand Journal of Geology and Geophysics **44**: 535-553.
- Nicolo, M.J., G.R. Dickens and C.J. Hollis (2010). "South Pacific intermediate water oxygen depletion at the onset of the Paleocene- Eocene Thermal Maximum as depicted in New Zealand margin sections." Paleoceanography **25**: PA4210
- Nicolo, M.J., G.R. Dickens, C.J. Hollis and J.C. Zachos (2007). "Multiple early Eocene hyperthermals: Their sedimentary expression on the New Zealand continental margin and in the deep sea." Geology **35**(8): 699-702.
- Nielsen, S.G., S. Mar-Gerrison, A. Gannoun, D. LaRowe, V. Klemm, A.N. Halliday, K.W. Burton and J.R. Hein (2009). "Thallium isotope evidence for a permanent increase in marine organic carbon export in the early Eocene." Earth and Planetary Science Letters **278**: 297-307.



- Norris, R.D. and U. Röhl (1999). "Carbon cycling and chronology of climate warming during the Palaeocene/Eocene transition." *Nature* **401**: 775-778.
- O'Brien, P.E., A.K. Cooper and C. Richter (1998). *Proceedings of the Ocean Drilling Program, Initial Reports, volume 188*. College Station, Texas, U.S. Government Printing Office.
- O'Brien, P.E., A.K. Cooper and C. Richter (2004). *Proceedings of the Ocean Drilling Program, Scientific Results, volume 188*. College Station, Texas, U.S. Government Printing Office.
- Pagani, M. (2002). "The alkenone-CO<sub>2</sub> proxy and ancient atmospheric carbon dioxide." *Philosophical Transactions: Mathematical, Physical and Engineering Sciences. Royal Society of London A* **360**: 609-632.
- Pagani, M., K.H. Freeman, K. Ohkouchi and K. Caldeira (2002). "Comparison of water column [CO<sub>2</sub>aq] with sedimentary alkenone-based estimates: A test of the alkenone-CO<sub>2</sub> proxy." *Paleoceanography* **17**: 1009.
- Pagani, M., J.C. Zachos, K.H. Freeman, B. Tipple and S. Bohaty (2005). "Marked decline in atmospheric carbon dioxide concentrations during the Paleogene." *Science* **309**: 600-603.
- Pagani, M., N. Pedentchouk, M. Huber, A. Sluijs, S. Schouten, H. Brinkhuis, J.S. Sinninghe Damsté and G.R. Dickens (2006). "Arctic hydrology during global warming at the Palaeocene/Eocene thermal maximum." *Nature* **442**: 671-675.
- Pagani, M., Z. Liu, J. LaRiviere and A.C. Ravelo (2010). "High Earth-system climate sensitivity determined from Pliocene carbon dioxide concentrations." *Nature Geoscience* **3**: 27-30.
- Paillard, D., L. Labeyrie and P. Yiou (1996). "Macintosh program performs time-series analysis." *EOS Transactions AGU* **77**: 379.
- Palmer, M.R., G.J. Brummer, M.J. Cooper, H. Elderfield, M.J. Greaves, G.J. Reichart, S. Schouten and J.M. Yu (2010). "Multi-proxy reconstruction of surface water pCO<sub>2</sub> in the northern Arabian Sea since 29 ka." *Earth and Planetary Science Letters* **295** 49-57.
- Panchuk, K., A.J. Ridgwell and K. L.R. (2008). "Sedimentary response to Paleocene-Eocene Thermal Maximum carbon release: A model-data comparison." *Geology* **36**(4): 315-318.
- Pearson, P.N. and M.R. Palmer (2000). "Atmospheric carbon dioxide concentrations over the past 60 million years." *Nature* **406**: 695-699.
- Pearson, P.N., P.W. Ditchfield, J. Singano, K.G. Harcourt-Brown, C.J. Nicholas, R.K. Olsson, N.J. Shackleton and M.A. Hall (2001). "Warm tropical sea surface temperatures in the Late Cretaceous and Eocene epochs." *Nature* **413**(4): 481-487.
- Pearson, P.N., B.E. Dongen, van, C.J. Nicholas, R.D. Pancost, S. Schouten, J.M. Singano and B.S. Wade (2007). "Stable tropical climate through the Eocene Epoch." *Geology* **35**(3): 211-214.
- Pearson, P.N., G.L. Foster and B.S. Wade (2009). "Atmospheric carbon dioxide through the Eocene-Oligocene climate transition." *Nature* **461**: 1110-1113.
- Pocknall, D.T. (1991). "Palynostratigraphy of the Te Kuiti Group (late Eocene - Oligocene), Waikato Basin, New Zealand." *New Zealand Journal of Geology and Geophysics* **34**: 407-417.
- Popp, B.N., E.A. Laws, R.R. Bidigare, J.R. Dore, K.L. Hanson and S.G. Wakeham (1998). "Effect of phytoplankton cell geometry on carbon isotopic fractionation." *Geochimica et Cosmochimica Acta* **62**: 69-77.
- Pross, J. and G. Schmiedl (2002). "Early Oligocene dinoflagellate cysts from the Upper Rhine Graben (SW Germany): paleoenvironmental and paleoclimatic implications." *Marine Micropaleontology* **45**: 1-24.
- Pross, J. and H. Brinkhuis (2005). "Organic-walled dinoflagellate cysts as paleoenvironmental indicators in the Paleogene; a synopsis of concepts." *Palaeontologische Zeitschrift Band* **79**(Heft 1): 53-59.
- Pujalte, V. and B. Schmitz (2006). "Abrupt climatic and sea level changes across the Paleocene-Eocene boundary, as recorded in an ancient coastal plain setting (Pyrenees, Spain)." *Climate and Biota of the early Paleogene*. Bilbao, Spain.
- Quattrocchio, M.E. and W.A.S. Sarjeant (2003). "Dinoflagellates from the Chorrillo Formation (Paleogene) of southern Chile." *Ameghiniana* **40**: 129-153.
- Quattrocchio, M.E. (2009). "Paleogene dinoflagellate cysts from Punta Prat, southern Chile." *Palynology* **33**: 141-156.
- Reichart, G.-J. and H. Brinkhuis (2003). "Late Quaternary *Protoperidinium* cysts as indicators of paleoproductivity in the northern Arabian Sea." *Marine Micropaleontology* **49**: 303-315.
- Reichart, G.-J., H. Brinkhuis, F. Huiskamp and W.J. Zachariasse (2004). "Hyperstratification following glacial overturning events in the northern Arabian Sea." *Paleoceanography* **19**: PA2013, doi:10.1029/2003PA000900.





## REFERENCES

- Richter, T.O., S. Gast, R., van der, Koster, A. Vaars, R. Gieles, H.C. De Stigter, H. Haas, de and T.C.E. Weering, van (2006). "The Avaatech XRF Core Scanner: technical description and applications to NE Atlantic sediments." New Techniques in Sediments Core Analysis. R. G. Rothwell. London, Geological Society London, Special Publication: 39–51.
- Robert, C. and J.P. Kennett (1994). "Antarctic subtropical humid episode at the Paleocene-Eocene boundary: clay mineral evidence." Geology **22**: 211–214.
- Roberts, A.P., S.J. Bicknell, J. Byatt, S.M. Bohaty, F. Florindo and D.M. Harwood (2003). "Magnetostratigraphic calibration of Southern Ocean diatom datums from the Eocene-Oligocene of Kerguelen Plateau (Ocean Drilling Program sites 744 and 748)." Palaeogeography, Palaeoclimatology, Palaeoecology **198**: 145-168.
- Röhl, U. and L.J. Abrams (2000). "High-resolution, downhole and nondestructive core measurements from Sites 999 and 1001 in the Caribbean Sea: application to the Late Paleocene Thermal Maximum." Proceedings of the Ocean Drilling Program, Scientific Results, volume 165. College Station, TX, Ocean Drilling Program: 191–203.
- Röhl, U., H. Brinkhuis, C.E. Stickley, M. Fuller, S.A. Schellenberg, G. Wefer and G.L. Williams (2004a). "Sea level and astronomically induced environmental changes in Middle and Late Eocene sediments from the East Tasman Plateau." Geophysical Monograph Series **151**: 127-151.
- Röhl, U., H. Brinkhuis, A. Sluijs and M. Fuller (2004b). "On the search for the Paleocene/Eocene boundary in the Southern Ocean: Exploring ODP Leg 189 Holes 1171D and 1172D, Tasman Sea." Geophysical Monograph Series **151**: 113-124.
- Röhl, U., T. Westerhold, T.J. Bralower and J.C. Zachos (2007). "On the duration of the Paleocene – Eocene thermal maximum (PETM)." Geochemistry, Geophysics, Geosystems **8**: Q12002.
- Rost, B., I. Zondervan and U. Riebesell (2002). "Light-Dependent Carbon Isotope Fractionation in the Coccolithophorid *Emiliana huxleyi*." Limnology and Oceanography **47**(1): 120-128.
- Roij, L., van (2009). "The Paleocene Eocene Thermal Maximum in the Gulf of Mexico: a low latitude paleoenvironmental reconstruction." University of Utrecht. **Master's thesis**.
- Sangiorgi, F., E.E. Soelen, van, D.J. Spofforth, H. Pälike, C.E. Stickley, K. St. John, N. Koç, S. Schouten, J.S. Sinninghe Damsté and H. Brinkhuis (2008). "Cyclicality in the middle Eocene central Arctic Ocean sediment record: Orbital forcing and environmental response." Paleoceanography **23**(PA1S08): doi:10.1029/2007PA001487.
- Schellenberg, S.A., H. Brinkhuis, C.E. Stickley, M. Fuller, F.T. Kyte and G.L. Williams (2004). "The Cretaceous/Paleogene Transition on the East Tasman Plateau, Southwestern Pacific." The Cenozoic Southern Ocean; Tectonics, Sedimentation and Climate Change Between Australia and Antarctica. N. Exon, J. P. Kennett and M. Malone. Washington, Geophysical Monograph Series **151**: 93-112.
- Schmitz, B., V. Pujalte and K. Nunez-Betelu (2001). "Climate and sea level perturbations during the Initial Eocene Thermal Maximum: evidence from siliciclastic units in the Basque Basin (Ermua, Zumaia and Trabakua Pass), northern Spain." Palaeogeography, Palaeoclimatology, Palaeoecology **165**: 299–320.
- Schouten, S., E.C. Hopmans, E. Schefuß and J.S. Sinninghe Damsté (2002). "Distributional variations in marine crenarchaeotal membrane lipids: a new tool for reconstructing ancient sea water temperatures?" Earth and Planetary Science Letters **204**: 265-274.
- Schouten, S., C. Huguet, E.C. Hopmans, M.V.M. Kienhuis and J.S. Sinninghe Damsté (2007a). "Analytical Methodology for TEX<sub>86</sub> paleothermometry by High-Performance Liquid Chromatography/ Atmospheric Pressure Chemical Ionization-Mass Spectrometry." Analytical Chemistry **79**: 2940–2944.
- Schouten, S., A. Forster, E.F. Panoto and J.S. Sinninghe Damsté (2007b). "Towards calibration of the TEX<sub>86</sub> palaeothermometer for tropical sea surface temperatures in ancient greenhouse worlds." Organic Geochemistry **38**: 1537-1546.
- Schouten, S., M. Woltering, W.I.C. Rijpstra, A. Sluijs, H. Brinkhuis and J.S. Sinninghe Damsté (2007c). "The Paleocene-Eocene carbon isotope excursion in higher plant organic matter: Differential fractionation of angiosperms and conifers in the Arctic." Earth and Planetary Science Letters **258**: 581–592.
- Schouten, S., J. Eldrett, D.R. Greenwood, I. Harding, M. Baas and J.S. Sinninghe Damsté (2008). "Onset of long-term cooling of Greenland near the Eocene-Oligocene boundary as revealed by branched tetraether lipids." Geology **36**(2): 147-150.



- Schrag, D.P., D.J. DePaolo and F.M. Richter (1995). "Reconstructing past sea surface temperatures: Correcting for diagenesis of bulk marine carbonate." *Geochimica et Cosmochimica Acta* **59**: 2265-2278.
- Seki, O., G.L. Foster, D.N. Schmidt, A. Mackensen, K. Kawamura and R.D. Pancost (2010). "Alkenone and boron-based Pliocene pCO<sub>2</sub> records." *Earth and Planetary Science Letters* **292**: 201-211.
- Sexton, P.F., P.A. Wilson and R.D. Norris (2006). "Testing the Cenozoic multisite composite δ<sup>18</sup>O and δ<sup>13</sup>C curves: New monospecific Eocene records from a single locality, Demerara Rise (Ocean Drilling Program Leg 207)." *Paleoceanography* **21**(PA2019).
- Shafik, S. (1996). "Calcareous microplankton biostratigraphy of the Eocene Browns Creek clay of the Aire district, Otway Basin of Southeastern Australia: An update." *AGZO Journal of Australian Geology and Geophysics* **16**(3): 333-344.
- Shafik, S. and M. Idnurm (1997). "Calcareous microplankton and polarity reversal stratigraphies of the Upper Eocene Browns Creek clay in the Otway Basin, southeast Australia: Matching the evidence." *Australian Journal of Earth Sciences* **44**: 77-86.
- Shea, D.J., K.E. Trenberth and R.W. Reynolds (1992). "A global monthly sea surface temperature climatology." *Journal of climate* **5**: 987-1001.
- Sijp, W.P., M.H. England and M. Huber (in press). "Effect of the deepening of the Tasman Gateway on the global ocean." *Paleoceanography*. doi:10.1029/2011PA002143.
- Siringan, F.P., R.V. Azanza, N.J.H. Macalalad, P.B. Zamora and M.Y.Y. Sta. Maria (2008). "Temporal changes in the cyst densities of *Pyrodinium bahamense* var. *compressum* and other dinoflagellates in Manila Bay, Philippines." *Harmful Algae* **7**: 523-531.
- Sloan, L.C. and D.K. Rea (1995). "Atmospheric carbon dioxide and Early Eocene climate: A general circulation modeling sensitivity study." *Palaeogeography, Palaeoclimatology, Palaeoecology* **119**: 275-292.
- Sluijs, A., H. Brinkhuis, C.E. Stickley, J. Warnaar, G.L. Williams and M. Fuller (2003). "Dinoflagellate cysts from the Eocene - Oligocene transition in the Southern Ocean: Results from ODP Leg 189." *Proceedings of the Ocean Drilling Program, Scientific Results, volume 189*. N. Exon and J. P. Kennett. College Station, Texas, U.S. Government Printing Office.
- Sluijs, A., J. Pross and H. Brinkhuis (2005). "From greenhouse to icehouse; organic walled dinoflagellate cysts as paleoenvironmental indicators in the Paleogene." *Earth-Science Reviews* **68**: 281-315.
- Sluijs, A., S. Schouten, M. Pagani, M. Woltering, H. Brinkhuis, J.S. Sinninghe Damsté, G.R. Dickens, M. Huber, G.-J. Reichart, R. Stein, J. Matthiessen, L.J. Lourens, N. Pedentchouk, J. Backman, K. Moran and Expedition 302 Scientists (2006). "Subtropical Arctic Ocean temperatures during the Palaeocene/Eocene thermal maximum." *Nature* **441**: 610-613.
- Sluijs, A. (2006). "Global Change during the Paleocene- Eocene Thermal Maximum." *LPP contributions series No. 21*. Utrecht University, Utrecht, the Netherlands. **PhD thesis**.
- Sluijs, A., G.J. Bowen, H. Brinkhuis, L.J. Lourens and E. Thomas (2007a). "The Palaeocene-Eocene thermal maximum super greenhouse: biotic and geochemical signatures, age models and mechanisms of global change." *Deep time perspectives on Climate Change: Marrying the Signal from Computer Models and Biological Proxies*. M. Williams, A. M. Haywood, F. J. Gregory and D. N. Schmidt. London, The Micropalaeontological Society, Special Publications. The Geological Society: 323-347.
- Sluijs, A., H. Brinkhuis, S. Schouten, S. Bohaty, C.M. John, J.C. Zachos, G.-J. Reichart, J.S. Sinninghe Damsté, E.M. Crouch and G.R. Dickens (2007b). "Environmental precursors to rapid light carbon injection at the Palaeocene/Eocene boundary." *Nature* **450**: 1218-1221.
- Sluijs, A., U. Röhl, S. Schouten, H.J. Brumsack, F. Sangiorgi, J.S. Sinninghe Damsté and H. Brinkhuis (2008a). "Arctic late Paleocene-early Eocene paleoenvironments with special emphasis on the Paleocene-Eocene thermal maximum (Lomonosov Ridge, Integrated Ocean Drilling Program Expedition 302)." *Paleoceanography* **23**(PA1S11, doi:10.1029/2007PA001495).
- Sluijs, A., H. Brinkhuis, E.M. Crouch, C.M. John, L. Handley, D. Munsterman, S.M. Bohaty, J.C. Zachos, G.-J. Reichart, S. Schouten, R.D. Pancost, J.S. Sinninghe Damsté, N.L.D. Welters, A.F. Lotter and G.R. Dickens (2008b). "Eustatic variations during the Paleocene-Eocene greenhouse world." *Paleoceanography* **23**: PA4216.
- Sluijs, A. and H. Brinkhuis (2009). "A dynamic climate and ecosystem state during the Paleocene-Eocene Thermal Maximum: inferences from dinoflagellate cyst assemblages on the New Jersey Shelf." *Biogeosciences* **6**(8): 1755-1781.



## REFERENCES

- Sluijs, A., S. Schouten, T.H. Donders, P.L. Schoon, U. Röhl, G.-J. Reichart, F. Sangiorgi, J.-H. Kim, J.S. Sinninghe Damsté and H. Brinkhuis (2009a). "Warm and Wet Conditions in the Arctic Region during Eocene Thermal Maximum 2." *Nature Geoscience* **2**: 777–780.
- Sluijs, A., H. Brinkhuis, G.L. Williams and R.A. Fensome (2009b). "Taxonomical revision of the *Spinidinium-Vozzhennikovia* group of organic walled, peridinioid dinoflagellate cysts." *Review of Palaeobotany and Palynology* **154**(1-4): 34-53.
- Spang, A., R. Hatzepichler, C. Brochier-Armanet, T. Rattai, P. Tischler, E. Spieck, W. Streit, D.A. Stahl, M. Wagner and C. Schleper (2010). "Distinct gene set in two different lineages of ammonia-oxidizing archaea supports the phylum Thaumarchaeota." *Trends in Microbiology* **18**: 331–340.
- Speelman, E.N., J.O. Sewall, D. Noone, M. Huber, A. Heydt, von der, J.S. Sinninghe Damsté and G.-J. Reichart (2010). "Modeling the influence of a reduced equator-to-pole sea surface temperature gradient on the distribution of water isotopes in the early/middle Eocene." *Earth & Planetary Science Letters* **298**(1-2): 57-65.
- Speijer, R.P. and T. Wagner (2002). "Sea-level changes and black shales associated with the late Paleocene thermal maximum: Organic geochemical and micropaleontologic evidence from the southern Tethyan margin (Egypt-Israel)." *Geological Society of America Special Paper* **356**: 533–549.
- St John, K. (2008). "Cenozoic Ice-Rafting history of the Central Arctic Ocean: Terrigenous sands on the Lomonosov Ridge." *Paleoceanography* **23**(PAIS05).
- Stap, L., L.J. Lourens, E. Thomas, A. Sluijs, S.M. Bohaty and J.C. Zachos (2010). "High-resolution deep-sea carbon and oxygen isotope records of Eocene Thermal Maximum 2 and H2." *Geology* **38**: 607–610.
- Sturbaut, E., R. Magioncalda, C. Dupuis, S. van Simaëys, E. Roche and M. Roche (2003). "Palynology, paleoenvironments, and organic carbon isotope evolution in lagoonal Paleocene-Eocene boundary settings in North Belgium." in: *Causes and consequences of Globally Warm Climates in the Early Paleogene*, Geological Society of America Special Paper. S. L. Wing, P. Gingerich, B. Schmitz and E. Thomas. Boulder, Colorado, Geological Society of America. **369**: 291–317.
- Stickley, C.E., H. Brinkhuis, K.L. McGonigal, G.C.H. Chapronière, M. Fuller, D.C. Kelly, D. Nürnberg, H.A. Pfuhl, S.A. Schellenberg, J. Schoenfeld, N. Suzuki, Y. Touchard, W. Wei, G.L. Williams, J. Lara and S.A. Stant (2004a). "Late Cretaceous - Quaternary biomagnetostratigraphy of ODP Site 1168, 1170, 1171 & 1172, Tasmanian Gateway." *Proceedings of the Ocean Drilling Program, Scientific Results, volume 189*. N. F. Exon, J. P. Kennett and M. J. Malone. College Station, Texas, U.S. Governmental Printing Office.
- Stickley, C.E., H. Brinkhuis, S.A. Schellenberg, A. Sluijs, U. Röhl, M. Fuller, M. Grauert, M. Huber, J. Warnaar and G.L. Williams (2004b). "Timing and nature of the deepening of the Tasmanian Gateway." *Paleoceanography* **19**: PA4027(1-18).
- Stickley, C.E., K.S. John, N. Koc, R.W. Jordan, S. Passchier, R.B. Pearce and L.E. Kearns (2009). "Evidence for middle Eocene Arctic sea ice from diatoms and ice-rafted debris." *Nature* **460**: 376-379.
- Stockmarr, J. (1972). "Tablets with spores used in absolute pollen analysis." *Pollen et Spores* **13**: 615–621.
- Stover, L.E. and G.L. Williams (1987). "Analyses of Mesozoic and Cenozoic organic-walled dinoflagellates 1977-1985." *AASP Contribution series* **18**: 1-243.
- Stover, L.E. and G.L. Williams (1995). "A revision of the Paleogene dinoflagellate genera *Areosphaeridium* Eaton 1971 and *Eatonicysta* Stover and Evitt 1978." *Micropaleontology* **41**(2): 97-141.
- Strong, C.P., C.J. Hollis and G.J. Wilson (1995). "Foraminiferal, radiolarian, and dinoflagellate biostratigraphy of late Cretaceous to middle Eocene pelagic sediments (Muzzle Group), Mead Stream, Marlborough, New Zealand." *New Zealand Journal of Geology and Geophysics* **38**: 171-212.
- Svensen, H., S. Planke, A. Malthe-Sørensen, B. Jamtveit, R. Myklebust, T.R. Eidem and S.S. Rey (2004). "Release of methane from a volcanic basin as a mechanism for initial Eocene global warming." *Nature* **429**: 542–545.
- Thomas, D.J., J.C. Zachos, T.J. Bralower, E. Thomas and S. Bohaty (2002). "Warming the fuel for the fire: Evidence for the thermal dissociation of methane hydrate during the Paleocene-Eocene thermal maximum." *Geology* **30**: 1067–1070.
- Thomas, D.J., T.J. Bralower and C.E. Jones (2003). "Neodymium isotopic reconstruction of the late Paleocene - early Eocene thermohaline circulation." *Earth and Planetary Science Letters* **209**(3-4): 309-322.
- Thomas, E. and N.J. Shackleton (1996). "The Palaeocene-Eocene benthic foraminiferal extinction and stable isotope anomalies." *Correlation of the Early Paleogene in Northwestern Europe*, Geological Society London Special Publication. R. W. O. B. Knox, R. M. Corfield and R. E. Dunay. London, Geological Society of London. **101**: 401–441.



- Tjallingii, R., U. Röhl, M. Kölling and T. Bickert (2007). "Influence of the water content on X-ray fluorescence core scanning measurements in soft marine sediments." Geochemistry, Geophysics, Geosystems, Technical Brief **8**: Q02004.
- Tripati, A. and H. Elderfield (2005). "Deep-Sea Temperature and Circulation Changes at the Paleocene-Eocene Thermal Maximum." Science **308**: 1894-1898.
- Truswell, E.M. (1997). "Palynomorph assemblages from marine Eocene sediments on the west Tasmanian continental margin and the South Tasman Rise." Australian Journal of Earth Sciences **44**: 633-654.
- Turich, C., K.H. Freeman, M.-A. Bruns, M. Conte, A.D. Jones and S.G. Wakeham (2007). "Lipids of marine Archaea: Patterns and provenance in the water-column and sediments." Geochimica et Cosmochimica Acta **71**: 3272-3291.
- Tyrrell, T., P.M. Holligan and C.D. Mobley (1999). "Optical impacts of oceanic coccolithophore blooms." Journal of Geophysical Research **104**(C2): 3223-3241.
- Uchikawa, J. and R.E. Zeebe (2010). "Examining possible effects of seawater pH decline on foraminiferal stable isotopes during the Paleocene-Eocene Thermal Maximum." Paleoceanography **25**: PA2216.
- Veevers, J.J. and J.R. Heirtzler (1974). Initial reports of the Deep Sea Drilling Project, volume 27. Washington, U.S. Government Printing Office.
- Veevers, J.J., C.M. Powell and S.R. Roots (1991). "Review of seafloor spreading around Australia. Synthesis of the patterns of spreading." Australian Journal of Earth Sciences **38**: 373-389.
- Villa, G., C. Fioroni, L. Pea, S. Bohaty and D. Persico (2008). "Middle Eocene-late Oligocene climate variability: Calcareous nannofossil response at Kerguelen Plateau, Site 748." Marine Micropaleontology **69**: 173-192.
- Villanoy, C., R.A. Corralet, G.S. Jacinto, N. Cuaresma and R. Crisostomo (1996). "Towards the development of a cyst-based model for *Pyrodinium* red tides in Manila Bay." Harmful Toxic Algal Blooms. T. Yasumoto, Y. Oshima and Y. Fukuyo. Paris, IOC of UNESCO: 189-192.
- Villanoy, C.L., R.V. Azanza, A. Altemerano and A.L. Casil (2006). "Attempts to model the bloom dynamics of *Pyrodinium*, a tropical toxic dinoflagellate." Harmful Algae **5**: 156-183.
- Wakeham, S.G., C.M. Lewis, E.C. Hopmans, S. Schouten and J.S. Sinninghe Damsté (2003). "Archaea mediate anaerobic oxidation of methane in deep euxinic waters of the Black Sea." Geochimica et Cosmochimica Acta **67**: 1359-1374.
- Walker, J.C.G. and J.F. Kasting (1992). "Effects of fuel and forest conservation on future levels of atmospheric carbon dioxide." Palaeogeography, Palaeoclimatology, Palaeoecology **97**: 151-189.
- Wall, D., B. Dale, G.P. Lohmann and W.K. Smith (1977). "The environmental and climatic distribution of dinoflagellate cysts in modern marine sediments from regions in the North and South Atlantic oceans and adjacent seas." Marine Micropaleontology **2**: 121-200.
- Walsh, E.M., A.E. Ingalls and R.G. Keil (2008). "Sources and transport of terrestrial organic matter in Vancouver Island fjords and the Vancouver-Washington Margin: A multiproxy approach using  $\delta^{13}\text{C}_{\text{org}}$ , lignin phenols, and the ether lipid BIT index." Limnology and Oceanography **53**(3): 1054-1063.
- Warnaar, J. (2006). "Climatological implications of Australian- Antarctic separation." LPP Contributions series no. 22. Utrecht University, Utrecht, the Netherlands. **PhD thesis**.
- Warnaar, J., P.K. Bijl, M. Huber, L.C. Sloan, H. Brinkhuis, U. Röhl, R. Sriver and H. Visscher (2009). "Orbitally forced climate changes in the Tasman sector during the Middle Eocene." Palaeogeography, Palaeoclimatology, Palaeoecology **280**: 361-370.
- Wei, W. and H.R. Thierstein (1991). "Upper Cretaceous and Cenozoic calcareous nannofossils of the Kerguelen Plateau (southern Indian Ocean) and Prydz Bay (East Antarctica)." Proceedings of the Ocean Drilling Program, Scientific Results, volume 119. J. Barron and B. Larsen. College Station, Texas, U.S. Government Printing Office: 467-494.
- Weijers, J.W.H., S. Schouten, O.C. Spaargaren and J.S. Sinninghe Damsté (2006). "Occurrence and distribution of tetraether membrane lipids in soils: Implications for the use of the TEX<sub>86</sub> proxy and the BIT index." Organic Geochemistry **37**: 1680-1693.
- Weijers, J.W.H., E. Schefuß, S. Schouten and J.S. Sinninghe Damsté (2007a). "Coupled thermal and hydrological evolution of tropical Africa over the last deglaciation." Science **315**: 1701-1704.
- Weijers, J.W.H., S. Schouten, J.C. v.d. Donker, E.C. Hopmans and J.S. Sinninghe Damsté (2007b). "Environmental controls on bacterial tetraether membrane lipid distribution in soils." Geochimica et Cosmochimica Acta **71**: 703-713.



## REFERENCES

- Weijers, J.W.H., S. Schouten, A. Sluijs, H. Brinkhuis and J.S. Sinninghe Damsté (2007c). "Warm Arctic continents during the Palaeocene–Eocene thermal maximum." *Earth and Planetary Science Letters* **261**: 230-238.
- Weijers, J.W.H., B. Bernhardt, F. Peterse, J.P. Werne, J.A.J. Dungait, S. Schouten and J.S. Sinninghe Damsté (2011). "Absence of seasonal patterns in MBT-CBT indices in mid-latitude soils." *Geochimica et Cosmochimica Acta* **75**: 3179-3190.
- Weiss, R.F. (1974). "Carbon dioxide in water and seawater: the solubility of a non-ideal gas." *Marine Chemistry* **2**: 203–215.
- Weller, P. and R. Stein (2008). "Paleogene biomarker records from the central Arctic Ocean (Integrated Ocean Drilling Program Expedition 302): Organic carbon sources, anoxia, and sea surface temperature." *Paleoceanography* **23**(PA1S17).
- Westerhold, T., U. Röhl, J. Laskar, I. Raffi, J. Bowles, L.J. Lourens and J.C. Zachos (2007). "On the duration of magnetochrons C24r and C25n and the timing of early Eocene global warming events: Implications from the Ocean Drilling Program Leg 208 Walvis Ridge depth transect." *Paleoceanography* **22**(PA2201).
- Willcox, J.B. and M.J. Stagg (1990). "Australia's southern margin: a product of oblique extension." *Tectonophysics* **173**: 269-281.
- Williams, G.L. and C. Downie (1966). "*Wetzeliella* from the London Clay." *Studies on the Mesozoic and Cainozoic dinoflagellate cysts*. R. J. Davey, C. Downie, W. A. S. Sarjeant and G. L. Williams, Bulletin of the British Museum (natural history) geology. Supplement 3: 82-198.
- Williams, G.L., H. Brinkhuis, M.A. Pearce., R.A. Fensome and J.W. Weegink (2004). "Southern Ocean and global dinoflagellate cyst events compared: Index events for the late Cretaceous - Neogene." *Proceedings of the Ocean Drilling Program, Scientific Results, volume 189*. N. F. Exon, J. P. Kennett and M. J. Malone: 1-98.
- Wilson, G.J. (1967a). "Some new species of lower Tertiary dinoflagellates from McMurdo Sound, Antarctica." *New Zealand Journal of Botany* **5**: 57-83.
- Wilson, G.J. (1967b). "Some species of *Wetzeliella* Eisenack (Dinophyceae) from New Zealand Eocene and Paleocene strata." *New Zealand Journal of Botany* **5**: 469-497.
- Wilson, G.J. and C.D. Clowes (1982). "*Arachnodinium*, a new dinoflagellate genus from the lower Tertiary of Antarctica." *Palynology* **6**: 97-103.
- Wilson, G.J. (1985). "Dinoflagellate biostratigraphy of the Eocene Hampden Section North Otago, New Zealand." *New Zealand Geological Survey Record* **8**: 93-101.
- Wilson, G.J. (1988). "Paleocene and Eocene dinoflagellate cysts from Waipawa, Hawkes Bay, New Zealand." *New Zealand Geological Survey Bulletin* **57**(1-96).
- Wilson, G.S., A.P. Roberts, K.L. Verosub, F. Florindo and L. Sagnotti (1998). "Magnetobiostratigraphic chronology of the Eocene - Oligocene transition in the CIROS-1 core, Victoria Land margin, Antarctica: Implications for Antarctic glacial history." *Geological Society of America Bulletin* **110**: 35-47.
- Wing, S.L., G.J. Harrington, F.A. Smith, J.I. Block, D.M. Boyer and K.H. Freeman (2005). "Transient Floral Change and Rapid Global Warming at the Paleocene-Eocene Boundary." *Science* **310**: 993-996.
- Wise jr., S.W. and R. Schlich (1989). *Proceedings of the Ocean Drilling Program, Initial Reports, volume 120*. College Station, Texas, U.S. Government Printing Office.
- Wise jr., S.W. and R. Schlich (1992). *Proceedings of the Ocean Drilling Program, Scientific Results, volume 120*. College Station, Texas, U.S. Government Printing Office.
- Woodburne, M.O. and J.A. Case (1996). "Dispersal, vicariance and the late Cretaceous to early Tertiary Land Mammal Biogeography from South America to Australia." *Journal of Mammalian Evolution* **3**(2): 121-161.
- Wrenn, J.H. and S.W. Beckman (1982). "Maceral, total organic carbon, and palynological analyses of Ross Ice Shelf Project Site J9 cores." *Science* **216**: 187-189.
- Wrenn, J.H. and G.F. Hart (1988). "Paleogene dinoflagellate cyst biostratigraphy of Seymour Island, Antarctica." *Geological Society of America Memoires* **169**: 321-447.
- Wuchter, C., B. Abbas, M.J.L. Coolen, L. Herfort, J. van Bleijswijk, P. Timmers, M. Strous, E. Teira, G.J. Herndl, J.J. Middelburg, S. Schouten and J.S. Sinninghe Damsté (2006a). "Archaeal nitrification in the ocean." *Proceedings of the National Academy of Sciences of the United States of America* **103**: 12317–12322.
- Wuchter, C., S. Schouten, S.G. Wakeham and J.S. Sinninghe Damsté (2006b). "Archaeal tetraether membrane lipid fluxes in the northeastern Pacific and the Arabian Sea: Implications for TEX<sub>86</sub> paleothermometry." *Paleoceanography* **21**: PA4208.



- Zachos, J.C., J.R. Breza and S.W. Wise jr. (1992). "Early Oligocene ice sheet expansion on Antarctica: Stable isotope and sedimentological evidence from Kerguelen Plateau, Southern Indian Ocean." Geology **20**: 659-573.
- Zachos, J.C., M. Pagani, L. Sloan, E. Thomas and K. Billups (2001). "Trends, rythms, and aberrations in global climate 65 Ma to present." Science **292**: 686-693.
- Zachos, J.C., M.W. Wara, S.M. Bohaty, M.L. Delaney, M.R. Petrizzo, A. Brill, T.J. Bralower and I. Premoli Silva (2003). "A transient rise in tropical sea surface temperature during the Paleocene-Eocene thermal maximum." Science **302**: 1551-1554.
- Zachos, J.C., U. Röhl, S.A. Schellenberg, A. Sluijs, D.A. Hodell, D.C. Kelly, E. Thomas, M. Nicolo, I. Raffi, L.J. Lourens, H. McCarren and D. Kroon (2005). "Rapid Acidification of the Ocean During the Paleocene-Eocene Thermal Maximum." Science **308**: 1611-1615.
- Zachos, J.C., S. Schouten, S. Bohaty, T. Quattlebaum, A. Sluijs, H. Brinkhuis, S. Gibbs and T. Bralower (2006). "Extreme warming of mid-latitude coastal ocean during the Paleocene-Eocene Thermal Maximum: Inferences from TEX<sub>86</sub> and isotope data." Geology **34**(9): 737-740.
- Zachos, J.C., S.M. Bohaty, C.M. John, H. McCarren, D.C. Kelly and T. Nielsen (2007). "The Palaeocene-Eocene carbon isotope excursion constraints from individual shell planktonic foraminifer records." Philosophical Transactions of the Royal Society A **365**: 1829-1842.
- Zachos, J.C., G.R. Dickens and R.E. Zeebe (2008). "An early Cenozoic perspective on greenhouse warming and carbon-cycle dynamics." Nature **451**: 279-283.
- Zachos, J.C., H. McCarren, B. Murphy, U. Röhl and T. Westerhold (2010). "Tempo and scale of late Paleocene and early Eocene carbon isotope cycles: Implications for the origin of hyperthermals." Earth and Planetary Science Letters **299**: 242-249.
- Zeebe, R.E. and J.C. Zachos (2007). "Reversed deep-sea carbonate ion basin gradient during the Paleocene-Eocene thermal maximum." Paleoceanography **22**: PA3201.
- Zeebe, R.E., J.C. Zachos and G.R. Dickens (2009). "Carbon dioxide forcing alone insufficient to explain Palaeocene-Eocene Thermal Maximum warming." Nature Geoscience **2**: 576-580.
- Zinsmeister, W.J. (1979). "Biogeographic significance of the late Mesozoic and early Tertiary molluscan faunas of Seymour Island (Antarctic Peninsula) to the final breakup of Gondwanaland." Historical biogeography, plate tectonics, and the changing environment. J. Gray and A. J. Boucot. Corvallis, Oregon State University: 349-355.











Met het begin van de industriële revolutie, ongeveer 150 jaar geleden, is een ongeëvenaard snelle stijging van de atmosferische druk van koolstofdioxide ( $p\text{CO}_2$ ) begonnen. Blijven de  $\text{CO}_2$  emissies onverminderd stijgen, dan wordt verwacht dat  $p\text{CO}_2$  waarden rond het begin van de 21<sup>e</sup> eeuw 1.000 deeltjes per miljoen in volume (ppmv) bereikt: veel hoger dan de  $\sim 390$  van vandaag de dag, laat staan de  $\sim 280$  van vlak voor de industrialisatie (IPCC, 2007). Het broeikasgas  $\text{CO}_2$  absorbeert de uitgaande langegolfstraling (warmte) en straalt het naar alle richtingen uit, waaronder naar de aarde. Hogere  $\text{CO}_2$  waarden zullen daarom naar verwachting resulteren in hogere oppervlaktetemperaturen. Bovendien is de verblijftijd van de uitgestoten  $\text{CO}_2$  lang genoeg om de Aarde de opwarmingseffecten te doen ervaren: de  $\text{CO}_2$  blijft zeker 100.000 jaar in het oceaan-atmosfeersysteem zitten (Walker en Kasting, 1992; Dickens, 2003; Archer, 2003). De klimaatrespons is reeds meetbaar bij veldobservaties (IPCC, 2007). Computermodelexperimenten worden uitgevoerd om de toekomstige klimaat- en milieu effecten gerelateerd aan de aangenomen verhoogde  $p\text{CO}_2$  te voorspellen. Een basale aanname in deze computermodellen is het actualiteitsprincipe: de klimaat-forceringen en terugkoppelingen die heden ten dage aan de orde zijn, zullen ook gelden voor de toekomst. De vraag is alleen of deze forceringen en terugkoppelingen wel hetzelfde zijn onder verschillende klimaatcondities. Een manier om de betrouwbaarheid van de computermodelvoorspellingen te testen is om te kijken in het geologische verleden, toen er condities heersten vergelijkbaar met die voor de toekomst worden verwacht. Reconstructies van de gevoeligheid en snelheid van aardse veranderingen bij perturbaties in het klimaatstelsel kunnen inzicht verschaffen voor toekomstige klimaatveranderingen.

Om een wereld te bestuderen met  $p\text{CO}_2$  die onze toekomstige benadert, kijken paleoklimatologen ver terug in de tijd. De beschikbare informatie geeft aan dat over de laatste 35 miljoen jaar  $p\text{CO}_2$  nooit boven de 1.000 ppmv is geweest. Verreweg de meeste tijd was  $p\text{CO}_2$  zelfs onder de 500 ppmv (Beerling en Royer 2011). De tijdsperiode voor 35 miljoen jaar geleden wordt gekenmerkt door  $p\text{CO}_2$  waarden die waarschijnlijk veel hoger dan 1.000 ppmv zijn geweest. Het bewijs voor veel warmere klimaatcondities is vooral overtuigend in poolgebieden. Vegetatiereconstructies van noordelijke hoge breedtegraden laten zien dat continenten rondom de Noordelijke IJszee tijdens het tijdvak Eoceen ( $\sim 56$  tot 34 miljoen jaar geleden) waren begroeid met (onder andere) *Metasequoia*, een boomsoort die nu alleen in gematigd regenwoud groeit (Francis, 1988). Krokodilschedels zijn gevonden in Alaska (Markwick, 1998), en pootafdrukken bewijzen dat voorvaderen van het Nijlpaard moerassen bevolkten op wat nu Spitsbergen is. Het is zelfs aangetoond dat sommige van deze zoogdieren het hele jaar door vertoefden in het noordelijke poolgebied (e.g., Eberle et al., 2009). Tijdens het toppunt van de Eocene warme periode, ongeveer 54 miljoen jaar geleden, groeiden er palmen rond de Noordelijke IJszee (Sluijs et al., 2009a), en rond 50 miljoen jaar geleden was de Noordelijke IJszee bedekt onder een dikke laag van de drijvende zoetwatervaren *Azolla* (Brinkhuis et al., 2006; Collinson et al., 2010). Het laatstgenoemde fenomeen, gecombineerd met de gereconstrueerde vegetatietypes op het omringende land doet vermoeden dat neerslag in ieder geval seizoenal nat moet zijn geweest op noordelijke hoge breedtegraden (Pagani et al., 2006; Speelman et al., 2010, Barke et al., 2011).



Op zuidelijke hoge breedtegraden zijn Paleogene macrofossielen gevonden in ontsluitingen op het Antarctische continent, die de aanwezigheid van loofbos bewijst (Francis and Poole, 2002). Biomen op Nieuw Zeeland (toentertijd 50° Zuid; Crouch, 2001)) bevatten een keur aan palmsoorten in het laat Eoceen (Hartwich et al., 2010). Studies aan kleimineraalcomposities in Eocene kustsedimenten wijzen op chemische verwerking onder invloed van regen in het Antarctische achterland (Ehrmann 1998). De ontdekking dat Antarctica nat en warm was, is opvallend omdat polaire gebieden ook in het Eoceen donker zijn voor de helft van het jaar. Om de Eocene warmte op polaire breedtegraden te verklaren werd een hypothese geopperd met de nadruk op het effect van de toenmalige continentenconfiguratie op het Zuidelijk Halfrond. Omdat Australië tijdens het grootste deel van het Eoceen nog min of meer aan Antarctica vastzat (Lawver en Gahagan, 2003), en ook de doorgang tussen Antarctica en Zuid Amerika nog niet open was (Lagabrielle et al., 2009), kon de –vandaag de dag isolerende- Antarctische circumpolaire stroming niet rond Antarctica stromen. In plaats daarvan zouden afgeleiden van warme, lage-breedtegraden-stromingen de Antarctische kustlijn hebben kunnen bereiken en opwarmen (Kennett 1977). Deze hypothese werd later in twijfel getrokken door resultaten van computer-modelexperimenten die oceaancirculaties simuleren (Sloan en Rea, 1995). Toepassingen van deze computer modellen op de Eocene situatie laten zien dat zelfs in afwezigheid van een isolerende circumpolaire stroming, de warme oceaanstromingen van lage breedtegraden niet de Antarctische kustlijn konden bereiken. In plaats daarvan circuleerde het oppervlakte water in de vorm van grote kloksgewijs circulerende stromingen, die het bereiken van de Antarctische kustlijn door warme stromingen effectief voorkwam (Sloan en Rea, 1995; Huber et al., 2004). De nu leidende hypothese die de warme condities in het vroeg Paleogeen verklaart dicht een belangrijke rol toe aan de hoge concentraties broeikasgassen, en de daarmee geassocieerde terugkoppelingen (Zachos et al., 2008) alhoewel voldoende direct bewijs, die deze hypothese ondersteunt, nog ontbreekt.

Vanaf 46 miljoen jaar geleden worden in de Arctische Oceaan *ice-rafted debris* en zee-ijs diatomeeën afgezet (Eldrett et al., 2007; St. John 2008; Stickley et al., 2009), wanneer Paleogene klimaatscondities hun topwarmte zijn gepasseerd. Desondanks wordt over het algemeen aangenomen dat de temperaturen en  $p\text{CO}_2$  concentraties in die tijd nog steeds te hoog waren om de aanwezigheid van grote hoeveelheden ijs op de polen toe te staan (DeConto et al., 2008). Op het Zuidelijk Halfrond laten resten van planktonische dinoflagellaten een opvallende verandering zien naar dominantie van vormen die endemisch zijn voor de zuidelijke hoge breedtegraden (Wrenn en Beckman, 1982; Brinkhuis et al., 2003a; Warnaar, 2006). Intuïtief doet zo'n endemische dinoflagellatenpopulatie een afkoeling van het oppervlaktewater in de Zuidelijke Oceaan vermoeden. Dit is niet in overeenstemming met de gereduceerde meridionale temperatuur-gradiënten zoals is gereconstrueerd met behulp van de randen van fossiele bladeren (Greenwood en Wing, 1995), wat eerder de migratie poolwaards dan het ontstaan van endemisme zou faciliteren. Bovendien, door de afwezigheid van fysieke barrières die de Zuidelijke Oceaan afscheidt van aangrenzende wateren, staat letterlijk niets in de weg voor de migratie van warme dinoflagellatensoorten poolwaards.



Algemeen bezien, terwijl een keur aan bewijs suggereert dat het vroeg Eoceen warm was, en het jongere deel van het Eoceen een afkoeling onderging richting de 'Ijskastwereld' van het Oligoceen en Neogeen, blijven nog steeds veel vragen bestaan, over de timing, gedrag en oorzaken van de Broeikas-Ijskast overgang. Een betere kennis van de klimaatsevolutie in de Zuidelijke Oceaan begint bij continue, chronostratigrafisch goed opgeloste tijdseries van vroeg-Paleogene temperatuur, klimaat- en biotische veranderingen. De opgeboorde sequentie van de Arctic Coring Expedition (Moran et al., 2006) heeft een uniek eerste inzicht gegeven in paleo-ecologische veranderingen tijdens de Paleogene broeikaswereld op de Noordpool, maar de sequentie is gefragmenteerd, van lage resolutie en met grote hiaten.

Het sedimentaire archief van de Zuidelijke Oceaan daarentegen is veelvuldig aangeboord door het *Deep Sea Drilling Project* (DSDP) en later het *Ocean Drilling Program* (ODP) en het nog lopende *Integrated Ocean Drilling Program* (IODP). Een probleem die de bestudering van deze boorkernen bemoeilijkt is de afwezigheid van voldoende biostratigrafische middelen om de sedimenten te dateren: conventionele, uit calciet bestaande microfossielen zijn typisch afwezig in sedimenten van hoge breedtegraden. Deels door die afwezigheid weten we nog maar weinig van de klimaatsevolutie in de Zuidelijke Oceaan ten tijde van het vroeg Paleogeen.

Een indirecte benadering om de Paleogene klimaatsevolutie van de Zuidelijke Oceaan te evalueren is opgeslagen in de compilatie van zuurstofisotopenanalyses aan benthische foraminiferen ( $\delta^{18}\text{O}$ ; Zachos et al., 2008). De  $\delta^{18}\text{O}$  waarde in benthische foraminiferen wordt vooral bepaald door watertemperatuur-veranderingen en veranderingen in de  $\delta^{18}\text{O}$  van het zeewater. Dit laatste wordt beïnvloedt door ijsvolume en saliniteit. In de afwezigheid van continentale ijskappen wordt zeewater  $\delta^{18}\text{O}$  dus vooral bepaald door saliniteitsschommelingen. De saliniteit en temperatuur van diepere wateren is afhankelijk van de bron en mechanismes van diep water formatie. De Zuidelijke Oceaan wordt algemeen gezien als de belangrijkste bron voor diepwater formatie in het Eoceen (Thomas et al., 2003). Dus, het signaal uit benthische foraminiferen die leefden in de diepere wateren bevat in feite de signatuur van de klimaatsevolutie van oppervlaktewateren van de Zuidelijke Oceaan.

De globale benthische  $\delta^{18}\text{O}$  compilatie (Zachos et al., 2008) laat een algemene afkoeling zien vanaf de Krijt-Tertiair grens, naar een minimum in het mid-Paleoceen (~58 miljoen jaar geleden; Zachos et al., 2008) Daaropvolgend stijgen de temperaturen gradueel tot ~52 miljoen jaar geleden, waar lange-termijn piektemperaturen voor het Cenozoicum worden bereikt tot ~50 miljoen jaar geleden: het *Early Eocene Climatic Optimum* (EECO). Hier bereiken diepere wateren temperaturen 13°C warmer dan vandaag de dag. De daaropvolgende 15 miljoen jaar, van 49 tot 34 miljoen jaar geleden worden gekenmerkt door graduele afkoeling van diepere wateren (Zachos et al., 2008), wat uiteindelijk uitmondt in het begin van het ontstaan van grootschalige glaciaties op Antarctica (Zachos et al., 1992), ongeveer 34 miljoen jaar geleden (Zachos et al., 2008). Omdat de aanwezigheid van continentale ijskappen voorafgaand aan het vroeg Oligoceen nog steeds ter discussie staat (Eldrett et al., 2007; St. John et al., 2008) is het vooralsnog onzeker hoeveel van de  $\delta^{18}\text{O}$  stijging



in het midden en laat Eoceen het gevolg is van afkoeling, hoeveel van ijsopbouw en hoeveel van een verandering in de bron voor diep water formatie.

Tijdens deze trends hebben verscheidene periodes van klimaatverandering plaats gehad met een meer kortdurend, *transient* karakter. Het *Paleocene-Eocene Thermal Maximum* (PETM) is een kortdurend (~150 kyrs) interval met 5 tot 8°C opwarming, zoals gedocumenteerd in sedimentaire opeenvolgingen van de tropen en in midden- en hoge breedtegraden op beide halfronden (Kennett en Stott, 1991; Sluijs et al., 2006; zie Sluijs et al. (2007a) voor een samenvatting). Tijdelijke opwarming tijdens deze periode valt samen met een duidelijke negatieve excursie in de stabiele koolstofisotopen compositie in sedimentaire componenten (Kennett en Stott, 1991; Sluijs et al., 2007a). Dit bewijst een input van <sup>13</sup>C-verarmd koolstof in het wereldwijde exogene koolstofreservoir. Omdat wijdverbreid bewijs bestaat dat de hoeveelheid koolstof die toegevoegd is tijdens de PETM van dezelfde orde van grootte is als aangenomen wordt voor onze toekomst als alle fossiele brandstof wordt opgebruikt, wordt deze periode veel gezien als beste analoog voor toekomstige klimaatsveranderingen. Jongere, minder extreme periodes met veel gelijkenissen met de PETM zijn ontdekt in het tijdsinterval vanaf de PETM (56 miljoen jaar geleden) tot 51 miljoen jaar geleden (bijv. Cramer et al., 2003; Nicolo et al., 2007; Stap et al., 2010; Zachos et al., 2010). Deze zogenoemde '*hyperthermals*' hebben verschillende acroniemen toegewezen gekregen en worden, net als de PETM, gekenmerkt door een shift naar lagere  $\delta^{13}\text{C}$  waarden van het exogene koolstofreservoir.

Een nog jongere, prominente verschijning van relatief kortdurende klimaatopwarming is het *Middle Eocene Climatic Optimum* (MECO; Bohaty en Zachos, 2003), wat rond 39 miljoen jaar geleden plaats vond (Bohaty et al., 2009). Net als de PETM en andere *hyperthermals*, valt de MECO in diepzeesequenties op door de carbonaatoplossing, welke intuïtief toe te schrijven is aan perturbaties van de koolstofcyclus. Verschillen met de *hyperthermals* zijn er ook, namelijk dat de MECO niet wordt gekarakteriseerd door een negatieve  $\delta^{13}\text{C}$  excursie. Dit doet vermoeden dat, mocht CO<sub>2</sub> stijging een rol spelen bij de klimaatverandering tijdens MECO, de oorsprong van die koolstof die in de atmosfeer gekomen is aanmerkelijk van andere aard is dan bij de *hyperthermals*.

In dit proefschrift komen een aantal nog openstaande vragen aan de orde om beter begrip te krijgen van de klimaatsevolutie in de Zuidelijke Oceaan, zoals: hoe zijn de oppervlaktewateren geëvolueerd in het vroeg-Paleoceen, vooral in vergelijking met de klimaatsevolutie zoals gereconstrueerd in the benthische isotopen? Hoe gevoelig waren de oppervlaktewateren in de Zuidelijke Oceaan voor klimaats-oscillaties op lange en korte termijn in het vroeg-Paleoceen? Wat was de biotische respons op temperatuur- en circulatieveranderingen? Wat was precies de rol van CO<sub>2</sub>, en wat van de opening en de daaropvolgende verdieping van de *Tasmanian Gateway*? Wat was de klimaatgevoeligheid van de Zuidelijke Oceaan in de Paleogene Broeikaswereld?



Om deze vragen te beantwoorden is een combinatie van micro-paleontologische en organisch geochemische technieken toegepast die uitermate bruikbaar bleek om klimaatverandering te reconstrueren op hoge breedtegraden. Anders dan de uit calciet bestaande microfossielen, zijn de fossiele resten van de in het oppervlaktewater levende dinoflagellaten, de dinoflagellaten 'cystjes', of dinocysten, wel zeer talrijk aanwezig in hoge breedtegradensedimenten. In de meeste gevallen, zeker bij zeer oude sedimenten, zijn de dinoflagellaten cysten zelfs het enig overgebleven biostratigrafische hulpmiddel, om de sedimenten met andere opeenvolgingen te kunnen correleren (Brinkhuis et al., 2003a; Eldrett et al., 2004; Williams et al., 2004). Bovendien bevatten assemblages van dinocysten bruikbare, kwantitatieve informatie over een keur aan fysische parameters van de oppervlaktewateren, zoals nutriënten, temperatuur, saliniteit en kustnabijheid (Dale 1996; Pross en Brinkhuis, 2005). Specifiek voor de Zuidelijke Oceaan ten tijde van het vroeg Paleogeen is de aanwezigheid van endemische vormen van dinocysten (Wrenn en Beckman 1982; Wrenn en Hart, 1988). Deze soorten werden aanvankelijk *transantarctic flora* genoemd, omdat aangenomen werd dat ze bewijs vormden voor de aanwezigheid van een transantarctische zeestraat (Wrenn en Beckman, 1982), en omdat blijkbaar in die tijd, dinoflagellaten onder de planten werden gerekend. Hoewel latere studies aantoonde dat dinoflagellaten zowel heterotrofe alsook autotrofe genera herbergt, en het vooralsnog niet evident is dat een transantarctische zeestraat daadwerkelijk bestond, wordt de term *transantarctic flora* desondanks toch nog gebruikt. Het werd duidelijk dat de *transantarctic flora* domineerde in die regio's die onder invloed waren van oceaanstromingen vanuit Antarctica (Huber et al., 2004). Deze observatie wijst intuïtief naar temperatuur als bepalende omgevingsfactor voor de biogeografische distributie van de endemische populatie, maar deze aanname is nog niet adequaat getest.

Bovenop de informatie verkregen door analyses van dinocysten kunnen organisch geochemische tools vaak worden ingezet op sedimenten die dinocysten bevatten, omdat de condities die nodig zijn om beide te preserven in het sediment vrijwel gelijk zijn. De organisch geochemische *toolbox* om klimaat te reconstrueren is de afgelopen jaren erg vergroot, met de ontwikkeling van nieuwe methodes, zoals de TEX<sub>86</sub> proxy voor zeeoppervlaktewatertemperatuur (Schouten et al., 2002; Kim et al., 2010) en pCO<sub>2</sub> gebaseerd op de stabiele koolstofsamenstelling van alkenonen (Pagani 2002). Door de palynologische en organisch geochemische tools te combineren op de grote hoeveelheid sedimentaire archieven uit de Zuidelijke Oceaan kan een betere reconstructie ontstaan van de dynamiek en hoge-resolutie klimaatevolutie van vroeg Paleogene zuidelijke hoge breedtegraden.

Dit proefschrift levert nieuwe inzichten in de paleomilieu- en paleoklimaatevolutie van de Zuidelijke Oceaan ten tijde van het vroeg Paleogeen. In **Hoofdstuk 1, 2 en 3** wordt een raamwerk gepresenteerd van de paleoklimaat en paleomilieu-evolutie in de Zuidelijk Oceaan, in termen van dinocyst bio-magnetostratigrafie, organische *biomarker* paleothermometrie en dinocysten biogeografie in de Zuidelijke Oceaan. De **Hoofdstukken 4, 5 en 6** richten zich specifiek op kritieke intervallen met snellere klimaatverandering, in chronologische volgorde.



In **Hoofdstuk 1** wordt een aan magnetostratigrafie gekalibreerd biostratigrafisch zonatieschema van organische dinoflagellaten cysten voorgesteld voor boven Paleocene tot boven Eocene sedimenten van de Zuid-Pacifische Oceaan. We vergelijken chronologieën van Ocean Drilling Program (ODP) Holes 1171D en 1172A/D met dat van Integrated Ocean Drilling Program (IODP) Hole U1356A, en vervolgens met dinocysten zonaties van Nieuw Zeeland. Gebaseerd op deze correlaties presenteren wij een gereviseerd magnetostratigrafisch ouderdomsmodel voor ODP Holes 1171D en 1172A/D en stellen een Zuid-Pacifische dinocysten zonatie voor, bestaande uit dertien dinocysten zones. De *South Pacific Dinocyst Zonation* is gekalibreerd naar de Internationale Tijdschaal van Gradstein et al. (2004), met toegevoegde onafhankelijke ouderdomsbepalingen uit stabiele koolstofisotopen profielen, zoals die gecorreleerd naar de *Paleocene-Eocene Thermal Maximum* en de *Middle Eocene Climatic Optimum*, en magnetostratigrafie.

In **Hoofdstuk 2** wordt een, in zijn continuïteit unieke en chronostratigrafisch goed gekalibreerde TEX<sub>86</sub> curve van zeewatertemperatuur gepresenteerd van ODP Leg 189 Hole 1172D op het East Tasman Plateau (~65° Zuid; Fig. 1 in *Introduction and Synopsis*). We laten zien de oppervlaktewatertemperatuur in de zuidwest Pacifische Oceaan steeg tot boven hedendaagse temperaturen in de tropen (tot 34°C) tijdens het vroeg Eoceen (53 miljoen jaar geleden) en dat het geleidelijk afkoelde tot ongeveer 21°C in het laat Eoceen (36 miljoen jaar geleden). Onze resultaten doen vermoeden dat er nagenoeg geen latitudinale temperatuursgradiënt bestond tussen subequatoriale en subpolaire breedtegraden ten tijde van het vroeg Eoceen (~55-50 miljoen jaar geleden). Deze latitudinale temperatuurgradiënt werd beduidend sterker in het midden Eoceen. Als de Eocene afkoeling het resultaat is van dalende atmosferische CO<sub>2</sub> concentraties (Zachos et al., 2008), dan zijn er in theorie additionele mechanismes nodig om de relatieve stabiliteit van tropische oppervlaktetemperaturen (Pearson et al., 2007) te verklaren bij evidente afkoeling op hogere breedtegraden.

Verschillende vroeg Paleogene plankton assemblages worden, in meer of mindere mate, gedomineerd door endemische soorten, ondanks warme condities op de polen en zwakke meridionale temperatuurgradiënten. Om de evolutie van het Paleogene plankton endemisme in zuidelijke polaire gebieden te documenteren, wordt in **Hoofdstuk 3** de verspreiding in ruimte en tijd van dinocysten onderzocht. Bovendien bepalen we hun respons op veranderingen in de regionale oppervlaktewatertemperatuur. Paleocene en vroeg Eocene (~65-50 miljoen jaar geleden) dinocystenassociaties waren voor het overgrote deel kosmopoliet van aard in de Zuidelijke Oceaan, maar een prominente shift van kosmopoliet-gedomineerde naar endemisch-gedomineerde assemblages (de zogeheten *transantarctic flora*) vond plaats rond de vroeg-midden Eoceen overgang (~50 miljoen jaar geleden). De geografische verspreiding en patronen in relatieve abundantie van de *transantarctic flora* komen sterk overeen met oppervlakteoceaanstromingen, zoals ze gereconstrueerd zijn met behulp van computermodelexperimenten, in het Eoceen. Dinocysten zijn kwantitatief vergeleken met de TEX<sub>86</sub>-gebaseerde zeewater-



temperatuurreconstructies zoals gepubliceerd in Hoofdstuk 2 voor het vroeg en midden Eoceen van ODP Site 1172. Een conclusie is dat het begin van de proliferatie van de *transantarctic flora* aan het begin van het midden Eoceen niet lineair is toe te schrijven aan regionale temperatuurreconstructies. Alleen wanneer de *transantarctic flora* goed en wel domineren in het midden Eoceen, mogelijk aangestuurd door productiviteitsveranderingen op oceaan-schaal, zien we een goede relatie tussen de relatieve abundantie van *transantarctic flora* en temperatuur.

In **Hoofdstuk 4** wordt een PETM sectie behandeld van ODP Hole 1172D. De organische paleothermometer TEX<sub>86</sub> laat zien dat de oppervlaktewatertemperatuur steeg van ~26°C naar ~33°C tijdens de PETM. Dergelijke temperaturen voor, tijdens en na de PETM zijn meer dan 10°C warmer dan die gesimuleerd worden door klimaatmodellen voor deze breedtegraad. Dus zou het zo kunnen zijn dat niet alleen Noordpool-, maar ook Zuidpooltemperaturen lager zijn ingeschat zijn in simulaties van voorbije broeikaswerelden door de modernste, meest geavanceerde en volledig gekoppelde klimaatmodellen. Er is een vroege verschijning van abundante *Apectodinium* spp. in Hole 1172D, in overeenstemming met andere secties met hoge sedimentaccumulatie, zoals in New Jersey. Dit doet eens te meer vermoeden dat milieuveranderingen aan de koolstofisotopenexcursie voorafgingen, op wereldwijde schaal. Organische dinoflagellaten cysten assemblages suggereren een versterkte aanvoer van riviermateriaal naar de boorplek ten tijde van de PETM, tegelijk met eustatische zeespiegelstijging. Bovendien zijn veranderingen in seizoensaliteit van het regionale hydrologische systeem, en wellicht stormactiviteit uit de assemblages te herleiden. Ten slotte laten de sterke variatie in dinoflagellaten cyst assemblages tijdens de PETM zien dat het zuidwest Pacificse klimaat significant varieerde over tijdschalen van 10<sup>3</sup> – 10<sup>4</sup> jaren, een ontdekking die in lijn is met vergelijkbare studies van de PETM op het continentale plat van New Jersey.

In **Hoofdstuk 5** wordt de rol onderzocht van het open gaan van een cruciale zeestraat in de Zuidelijk Oceaan, de *Tasmanian Gateway*, in Antarctische klimaatverandering. Proxy gegevens worden gepresenteerd van recentelijk opgeboorde sedimenten van het Wilkes Land continentaal plat, voor de kust van Antarctica (Escutia et al., 2011), welke afgezet zijn aan de westkant van de *Tasmanian Gateway* in de *Australo-Antarctic Gulf*. Geïntegreerde analyses van zowel mariene als terrestrische microfossielen en organisch geochemische componenten laten een sterke afkoeling zien van oost-Antarctische wateren (3-4°C) en aangrenzende landmassa's (6°C), rond 50 miljoen jaar geleden. Opvallend is dat deze afkoeling samenvalt met het begin van het overheersen van typisch zuidwest Pacificsch fytoplankton welke gemigreerd zijn via een blijkbaar ondiepe zuidelijke opening van de *Tasmanian Gateway*. Tezamen impliceren deze observaties dat het begin van de *Antarctic Counter Current* door de *Tasmanian Gateway* de invloed van de warmere *Proto-Leeuwin Current* heeft geminimaliseerd. Dit suggereert een sterke rol voor de ondiepe opening van de *Tasmanian Gateway* in Antarctische afkoeling, wat deze regio voorbereidt op grootschalige cryosfeerontwikkeling ten tijde van de Eoceen-Oligoceengrens rond 34 miljoen jaar geleden.





De lange-termijn warmte in het Eoceen (~56-34 miljoen jaar geleden) wordt alom in verband gebracht met verhoogde atmosferische druk van koolstofdioxide ( $p\text{CO}_2$ ). Echter, dit verband is nog niet vastgesteld voor korte-termijn perturbaties. In **Hoofdstuk 6** worden zowel  $p\text{CO}_2$ - als zeevatertemperatuurreconstructies getoond voor een periode van tijdelijke wereldwijde opwarming: de *Middle Eocene Climatic Optimum* (MECO; ~39 miljoen jaar geleden). Organische moleculaire paleothermometrie laat een opwarming van zuidwest Pacifische oppervlaktewateren van 3 tot 6°C zien, terwijl  $p\text{CO}_2$  gelijktijdig twee- tot driemaal zo hoog wordt. De evidente overeenstemming tussen zeevatertemperatuur- en  $p\text{CO}_2$  trends tijdens de MECO doen vermoeden dat verhoogde  $p\text{CO}_2$  concentraties een grote rol speelden in wereldwijde opwarming ten tijde van de MECO.

Samenvattend levert dit proefschrift een gedetailleerde weergave van de vroeg Paleogene transitie van een Broeikas- naar een Ijskastwereld in de Zuidelijk Oceaan. De dinocystenzonatie die een groot deel van het vroeg Paleogeen bestrijkt, kan worden gebruikt als leidraad voor toekomstige biostratigrafie en ouderdomsbepalingen, wat cruciaal is gezien de afwezigheid van alternatief biostratigrafisch gereedschap in de Paleogene Zuidelijke Oceaan. De zeevatertemperatuurevolutie in de zuidwest Pacifische Oceaan volgt die in zuurstof isotopen in benthische foraminiferen, wat doet vermoeden dat de zuid Pacifische Oceaan een sector was waar diep water werd gevormd. Echter, absolute temperaturen blijken veel hoger dan die bepaald met benthische foraminiferen. Deels kan dit het gevolg zijn van seizoenale afwijkingen, bijvoorbeeld dat het diepwater met name gevormd wordt in winter en dat de gereconstrueerde oppervlaktewatertemperaturen in de Zuidelijke Oceaan vooral naar zomertemperaturen neigen. De biotische reactie op de oppervlakte-watertemperatuurevolutie in de Zuidelijke Oceaan is controversieel: het domineren van endemische dinocysten assemblages lijkt niet gerelateerd aan temperatuur. De werkhypothese was intuïtief dat de verspreiding van een endemische fytoplanktongemeenschap op hoge breedtegraden het resultaat was van een succesvolle concurrentiestrijd met warmwatersoorten ten tijde van afkoeling. Nu blijkt dat de zeevatertemperatuur niet verantwoordelijk kan worden gehouden voor het begin van de wijde verspreiding van de endemische planktonsoorten, is er een alternatieve hypothese opgesteld, die een rol toedicht aan nutriëntentoeename in de oppervlaktewateren in het midden Eoceen. Inderdaad, verscheidene onafhankelijke proxies laten gezamenlijk een verschuiving naar meer nutriëntentoevoer zien, beginnende in het late vroeg Eoceen (~50 miljoen jaar geleden), van export productiviteitstoename in de gehele Pacifische Oceaan tot een versterking van de gradiënt van stabiele koolstofisotopen tussen oceanen. De PETM is ook een opvallend interval in de Zuidelijke Oceaan gekenmerkt door zeer snelle opwarming van de oppervlaktewater-temperatuur: 5-8°C. Ook hier is een superdominantie van tropische representanten van dinocystengenus *Apectodinium* vastgesteld. Net als bij andere PETM secties is ook in de zuid Pacifische Oceaan een nadrukkelijke milieuverandering zichtbaar voordat de negatieve koolstof-isotopenexcursie zich voordoet. Dit is in samenspraak met verdenkingen dat initiële klimaatveranderingen vooraf gingen aan de uitstoot van koolstof verantwoordelijk voor de koolstof-isotopenexcursie. Vervolgens zou dit kunnen betekenen dat de koolstofisotopenexcursie een respons is op klimaatverandering, in plaats van een forcering. Een ander



voortdurend debat dat bediscussieerd wordt in dit proefschrift is de rol van het open gaan van bepaalde zeestraten en hun rol in klimaatverandering. Recentelijk (2010) opgeboorde sedimenten van het Wilkes Land continentaal plat, Antarctica, laten zien de doorstroming van de *Antarctic Counter Current* rond de vroeg-midden Eoceen overgang (52-50 miljoen jaar geleden) begon, gelijktijdig met een versterkte afkoeling van Antarctische landmassa's en kustwateren. Deze opening van de *Tasmanian Gateway* vond plaats op het moment dat Aarde langzaam maar zeker begon af te koelen naar 'ijskast'-condities zoals de afgelopen 35 miljoen jaar bestaan. Daarom zou het opengaan van de *Tasmanian Gateway* wel eens het pad vrij kunnen hebben gemaakt voor klimaatafkoeling, waar atmosferische CO<sub>2</sub> druk waarschijnlijk nog steeds een grote forceringsfactor was in Paleogene klimaatsevolutie. Inderdaad, we zien desondanks dat de relatief kortdurende klimaatverandering van de MECO samenvalt met een sterke toename in de atmosferische CO<sub>2</sub> concentraties, wat een grote rol toedicht aan CO<sub>2</sub> als forcering van klimaatveranderingen.





## Acknowledgements

This is where it has to happen. It was an intense feeling of shame that I felt putting just my own name on the front cover of this thesis. Rather, I would have liked to put all the names listed below on the front cover and my name here. Oh well, I guess I have to obey the rules...

In springtime 2006, after the Master's course 'Extreme Climate Transitions' I thought: let's ask that Henk Brinkhuis guy whether he has a Master's internship subject for me. From that day onwards, Henk has supervised me in the typical Brinkhuis way: letting go where it is possible and helping out wherever he could. After my graduation in September 2007, I was really hoping to continue this work in a PhD, which worked out really well thanks to the Faculty of Science and the LPP Foundation. I applied (after encouragements by Henk) for the IODP expedition to Wilkes Land, Antarctica. Subsequently, Henk was asked to become co-chief of the Leg. Coincidence dictated that Dan, his brother, became videographer, and I was invited to sail as palynologist. This is just one example where sheer coincidence and serendipity has brought the most brilliant things together. For me it suffices to say that Henk is the 'totaalsupervisor'. With 'totaalvoetbal', the Dutch soccer coach Rinus Michels led Dutch teams to superior levels in the 70's and 80's. Soccer players were encouraged to show up at different positions on the pitch all the time, and therefore the ball circulated very quickly. Henk gave me the opportunity to show up everywhere in the 'scientific pitch' all the time during my Master's and PhD. Besides supervising, he has always been and still is in for good fun outside the University, with the endless poker nights, and nice 'Christmas' (November through March) dinners at his home. Likewise, Dutch soccer teams of the 70's were quite notorious for their entertainment outside the soccer pitch as well...

Appy was the perfect counterpart of Henk's at the university. Appy, your discussions really helped me a lot in perfecting the paper manuscripts and it worked very efficient to have both you and Henk so close together. I really appreciated the debates over coffee, on any subject, also outside of academia ('...that goal was clearly offside...'). Appy, it felt like I was always welcome in your office, and couldn't ask too much questions. It is a habit I would like to have a bit more.

Stefan, I visited the NIOZ way too little, and in my memory it was always during the harsh part of the year. Even though, while stormy and cold outside, within your group there was always the feeling of a warm welcome. It was really good fun traveling all the way up to the island of Texel, because I knew who were waiting there for me. Thank you so much for the pleasant cooperation, and I hope that the finishing of this thesis is not the end of that.

I considered the Laboratory of Palaeobotany and Palynology in Utrecht as second home. The atmosphere was really good, optimistic even in harsh times. There was always time for a coffee and a chat: the coffee corner was equipped with an invaluable espresso machine around which all the magic happens. There are so many

## ACKNOWLEDGEMENTS

true heroes from LPP to be acknowledged here, in the absence of whom chaos would reign: Natasja Welters, Jan v Tongeren, Leonard Bik, Marjolein Mullen, Ton v Druten, Hans v Aken and from the LPP Foundation: Wim Sluis.

Francesca Sangiorgi: you brought the Mediterranean spice into the group: something that us sober Dutchies could really use! Also the contact with Andy Lotter, Friederike Wagner en Wolfram Kürschner was very pleasant.

Then my fellow PhD's. Being in the group now for over 5 years, I have met so many PhD students, and that large group provided a vivid atmosphere at the 3<sup>rd</sup> floor of the Earth Sciences Building: Jeroen, Gianluca, Maaike, Emilia, Frederike, Peter, Nina, Micha, Judith, Maarten.

Sander, Emmy, Alex, Mirja, Johan, Niels, Joost, Arjen and Mariska have the pleasure to keep the nice atmosphere going in the lab. Good luck with your PhDs you guys!

Students came and went over the past years, and it is always nice to see your own enthusiasm being conveyed to new bright people: Willemijn, Linda, Esther, Marcel, Michiel and Luuk, and all the others in the student room.

Many thanks go out to the people from Geochemistry ('downstairs'). Although they had every reason to get absolutely nuts from the invasion of their lab by LPP people ('this is person x, he/she is doing a master's thesis with us and would like to run some TEX<sub>86</sub> as well...') but no, you guys always helped a lot in the lab, and everybody cooperated to make things happen. Gert-Jan, your input in manuscripts was spot on at the right time. Thanks also to Jack Middelburg, Jaap Sinninghe Damsté, Eveline Speelman, Elizabeth v Benthum, Els v Soelen, Julia v Winden, Cornelia Blaga, Jos Wit, Marieke Lammers, Laura Buckles, Lennart de Nooijer, Johan Weijers, Klaas v Nierop, Gijs Nobbe, Anita Tolboom, Arnold v Dijk and Jan Kubiak.

At the NIOZ on Texel, numerous people have helped out with the analyses. Endless thanks go out to Jort Ossebaar, Ellen Hopmans, Irene Rijpstra, Jan de Leeuw, Anhelique Metsers, Marianne Baas en Michiel Kienhuis. Also the OiO's out there were helpful in the lab and good company at lunches.

Good discussions were also very much appreciated with Lucas Lourens, Jan-Willem Zachariasse, Albert vd Meulen, Poppe de Boer, Lucy Stap and Hemmo Abels, from the Stratigraphy and Paleontology group.

The IODP Expedition 318 to Wilkes Land, Antarctica has offered me the opportunity to meet the nicest people, both in academia and from the Integrated Ocean Drilling Program. In particular Carlota Escutia, Jörg Pross, Lineth Contreras, Cathy Stickley, James Bendle, Ursula Röhl, Steve Bohaty, Sandra Passchier, Rob & Rob (McKay and Dunbar), Lisa Tauxe and Tina vd Flierdt really learned me a lot on the ship and post-cruise, and we had a great time on the ship. Also the IODP folks: Adam

Klaus, Chad Broyles, John Firth, and shiploads of other people I now forget: you are great; let's all hope this work can be continued.

Dan Brinkhuis, the 'lean mean video machine', is thanked for loads of occasions where he popped up, of course during Expedition 318, where he helped out a lot with my blog video's and kept spirits up on the ship, but also just for an espresso at the University, with the *Academische Jaarprijs*, during poker or at IODP science meetings: it was always good fun, also because you are so enthusiastic about our stuff!

Bert Vermeersen and Paolo Stocchi, you have been the most interesting physicists I have met, not only in terms of science (tell me, how does it feel to see so many geologists busting their brains from your science?) but also on occasions outside of science we had a good time. I hope our cooperation can be continued!

The Urbino Summer School of Paleoclimatology was like a professional playground for me: I got to meet the most interesting people, team up in discussions with beers and good food, and experience the birth of so many new projects, views, opinions. That worked really inspiring and set me off in science right from the start. Many thanks therefore go out to Simone Galeotti and his Italian co-workers who made the summer schools logistically possible, but also people like Matthew Huber, Paul Pearson, Robert DeConto, James Zachos, Rich Pancost, Jerry Dickens and loads of people I forget now for so many interesting discussions by the pool.

Sander, my roomy for the vast majority of my PhD time, we could really enjoy ourselves over many things (funny news items, good music) and discuss new data hot off the press, but also (and that was sometimes even more valuable) be silently working all day. Thanks a lot for sharing a room! Other than that, the many conference trips were much more fun with you being around. Emmy: many thanks for keeping the office of Sander and me a bit joyous with your visits. If it weren't for you, our office would have been too much work and too little fun! You were the often-necessary distraction from too intense workdays. Also with both you guys I had really good fun in our days in the Board of the PPGU. We successfully organized symposia and excursions: it was great fun!

Thanks to the institutions that made working with the ocean sediments possible in the first place. The research presented in this thesis used samples and data provided by the Deep Sea Drilling Project, (DSDP) the Ocean Drilling Program (ODP) and the Integrated Ocean Drilling Program (IODP). DSDP, ODP and IODP were sponsored by the U.S. National Science Foundation (ODP and IODP were also sponsored by other participating countries) under the management of Joint Oceanographic Institutions (JOI) Inc. The Shipboard Scientific Party of IODP Expedition Leg 318 is thanked for providing (shipboard) data.

Last but not least, my parents for making it financially possible for me to go to the university, but most of all for being interested and loving like only parents can.

**Cheers you all!**





*'For whatever we lose (like a you or a me)  
it is always ourselves we find in the sea'*

- ***E.E. Cummings (1894-1962)***





## Curriculum Vitae

Peter Bijl werd op 21 oktober geboren, in Hoogeveen, maar groeide op in Papendrecht. Na zijn VWO-examen aan De Lage Waard in Papendrecht in 2002 begon hij zijn studie Geologie aan Universiteit Utrecht. In het tweede jaar volgde hij het *Bachelor track Biogeology*, die hij afsloot met een praktisch onderzoek bij de leerstoelgroep Stratigrafie en Paleontologie van de Universiteit Utrecht, naar benthische foraminiferen assemblageveranderingen in de Waddenzee over de afgelopen 150 jaar. In 2005 startte Peter de *Master Biogeology* aan de Universiteit Utrecht, waarin hij in april 2006 zijn afstudeerscriptie begon bij Henk Brinkhuis en Appy Sluijs van de leerstoelgroep Palaeoecologie van de Universiteit Utrecht. Hierbij keek hij naar paleomilieuveranderingen in de Zuid Pacifische Oceaan ten tijde van het Paleoceen-Eoceen. Aan de hand van studies naar dinoflagellaten cysten assemblages werden oppervlaktewater veranderingen gereconstrueerd. Daarnaast heeft hij voor zijn afstudeerscriptie veranderingen in elementenverhoudingen geanalyseerd in boorkernen met behulp van een *X-ray fractionation scanner* bij Ursula Röhl aan de Bremen Universiteit. Ook heeft hij op het NIOZ Koninklijk Nederlands Instituut voor Zeeonderzoek op Texel organisch geochemische analyses uitgevoerd. Tijdens zijn master stage was Peter betrokken bij het winnende project van de Academische Jaarprijs. Het project had als doel wetenschappelijke bevindingen van de studie naar de Paleogene broeikaswereld en de lessen voor toekomstige klimaatverandering naar het middelbaar onderwijs te over te brengen. Middels informatieve clips, een website en prijsvraag voor bovenbouw HAVO/VWO werden leerlingen bekend met het aardwetenschappelijk onderzoek. Na het behalen van zijn *MSc.* in 2007 begon hij in januari 2008 zijn promotieonderzoek bij de leerstoelgroep Palaeoecologie, onder begeleiding van Henk Brinkhuis, Stefan Schouten (NIOZ) en Appy Sluijs.



## Peer-reviewed articles

Warnaar, J., **P.K. Bijl**, M. Huber, L.C. Sloan, H. Brinkhuis, U. Röhl, R. Sriver and H. Visscher (2009). "Orbitally forced climate changes in the Tasman sector during the middle Eocene." *Palaeogeography, Palaeoclimatology, Palaeoecology* 280: 361-370.

**Bijl, P.K.**, S. Schouten, H. Brinkhuis, A. Sluijs, G.-J. Reichert and J.C. Zachos (2009). "Early Palaeogene Temperature Evolution of the Southwest Pacific Ocean." *Nature* 461: 776-779.

**Bijl, P.K.**, A.J.P. Houben, S. Schouten, S.M. Bohaty, A. Sluijs, G.-J. Reichert, J.S. Sinninghe Damsté and H. Brinkhuis (2010). "Transient Middle Eocene Atmospheric Carbon Dioxide and Temperature Variations." *Science* 330: 819-821.

Escutia, C., H. Brinkhuis, A. Klaus and **Expedition 318 Scientists** (2010). "Wilkes Land Glacial History: Cenozoic East Antarctic Ice Sheet evolution from Wilkes Land margin sediments." *Proceedings of the Integrated Ocean Drilling Program, Preliminary Reports*, volume 318.

Sluijs, A., **P.K. Bijl**, S. Schouten, U. Röhl, G.-J. Reichert and H. Brinkhuis (2011). "Southern Ocean warming and hydrological change during the Paleocene-Eocene thermal maximum." *Climate of the Past* 7: 47-61.

**Bijl, P.K.**, J. Pross, J. Warnaar, C.E. Stickley, M. Huber, R. Guerin, A.J.P. Houben, A. Sluijs, H. Visscher and H. Brinkhuis (2011). "Environmental forcings of Paleogene Southern Ocean dinoflagellate biogeography." *Paleoceanography* 26: PA1202.

Houben, A.J.P., **P.K. Bijl**, G.R. Guerin, A. Sluijs, H. Brinkhuis (2011). "*Malvinia escutiana*, a new biostratigraphically important Oligocene dinoflagellate cyst from the Southern Ocean." *Review of Palaeobotany and Palynology* 165: 175-182.

Escutia, C., H. Brinkhuis, A. Klaus and **Expedition 318 Scientists** (2011). "Proceedings of the Integrated Ocean Drilling Program, Initial Results, volume 318." Tokyo (Integrated Ocean Drilling Program Management International, Inc.).